Kingdom of Saudi Arabia
Ministry of Education
Jazan University

JAZAN UNIVERSITY

JOURNAL OF
JAZAN UNIVERSITY
For
Applied Sciences

A Refereed Scientific Periodical

ISSN:1658-6913

To Vol. 11 No 2 October 2023(Rabi` al-Thani)

Publication Rules

The University of Jazan provides an opportunity for scholars to publish their scholarly work on research. The editorial board will consider manuscripts from all fields of knowledge. Manuscripts submitted in either Arabic or English, and if the due accepted for publication, may not be published elsewhere, without permission of the Editor-in-Chief. The journal issues one volume per year. The types of manuscript classification used by the Editorial Board run as follows:

1. **Article:**
   An author's original work contributing new knowledge to the field in which research was conducted.
2. **Review Article:**
   A critical synthesis of the current literature in a particular filed, or a synthesis of the literature in a particular field during an explicit period of time.
3. **Brief Article:**
   A short article (note) with the characteristics of an article.
4. Book Reviews
5. **Forum:**
   Letters to the editor, comments, responses, preliminary results or findings, and miscellany

General Instructions

1. Submission of manuscripts:

Original manuscripts should be typewritten (one side only), using an A4 size paper, double spaced along with 3 copies. All pages are to be numbered consecutively, including tables and graphs. Tables, other illustrations, and references should be presented on separate sheets with their proper text position indicated.

2. Abstracts:

Manuscripts for articles, review articles, and brief articles require both Arabic and English abstracts, using no more than 200 words, in single column (13cm wide), for each version.

3. Tables and other illustrations:

Tables, charts, figures, and plates should fit the journal's page size (12.5 com x 18cm). All inner drawings must be presented on high quality. Tracing paper is necessary, using black Indian ink as well. Photographs may be submitted, but on glossy print paper in either black or color.

4. Abbreviations and Units:

A4 sizes and quantities should be expressed according to international standards. Standardized abbreviation should only be used. The names of periodicals should be abbreviated in accordance with the words of scientific periodicals.

5. Title Page:

Should contain the title, name of the authors, name and address of the institution, where the work was carried out. The title should be brief and use strong keywords. Scientific names of organism should be clearly stated and should be typed italic.

6. Text:

The organization of the manuscript should be as follows: Introduction, materials, results, discussion, and references. Results and discussions can be combined in one section. Acknowledgement (if needed) should be brief and added before the reference sections.

1. References:

Citation of the references (within the text) should be indicated by author. Date, style, and references should be listed in an alphabetical order and conform to the following examples: Periodical citations in the text are to be enclosed in one line brackets, e.g.(6).

Periodical references are to be presented in the following

form:

References number in line brackets ( ), author's name followed by a given name and/or initials, the title of an article or periodical (italicized), volume number, year of publication (in parentheses) and pages e.g.

Basahy, A.Y. (1992). Protein and Amino Acid contents in seeds of some soybean cultivate (Glycin Max 1) Arab Gulf J. Sci. Res. 11(2), 221-228.

Book Citation:

Book references should include the following:

Reference number ( ), author's surname followed by a given name and/or title of the book (italicized), place of publication, publisher, and year of publication.

Example:

Lehman. H.C. (1953). Age and Achievement. Princeton: Princeton University Press.

2. Content Notes:

Content notes are to be presented on separate sheets. They will be printed below a solid line separating the content notes from the text.

9. The manuscripts and forum items submitted to the journal for publication contain the author's conclusions and opinions, and if published they do no bear a conclusion or opinion of the Editorial Board.

10. Authors will be provided with 20 reprints free of charge, along with two issues of the journal. Additional copies could be purchased, if ordered when the proofs are returned. Price will be shown on the order form.

11. It is the responsibility of the researcher to make sure that the manuscript is free of linguistic, grammatical and typo errors.

12. The editors' board has the right to set priorities of publishing the research.

13. The journal is not obligated to repeat the research it reaches, whether it was approved for publication or not.

14. All the received research is subject to primary examination by the editorial board in order to determine their eligibility for arbitration. The editorial board is entitled to excusing itself from accepting the research without giving reasons.

15. The journal is published twice a year.

Kingdom of Saudi Arabia
Ministry of Education
Jazan University

JOURNAL OF
JAZAN UNIVERSITY

For

Applied Sciences

A Refereed Scientific Periodical

To Vol. 11 No 2 October 2023(Rabi` al-Thani)

ISSN:1658-6913

Journal Jazan University

for applied sciences

Correspondence

All correspondence should be directed to:
Editor-in-chief of Jazan University Journal of Applied Sciences, Jazan - University City
Administrative Tower - PO Box 114 - Zip Code 4514, Kingdom of Saudi Arabia
jas@jazanu.edu.sa

فهرس المحتويات

الموضوع **صفحة**

Soil Properties and Contaminants May Play a Significant Role in the Interference Level of Biochar with Colorimetric Soil Enzyme Assay of β-glucosidase

Abdurrahman S. Masrahi

Department of Biology, Faculty of Science, Jazan University, Jazan, Saudi Arabia.

Abstract

Biochar (BC) has recently received much attention as a soil conditioner or amendment. Measuring soil enzyme activities in BC-amended soils has shown some contradictions due to the possible interference of BC with colorimetric enzyme assays. This interference has mainly been attributed to only BC, needing to consider soil properties and the presence of contaminants. This study aims to evaluate the effects of soil types differing in chemical and physical properties and the presence of contaminants in the interference of BC with a colorimetric assay of β-glucosidase using three different BC application rates: 0, 2, and 5 %. Three different soils were collected from different sites: soil near a cement factory (CES), soil near a wastewater treatment plant (WWS), and soil near an agricultural farm (PMS). Concentrations of several heavy metals in the polluted soils (WWS and CES) were determined using ICP-AES. The results showed that 2 and 5 % BC rates significantly ($p < 0.05$) underestimated β-glucosidase activity in the WWS soil.
In contrast, only the 5 % rate significantly underestimated enzyme activity in the PMS soil. No significant interference was found in the case of CES soil. Overall, the results illustrated that depending on the chemical and physical characteristics of the soil, BC can interfere differently with colorimetric assays of β-glucosidase activity. Also, the presence of heavy metals may have a role in this interference. However, more research is needed to fully understand the role of soil properties and contaminants in such interference.

Keywords: biochar; β-glucosidase; soil properties and contaminants; heavy metals; colorimetric enzyme assays.

1. INTRODUCTION

The many benefits biochar (BC) provides to plants, soil, and the environment have recently made it a hot topic. Higher populations of beneficial soil bacteria, greater soil fertility, increased carbon sequestration (lessening greenhouse gas emissions), and soil retention of water and nutrients are a few of these benefits. (Atkinson et al., 2010). Biochar has a large surface area and various cation exchange capacities (CEC). Such properties of BC highly depend on the activation processes used (Azargohar and Dalai, 2008). Therefore, the application of BC will raise soil CEC (Joseph et al., 2009), increasing soils' ability to adsorb ions and preventing nutrient leaching (Yao et al., 2011). However, there is increased evidence indicating that the characteristics of BC, including the feedstock, physicochemical nature, pyrolysis temperature, age, and quantity of BC supplied, can affect how much of a change in soil properties they can produce (Amini et al., 2016; Dahlawi et al., 2018).

Beside chemical indicators of soil quality, soil enzymes are one of the major indicators of soil health (e.g., soil that functions normally and is free of diseases) (Alkorta et al., 2003). Determination of soil enzyme activities is mostly based on colorimetric methods using a spectrophotometer. However, since BC is frequently used as a soil conditioner, studies on soil enzyme activities in soil amended with BC have shown contradictory results. For example, a study by Liu et al. (2017) reported a significant increase in alkaline phosphatase activities in soil amended with rice husk BC produced at a temperature of 400 °C. In addition, Günal et al. (2018) reported that applying different types of BC in different agricultural soils varying in textures decreased β-glucosidase enzyme activity. However, the chemical properties of soils reported in their study (EC, pH, and CaCO3) were relatively similar. The enzyme β-glucosidase is a major player in the carbon cycle in soil ecosystems (Günal et al., 2018). In a recent study by Lopes et al. (2021), long-term application of BC in doses up to 30 Mg ha-1 (approximately 3% w/w) in sugarcane fields enhanced the activities of β-glucosidase, acid phosphatase, arylsulfatase, and urease. However, they reported that greater doses decreased these enzymes' activity and the soil's overall microbial quality over time.

Studies on the impact of BC on soil microbial activity need to be better understood, largely because the materials that make up the BC vary and because of how much carbon is present in BC (Song et al., 2020; Amoah-Antwi et al., 2020). In addition, recent studies that evaluated the interference of BC with colorimetric soil enzyme assays (Jindo et al., 2014; Masrahi, 2018., Cardelli et al., 2019; Wojewódzki et al., 2022) have primarily focused on and attributed the interference to BC alone, with no attention to the role of soil contaminants or chemical properties. For example, Cardelli et al. (2019) reported that in two soils differing in texture and cation exchange capacities, potential activities of β-glucosidase, phosphatase, and arylsulphatase did not change with the addition of 2 % BC. However, both soils in their study were collected from the same area. Moreover, in a recent study conducted by Wojewódzki et al. (2022), the response of soil enzymatic activity to BC amendment was highly dependent on the type of BC feedstock and incubation time. Nevertheless, they only used one type of soil (sandy loam) mixed with different types of BC. Therefore, this study aims to test if different soil types, in terms of chemical and physical properties and the presence of contaminants, could play a role or affect BC interference with a

colorimetric assay of β-glucosidase under different BC application rates.

2. MATERIAL AND METHODS

2.1.Soil samples

Soil samples were collected from three locations, representing high chemical and physical properties variations. These locations were as follows: CES: soil from an area adjacent to a cement factory located in Jazan region, Saudi Arabia (16°43'36.3 "N latitude and 43°02'29.7 "E longitude); WWS: soil nearby a wastewater treatment plant's (WWTP) discharge point located in Makkah city, Saudi Arabia (21°15'19.8 "N latitude and 39°42'41.3 "E longitude); PMS: soil near an agricultural farm of Panicum maximum located in Makkah city (21°14'08.4 "N latitude and 39°42'12.4 "E longitude). All soil samples were air-dried and sieved with a 2mm pore-size sieve. The CES and WWS soils represents polluted soils, since the presence of contaminants such as heavy metals (in both soils), pharmaceuticals, and micropollutants such nanoparticles (more likely in the WWS soil) is most likely high (Cabeza et al., 2008; Dong et al., 2015; Rogowska et al., 2020).

2.2.Chemical and physical properties of soils

Soil textures were determined using the hydrometer method (Bouyoucos, 1962). The percentage of soil organic matter (SOM %) was determined using the wet oxidation method (Walkley and Black, 1934). Soil pH and electrical conductivity (EC) were measured with a pH meter using a 1:2.5 soil: water suspension. The chemical and physical properties of all soils are listed in **Table 1**.

2.3. Heavy metal concentrations in contaminated soils

To better evaluate the possible role of soil contaminants in the interference of BC with soil enzyme activity, the concentration of heavy metals in the contaminated soils (CES and WWS) was determined using Inductively Coupled Plasma-Atomic Emission Spectrometry (ICP-AES), according to the standard US-EPA 6010B method (EPA, 1996).

2.4. Biochar

The biochar used in this study was obtained from SoilFixer, AC Innovations Ltd., Newcastle upon Tyne, UK. The BC's physical and chemical properties are listed in **Table 2**, as reported by the manufacturer. The obtained BC particle sizes were in the range of 2-8mm, which was then grounded to pass a two mm sieve before use in the current study.

2.5.Experimental design

Air-dried soil samples were mixed with BC in three replicates using three different rates: zero (0) as control, two (2), and three (3) % (w/w). Soil/soil-BC samples were incubated for 60 days prior to analysis.

2.6. β-glucosidase enzyme assay

Potential soil β-glucosidase activity was measured using a modified assay of Tabatabai (Tabatabai and Bremner, 1969; Tabatabai, 1994) by Margenot et al. (2018) and Daughtridge et al. (2021). Briefly, 1 g of air-dried soil/soil with BC was incubated in a *p*-nitrophenyl-β-D-glucopyranoside substrate (Sigma-Aldrich, USA) along with a modified universal buffer solution at 37°C and pH 6. After one hour, the reaction was stopped with 0.1 M Trizma base, followed by 2 M $CaCl_2$ to flocculate. Supernatants were then transferred into microcentrifuge tubes and centrifuged at 14,000 rpm for 1.45 min. Formation of *p*-nitrophenol was then determined colorimetrically using a microplate spectrophotometer at 410 nm, and expressed as the mean of three replicates in μmol g^{-1} h^{-1}.

2.7. Statistical analysis

Treatment effects were statistically analyzed using analysis of variance

(ANOVA) in SAS software (v 9.4). Differences between treatments were determined using Fisher's least-significant-difference (LSD) test at a *p*-value of <0.05.

3. RESULTS

3.1. Heavy metal concentrations in contaminated soils

In the contaminated soils of our study (CES and WWS), we determined concentrations of 8 heavy metals using ICP-AES (**Table 3**). In the CES soil, chromium and nickel were relatively high (25 and 20 ppm, respectively) compared to WWS soil (16 and 14 ppm, respectively). On the other hand, zinc was relatively high in WWS soil (60 ppm) compared to CES soil (44 ppm). The remaining heavy metals (arsenic, cadmium, cobalt, copper, and lead) showed relatively similar concentrations in both soils.

Table 1. Characteristics of the soils used in this study. PMS: soil near an agricultural farm of *Panicum maximum*. WWS: soil nearby a wastewater treatment discharge point. CES: soil from an area contaminated with cement.

Parameter	PMS soil	WWS soil	CES soil
Clay (%)	24	2	26
Silt (%)	6	0	40
Sand (%)	70	98	34
Soil organic matter (%)	0.6	0.4	0.6
pH	7.5	6.7	7.8
EC (dS/m)	2.7	4	1.1

Table 2. Properties of biochar used in this study.

Property	Specification/Value
Pyrolysis temperature	500 °C
Feedstock material	Mixed hard woods
Total organic matter	92 % total mass
Total carbon	84 % total mass
Total ash	8 % total mass
pH	8.5

Table 3. Heavy metal concentrations in contaminated soils. CES: soil from an area contaminated with cement. WWS: soil nearby a wastewater treatment discharge point.

Heavy metal	CES soil	WWS soil
Arsenic (mg/kg)	<5	<5
Cadmium (mg/kg)	<1	<1
Chromium (mg/kg)	25	16
Cobalt (mg/kg)	9	6
Copper (mg/kg)	18	20
Lead (mg/kg)	5	6
Nickel (mg/kg)	20	14
Zinc (mg/kg)	44	60

3.2. β-glucosidase enzyme activity

Potential soil β-glucosidase enzyme activities as affected by BC amendment rate varied significantly (**Table 4 and Figure 1**) in each soil type. In PMS soil, the activity of β-glucosidase was significantly reduced with the 5 % BC application rate, while no significant difference was found with 2 % BC. For WWS soil, both 2 and 5 % BC rates resulted in a significant reduction of β-glucosidase enzyme activities. However, no significant differences were found in all BC application rates in the case of CES soil. Analysis of variance (ANOVA) revealed that both soil type and BC application rate have significant effects on β-glucosidase enzyme activity (*p*-values <.0001 and 0.03, respectively). In contrast, no interaction effects between BC application rates and soil type were found.

Table 4. Results of analysis of variance (ANOVA).

Source of variation	*df*	Sum of Squares	Mean Square	F Value	Pr > F
Soil type	2	0.75461356	0.37730678	126.03	<.0001
BC application rate	2	0.02430289	0.01215144	4.06	0.0351
Soil type × BC application rate	4	0.00901222	0.00225306	0.75	0.5692

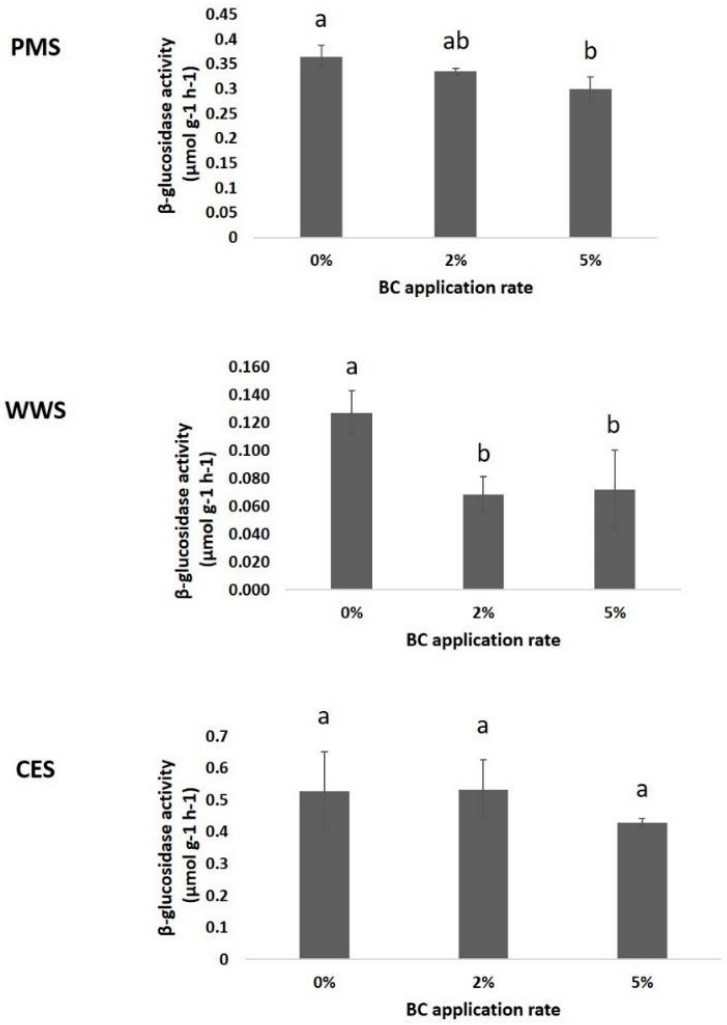

Figure 1. Potential soil β-glucosidase enzyme activities for three different soil types under three different biochar (BC) application rates. PMS: soil near an agricultural farm of Panicum maximum. WWS: soil nearby a wastewater treatment discharge point. CES: soil from an area contaminated with cement. Data are means ± s.d (n=3). Different letters indicate a significant difference ($p < 0.05$).

4. DISCUSSION

The current study showed that BC significantly interferes with the colorimetric assay of soil β-glucosidase activity. However, the level of this interference differed between the different soil types used in this study. Only the 5 % BC application rate for the PMS soil resulted in a significant underestimation of soil β-glucosidase activity, while no interference was found with the 0 and 2 % BC rates. The results of the current study agree with the study by Cardelli et al. (2019), where 2 % BC did not interfere with the colorimetric assay of soil β-glucosidase activity. However, this was not the case with the other two soils in our study. In the WWS soil, both 2 and 5 % BC application rates significantly underestimated the enzyme activity. Soil contaminants may have a role in the interference level of BC with the colorimetric enzyme assays. Biochar has been widely used to remove contaminants

from soil and water, such as heavy metals and organic pollutants, by adsorption on BC surfaces (Zhang et al., 2013). Biochar possesses negatively charged surfaces with hydrophobic properties. Recent research evidence has suggested that the primary mechanism by which BC reduces enzyme activity is through direct sorption of the enzyme into BC (Foster et al., 2018). Therefore, this may cause either a direct alteration to the enzyme active site or rotation of the active site toward the BC surface (Leprince et al., 1996). Therefore, this may explain the underestimation of β-glucosidase activity in PMS and WWS soils.

In the case of CES soil, BC did not significantly affect the potential activity of soil β-glucosidase. One possible explanation is that the higher surface area of CES soil, due to higher silt and clay percentages than the other two soils, resulted in higher cation exchange capacity. Therefore, this may have caused higher cation competition on BC surfaces (Tong et al., 2011), possibly resulting in less sorption of enzyme/substrate into BC surfaces. Fidel et al. (2018) have demonstrated the importance of solution pH and chemical composition in influencing BC's cations and anions sorption capacities. Recently, Guo et al. (2020) reported that BC has a high affinity for hexavalent chromium (Cr^{6+}) adsorption, a form of Cr that is highly found in cement and mining sites (Dhal et al., 2013). Biochar also has been shown to have strong adsorption capacities for other heavy metals such as nickel (Ni^{2+}) (Shen et al., 2017). Another explanation could be related to the fact that adsorption of contaminates such as positively charged heavy metals may reduce the release of substances from BC surfaces, therefore reducing the interference of such substances with color intensity in the solution used for spectrophotometer reading (Cardelli et al., 2019). In this study, chromium and nickel were relatively higher in CES soil than in WWS soil, which may explain their role in minimizing BC interference with the enzyme activity in CES soil. However, it is worth mentioning that there is a lack of research data in the literature regarding the response of soil β-glucosidase activity to increased heavy metals concentrations (Aponte et al., 2020), which raises the need for more research on the influence of such factors on soil enzyme activities.

5. CONCLUSION

In the current study, it seems that the interference of BC with the colorimetric assay of soil β-glucosidase activity varies based on the soil's chemical and physical properties. Consequently, research studies based on colorimetric soil enzyme assays in BC-amended soils should account for the role of soil properties and contaminants to accurately measure the potential activity of the enzymes. However, numerous studies are still needed to fully unravel and fill the gaps concerning the mechanisms in which the above factors interfere with colorimetric enzyme assays in BC-amended soils.

REFERENCES

Alkorta, I., Aizpurua, A., Riga, P., Albizu, I., Amézaga, I., & Garbisu, C. (2003). Soil enzyme activities as biological indicators of soil health. Reviews on environmental health, 18(1), 65-73.

Amini, S., Ghadiri, H., Chen, C., & Marschner, P. (2016). Salt-affected soils, reclamation, carbon dynamics, and biochar: a review. Journal of Soils and Sediments, 16, 939-953.

Amoah-Antwi, C., Kwiatkowska-Malina, J., Thornton, S. F., Fenton, O., Malina, G., & Szara, E. (2020). Restoration of soil quality using biochar and brown coal waste: A review. Science of the Total Environment, 722, 137852.

Aponte, H., Meli, P., Butler, B., Paolini, J., Matus, F., Merino, C., . . . Kuzyakov, Y. (2020). Meta-analysis of heavy metal effects on soil enzyme activities. Science of the Total Environment, 737, 139744.

Atkinson, C. J., Fitzgerald, J. D., & Hipps, N. A. (2010). Potential mechanisms for achieving agricultural benefits from biochar application to temperate soils: a review. Plant and soil, 337, 1-18.

Azargohar, R., & Dalai, A. (2008). Steam and KOH activation of biochar: Experimental and modeling studies. Microporous and Mesoporous Materials, 110(2-3), 413-421.

Cabeza, Y., Candela, L., Ronen, D., & Teijon, G. (2012). Monitoring the occurrence of emerging contaminants in treated wastewater and groundwater between 2008 and 2010. The Baix Llobregat (Barcelona, Spain). Journal of hazardous materials, 239, 32-39.

Cardelli, R., Becagli, M., Marchini, F., & Saviozzi, A. (2019). Biochar impact on the estimation of the colorimetric-based enzymatic assays of soil. Soil Use and Management, 35(3), 478-481.

Dahlawi, S., Naeem, A., Rengel, Z., & Naidu, R. (2018). Biochar application for the remediation of salt-affected soils: Challenges and opportunities. Science of the Total Environment, 625, 320-335.

Daughtridge, R. C., Nakayama, Y., & Margenot, A. J. (2021). Sources of abiotic hydrolysis of chromogenic substrates in soil enzyme assays: Storage, termination, and incubation. Soil Biology and Biochemistry, 158, 108245.

Dong, Z., Bank, M. S., & Spengler, J. D. (2015). Assessing metal exposures in a community near a cement plant in the Northeast US. International Journal of Environmental Research and Public Health, 12(1), 952-969.

Environmental Protection Agency, U. (1996). Method 6010B: Inductively coupled plasma-atomic emission spectrometry. SW-846 test methods for evaluating solid wastes.

Fidel, R. B., Laird, D. A., & Spokas, K. A. (2018). Sorption of ammonium and nitrate to biochars is electrostatic and pH-dependent. Scientific reports, 8(1), 17627.

Foster, E. J., Fogle, E. J., & Cotrufo, M. F. (2018). Sorption to biochar impacts β-glucosidase and phosphatase enzyme activities. Agriculture, 8(10), 158.

Günal, E., Erdem, H., & Demirbaş, A. (2018). Effects of three biochar types on activity of β-glucosidase enzyme in two agricultural soils of different textures. Archives of Agronomy and Soil Science, 64(14), 1963-1974.

Guo, X., Liu, A., Lu, J., Niu, X., Jiang, M., Ma, Y., . . . Li, M. (2020). Adsorption mechanism of hexavalent chromium on biochar: kinetic, thermodynamic, and characterization studies. ACS omega, 5(42), 27323-27331.

Jindo, K., Matsumoto, K., García Izquierdo, C., Sonoki, T., & Sanchez-Monedero, M. (2014). Methodological interference of biochar in the determination of extracellular enzyme activities in

composting samples. Solid Earth, 5(2), 713-719.

Joseph, S., Peacocke, C., Lehmann, J., & Munroe, P. (2009). Developing a biochar classification and test methods. Biochar for environmental management: science and technology, 1, 107-126.

Leprince, F., & Quiquampoix, H. (1996). Extracellular enzyme activity in soil: effect of pH and ionic strength on the interaction with montmorillonite of two acid phosphatases secreted by the ectomycorrhizal fungus Hebeloma cylindrosporum. European Journal of Soil Science, 47(4), 511-522.

Margenot, A. J., Nakayama, Y., & Parikh, S. J. (2018). Methodological recommendations for optimizing assays of enzyme activities in soil samples. Soil Biology and Biochemistry, 125, 350-360.

Masrahi, A. S. J. (2018). Interactions of Arbuscular Mycorrhizal Fungi with Rhizosphere Communities in Saline Soils.

Rogowska, J., Cieszynska-Semenowicz, M., Ratajczyk, W., & Wolska, L. (2020). Micropollutants in treated wastewater. Ambio, 49, 487-503.

Shen, Z., Zhang, Y., McMillan, O., Jin, F., & Al-Tabbaa, A. (2017). Characteristics and mechanisms of nickel adsorption on biochars produced from wheat straw pellets and rice husk. Environmental Science and Pollution Research, 24, 12809-12819.

Song, X., Razavi, B. S., Ludwig, B., Zamanian, K., Zang, H., Kuzyakov, Y., . . . Gunina, A. (2020). Combined biochar and nitrogen application stimulates enzyme activity and root plasticity. Science of the Total Environment, 735, 139393.

Tabatabai, M. (1994). Soil enzymes. Methods of soil analysis: Part 2 Microbiological and biochemical properties, 5, 775-833.

Tabatabai, M. A., & Bremner, J. M. (1969). Use of p-nitrophenyl phosphate for assay of soil phosphatase activity. Soil Biology and Biochemistry, 1(4), 301-307.

Tong, X.-j., Li, J.-y., Yuan, J.-h., & Xu, R.-k. (2011). Adsorption of Cu (II) by biochars generated from three crop straws. Chemical Engineering Journal, 172(2-3), 828-834.

Wojewódzki, P., Lemanowicz, J., Debska, B., & Haddad, S. A. (2022). Soil enzyme activity response under the amendment of different types of biochar. Agronomy, 12(3), 569.

Yao, Y., Gao, B., Inyang, M., Zimmerman, A. R., Cao, X., Pullammanappallil, P., & Yang, L. (2011). Biochar derived from anaerobically digested sugar beet tailings: characterization and phosphate removal potential. Bioresource technology, 102(10), 6273-6278.

Zhang, X., Wang, H., He, L., Lu, K., Sarmah, A., Li, J., . . . Huang, H. (2013). Using biochar for remediation of soils contaminated with heavy metals and organic pollutants. Environmental Science and Pollution Research, 20, 8472-8483.

الدور الهام الذي قد تلعبه خصائص التربة وملوثاتها في مستوى تداخل الفحم الحيوي مع تقدير نشاط إنزيم β-glucosidase في التربة باستخدام جهاز قياس الطيف الضوئي

عبدالرحمن سليمان مسرحي

قسم الأحياء، كلية العلوم، جامعة جازان

الملخص

الفحم الحيوي لاقى الكثير من الاهتمام مؤخرًا فيما يخص استخدامه كمحسّن وداعم للتربة. قياس أنشطة إنزيمات التربة المضاف إليها الفحم الحيوي أظهر حديثاً أن هناك تداخل وتعارض بين طريقة قياس أنشطة الأنزيمات المعتمدة على جهاز قياس الطيف الضوئي وبين جزيئات الفحم الحيوي. هذه التداخلات غالباً ما تعزى لوجود حبيبات الفحم الحيوي فقط، دون مراعاة خصائص التربة ووجود الملوثات. الهدف من هذه الدراسة هو تقييم تأثيرات أنواع التربة المختلفة في الخواص الكيميائية والفيزيائية ووجود الملوثات في مستوى التعارض مع قياس نشاط إنزيم β-glucosidase في وجود حبيبات الفحم الحيوي بنسب متفاوتة: ٠، ٢، و5 %. تم جمع ثلاثة أنواع مختلفة من التربة من مواقع مختلفة: تربة بالقرب من مصنع إسمنت (CES)، تربة بالقرب من محطة معالجة مياه صرف صحي (WWS)، وتربة قريبة من مزرعة (PMS). المعادن الثقيلة في الترب الملوثة (CES و WWS) تم تحديد تراكيزها باستخدام ICP-AES. أظهرت النتائج أن تركيز ٢ و٥ % من الفحم الحيوي قللت بشكل كبير ($p < 0.05$) من تقدير نشاط إنزيم β-glucosidase في تربة WWS. في المقابل، فقط تركيز ٥ % قلل بشكل كبير من تقدير نشاط الإنزيم في تربة. لم يتم ملاحظة تداخل بين الفحم الحيوي ونشاط إنزيم β-glucosidase في تربة CES. بشكل عام ، أوضحت النتائج أنه اعتمادًا على الخصائص الكيميائية والفيزيائية للتربة، يمكن أن يتداخل الفحم الحيوي بشكل مختلف مع تقديرات نشاط إنزيم β-glucosidase المعتمدة على جهاز قياس الطيف الضوئي. أيضًا، قد يكون لوجود المعادن الثقيلة دور في هذا التداخل. بناء على ذلك، هناك حاجة إلى مزيد من الأبحاث لفهم دور خصائص التربة والملوثات في مثل هذا التداخل بشكل كامل.

الكلمات المفتاحية: الفحم الحيوي - إنزيم β-glucosidase – خصائص وملوثات التربة – المعادن الثقيلة - قياس أنشطة الأنزيمات المعتمدة على جهاز قياس الطيف الضوئي.

Basket study 2: Monitoring of Arsenic Contamination in Culturally Relevant Crops in Jazan Region, KSA.

Tawfiq H. Alfaifi
Biology Department, Faculty of Science, Jazan University, Saudi Arabia.
Contact information: Biology Department, Faculty of Science, Jazan University, the Kingdom of Saudi Arabia

Abstract

The main objective of this study is to assess the levels of arsenic contamination in locally farmed products, fruits and vegetables of the Jazan region in the south of the Saudi Kingdom. This paper begins with a comprehensive review of arsenic assimilation by fruits and vegetables worldwide as a baseline for our study. Then, The collections of local fruits and vegetables from local markets were imported to the lab and prepared for analysis: tomato (*Solanum Lycopersicum*), pepper (*Capsicum annuum*), eggplant (*Solanum melongena*), watermelon (*Citrullus lanatus*), cucumber (*Cucumis sativus*), Christ's thorn jujube (*Ziziphus spina-christi*), banana (*Musa balbisana*), papaya (*Carica papaya*), fig (*Ficus carica*), mango (*Mangifera indica*), carrot (*Daucus carota*), okra (*Hibiscus esculentus*), Manila tamari (*Pithecellobium dulce*), and guava (*Psidium guajava*). The analysis of arsenic was conducted using inductively coupled plasma atomic emission spectroscopy (ICP-AES). The results showed that all the products offered on the streets and brought to farmer's markets have low levels of arsenic contamination in edible parts. The comparison of the results in this study to those of Codex Alimentarius (CA) maximum levels (ML) of arsenic in commodities allowed for human consumption shows that they are less than that of CA. The study concluded that 1) relevant crops in the region produced in local farms and introduced to the local markets are safe in relevant to arsenic contamination, and 2) farms and irrigation water of the Jazan region are not an arsenic threatening to human health.

Keywords: Arsenic, Contamination, Pollution, Cancer, Soils, Fruits, Vegetables

Introduction

Human health has been a concerning issue since many threats surround it. One of these threats is severe pollution from heavy metals to the environment and food. One of the most toxic elements that creates human health issues is arsenic. Arsenic can be found in more than 200 minerals, such as elemental arsenic, arsenite, arsenate, sulfides, oxides, igneous rocks, and sedimentary rocks (Garelick et al., 2009). Contamination by arsenic in the environment occurs mainly by natural interactions of environmental elements or is triggered by the hands of humans from its storage locations. Weathering and erosion of arsenic-containing rocks, emissions of volcanoes, and biological activities are natural sources of arsenic and anthropogenic activities worldwide, such as mining activities and wood preservative facilities (Wang and Mulligan, 2006; Villaescusa and Bollinger, 2008; Vladimir et al., 2020; Lee et al., 2021).

Arsenic may move to different environments in different ways. One is the air movement from the source to the sink (Duan and Tan, 2013). In addition, arsenic might take water trajectories to move from one point to another in soils (Anwar et al., 2002**).** Furthermore, arsenic can accumulate and be dispersed by animals such as moths (Andrahennadi, and Pickering, 2008; Mogren and Trumble, 2010). Thus, contamination by arsenic might not be expected and avoided.

When arsenic is freed from its source, it enters the food chain through plants moving to the top of the food pyramid as other elemental toxicants do (Pullyottum et al., 2020; Pogányová et al., 2020). There is plenty of research that confirms the absorption of arsenic by plants. Grasses on which cattle graze are a source of arsenic when they grow on contaminated sites (Belozubova and Zubkova, 2021). Trees were also found to take up arsenic in different plant organs in the vicinity of elements contamination sites, the maritime pine tree for example (Favas et al., 2013). Aquatic plants, moreover, are exposed to arsenic contamination (Ma et al., 2018). Thus, arsenic contamination is considered a serious threat to plants, animals, and, eventually, humans.

The WHO threshold for arsenic in drinking water is 10 μg/L, and critical health issues appear when it exceeds that level, such as skin lesions as early signs of arsenic contamination (Bardach et al., 2015). Human exposure to arsenic has been studied and found to be associated with many diseases. During a 39.5-year exposure to As in drinking water, arsenic was found to be associated with lung cancer, myocardial infarction, and peripheral arterial disease (D'Ippoliti et al., 2015). The chance of having blood pressure and circulatory problems increases as the exposure to arsenic loaded in drinking water increases (Zierold et al., 2004). Eventually, mortalities have been noticed to increase as the concentration of arsenic increases in water (Argos et al., 2010)

Several studies have investigated fruit and vegetable contamination levels by arsenic in food when they grow on contaminated sites. A study by (de las

Torres et al., 2020) found that strawberry fruits absorb arsenic in their organs from roots to fruits (0.22–0.30 mg/ kg), indicating that strawberries might be a source of human health hazards. Other studies on mango fruits (*Mangifera indica* L.) found that the arsenic in the fruits might reach 50 µg/ kg (Liao et al., 2014). Pepper (*Capsicum annum* L.) was studied and found that the second most arsenic-concentrated organs, after roots, were the fruits, 0.059 and 0.082 (fruits) and 7.8 and 10.0 (roots) mg/ kg (Száková et al., 2007), with values of 111 mg/ kg in other studies (Salas-Muñoz et al., 2022). In tomatoes (*Lycopersicon esculentum*), arsenic in the organic forms of methylarsonic and dimethylarsinic acids added to soils resulted in higher As- assimilation in the fruits than when it is in inorganic forms, which means tomato fruits take up As whatsoever (Tlustoš et al., 2006). In addition, garlic (*Allium sativum* L.) was found with As- values of 100 mg/ kg (Salas-Muñoz et al., 2022). Leafy vegetables are much worse at arsenic intake, such as radishes, arum leaves, gourd leaves, red amaranthus, and spinach, with As- values ranging from 41–464 ug/ kg (Rahman et al., 2013). Thus, fruits and vegetables must be under control and closely supervised for their high capacity for pollutant absorption and storage.

This study is conducted in the Jazan region, south of Saudi Arabia. This study aims to measure the levels of arsenic contamination in fruits and vegetables brought to the market by local farmers immediately from local farms. By studying these crops, we should know whether there is an arsenic contamination in the region or no, and the presence of a human health risk as a result. By studying the contamination of arsenic in food, we would know what plans and actions should be taken if there is a contamination risk.

Methodology

Fruits and vegetable market

The Jazan region is where various fruits and vegetables have been farmed and cultivated either for self-consumption or to offer to the market, Image 1. The market could be a center store such as supermarkets or small stalls on the streets. They sell a variety of fruits and vegetables, such as mango fruits, dates, papaya, watermelon, zucchini, carrots, cucumber, tomato, okra, lettuce, spinach, radish, fig, eggplant, pepper, and mint. Farmers bring seasonal fresh fruits daily, usually to where people can buy them.

Image 1. The location of Jazan Province in Saudi Arabia (Google Mapping)

Sampling

Along a road approximately 60 km from the center of Jazan city to a rural area in the same region, fruits and vegetables were bought from sellers offering their crops on the street ,Table (1). To avoid any bias, fruits and vegetables were bought as if they were for home consumption. The fruits and vegetables were not taken from one seller or point; we brought the goods from different sellers alongside the road. We asked the seller to give us one kilogram of the product. The product could be brought from more than one seller. Then, samples were immediately taken to the lab for preparation.

Table 1. Shows the fruits and vegetables collected from the market. The scientific names are taken from https://usdasearch.usda.gov/

Number of sample	**Scientific Name**	**Common Name**
1	*Solanum lycopersicum* L.	Tomato
2	*Capsicum annuum* L.	Pepper
3	*Solanum melongena* L.	Eggplant
4	*Citrullus* spp.	Watermelon
5	*Cucumis sativus* L.	Cucumber
6	*Ziziphus spina-christi* (L.)	Christ's thorn jujube
7	*Musa balbisana* Colla	Banana
8	*Carica papaya* L.	Papaya
9	*Ficus carica* L.	Fig
10	*Mangifera indica* L.	Mango
11	*Daucus carota* L.	Carrot
12	*Hibiscus esculentus* L.	Okra
13	*Pithecellobium dulce* L.	Manila tamari
14	*Psidium guajava* L.	Guava

Preparing samples in the lab

Fruits and vegetables were taken to the lab of the science college at Jazan University. The edible parts were washed with tap water to mimic people's practices with these products. Then, they were dried in an oven at 80 C° until we obtained a steady weight. Subsamples which are three samples of each product, regardless the point where it was bought, were chosen randomly from each whole product to prepare each sample as a replicate for acid digestion later and for the calculation of the average value of detected arsenic.

Digestion and analysis

The subsamples prepared above were processed by the dry-ash method. The dried subsamples were then powdered manually using a clean grinder. The grinder was swiped after each sample with alcoholic wipes to avoid cross-contamination of the samples.

Fourteen grams (per each subsample) were placed in a silica crucible, and a few drops of concentrated nitric acid were added. The dry-ash process was administered in a muffle furnace by a stepwise increase in the temperature up to $550C^{\circ}$, and the subsamples were left to ash at this temperature for 6 hours.

After that, one to two grams of the powder was digested in HCl (7.5 ml conc) and HNO_3 (2.5 ml conc.), 75 % HCL TO 25% HNO_3. Then, the samples were filtered using Whatman, Ashless, Diameter 125 mm, and extra HCL (5 ml) and reagent water (20 ml) were added to the samples to wash the filters. Then, digested samples were sent for analysis using inductively coupled plasma-atomic emission spectroscopy ICP-AES within the Center for Environmental Research and Studies at Jazan University.

Blank samples were made of nitric acid, hydrochloric acid, and deionized water with the same concentrations above. The spectrometer software then automatically subtracts the blank from the concentrations detected in the samples. A standard for arsenic used (catalog No. 01969-100ML-F, SIGMA ALDRICH). **US EPA 3050B, Acid Digestion of Sediments, Sludge, and Soils 1996**.

Results and Discussion

Table (2) shows the results of arsenic levels in the samples from high to low. They are set from the highest to the lowest: Papaya (0.05) >> Pepper (0.019) >>Manila tamari (0.017) >> Cucumber (0.015) >>Banana (0.014) >>Eggplant (0.013) >>Christ's thorn jujube and Okra (0.012) >>Carrot (0.011) >>Fig and Guava (0.01) >>Mango (0.006) >>Tomato (0.002), Figure 1.

Table 2. Fruit and vegetable concentrations of arsenic in ppm

Number of the sample	Common Name	results of As in ppm/ dry weight	St. dev.
1	Tomato	0.002	0.001
2	Pepper	0.019	0.002
3	Eggplant	0.013	0.000
4	Watermelon	0.008	0.001
5	Cucumber	0.015	0.006
6	Christ's thorn jujube	0.012	0.003
7	Banana	0.014	0.003
8	Papaya	0.050	0.005
9	Fig	0.010	0.002
10	Mango	0.006	0.004
11	Carrot	0.011	0.001
12	Okra	0.012	0.005
13	Manila tamari	0.017	0.008
14	Guava	0.010	0.004

Figure 1. concentrations of arsenic in vegetables and fruits

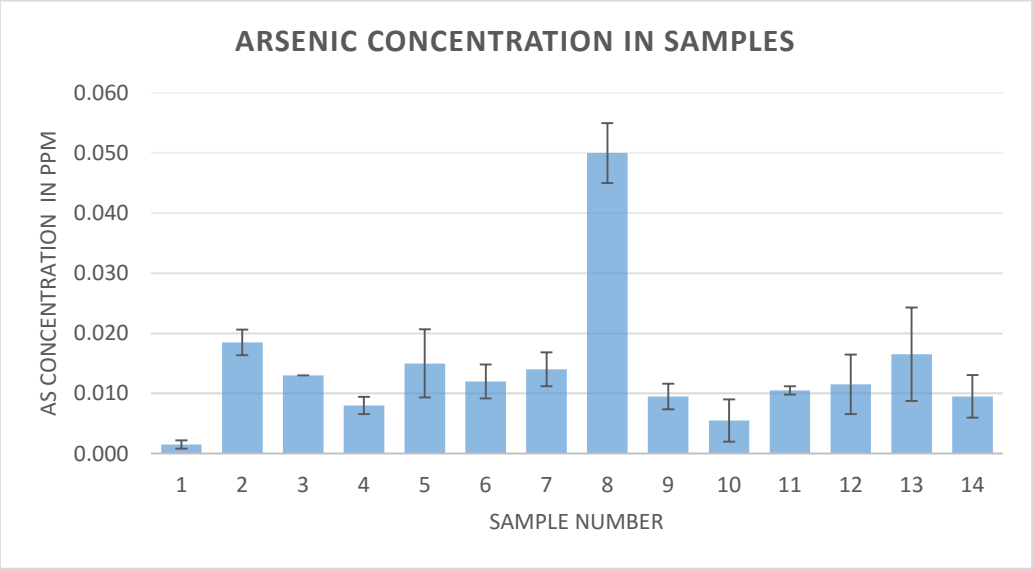

** Each number on the ***X***-axis is related to its sample from Tables 1 and two (Excel program)

Plants, unfortunately, cannot avoid arsenic absorption in the environment during their growth since it is from the natural components of soils and rocks (Li et al., 2019). Thus, our plants in this study showed levels of arsenic in the tissues.

One of many indications that might clue on the contamination of soils with arsenic is the concentration of arsenic in plant tissues. As the concentrations of arsenic increase in soils, the concentrations of it increases in plants tissues (Roychowdhury et al., 2002; Ramirez-Andreotta et al., 2013). Therefore, these results obtained from our market scanning project might indicate that the soils where these crops grown in are at low levels of arsenic to the extent that it can be neglected when compared with other assessment studies on crops grown in As- contaminated soils .

In previous study by Alfaifi (2022), some areas in the region might be polluted with arsenic since they are near manufacturing activities. Almost, our plants in this project showed low levels of arsenic in the edible parts, ranging from 0.002 to 0.05 ppm. Low levels of arsenic contamination in the plants tissiues means that the agricultural activities practiced in areas that are far from pollution centers.

These families in our study had been witnessed accumulating arsenic in their tissues when grown in soils contaminated with arsenic as it is mentioned in the introduction. As a result, if there were a chance of increasing arsenic concentrations in soils, at least one family would show an increasing arsenic sign in plant tissues.

As illustrated above, arsenic might travel to soils and farms taking water trajectories. One way of arsenic movement is through the irrigation of crops using well waters. Al-Farraj et al. (2013) found that groundwater in some Saudi regions are loaded with unacceptable levels of arsenic, which might create arsenic pollution to plants and then to human. However, Jazan region might not be contaminated with arsenic in its groundwater since our plant tissues showed no sign of As contamination.

Codex Alimentarius Comparison

Codex Alimentarius (CA) is a guideline and standards collections related to food and contaminants in food recommended by the Codex Alimentarius Commission (CAC). Food codes are recommended to apply to food and feed. It reveals plants samples that are internationally traded and the allowed maximum levels of toxicants in the tissues of those plants. We should compare our results with CAC maximum levels (ML) allowed for a commodity. Unfortunately, their survey does not consider the specific commodities in our study. However, the comparison would be fulfilled with the CA products' maximum level of arsenic in some other commodities provided on the website. The maximum number of ML was 0.5 mg/kg in salt and food grade, while the lowest value was 0.01 mg/kg in fat spreads and blended spreads. None of our results meets the maximum level of 0.5, Table 2.

Health Risk Assessment

Antoine et al. (2017) argued that low levels of arsenic, for example, in carrots, bananas, and tomatoes with values of 0.004, 0.104, and 0.012 mg/kg fresh weight, respectively, would not threaten consumers' health. In our study, value of arsenic in an approximately: 1) a 30-gram carrot would be 0.005 µg/g fresh weight, 2) an 85-gram banana would be 0.002, and in 3) a 30-gram tomato would be 0.0003 µg/g fresh weight. Our values are much lower than being associated with As- human health issues.

Conclusion

The analysis of a variety of culturally relevant crops may indicate the status of the environmental conditions regarding contamination with arsenic. The assessment of arsenic levels in this project indicates that each of water resources used for irrigation and farming soils are almost safe from being contaminated with arsenic. Chosen crops in this study are related to several families with several physiological behaviors, and most of those families had proven their accumulation of arsenic in other studies when they are exposed to As-contaminations; However, no As-contamination noticed in this study.

Based on these results, no contamination by arsenic is traced in the region, and the detected low values might be naturally occurring. In addition, this study might elect Jazan as one of the ideal regions in Saudi Arabia to produce crops and offer them in the market. With more civil advances, more restrictions should be imposed to not allow for As-contamination to occur. More studies should be suggested on crops and arsenic contamination monitoring yearly to prevent arsenic contamination and make an early alarm if needed.

Acknowledgments

The authors would like to thank Prof. Dr. Zarraq AL-Faifi, Head of the Center for Environmental Research and Studies, Faculty of Science, Jazan University, for his cooperation and all staff members in the center for analyzing the samples for this study.

References

Alfaifi, T. (2022). Evaluation and Assessment of Metal (loids) Adsorptions by Cenchrus ciliaris L. in a Cement Contaminated Area. *BioResources*, 17(3), 4360-4377.

Al-Farraj, A. S., Al-Wabel, M. I., El-Saeid, M. H., El-Naggar, A. H., and Ahmed, Z. (2013). Evaluation of groundwater for arsenic contamination using hydrogeochemical properties and multivariate statistical methods in Saudi Arabia. *Journal of Chemistry*, 2013.

Anawar, H. M., Akai, J., Mostofa, K. M. G., Safiullah, S., and Tareq, S. M. (2002). Arsenic poisoning in groundwater: health risk and geochemical sources in Bangladesh. *Environment International*, 27(7), 597-604.

Andrahennadi, R., and Pickering, I. J. (2008). Arsenic accumulation, biotransformation and localisation in

bertha armyworm moths. *Environmental Chemistry*, 5(6), 413-419.

Antoine, J. M., Fung, L. A. H., and Grant, C. N. (2017). Assessment of the potential health risks associated with the aluminum, arsenic, cadmium and lead content in selected fruits and vegetables grown in Jamaica. *Toxicology reports*, 4, 181-187.

Argos M, Kalra T, Rathouz PJ, Chen Y, Pierce B, Parvez F, Islam T, Ahmed A, Rakibuz-Zaman M, Hasan R, Sarwar G, Slavkovich V, van Geen A, Graziano J, and Ahsan H. (2010). Arsenic exposure from drinking water, and all-cause and chronic-disease mortalities in Bangladesh (HEALS): a prospective cohort study. *The Lancet*, *376*(9737), 252-258.

Bardach E. A, Ciapponi A,Soto N, Chaparro R. M, Calderon M, Briatore A, Cadoppi N, Tassara R, and Litter I. M. (2015). Epidemiology of chronic disease related to arsenic in Argentina: A systematic review. *Science of the Total Environment*, 538, 802-816.

Belozubova, N. Y., and Zubkova, V. M. (2021). Biogeochemical Activity of Pasture Plant Species in the Absorption of Lead, Cadmium, and Arsenic under the Conditions of the Volgograd Region. *Arid Ecosystems*, 11(3), 287-292.

"Codex Alimentarius International Foods Standards." *Fao.org*, FAO of the UN, 2017, www.fao.org/fao-who-codexalimentarius/sh-proxy/en/?lnk. [Accessed 14 Jan 2023].

D'Ippoliti, D., Santelli, E., De Sario, M., Scortichini, M., Davoli, M., and Michelozzi, P. (2015). Arsenic in drinking water and mortality for cancer and chronic diseases in Central Italy, 1990-2010. *PLoS One*, 10(9), e0138182.

de Las Torres, A. I. G., Giráldez, I., Martínez, F., Palencia, P., Corns, W. T., and Sánchez-Rodas, D. (2020). Arsenic accumulation and speciation in strawberry plants exposed to inorganic arsenic enriched irrigation. *Food chemistry*, 315, 126215.

Duan, J., and Tan, J. (2013). Atmospheric heavy metals and arsenic in China: situation, sources and control policies. *Atmospheric Environment*, 74, 93-101.

Favas, P. J. C., Pratas, J., and Prasad, M. N. V. (2013). Temporal variation in the arsenic and metal accumulation in the maritime pine tree grown on contaminated soils. *International Journal of Environmental Science and Technology*, 10(4), 809-826.

Garelick, H., Jones, H., Dybowska, A., and Valsami-Jones, E. (2009). Arsenic pollution sources. *Reviews of Environmental Contamination Volume* 197, 17-60.

Lee, Y. S., Kim, M. S., Wee, J., Min, H. G., Kim, J. G., and Cho, K. (2021). Effect of bioavailable arsenic fractions on the collembolan community in an old abandoned mine waste. *Environmental geochemistry and health*, 43(10), 3953-3966.

Li, J., Zhao, Q., Xue, B., Wu, H., Song, G., and Zhang, X. (2019). Arsenic and nutrient absorption characteristics and antioxidant response in different leaves of two ryegrass (Lolium perenne) species under arsenic stress. *PLoS One*, 14(11), e0225373.

Liao, X., Fu, Y., He, Y., and Yang, Y. (2014). Occurrence of arsenic in fruit of mango plant (Mangifera indica L.) and its relationship to soil properties. *Catena*, 113, 213-218.

Ma, Z., Lin, L., Wu, M., Yu, H., Shang, T., Zhang, T., and Zhao, M. (2018). Total and inorganic arsenic contents in seaweeds: Absorption, accumulation, transformation and toxicity. *Aquaculture*, 497, 49-55.

Mogren, C. L., and Trumble, J. T. (2010). The impacts of metals and metalloids on insect behavior. *Entomologia Experimentalis et Applicata*, 135(1), 1-17.

Pogányová, A., Janiga, M., and Solár, J. (2020). Heavy metals compounds from tailing pond sludge and their distribution to the tissues of the selected common Poaceae species and crop plants. *Oecologia Montana*, 29(2), 71-78.

Pullyottum Kavil, S., Ghosh, D., Pašić, I., and Routh, J. (2020). Temporal dynamics of arsenic uptake and distribution: food and water risks in the Bengal basin. *Toxicological & Environmental Chemistry*, 102(1-4), 62-77.

Rahman, M. M., Asaduzzaman, M., and Naidu, R. (2013). Consumption of arsenic and other elements from vegetables and drinking water from an arsenic-contaminated area of Bangladesh. *Journal of hazardous materials*, 262, 1056-1063.

Ramirez-Andreotta, M. D., Brusseau, M. L., Artiola, J. F., and Maier, R. M. (2013). A greenhouse and field-based study to determine the accumulation of arsenic in common homegrown vegetables grown in mining-affected soils. *Science of the Total Environment*, 443, 299-306.

Roychowdhury, T., Uchino, T., Tokunaga, H., and Ando, M. (2002). Survey of arsenic in food composites from an arsenic-affected area of West Bengal, India. *Food and Chemical Toxicology*, 40(11), 1611-1621.

Salas-Muñoz, S., Valdez-Valdez, E., Mauricio-Castillo, J. A., Salazar-Badillo, F. B., Vega-Carrillo, H. R., and Salas-Luevano, M. A. (2022). Accumulation of As and Pb in vegetables grown in agricultural soils

polluted by historical mining in Zacatecas, Mexico. *Environmental Earth Sciences*, 81(14), 1-12.

Száková, J., Tlustoš, P., Goessler, W., Pavlíková, D., and Schmeisser, E. (2007). Response of pepper plants (Capsicum annum L.) on soil amendment by inorganic and organic compounds of arsenic. *Archives of environmental contamination and toxicology*, 52(1), 38-46.

Tlustoš, P., Száková, J., Pavlíková, D., and Balík, J. (2006). The response of tomato (Lycopersicon esculentum) to different concentrations of inorganic and organic compounds of arsenic. *Biologia*, 61(1), 91-96.

Villaescusa, I., and Bollinger, J. C. (2008). Arsenic in drinking water: sources, occurrence and health effects (a review). *Reviews in Environmental Science and Bio/Technology*, 7(4), 307-323.

Vladimír, F., Moreno-Jimenez, E., Bucheli, T. D., Jana, F., Gerhard, S., and Schmidt, H. P. (2020). Engineered Pyrogenic Materials as Tools to Affect Arsenic Mobility in Old Mine Site Soil of Mediterranean Region. *Bulletin of Environmental Contamination and Toxicology*, 104(2), 265-272.

Wang, S., and Mulligan, C. N. (2006). Occurrence of arsenic contamination in Canada: sources, behavior and distribution. *Science of the total Environment*, 366(2-3), 701-721.

Zierold, K. M., Knobeloch, L., and Anderson, H. (2004). Prevalence of chronic diseases in adults exposed to arsenic-contaminated drinking water. *American journal of public health*, 94(11), 1936-1937.

دراسة السلة الغذائية ٢: رصد التلوث بالزرنيخ في بعض أنواع المحاصيل الشعبية في منطقة جازان، المملكة العربية السعودية

توفيق بن هادي الفيفي

قسم الأحياء ، كلية العلوم ، جامعة جازان ، المملكة العربية السعودية

الهدف الأساسي من هذه الدراسة هو تقييم مقدار التلوث بالزرنيخ في المحاصيل الزراعية المحلية، فواكه وخضار منطقة جازان، المملكة العربية السعودية. هذه الورقة تبدأ بمراجعة تلوث الفواكه والخضار بالزرنيخ عالميا لتكون قاعدة لهذه الدراسة. بعد ذلك، بدأ تجميع العينات المحلية ثم ارسالها الى المختبر لتحضيرها وتحليلها: الطماطم ، الفلفل و الباذنجان، البطيخ الصيفي، والخيار، النبق، الموز، التين، المانجو، الجزر، البامية، اللوز الهندي و الجوافة. تحليل الزرنيخ في الانسجة كان بواسطة جهاز Inductively Coupled Plasma Atomic Emission Spectroscopy (ICP-AES)

نتائج التحليل أظهرت ان كل هذه المنتجات المعروضة للبيع على الشوارع والمنتجة محليا بها كميات قليلة جدا من الزرنيخ غير ضارة في اجزائها المستخدمة للغذاء. من خلال المقارنة بين نتائج هذه الدراسة و

Codex Alimentarius (CA)

وجدنا ان مستويات الزرنيخ في هذه الدراسة اقل من تلك المسموح بها. هذه الدراسة انتهت بثلاث نقاط هي :١) هذه المنتجات المحلية أمنة من حيث استخدامها كغذاء للإنسان من حيث قلة مستويات الزرنيخ فيها. ٢) عمليات الزراعة في منطقة جازان بما فيها مياه الري ليست مصدر تهديد للإنسان بالتلوث بالزرنيخ.

الكلمات المفتاحية: الزرنيخ، التلوث ، مرض السرطان، التربة، الفواكه، الخضروات.

Recent Developments in use of Modified Organic Materials as Sodium-Ion Battery Electrodes

Ahmed A. Alzharani

Department of Chemistry, Faculty of Science, Al Baha University, Albaha, Saudi Arabia

Abstract

Sodium is the most well-known, affordable, and plentiful metal ion source. Sodium-ion batteries have advanced rapidly in the later years. Organic polymers & the carbon materials they are derived from are essential for green and sustainable development when used as the positive and anode of sodium-ion batteries because they are abundant in resources, have a little environmental impact, and have manageable structural designs. Because of their inherent flexibility, organic polymers are also very useful in flexible sodium-ion batteries. In relation to sodium-ion batteries, the evolution of flexible organic polymer materials and flexible carbon materials derived from flexible polymer materials is discussed. Various processing methods and precursors for polymer-based carbon compounds were applied. Flexible renewable polymer materials are expected to evolve in the future. For devices used for the storage of electrochemical energy, sodium is a widely available metal that makes an excellent substitute. The main impediment to the enhancement of sodium- ion batteries having enough life span is an absence of adequate electrode substances for sodium ion reversible redox reactions. Redox-active polymers offer the right set of circumstances for the enhancement of novel electrode substances for sodium ion batteries due to their flexibility in structure, the functionality of their tenable surface, as well as their affordability. This overview summarizes current developments in polymeric azo-compound materials for use in sodium-ion batteries. Several issues with polymer electrode materials and processes will be addressed so that an electrochemical show of polymer materials used as Na^+ battery electrodes may be enhanced. The current review concentrates on the most up -to - date developments in the sodium-ion battery.

Keywords: Sodium-Ion Batteries; Advanced materials; Electrode materials; Sustainable development; Organic polymers; Azo-COFs; Azo-MOFs.

Introduction

Authorities in various research fields are enforcing environmentally friendly building practices to keep the environment safe, clean, and cost- and energy-efficient. Significant advances in the energy storage field prompted the use and development of sodium-ion batteries, which are inexpensive and widely available. It is obvious that burning fossil fuels produces significant CO_2 emissions as the world's energy demand rises rapidly [1]. It was predicted that it would have several significant effects on our ecosystem, including desertification and global warming [2-4]. Major research projects are now focusing on utilizing and exploiting renewable energy sources in response to growing concerns about excessive energy consumption and environmental damage. However, the cost of producing cleaner, more sustainable energy from resources such as solar, wind, and geothermal resources has steadily declined since the turn of the century. As a result, developing high-efficiency energy storage (EES) and conversion technology is one of the best ways to tackle the challenges [2-4]. It is critical to develop large-scale, ecologically friendly electrical energy storage devices for stationary applications in order to successfully accumulate and use these energy resources [5]. A variety of technologies, including compressed-air energy storage, pumped-hydroelectric storage, batteries, and capacitors, have been assessed as grid-scale solutions for ESSs [6]. Pumped-hydroelectric storage currently stores approximately 98% of the energy consumed globally [4-7]. However, sustainable energy generation is frequently irregular and constrained by geological factors. This is for its high-energy density, low cost, ability to achieve its aim with little waste, and the extended number of charge/discharge cycles it is capable of, contemporary large-scale energy production facilities recommend storing energy electrochemically [7, 8]. Because of their high operating voltage, long cycle durations, little maintenance requirements, and high energy density, secondary batteries are viewed by some as the most promising EES technology [5-9].

Since the early 1990s, when Li-ion batteries (LIBs) became popular in moveable electronics, fabrication techniques and LIB performance have advanced to the point where they can now be used as the primary source of power. Advanced electronics, hybrid electric vehicles (HEVs), and pure electric cars are examples of mid-size applications where LIB technology has advanced quickly and reached the market (EVs). There has also been an increase in the number of grid-scale LIB prototypes linked to sources of

renewable energy like wind or solar power [4-10]. However, a number of significant barriers to LIB adoption exist, including the cost of processing fabrication and raw materials for grid-scale ESSs [11]. Because of their low cost, easy access to abundant sodium supplies, and high energy density, Na^+ batteries (SIBs) have emerged as the energy-storing technology with the most potential [8-10]. LIBs and SIBs have similar chemistry, so they can both be refilled, and sodium ions can be used as charge carriers. Because LIBs and SIBs can be made using the same technology, the fabrication processes for SIB production lines are less complex [3-12]. Furthermore, SIBs and LIBs have a similar work principle with regard to energy density and reaction kinetics. SIBs are less electroactive than Li because they have a higher redox potential and a larger ionic radius, as shown in table 1. Sodium storage materials have significantly lower energy densities as anode materials than LIBs [5, 13].

Table 1. Comparison between sodium and lithium

Properties	Sodium	Lithium
Atomic Weight (g mol^{-1})	22.989769	6.941
Cation Size (Radius, Å)	1.06	0.76
Melting Point (^oC)	97.7	180.5
E°(V) (vs. SHE)	-2.7	-3.05
Capacity (mAh g-1)	1165	3829
Costs ($ ton^{-1})	150	5000

SIBs were ignored for decades because of their lower energy density & the lack of suitable cathode/anode material [8-10]. Organic materials, which can be produced from biomass resources, have advantages over inorganic materials in that they contain natural elements that are abundant in C, H, O, N, and S [10-12]. Organic materials, due to their adaptability, can have their molecular structure and functional groups modified in a way that enhances their electrochemical properties for use in sodium-ion batteries [2, 11]. Despite these disadvantages, organic electrode materials have a number of flaws, including small organic molecules that dissolve in non-protonic electrolytes and significantly lower capacity [8]. As a result, making electrode materials from polymers makes sense. Polymers can be made into flexible free-standing components for SIBs as cathodes owing to

their inherent flexibility [3]. Hard carbon (HC) has a great changeable capacity in around 300 mAh g^{-1} & demonstrated effective electrochemical insertion of sodium comparable to graphite's 372 mAh g^{-1} lithium storage capacity [14,15]. In the meantime, SIBs claim that they will eventually affordably replace LIBs. Because of their abundant Na resource base, simplicity of exploitation, and affordability, SIBs have recently been the focus of extensive research [16-23]. It is a good competitor for large-scale energy storage; additionally, sodium's half-cell potential is around $3x10^{-1}$ volt over of the half-cell potential of lithium.[2] Unlike LIBs, SIBs do not have over-discharge characteristics, allowing them to discharge to zero volts while maximizing energy density. The lower operating voltage of SIBs as contrasted with LIBs is what makes this possible, allowing the use of electrolytes which have lower decomposition potentials and thus improving safety.

Table 2 lists the reported organic electrode materials' properties, species, discharge potential, and positions of electrodes (commonly used in SIBs). Organic electrode components have three types of classification: C=O-, C=N-, & N=N-bonded compounds. Quinones & ketones have greater reduction-oxidation potential when employed as cathode materials than carboxylic acid derivatives, which are commonly used as anode materials. On the other hand, anhydride compounds possess higher specific capacities and last longer in cycles [24].

Organic small molecules with a variety of groups, such as C=O (ketones and quinones, anhydrides, carboxylates, & imides compounds), C=N (Schiff bases, pteridine derivatives), and N=N (azo derivatives), have been shown to be electroactive sites electrode compounds for SIBs. Pteridine is an aromatic chemical formed by the union of pyrimidine and pyrazine rings. Carbonyl compounds that have a C=O link are the organic electrode materials that are researched most frequently due to their distinct multielectron reaction, high theoretical capacity, and vast range of structural variations [25-62]. Conjugated structure and plane structure are both important in the preservation of the electrochemical activity of Schiff base and pteridine derivatives with a C=N bond. [63–68].

It is now known that azo components with N=N bonds can be used as OSIB electrode components; the N=N link has been shown in experiments to act as an electrochemical activity group, forming a reversible bond with Na ions [69].

The majority of electrode materials used today are organic small-molecular substances from three main classes:

carbonyl compounds, Schiff base derivatives, and azo derivatives. Quinones and carbonyl compounds have a higher redox potential [14]. The Na insertion voltage of carboxylic acids is lower than that of anhydride compounds, which have a greater specific capacity & longer cycle life. As the cathode and anode for SIBs, redox polymer elements such as azo conductive polymers, conjugated microporous polymers, organometallic polymers, COF and MOF were used [70]. Organometallic and organic radical polymers frequently have faster kinetic properties, despite their low capacity.

Materials made of covalent organic frameworks (COF) and metal-organic frameworks (MOF) have excellent structural stability, and their shape and nanostructures can be easily changed to admit more Na^+ ions [71-72].

In redox polymers, reversible oxidation and reduction processes are possible. The side chains or primary polymer backbones of these materials contain active regions where these redox reactions occur. Because of their limited solubility, mechanical and thermal stability, and safety, redox polymers are viable solutions. The electrochemical attributes of the electrode materials & stability of the cycle were the primary criteria [1,73]. They have redox potential, capacity, cycle life, and rate capability and were originally used as battery electrode materials.

The battery's specific energy is computed by multiplying the cell voltage (V) by the specific capacity (mAh g^{-1}) [3, 8]. Because of the increased specific capacity of the cathode and anode potential differences of the active materials [4, 5], more energy can be stored in the battery system.

To improve performance, rechargeable batteries with quick kinetics and multielectron redox-active sites are desirable. For rechargeable batteries, it is also necessary to resolve the solubility of active components in the electrolyte [75-76]. On the other hand, azo derivations based on the N=N bond may make it easier to build SIBs with high capacity and rate [1,9,11]. Because azo compounds have two electrons, they can carry out redox reactions based on N=N/N-N and N=N group conjugation with rapid redox kinetics and enormous capacities [74-76]. Azo compounds with fast kinetics, numerous electron redox processes, and adaptable architectures are among the candidates for improving battery performance in this area.

Because sodium sources are cheap and plentiful, and because their reaction potential is similar to that of lithium (2.71 V for Na/Na+ vs 3.04 V for Li/Li+) [77-79], SIBs are regarded as an alternative to LIBs. SIBs lack the high energy density

and consistent cycle life of LIBs due to Na+ having an ion size 1.4 times larger than Li+, resulting in a more drastic volume shift during the sodiation and desodiation processes as well as more difficult intercalation chemistry [78]. An assortment of inorganic materials was developed to replace graphite as well as LiCoO2 in SIBs to improve their electrochemical performance.

However, none of those inorganic compounds comes close to the efficiency of LIBs. OEMs stand out as desirable electrode materials for SIBs due to their characteristics of being plentiful, light, affordable, environmentally sustainable, and recyclable. Sodium 4,4′-stilbene-dicarboxylate (SSDC) was described as a rapid charge/discharge organic anode for SIBs by Wang et al. [79]. The design approach for the rapid charge/discharge organic anode entails expanding the organic framework's conjugated structure. The SSDC demonstrates the consistent cycle life in SIBs by providing a reversible initial capacity of 160 mAh g^{-1} and maintaining 112 mAh g^{-1} after 400 cycles.

To demonstrate rapid charge/discharge capability, the SSDC may produce reversible capacities of 90 and 72 mAh g^{-1} at high current densities of 5 and 10 mAh g^{-1}. The extended -conjugated system improves charge transport and evens out the charged and discharged states of SSDC. It is responsible for SSDC's rapid charge/discharge capabilities. Zhao et al. reported that organic thiocarboxylate electrodes [79] increase the organic anode’s capacity in SIBs, in which sulfur replaces oxygen as the redox centers.

Table 2. Overview of the reported organic electrode material's types, characteristics, electrode locations (often utilized in SIBs), and discharge potential.

Molecular weight (Working principles)	Types	Characteristics	Electrode (charge/discharge potential)
Containing a small molecule and carbonyl groups (C=O)	Quinones and ketones Carboxylates Anhydrides Imides	Greater redox potentials Lower Na-insertion voltage High specific capacity and long cycle life High solubility in electrolyte	Cathode (≈0.5–2.7 V) Anode (≈0.2–0.7 V) Cathode/anode (≈0.5–1.6 V) Cathode/anode (≈0.6–2.5 V)
Containing (C=N)	Schiff bases and Pteridine derivatives compounds (pyrimidine and pyrazine rings.)	Modifiable electrochemical activity	Anode (≈0.2–1 V) Cathode (1.6–1.9 V)
Containing (N=N)	Azo-compounds, Conductive polymers	Further study needed Faster kinetic properties	Anode (≈1.0–1.5 V) Cathode (≈2.5–3.4 V)
Macromolecular Doping	Nitroxyl radical polymers Organometallic polymers COFs MOFs	High electrochemical activity Good stability, consistent and stable nanostructures	Cathode (≈2.2–3.4 V) Cathode (3.1–3.4 V) Cathode/anode (1.3–2.7 V) Cathode/anode (1.3–2.7 V)

The reaction mechanism of thiocarboxylate electrodes is exactly like that of carboxylate electrodes; however due to an interaction between sodium ions and the benzene ring, the thiocarboxylate electrode's capacity can increase to 567 mAh g^{-1} at 50 mAh g^{-1}. The sulfur doping of carboxylate electrodes improves electron density and conductivity while increasing battery capacity. Even at a high current density of 2 mAh g^{-1}, the thiocarboxylate electrode can maintain a reversible capacity of 300 mAh g^{-1}. This OEM is utilized to create flexible organic batteries as a proof of concept. The good performance and possible applications of carboxylate and thiocarboxylate electrodes [77-79] demonstrate carboxylate-based

organic compounds' interest as SIB anodes. The current study focuses on polymeric azo-compound materials (PAMs) as active components for SIBs, describes some material design concerns and electrochemical reaction methods, and highlights recent advances in this field.

2. As Electrode Materials, Polymers Containing Conjugated Azo Compounds are Used

Polymeric polymers based on conjugated azo compounds are frequently used to make modified electrode components for SIBs. The azo group (N=N), a distinct kind of organic electrode component, functions as a redox center for reversible electrochemical interactions with sodium ions. SIBs can be generated at a high rate and with a lengthy cycle life due to the reversible reaction with Na-ions [80]. Batteries have desirable properties. They are lightweight, flexible, and sustainable due to the organic components of small molecules and polymers. The abundance, adjustable redox properties, and relative affordability of organic materials are major advantages [81-84]. Other organic compounds, such as polymers and small compounds, have also been investigated for their potential use as electrodes. However, due to their extraordinary solubility within organic electrolyte materials, using small components as electrode molecules has several drawbacks and practical challenges. Wang et al. [81-84] described a class of organic components with an azo group (N=N) for the lithiation/delithiation redox reaction. The lithium salt of azobenzene-4,4′-dicarboxylic acid is one of the organic compounds whose reaction mechanism and electrochemical activity have been studied [13-85]. (ADALS).

At 0.5 C (equal to 95 mAh g^{-1}), ADALS can still offer a capacity of 190 mAh g^{-1} and retain 90%, 71%, or 56% of the capacity when the current density is elevated to 2 C, 10 C, or 20 C, respectively. Furthermore, ADALS has one of the best performances of any organic compound, retaining 89% of its initial capacity after 5,000 cycles at 20 degrees Celsius and degrading only moderately (0.0023% per cycle). The improved redox performance of ADALS in sodium ion batteries [13] shows that azo components are widely used as electrode materials in alkali-ion batteries.

The ADALS-based electrode has one of the top electrochemical presentations among organic electrodes as a model azo compound. With reversible capacities of 179 mAh g^{-1} at 0.5 C for 100 cycles, 146 mAh g^{-1} at 2 C for 2,000 cycles, and 93 mAh g^{-1} at 20 C for 5,000 cycles [13], it has good cycling stability and rapid

charge/discharge capabilities. Because SIBs perform well electrochemically, azo compounds may be suitable as electrode materials for all alkali-ion battery types. Unfortunately, high-rate operation is not possible for azo compounds with aromatic cores. Exhibiting exceptional capabilities, it leads one to believe that N=N extended-conjugated structures play a part in LIBs' high-rate capability [13].

Because of organic electrolytes solubility with cathode material, azo compounds frequently exhibit poor cycling performance. However, by changing the structure, such as by including other carboxylate groups, or by using a different technique to address the issues, its performance can be improved [13].

To overcome this barrier, El-Kaderi et al. synthesized extremely porous azo-linked polymer networks & covalent organic frameworks to explore the electrochemical behavior and reaction mechanism of porous organic polymers (POPs), which present a once-in-a-lifetime opportunity to create a substance that can improve battery performance as well as stability [83-86]. Polymer materials are suitable platforms for electrochemical energy storage applications because of their great number of redox-active sites, high surface areas, and conjugated frameworks. The properties of porous organic polymers β their crystalline complements, covalent organic frameworks (COFs), enable high-rate charge storage and rapid ion transport in Li/Na ion batteries [83-87].

Azo compounds electrochemical properties and reaction mechanisms have also been investigated. In SIBs, Luo et al. [83-86] investigated azobenzene, 4-(phenylazo) benzoic acid sodium salt (PBASS), and azobenzene 4,4′-dicarboxylic acid sodium salt (ADASS). The cycle's stability is extremely low due to the components' solubility in organic electrolytes. PBASS and ADASS were created to address this issue by incorporating carboxyl groups. As a result, the ADASS had a high specific capacity (170 mAh g^{-1} at 0.2 C), a high-rate capacity, and a long cyclic stability (a reversible capacity of 98 mAh g^{-1} after 2000 cycles at 20 C). [83-87].

Alzharani et al. and others reported on the synthesis of azobenzene partially reduced graphene oxide molecules (AB-PRGO) for sodium ion batteries [85]. In half-cell Na-ion batteries, AB-PRGO was used as a new cathode material (SIBs). The results showed that the AB-PRGO-based SIB had great cyclic stability, good rate capability, & great specific capacity under a defined potential window (0.01-3.0 V), reaching a specific capacity of 160 mAh g^{-1} at 50 mA g1 and sustaining the capacity for 50 cycles [84-87]. Because the polymer structure in organic electrolytes have high

solubility resistance, converting tiny molecules into polymers is an efficient technique for improving cycle performance [86, 87]. Polymer electrode materials are also prone to electrochemical polarization & insufficient ion/electron transport [86]. Also, the inactive links added during polymerization decrease the weight ratio of active units in polymer electrode materials, limiting their theoretical capacity [18, 86].

The NO_2 to azo group translation was proposed to enhance the enactment of batteries because it undergoes its first irreversible reduction & produces a stable azo-linked polymer [87]. When the C=O link in 2,7-dinitropyrene-4,5,9,10-tetraone (PT-2NO_2) was broken during discharge, it was changed into a conjugated azo polymer. Despite its small Coulombic efficiency (charge/discharge capacity=301.3/250.4 mAh g^{-1} [84-87]), PT-2NO2 has a high electron mobility.

Organic electrode materials have come under increasing scrutiny in the field of Na-metal batteries because of their enormous assets, pliability, and environmental friendliness. Despite this, the electrolyte's inability to stabilize organic small molecules does cause a decrease in battery capacity & a shorter cycle life. To tackle these issues, we propose p-PADA, a linear polymer with active centers N=N and C=N. The p-PADA electrode stands out due to its impressive rate performance, rapid reaction kinetics, and highly conjugated and polymerized structure. After 1000 cycles, p-PADA still has a specific capacity of 313 mAh g^{-1} when the current density approaches 5 mAh g^{-1}. According to this research, polymerization is a viable technique for developing the electrochemical properties of organic substances [88].

3.Organometallic Compounds with Azo-functional Groups for Sodium-ion Battery Modification

Organometallic compounds containing azo-functional groups, such as azo polymers, COFs, and MOFs, are now frequently used to modify sodium-ion batteries. Table 3 shows the electrochemical properties of several electrode materials made of azo polymers, COFs, and MOFs. When metal ions or clusters with organic linkers self-coordinate, a metal-organic framework (MOF) is formed, which is a type of inorganic-organic hybrid material. MOFs have been reported to be widely used in a variety of applications due to their many exceptional properties, which include a customizable structure, superior thermal stability, high porosity, massive surface areas, and abundant groups [17]. Supercapacitors and other energy storage

technologies, particularly MOFs and their derivatives, have sparked considerable interest [1-6].

LIBs are lithium-ion batteries. [20-26] Li-S batteries, [34-36] fuel cells, [27-33] solar cells. In such circumstances, pristine MOFs are calcined to produce electrode materials like hard carbon, porous metal oxides, or metal oxide/carbon composite compounds, with MOFs acting as precursors or templates. Although the majority of the MOFs had structural stability issues or experienced significant capacity loss while cycling, they all demonstrated good cycling performance and reversible capacity. Metal-organic frameworks with redox activity are currently being researched as anode materials for LIBs, despite their difficulty to obtain [85]. One method for creating redox active MOFs for LIBs is to use oxidation-reduction active metal sites and/or a ligand [32].

COFs, porous frameworks made by covalently linking two or more different types of organic molecules [85], can also improve the azo compounds' battery performance. Planar compounds with conjugated systems are commonly used in the synthesis of COFs with two-dimensional (2D) -conjugated structures. Furthermore, because -stacking improves electron conductivity while decreasing solubility, COFs have lately been employed as active components for LIBs. Covalent organic frameworks (COFs) have been looked at closely in recent times due to their unusual structural skeleton, high porosity, high crystallinity, ease which they can be modified chemically, and exceptional durability in a variety of demanding conditions. A 2D COF has been used in a variety of energy storage & conversion applications.

According to Lu et al., the 2D COF coupled to -ketoenamine and anthraquinone has good capacity when used in the anode compound in sodium-ion batteries due to its abundant carbonyl (C=O) group composition (SIBs). The anode material in LIBs, according to Feng et al., is a 2D polyarylimide-based COF with good rate capability and cycle stability [38]. According to this groundbreaking study, a COF can be the most suitable electrode material for LIBs or SIBs [30].

Metal-organic frameworks (MOFs) are porous frameworks formed by coordination bonding between metal ions and organic ligands. Because of their insoluble nature in organic solvents, MOFs have been used recently as active components to enhance the rate and cycle performances of organic compounds. Azo-MOFs perform exceptionally well as anode active materials due to the presence

of open, negatively charged oxygen atoms linked by N=N groups.

The improved battery performance of azo polymers and frameworks is due to their insolubility in organic solvents as well as their varied HOMO and LUMO energies, as previously established. These findings show that it is possible to meet these goals and that the soft crystal properties of COFs and MOFs facilitate the development of azo compounds as the active substances of rechargeable batteries with superior capacity and high-rate capability.

Table 3. List of the electrochemical characteristics of several electrode materials made of azo polymers, COFs, and MOFs.

Polymer Electrode Materials	Rate	Sp. Capacity ($mAhg^{-1}$)	Capacity retention (current density, cycles)	AM : C : binder (binder)	AM loading ($mg\ cm^{-2}$)	Ref
ADALS	0.5 C	190	89% (2C, 5000)	60:30:10 (PVDF)	~1.5	24
PBASS	0.2 C	162	dissolves into the electrolyte/severe shuttle reaction	60:30:10 (PVDF)	-	13
ADASS	0.2 C	113	0.2 C after 1000 cycles	60:30:10 (PVDF)	-	13
ALP-8	0.3 C	170	90% (0.08 Ag^{-1}, 150)	6:3:1 (Na alginate)	~1	27
PT-2NO2	50 mAg^{-1}	153.9	120 cycles	4:5:1 (PVDF)	-	31
CPL-4	50 mAg^{-1}	91 mAg^{-1}	100 cycles	30:60:10 (PVDF)	-	23
Tp-Azo-COF	1000 mAg^{-1}	305.97 mAg^{-1}	100% 1000 mAg^{-1}, 3000)	80:10:10 (PVDF)	~ 3.15	30
AB-PRGO	50 mAg^{-1} 100 mAg^{-1}	160 140	95% (0.1 A g^{-1}, 100)	7:2:1 (PVDF)	~1	28

To meet the demands of sustainable energy systems, grid-scale energy storage devices with reasonably priced and effective electrodes are required. Because of their wide availability, low cost, and electrochemistry, SIBs receive a lot of consideration as potential grid-scale energy storage devices. Despite the enormous efforts made over the last decade to improve the development of SIBs and the remarkable advances made, more advancements regarding energy/power density and extended cyclic stability are still required for commercialization.

A brief discussion of many fascinating cathodes and anodes, as well as the most recent developments in electrode materials for SIBs, is included. Furthermore, structural, and compositional optimizations, challenges, and opportunities are being investigated in order to enhance the electrochemical capabilities of SIB electrode materials. We are confident that, with active research efforts, sodium-ion batteries with long lifespans and low operating costs will soon be commercially available for use in many energy storage applications, despite the possibility of significant challenges [87-91].

Due to the abundance of sodium, its affordability, and its comparable electrochemical performance, SIBs have become a potential replacement for LIBs in energy storage implementations. In contrast to Li^+, Na^+ has a high molar mass and a large radius, resulting in significant volume strain throughout charge/discharge, a limited reversible capacity, & unstable cycling. Graphene has sparked a lot of interest as a potential anode compound for SIBs because of its exceptional physical & chemical things [87-91].

Graphene, when combined with other nanomaterials in electrodes, can accelerate reaction kinetics, accommodate significant volume changes, and improve electrical conductivity. This research examines the most recent developments in the fabrication of sodium ion storage mechanisms, structural configuration, and electrochemical enactment of graphene-based cathodes for SIBs. Several issues and potential solutions for improving the shortage presentation of graphene-based electrodes for storage energy are also discussed [91-94].

As the demand for sustainable energy sources grows, SIBs are becoming a more viable substitute for LIBs for building large energy storage grid applications. However, the inefficiency of current electrode compounds, particularly cathodes, has hampered the commercialization of SIBs thus far. Considering the extensive research on

layered transition metal oxides, Prussian blue analogues, and polyanionic chemicals, this brief review calls attention to the inherent problems and appropriate solutions. Furthermore, the commercial viability of currently available materials is evaluated in light of pertinent factors. The information in this review could be used to develop cutting-edge cathode materials [91-93].

4. Polymeric Azo-Materials for Sodium-ion Electrode Development

Even though there are a wide variety of organic electrode materials on the market right now, it may be difficult to find any that meet the sophisticated requirements of SIBs. There are several issues with the present organic electrode materials for SIBs that require immediate attention.

I) Organic Compounds' Chemical Stability is Poor

The chemical bond strength between molecules has a significant impact on the chemical stability of organic materials.

Most organic compounds are made up of covalent bonds, which are susceptible to free radical formation throughout the charge/discharge process & to interactions with main chain active groups. As a result, when side reactions occur, organic electrode materials are rendered inactive. Another factor that contributes to particle pulverization and simple separation from the current collector is the significant volume expansion of organic material [94-97]. The morphology and molecular structure of the organic material must be optimized in order to maximize the stability of the electrode material [94-97].

II) Organic substances, particularly small organic molecules, have high innate solubilities in organic electrolytes. Organic electrode materials' high solubility is the root cause of their rapid capacity attenuation and poor cycle stability [98, 99]. Even though it accelerates electrochemical activities in solution phases, the main barrier to using organic materials in SIBs is their solubility. This issue can be solved by employing the appropriate molecular synthesis or by relating them to inorganic materials. Aqueous electrolytes could also be a viable option [100-102].

III) Inadequate Electric Conductivity

Because most organic molecules are covalent compounds, they lack unbound electrons or ions. As a result, they have a low charge transfer rate. OSIBs' overall energy density is reduced due to the need to use a significant quantity of carbon as conductive additives while creating the electrodes [103-106]. To improve the transfer ability of organic electrode materials, molecular design [107], doping [108], composites of conductive polymers

or inorganic conductive materials [109-111], and molecular design can be used.

Polymers will be used in the next generation of organic batteries due to their adaptability and the benefits of azo-polymeric electrode materials. The development of rechargeable polymer batteries will undoubtedly increase research interest. It is very possible that new, innovative polymer electrode materials with novel structures and properties will lay the foundations for the development of long-lasting energy storage technologies.

OEMs are one of the materials with the most potential for use in the next iteration of rechargeable batteries, due to their abundant resources, sustainability, high theoretical capacity, and structural designability. OEMs, on the other hand, typically have poor stability in common organic electrolytes and poor electronic conductivity, which contributes to their declining output capacity and rate capability. To consider new OEMs, it is necessary to understand the issues at both the microscale and macroscale levels. [112] provides a comprehensive explanation of the challenges and cutting-edge techniques for improving the electrochemical enactment of redox-active materials for long-lasting secondary batteries.

Characterization tools and computational methodologies have been developed to help understand the complex redox reaction processes and validate the organic radical intermediates of OEMs. Also shown are the future of OEMs and the structural design of complete cells based on OEMs. This assessment will draw attention to OEMs thorough understanding and advancement of sustainable secondary batteries [112].

These two organic battery problems have piqued the interest of many researchers. Numerous of tremendous reviews [113-118] have provided a thorough overview of OEM development and applications for nonaqueous alkali-ion batteries and all-solid-state batteries. In contrast to other studies, this one discusses OEM applications in dual-ion batteries, multivalent metal batteries, aqueous batteries, all-solid-state batteries, and harsh environments, as well as the underlying reaction processes of OEMs in metal ion batteries.

Organic electrode materials face many challenges, but they can be overcome by watchful organic molecule synthesis & modification. Fundamentally, there are 3 main strategies: morphological control, function-oriented molecular design and a combination of organic and inorganic materials. These strategies improve SIB capacity, rate performance, and cycle

stability by making acceptable changes to organic molecules' conductivity, solubility, theoretical capacity, and working voltage.

4.1. Molecular Design for Function

Designability is one of the most notable properties of molecular structures in organic materials. Careful molecular engineering can be used to develop organic molecule targeting strategies. The following points, in particular, can be modified:

1) The addition of electron-withdrawing (NO_2, CN, F, Cl, Br, SO_3Na, OCH_3)/electron-donating (NR_2, NHR, NH2, OH, OR, OCOR, R, Ph, R = alkyl) groups efficiently lowers/increases the working voltage in SIBs. Adding halogen atoms like fluorine, chlorine, or bromine to benzoquinone derivatives, for example, may increase their redox potential but will not increase their molecular weight [119].

2) The rate performance of organic materials can be improved by increasing the degree of -conjugation of the electrochemical active center unit. The conjugation system extension helps to build a tolerance to the quick insertion and extraction of Na^+ ions as well as the rapid transfer and collection of charge during the fast charge and discharge process. Furthermore, the increased -conjugation system may lead to a layer of molecular order via strengthened molecular connections.

High-polarity salts have been developed to reduce electrolyte solubility [120-121]. One advantage of salinizing organic molecules is that it increases their polarity, which aids in the prevention of organic electrode material dissolution in aprotic electrolytes. Strong hydrophilic solid organic salts, such as NaO/KO/CaO, on the other hand, can form coordination bonds that can slightly obstruct the dissolution of organic electrode materials. Even after 300 cycles as an anode material in SIBs, the organic salt (Ca2BTEC) produced by $Ca2^+$ and H4BTEC (1,2,4,5-benzenetetracarboxylic acid) demonstrated a reversible capacity of 140 mAh g^{-1} [123].

4) Polymerization is another effective technique for increasing the usefulness of organic materials in SIBs. First, the dissolution of the organic material can be greatly reduced due to the polymer's rapidly increasing molecular weight (Mw). Second, by copolymerizing with other electrochemical active units and 3D porous polymers, the theoretical capacity can be increased.

4.2. Micromorphology Control

Because material morphology influences the electron and ion transport channels, controlling the micromorphology of battery materials is critical. In general, increasing capacity and performance by

nanomerizing electrode materials is an effective strategy. In addition to particle size, the morphology, crystal structure, and crystallinity of electrode components must be regulated during the production of nanostructured electrode components. In addition to fully utilizing the benefits of nanoparticles when used as the electrode component for SIBs, nanostructured materials have the ability to mitigate and outperform the disadvantages of nanomaterials due to their distinct structural features, thus improving the functionality of SIBs. Compact size, short sodium ion insertion/detachment distance, exceptional, large specific surface area, more active sodium insertion sites, kinetic performance, low polarization, and high reversible capacity are just a few of the electrode's charging and discharging characteristics. The research community has been very interested in nano electrode materials for SIBs. Nano electrode materials can be manufactured in a variety of ways and in a variety of forms.

5. Novel Electrode Components for Rechargeable Green Na-ion Batteries

Recent organic materials, as well as organic polymers of the redox-active porous type, are widely used for the modification of electrode materials for environmentally friendly rechargeable sodium-ion batteries.

5.1. New Electrode Materials for Green Rechargeable Na-ion Batteries Using Porous Organic Polymers that are Redox Active

While switching from lithium to sodium may reduce lithium shortages and costs, rechargeable batteries with redox-active organic materials could potentially transform the industry by providing lightweight, flexible, and environmentally friendly batteries. The first highly porous azo-linked polymer-based redox-active electrode material for rechargeable sodium-ion batteries is presented here (ALPs). Strongly cross-linked polymers, such as ALPs, avoid the problem that small organic molecules have with organic electrodes dissolving quickly in common electrolytes [124]. Because of their high surface area and -conjugated microporous structure, electrolytes can more easily bind to the pores of ALPs, which accelerates ion transport and charge transfer rates. Over 150 charge/discharge cycles, a 96% Coulombic efficiency was maintained, with a mean specific capacity of 170 mA h g1. The use of extremely porous azo-linked polymers (ALPs) as new redox active electrode materials for sodium-ion batteries is described by Alzharani et al. [124-126]. Because of their strong cross-linking, ALPs would address the solubility issue that is common in small biological compounds and contributes a rapid

reduction of the capacity. The polymer's large surface area and conjugated microporous structure can also bind electrolytes, accelerating ionic transport. ALP-8 is an azo-linked polymer (Scheme 1).

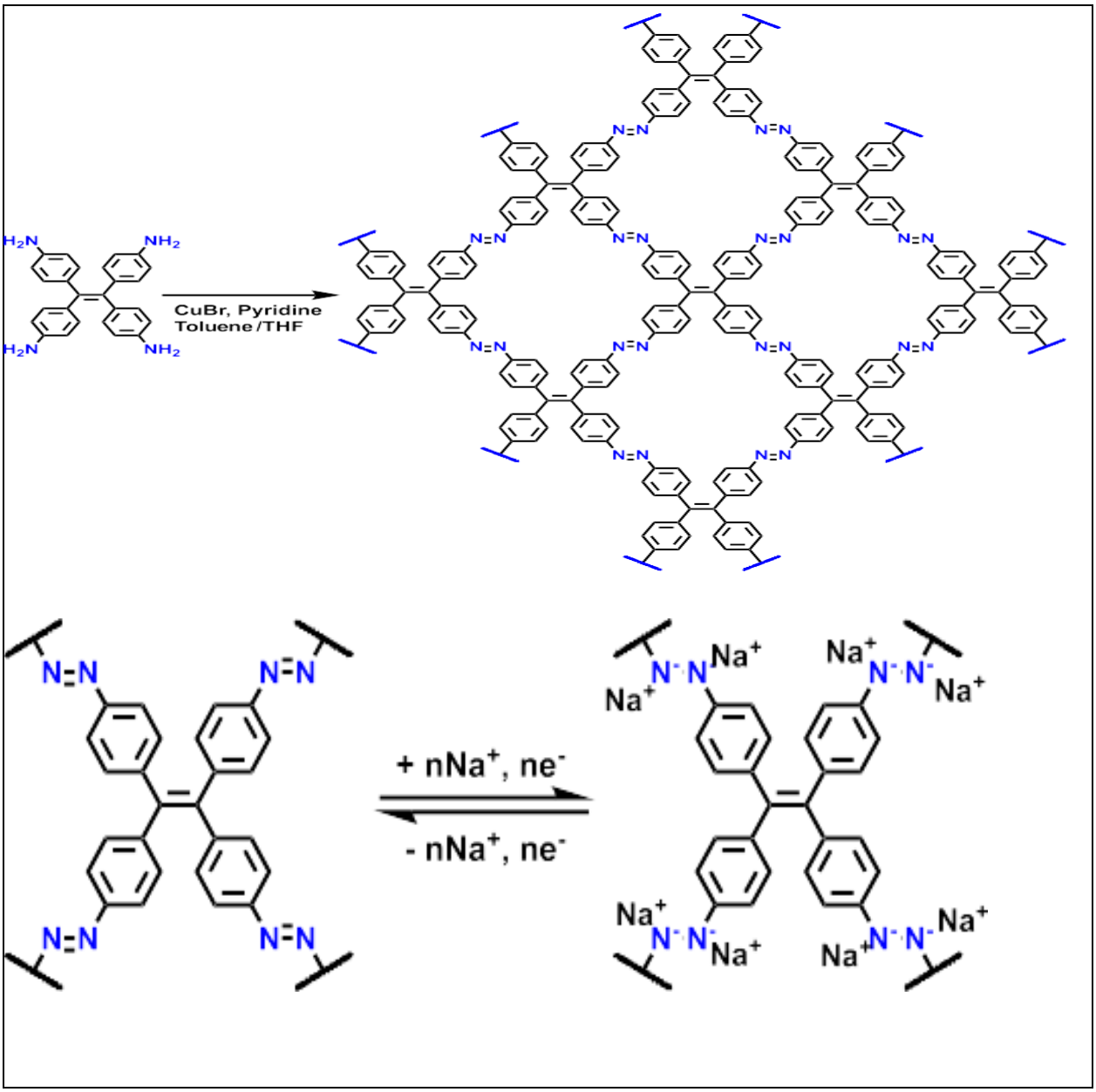

Scheme 1. The synthesized Azo-materials (ALP-8) [124] and their sodium ion redox mechanism.

In such porous materials, the redox-active sites required for charge storage capacity are provided by the nitrogen-nitrogen double bonds, or azo-bonds, in the framework without threatening the physical and chemical stability of the electrodes. In this study, as cathode,

1,1,2,2-tetrakis(4-aminophenyl)-ethene was homocoupled with a CuBr/pyridine catalyst to produce ALP-8 using a previously published method [125]. The produced electrodes were tested in CR2032 half coin cells with the electrolyte of 1 M NaPF6 in DEGDME and Na metal used as both the counter and reference electrodes to determine the electrochemical activity of ALP-8 in SIBs. The CV analysis was implemented at a scan rate of 0.1 mv/s and over a possible range of 0.01 to 3.0 V. **(Figure 1a).**

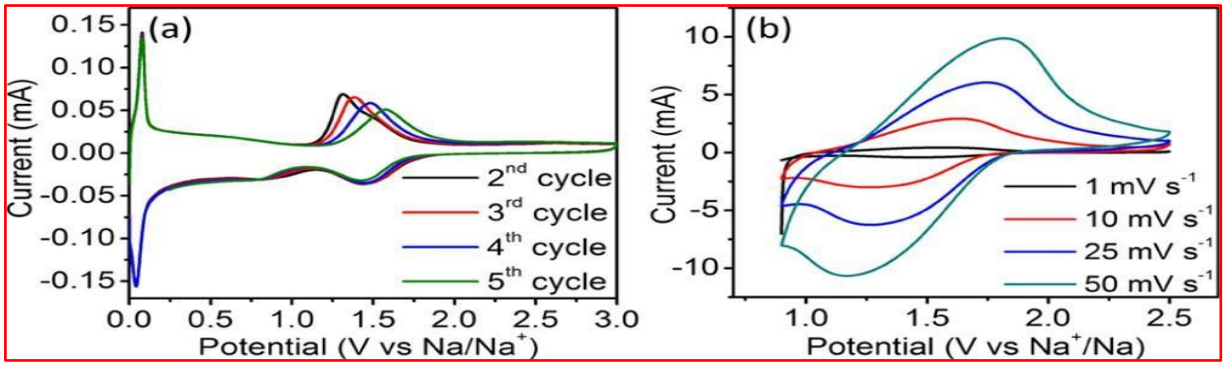

Figure 1. Cyclic voltammetry profile for the APL-8 at (a) 0.1 mVs^{-1} at the potential range (0.01-3 V) , (b) with various scan rates at potential range (0.9-2.5 V) vs (Na^+/ Na).

The CV profile may show a broad cathodic peak that varies with the number of cycles. The broad anodic peak exceeds 1.5 V, indicating the existence of a significantly irreversible reaction at a low scan rate. Nonetheless, these variances are absent at greater scan rates (Figure 1b), which demonstrates that the side reactions can only be the result of sluggish electron transfer rates. The anodic & cathodic peaks represent the azo core's semi-reversible reduction, or sodiation, and oxidation, or desodiation, processes, respectively. The absence of corresponding electroactive sites on the polymer as a result of conjugation errors is represented by the single, broad anodic and cathodic peaks. Broad CV bands imply that sodiation is a mixed process that involves both surface pseudocapacitive Na+ storage and Na+ injection into the polymer [127]. This is demonstrated by the CV profiles obtained at various scan rates (Figure 1b). The slopes of the anodic and cathodic logarithmic curves were 0.82 and 0.79, respectively, demonstrating that Na^+ ion diffusion is a surface-limiting redox process and not a rate-limiting process [128-130]. Galvanostatic charge/discharge tests were performed against a Na+/Na reference electrode in the potential range of 0.01-3.0 V in order to determine the electrode's effectiveness in reversible Na+

ion storage. In this work, charge corresponds to desodiation and discharge to sodiation. Figure 2a depicts the charge/discharge profile at 0.3 C (1 C = 278 $mAhg^{-1}$) current density. In the first cycle, a greater discharge capacity of 315 $mAhg^{-1}$ was observed. This figure exceeds the theoretical ALP-8 capacity (278 $mAhg^{-1}$) for a four-electron redox reaction (Scheme 1). Therefore, the first discharge capacity can be equal to the total of the irreversible capacity generated by the SEI and the reversible capacity. The complex electrical properties of the amorphous framework, redox reactions, and Na^{+} insertion is what causes the sloping charge/discharge curves (Figure 2a). It demonstrated exceptional cycling performance for an ALP-8 electrode by producing a reversible capacity of 194 $mAhg^{-1}$ at 0.3 C (2nd cycle, Figure 2b), which is 70% of the theoretical capacity. After 150 cycles, the battery retained more than 90% of its capacity, with a specific discharge capacity of $mAhg^{-1}$ (Figure 2c). These findings show that the ALP-8 polymer can reversibly accept 2.5 Na+ ions in a single repeat unit. As shown in Figure 2d, the rate capability was tested by measuring the discharge capacities at different current densities ranging from 0.3 to 40 C at a working potential of 0.01-3 V versus Na/Na+.

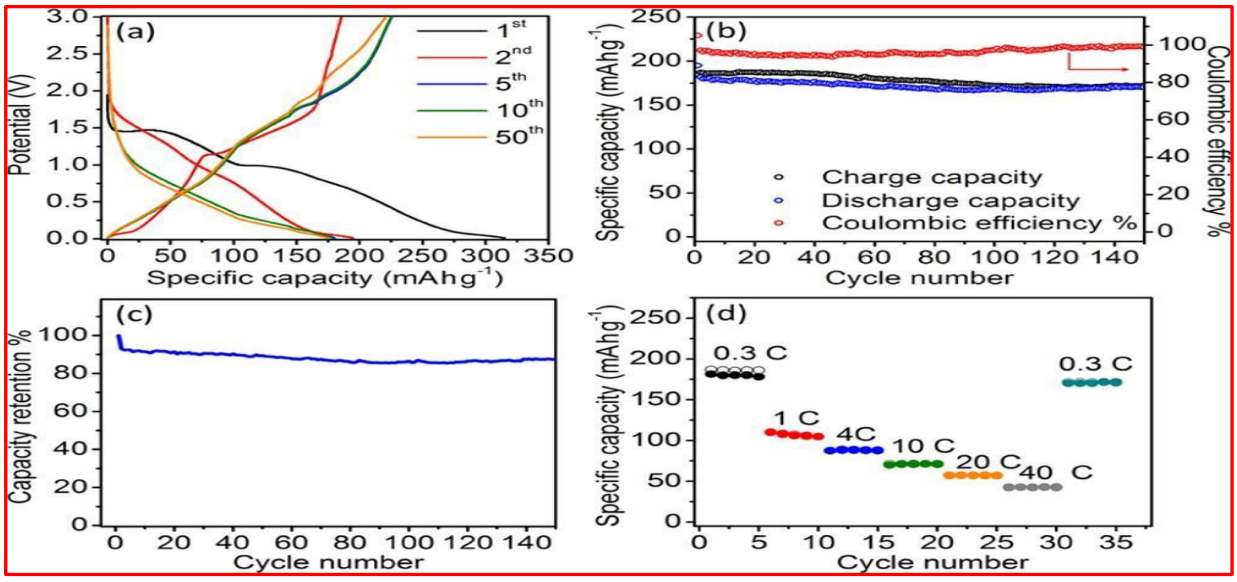

Figure 2. (a) Profiles of galvanostatic charge/discharge of ALP-8 battery at 0.3 C, (b) Columbic efficiency and cycle stability, (c) Retention of capacity at 0.3 C, and (d) Rate capability at different current densities, 0.3−40 C (filled/unfilled charge/discharge capacity). (1 C = 278 $mAhg^{-1}$)

El-Kaderi et al. determined the following significant points in 2019 [124-133] as a key outcome of the described research:

- The high conjugated microporous framework provides an electrode that is stable with rapid ion transport & charge transfer rates.
- A specific capacity of up to 170 $mAhg^{-1}$ was achieved at a 0.3 C rate. At the same time, a Coulombic efficiency of above 96% was retained.
- The superior cycle stability surpasses most other state-of-the-art organic polymer electrode components reported in the literature [125-133] and can be attributed to the highly cross-linked framework's insoluble nature, which gets rid of the complications of dissolution in the electrolyte and thus lessens capacity fading while increasing ionic conductivity.
- The ALP-8-based electrode has great rate capability and stability over 150 cycles.

Alzharani et al, 2022 recently reported the new surface modified reduced graphene oxide as a new material for application in the improved modified electrode materials used for environmentally friendly rechargeable SIBs. The following are some of the current study's key findings:

1- The employment of redox-active sites in the organic components in rechargeable batteries could potentially advance the field of energy storage by enabling lightweight and flexible safe batteries. Furthermore, substituting sodium for lithium significantly reduces the limited supply and costliness of lithium for Li^{+} batteries (LIBs).

2- Covalently bound azo compounds were used to cross-link graphene oxide (GO) nanosheets to enable sodium-ion insertion and improve the capacity of charge storage. The diamine functional groups of p-phenylenediamine (PPD) were transformed into diazonium salts (DSs), which were then electrophilically substituted with GO nanosheets to create azobenzene partially reduced AB-PRGOs for sodium-ion battery storage.

3- Some of the methods used to characterize the as-synthesized AB-PRGO include advanced spectroscopy techniques such as X-ray diffraction (XRD), FT-IR, nitrogen adsorption/desorption isotherm, Raman spectroscopy, XPS, SEM, and TEM to confirm

the structural materials of the cathode sides.

4- The AB-PRGO was employed as a novel cathode material in half-cell Na^+ batteries (SIBs). In a defined possible window (0.01-3.0 V), the AB-PRGO-based SIB has good cyclic stability, a great specific capacity, as well as a great rate capability, reaching a specific capacity of 160 $mAhg^{-1}$ at 50 $mAhg^{-1}$ which it can maintain for 50 cycles. This work paves the way for the development of better organic electrode compounds for SIBs.

6. Conclusion

Finally, because of the amount of sodium, structural diversity, composition tenability, and variety of functional groups, polymer electrode materials have shown enormous possibility for use in Na-ion batteries. Polymer batteries are thought to be the future energy storage technology. Research into various polymer electrode materials for Na-ion batteries is still in its early stages. New polymeric materials with different structures are needed for sodium-ion battery applications. Radicals, heteroatoms in conjugated systems, and carbonyl groups may be active locations for interacting with sodium ions, according to newly emerging knowledge of sodium-ion storage mechanisms in polymer electrode materials. As a result, innovative polymers with a high density of these active components are highly desired. The most greatest promising material for Na-ion battery modification is the redox-active porous type, which is frequently used for modification of the electrode compounds toward environmentally friendly rechargeable sodium-ion batteries.

Table 4: List of Abbreviations

The abbreviations	Definition
Azo	Type of organic compound containing nitrogen
COFs	Covalent Organic Frameworks
Azo-COFs	Azo compound with Covalent Organic Frameworks
MOFs	Metal-Organic Frameworks
Azo-MOFs	Azo- Metal-Organic Frameworks
(LIBs)	Li-ion batteries
EES technology (ESSs)	Electrochemical Energy Storing
(HEVs),	Hybrid Electric Vehicles
EVs	Electron Volts
(SIBs)	Na^+ batteries (Sodium Ion Batteries)
(HC)	Hard Carbon
(V)	Cell Voltage
OEMs	Organic Electric Materials
(SSDC)	Sodium 4,4′-stilbene-dicarboxylate
(PAMs)	polymeric azo-compound materials
(ADALS)	The lithium salt of azobenzene-4,4′-dicarboxylic acid
(POPs)	Porous Organic Polymers
(PBASS)	azobenzene, 4-(phenylazo) benzoic acid sodium salt
(AB-PRGO)	azobenzene partially reduced graphene oxide molecules
(PT-2NO_2)	2,7-dinitropyrene-4,5,9,10-tetraone
p-PADA	a linear polymer with active centers N=N and C=N.
(2D)	two-dimensional -conjugated structures
2D COF	two-dimensional- Covalent Organic Frameworks
HOMO	High-occupied molecular orbitals.
LUMO	Low- unoccupied molecular orbitals.
OEMs	Are one of the materials with the most potential for use in the next iteration of rechargeable batteries.
(Ca2BTEC)	the organic salt produced by Ca^{2+} and H4BTEC (1,2,4,5-benzenetetracarboxylic acid)
(ALPs)	The first highly porous azo-linked polymer-based redox-active electrode material for rechargeable sodium-ion batteries
ALP-8	is a type of an azo-linked polymer
CV	Cyclic voltammetry profile (cyclic Voltamogram)
(GO)	graphene oxide
(PPD)	p-phenylenediamine
AB-PRGOs	azobenzene partly reduced graphene oxide

7. References

1. Amin K, Mao L, Wei Z (2019) Recent Progress in Polymeric Carbonyl-Based Electrode Materials for Lithium and Sodium Ion Batteries. Macromol Rapid Commun 40 (1) e1800565.
2. Bhosale ME, Chae S, Kim J M, Choi JY (2018) Organic small molecules and polymers as an electrode material for rechargeable lithium ion batteries. Journal of Materials Chemistry A 6 (41) 19885.
3. Cao X, Liu J, Zhu L, Xie L (2019) Polymer Electrode Materials for High- Performance Lithium/Sodium- Ion Batteries. A Review. Energy Technology 7 (7)1800759.
4. Wang TW (2018) Electrode Materials for Sodium- Ion Batteries: Considerations on Crystal Structures and Sodium Storage Mechanisms. Electrochemical Energy Reviews 1 (38) 1:200.
5. Zhao Q, Whittaker A K, Zhao XS(2018) Polymer Electrode Materials for Sodium-ion Batteries. Materials (Basel) 11 (12) 2567.
6. Abdelkader A A, Norouzi N, Rodene DD, Alzharani A, Gupta RB, El-Kadri HM (2020) Electrocatalytic Cathodes Based on Cobalt Nanoparticles Supported on Nitrogen-Doped Porous Carbon by Strong Electrostatic Adsorption for Advanced Lithium–Sulfur Batteries. Energy & Fuels 34 (10)13038.
7. Kim H, Kim H, Ding Z, Lee MH, Lim K, Yoon G, Kang K (2016) Recent Progress in Electrode Materials for Sodium-Ion Batteries. *Advanced Energy Materials 6* (19) 1600943.
8. Li M, Zhu K, Zhao H, Meng Z(2022) Recent Progress on Graphene-Based Nanocomposites for Electrochemical Sodium-Ion Storage. Nanomaterials (Basel)12 (16) 2837.
9. Mauger A, Julien CM (2020) State-of-the-Art Electrode Materials for Sodium-Ion Batteries. Materials (Basel) 13 (16) 3453.
10. Yin X, Sarkar S, Shi S, Huang Q A, Zhao H, Yan L, Zhao Y, Zhang J(2020) Recent Progress in Advanced Organic Electrode Materials for Sodium- Ion Batteries: Synthesis, Mechanisms, Challenges and Perspectives. Advanced Functional Materials **30** (11)1908445.

11. Shea J J, Luo C (2020) Organic Electrode Materials for Metal Ion Batteries. ACS Appl Mater Interfaces 12 (5), 5361.
12. Mishra K, Yadav N, Hashmi S A (2020) Recent progress in electrode and electrolyte materials for flexible sodium-ion batteries. Journal of Materials Chemistry A 8 (43) 22507.
13. Luo C Borodin O Ji X Hou S Gaskell K J Fan X Chen J Deng T Wang R Jiang J Wang C(2018) Azo compounds as a family of organic electrode materials for alkali-ion batteries. Proc Natl Acad Sci U S A 115 (9) 2004.
14. Wasalathilake K C, Li H, Xu L, Yan C (2020) Recent advances in graphene based materials as anode materials in sodium-ion batteries. Journal of Energy Chemistry 42, 91.
15. Zhang Y, Xia X, Liu B, Deng S, Xie D, Liu Q, Wang Y, Wu J, Wang X , Tu J (2019) Multiscale Graphene-Based Materials for Applications in Sodium Ion Batteries. Advanced Energy Materials **9** (8) 1803342.
16. Huang S F, Wang M, Jia P , Wang B , Zhang J J, Zhao Y F (2019) N-graphene motivated SnO2@SnS2 heterostructure quantum dots for high performance lithium/sodium storage. Energy Storage Mater 20, 225.
17. Shi S S, Li Z P, Sun Y , Wang B , Liu Q N , Hou Y L , Huang S F , Huang J Y , Zhao Y F (2018) A covalent heterostructure of monodisperse Ni2P immobilized on N, P-co-doped carbon nanosheets for high performance sodium/lithium storage. Nano Energy 48, 510.
18. Wang T Y, Su D W , Shanmukaraj D , Rojo T F , Armand M, Wang G X (2018) Electrode Materials for Sodium-Ion Batteries: Considerations on Crystal Structures and Sodium Storage Mechanisms , Electrochem. Energy Rev1, 200.
19. Gao G, Tie D, Ma H, Yu H, Shi S, Wang B, Xu S, Wang L, Zhao Y F (2018) Interface-rich mixed P2 + T phase NaxCo0.1Mn0.9O2 ($0.44 \leq x \leq 0.7$) toward fast and high capacity sodium storage , J. Mater. Chem. A 6, 6675.
20. Tie D, Gao GF, Xia F, Yue R Y , Wang Q J, Qi R J , Wang B, Zhao Y F (2019) Modulating the Interlayer Spacing and Na+/Vacancy Disordering of P2-Na0.67MnO2 for Fast Diffusion and High-Rate Sodium Storage.

ACS Appl. Mater. Interfaces11, 6978.

21. Pan H L , Hu Y S , Chen L Q (2013) Room-temperature stationary sodium-ion batteries for large-scale electric energy storage , Energy Environ. Sci 6, 2338.
22. Hwang J Y , Myung S T , Sun Y K (2017) Sodium-ion batteries: present and future Chem. Soc. Rev 46, 3529.
23. Sakaushi K, Antonietti M (2015) Carbon- and Nitrogen-Based Organic Frameworks. Acc. Chem. Res 48, 1591.
24. Yin PX, Sarkar S, Shi S, Huang Q, Zhao H, Yan L, ZhaoY , Zhang J(2020) Recent Progress in Advanced Organic Electrode Materials for Sodium-Ion Batteries: Synthesis, Mechanisms, Challenges and Adv. Funct. Mater 30, 1908445
25. Lee M, Hong J, Lopez J, Sun Y M, Feng D W, Lim K, Chueh W C, Toney M F, Cui Y, Bao Z A (2017) High-performance sodium–organic battery by realizing four-sodium storage in disodium rhodizonate. Nat. Energy 2, 861.
26. Kim H, Kwon J E , Lee B, Hong J, Lee M, Park S Y, Kang K (2015) High Energy Organic Cathode for Sodium Rechargeable Batteries , Chem. Mater 27, 7258.
27. Chen H Y , Armand M, Demailly G, Dolhem F, Poizot P, Tarascon J M (2008) From Biomass to a Renewable LiXC6O6 Organic Electrode for Sustainable Li-Ion Batteries , ChemSusChem 1(4) 348.
28. Song Z P, Qian Y M , Liu X Z, Zhang T, Zhu Y B, Yu H J, Otanibd M, Zhou H S (2014) A quinone-based oligomeric lithium salt for superior Li–organic batteries Energy Environ. Sci. 7, 4077.
29. Zhu Z Q, Li H , Liang J, Tao Z L (2015) The disodium salt of 2,5-dihydroxy-1,4-benzoquinone as anode material for rechargeable sodium ion batteries. J. Chen, Chem. Commun. 51, 1446.
30. Wang Y Q, Ding Y, Pan L J, Shi Y, Yue Z H, Shi Y, Yu G H (2016) Understanding the Size-Dependent Sodium Storage Properties of Na2C6O6-Based Organic Electrodes for Sodium-Ion Batteries. Nano Lett 16, 3329.
31. Luo C, Wang J J, Fan X L, Zhu Y J, Han F D, Suo L M, Wang C S (2015) Roll-to-roll fabrication of organic nanorod electrodes for

sodium ion batteries. Nano Energy 13, 537.

32. Wu X Y, Ma J, Ma Q D, Xu S Y , Hu Y S, Sun Y, Li H, Chen L Q , Huang X J (2015) A spray drying approach for the synthesis of a Na2C6H2O4/CNT nanocomposite anode for sodium-ion batteries , J. Mater. Chem. A 3, 13193.
33. Chen L, Zhao Y M (2019) Exploration of p-Na2C6H2O6-based organic electrode materials for sodium-ion and potassium-ion batteries. Mater. Lett 243, 69.
34. Zheng S B, Hu J Y, Huang W W (2017) An inorganic–organic nanocomposite calix[4]quinone (C4Q)/CMK-3 as a cathode material for high-capacity sodium batteries. Inorg. Chem. Front 4, 1806.
35. Yan B, Wang L J, Huang W W , Zheng S B, Hua P D, Du Y Y (2019) High-capacity organic sodium ion batteries using a sustainable C4Q/CMK-3/SWCNT electrode. Inorg. Chem. Front. 6, 1977.
36. Xiong W X, Huang W W, Zha ng M, Hu P , Cui H M, Zhang Q C (2019) Pillar[5]quinone–Carbon Nanocomposites as High-Capacity Cathodes for Sodium-Ion Batteries , Chem. Mater. 31, 8069.
37. Huang W W, Zhang X Q, Zheng S B, Zhou W J, Xie J, Yang Z N, Zhang Q C (2020) Calix[6]quinone as high-performance cathode for lithium-ion battery *Science China Materials* **63**,339.
38. Wang C L, Fang Y G, Xu Y, Liang L Y, Zhou M, Zhao H P, Lei Y(2016) Manipulation of Disodium Rhodizonate: Factors for Fast-Charge and Fast-Discharge Sodium-Ion Batteries with Long-Term Cyclability. Adv. Funct. Mater 26, 1777.
39. Deng W W, Liang X M, Wu X Y, Qian J F, Cao Y L, Ai X P, Feng J W, Yang H X (2013) A low cost, all-organic Na-ion Battery Based on Polymeric Cathode and Anode. Sci. Rep. 3, 2671.
40. Song Z P, Qian Y M, Zhang T, Otani M, Zhou H S (2015) Poly(benzoquinonyl sulfide) as a High-Energy Organic Cathode for Rechargeable Li and Na Batteries. Adv. Sci. 2, 1500124.
41. Wu D B, Huang Y H, Hu X L (2016) A sulfurization-based oligomeric sodium salt as a high-performance organic anode for sodium ion batteries. Chem. Commun. 52, 11207.

42. Zhu L M, Liu J B, Liu Z Q, Xie L L, Cao X Y (2019) Chem Electro Chem 2019, 6, 787-792. ; Chihara K, Chujo N, Kitajou A, Okada S (2013) Cathode properties of Na2C6O6 for sodium-ion batteries. Electrochim. Acta 110, 240 .
43. Luo C, Zhu Y J, Xu Y H, Liu Y H, Gao T, Wang J, Wang C S (2014) Graphene oxide wrapped croconic acid disodium salt for sodium ion battery electrodes. J. Power Sources 2014, 250, 372.
44. Yao M, Kuratani K, Kojima T, Takeichi N, Senoh H, Kiyobayashi T (2015) Molecular ion battery: a rechargeablesystem without using any elemental ions as a charge carrier , Sci. Rep. 4, 3650.
45. Zhu H, Yin J, Zhao X, Wang C Y, Yang X R (2015) Humic acid as promising organic anodes for lithium/sodium ion batteries. Chem. Commun.51, 14708.
46. Zhao L, Zhao J M, Hu Y S, Li H , Zhou Z B, Armand M, Chen L Q (2012) Disodium Terephthalate (Na2C8H4O4) as High Performance Anode Material for Low-Cost Room-Temperature Sodium-Ion Battery. Adv. Energy Mater 2, 962.
47. Park Y, Shin D S, Woo S H, Choi N S, Shin K H, Oh S M, Lee K T, Hong S Y (2012) Sodium Terephthalate as an Organic Anode Material for Sodium Ion Batteries. Adv. Mater. 2012, 24, 3562.
48. Ma C, Zhao X L, Kang LT, Wang K X, Chen J S, Zhang W Q, Liu J J (2018) Non-Conjugated Dicarboxylate Anode Materials for Electrochemical Cells. Angew. Chem. 30, 9003.
49. Wu D B, Luo K, Du S Y, Hu X L (2018) A low-cost non-conjugated dicarboxylate coupled with reduced graphene oxide for stable sodium-organic batteries. Power Sources 398, 99.
50. Abouimrane A, Weng W, Eltayeb H, Cui Y J, Niklas J, Poluektova O, Amine K (2012) Sodium insertion in carboxylate based materials and their application in 3.6 V full sodium cells. Energy Environ. Sci. 5, 9632.
51. Choi A, Kim Y K, Kim T K, Kwon M S, Lee K T, Moon H R (2014) 4,4′-Biphenyldicarboxylate sodium coordination compounds as anodes for Na-ion batteries. J. Mater. Chem. A 2, 14986.
52. Wang C L, Xu Y, Fang Y G, Zhou M, Liang L Y, Singh S, Zhao H P, Schober A, Lei Y (2015) Extended π-Conjugated System for Fast-Charge and -Discharge Sodium-Ion

Batteries. J. Am. Chem. Soc. 2015, 137(8) 3124.

53. Veerababu M, Varadaraju U V, Kothandaraman R (2015) Improved electrochemical performance of lithium/sodium perylene-3,4,9,10-tetracarboxylate as an anode material for secondary rechargeable batteries. Int. J. Hydrogen Energy 40(43) 14925.
54. Zhao H Y, Wang J W, Zheng Y H, Li J, Han X G, He G, Du Y P (2017) Angew. Chem 129(48) 5536.
55. Wan F., Wu X L, Guo J Z, LiJ Y, Zhang J P, Niu L, Wang R S (2015) Nano effects promote the electrochemical properties of organic Na2C8H4O4 as anode material for sodium-ion batteries. Nano Energy 13, 450 - 457.
56. Luo W, Allen M, Raju V, Ji X L (2014) An Organic Pigment as a High-Performance Cathode for Sodium-Ion Batteries. Adv. Energy Mater 4(15)1400554.
57. Wang H G, Yuan S, Si Z J, Zhang X B (2015) Multi-ring aromatic carbonyl compounds enabling high capacity and stable performance of sodium-organic batteries. Energy Environ. Sci. 2015, 8(11) 3160 - 3165.
58. Banda H, Damien D, Nagarajan K, Raj A, Hariharan M, Shaijumon M M (2017) Twisted Perylene Diimides with Tunable Redox Properties for Organic Sodium-Ion Batteries. Adv. Energy Mater 7, 1701316.
59. Deng W W, Shen Y F, Qian J F, Cao Y L, Yang H X (2015) A Perylene Diimide Crystal with High Capacity and Stable Cyclability for Na-Ion Batteries. ACS Appl. Mater. Interfaces 2015, 7, 21095 - 21099.
60. Zhao Q L, Gaddam R R, Yang D F, Strounina E, Whittaker A K, Zhao X S (2018) Pyromellitic dianhydride-based polyimide anodes for sodium-ion batteries. Electrochim. Acta 265, 702 -708.
61. Li L, Hong Y J, Chen D Y, Lin M J (2017) Molecular Engineering of Perylene Imides for High-Performance Lithium Batteries: Diels–Alder Extension and Chiral Dimerization. Chem. - Eur. J 23(65) 16612 - 16620.
62. Deng W W, Shen Y F, Qiana J F, Yang H X (2015) A polyimide anode with high capacity and superior cyclability for aqueous Na-ion batteries. Chem. Commun. 51, 5097 - 5099.

63. López-Herraiz M, Castillo-Martínez E, Carretero-González J, Carrasco J, Rojo T, Armand M (2015) Oligomeric-Schiff bases as negative electrodes for sodium ion batteries: unveiling the nature of their active redox centers. Energy Environ. Sci. 8, 3233- 3241.

64. Kaim W, Schwederski B, Heilmann O, Hornung F M (1999) Coordination compounds of pteridine, alloxazine and flavin ligands: structures and properties. Coord. Chem. Rev.182, 323- 343.

65. Hong J Y, Lee M, Lee B, Seo D H, Park C B, Kang K (2014) Biologically inspired pteridine redox centres for rechargeable batteries. Nat. Commun. 5, 5335.

66. Chen Y Q, Manzhos S (2015) Lithium and sodium storage on tetracyanoethylene (TCNE) and TCNE-(doped)-graphene complexes: A computational study. Mater. Chem. Phys. 156, 180 - 187.

67. Precht R, Stolz S, Manke E, Jaegemann W, Hausbrand R (2016) Investigation of sodium insertion into tetracyanoquinodimethane (TCNQ): results for a TCNQ thin film obtained by a surface science approach, Phys. Chem. Chem. Phys. 18, 3056- 3064 .

68. Chen Y, Manzhos S (2016) A comparative computational study of lithium and sodium insertion into van der Waals and covalent tetracyanoethylene (TCNE)-based crystals as promising materials for organic lithium and sodium ion batteries. Ph ys. Chem. Chem. Phys.18, 8874 - 8880.

69. Luo C, Xu G L, Ji X, Hou S, Chen L, Wang F, Jiang J J, Chen Z, Ren Y, Amine K, Wang C S (2018) Reversible Redox Chemistry of Azo Compounds for Sodium-Ion Batteries. Angew. Chem., Int. Ed. 57, 2879 -2883.

70. Li Q, Wang H, Wang H G, Si Z, Li C, Bai J(2020) A Self-Polymerized Nitro- Substituted Conjugated Carbonyl Compound as High-Performance Cathode for Lithium-Organic Batteries. ChemSusChem.13 (9), 2449-2456.

71. Rambabu D, Lakraychi A E, Wang J, Sieuw L, Gupta D, Apostol P, Chanteux G, Goossens T, Robeyns K,Vlad A(2021) An Electrically Conducting Li-Ion Metal- Organic Framework. J Am Chem Soc143 (30) 11641-11650.

72. Halder A, Ghosh M, Khayum M A, Bera S, Addicoat M, Sasmal H S, Karak S, Kurungot S, Banerjee R(2018) Interlayer Hydrogen-

Bonded Covalent Organic Frameworks as High-Performance Supercapacitors. J Am Chem Soc 140 (35) 10941- 10945.

73. Priyanka Gupta S P, Ali Haider M, Suddhasatwa B(2022) Understanding the Design of Cathode Materials for Na-Ion Batteries. ACS Omega 7, 10.
74. An S Y, Schon T B, McAllister B T, Seferos D S (2020) Design strategies for organic carbonyl materials for energy storage: small molecules, oligomers, polymers and supramolecular structures. EcoMat 2 (4)1.
75. Desai A V,Morris R E, Armstrong A R(2020) Advances in Organic Anode Materials for Na-/K-Ion Rechargeable Batteries. ChemSusChem. 13 (18), 4866-4884.
76. Zeng M, Xiao Y, Liu J, Yang K, Fu L(2018) Exploring Two-Dimensional Materials toward the Next-Generation Circuits: From Monomer Design to Assembly Control. Chem Rev 118 (13) 6236-6296.
77. Luo C, Fan X, Ma Z, Gao T, Wang C (2017) Self-Healing Chemistry between Organic Material and Binder for Stable Sodium Ion Batteries. Chem. 3 (6) 1050−1062.

Luo C, Zhu Y, Xu Y, Liu Y, Gao T, Wang J, Wang C (2014) Graphene Oxide Wrapped Croconic Acid Disodium Salt for Sodium Ion Battery Electrodes. J. Power Sources.250, 372−378.

78. Wang C, Xu Y, Fang Y, Zhou M, Liang L, Singh S, Zhao H, Schober A, Lei Y (2015) Extended π-Conjugated System for Fast-Charge and -Discharge Sodium-Ion Batteries. J. Am. Chem. Soc. 137 (8) 3124−3130.
79. Zhao H, Wang J, Zheng Y, Li J, Han X, He G, Du Y(2017) Organic Thiocarboxylate Electrodes for a Room-Temperature Sodium-Ion Battery Delivering an Ultrahigh Capacity. Angew. Chem., Int. Ed. 56 (48) 15334−15338.
80. Shimizu, T.; Mameuda, T.; Toshima, H.; Akiyoshi, R.; Kamakura, Y.; Wakamatsu, K.; Tanaka, D.; Yoshikawa, H., Application of Porous Coordination Polymer Containing Aromatic Azo Linkers as Cathode-Active Materials in Sodium-Ion Batteries. ACS Applied Energy Materials **2022,** 5 (4), 5191-5198.
81. Luo C, Xu G L, Ji X, Hou S, Chen L, Wang F, Jiang J, Chen Z, Ren Y, Amine K, Wang C (2018)

Reversible Redox Chemistry of Azo Compounds for Sodium-Ion Batteries. Angew Chem Int Ed Engl 57 (11) 2879-2883.

82. Sun Z, Liu H, Shu M, Lin Z, Liu B, Li Y, Li J, Yu T, Yao H, Zhu S, Guan S (2022) pi-Conjugated Hexaazatrinaphthylene-Based Azo Polymer Cathode Material Synthesized by a Reductive Homocoupling Reaction for Organic Lithium-Ion Batteries. ACS Appl Mater Interfaces 14 (32) 36700-36710.
83. Wang Y, Yang Z, Xia T, Pan G, Zhang L, Chen H, Zhang J (2019) Azo- Group- Containing Organic Compounds as Electrode Materials in Full- Cell Lithium- Ion Batteries. ChemElectroChem.6 (19), 5080-5085.
84. Weeraratne K S, Alzharani A A, El-Kaderi H M(2019) Redox-Active Porous Organic Polymers as Novel Electrode Materials for Green Rechargeable Sodium-Ion Batteries. ACS Appl Mater Interfaces 11 (26) 23520-23526.
85. Alzharani A, Shehab M K, Rodene D D, Ahmed J U, Bakry A M, Kaid M M, El-Kaderi H M (2022) Surface Modification of Partially Reduced Graphene Oxide for Advanced Electrode Material in Rechargeable Sodium Batteries. Energy & Fuels. 36 (9) 4967-4977.
86. Lei Z, Yang Q, Xu Y, Guo S, Sun W, Liu H, Lv L P, Zhang Y, Wang Y(2018) Boosting lithium storage in covalent organic framework via activation of 14-electron redox chemistry. Nat Commun 9 (1) 576.
87. Zhao G, Zhang Y, Gao Z, Li H, Liu S, Cai S, Yang X, Guo H, Sun X (2020) Dual Active Site of the Azo and Carbonyl-Modified Covalent Organic Framework for High- Performance Li Storage. ACS Energy Letters 5 (4) 1022-1031.
88. Jiawen W, Yifan Tong Dr, Weiwei Huang p, Qichun p ,Zhang Q (2022) Conjugated Azo Compounds as Active Materials for Rechargeable Sodium-Metal Batteries with High-R ate Performance 6(2) e202200413.
89. Wang C L, Fang Y G, Xu Y, Liang L Y, Zhou M, Zhao H P, Lei Y (2016) Manipulation of Disodium Rhodizonate: Factors for Fast-Charge and Fast-Discharge Sodium-Ion Batteries with Long-Term Cyclability. Adv. Funct. Mater. 26(11) 1777 - 1786.
90. Luo C, Zhu Y J, Xu Y H, Liu Y H, Gao T, Wang J, Wang C S (2014)

Graphene oxide wrapped croconic acid disodium salt for sodium ion battery electrodes. J. Power Sources 250, 372-378.

91. Yongjin F, Lifen X, Zhongxue C, Xinping A, Yuliang C, Hanxi Y(2018) Recent Advances in Sodium-Ion Battery Materials, *Electrochemical Energy1*,294–323.
92. Wasalathilake K, Henan Li, Xu L, Yan C (2020) Recent advances in graphene-based materials as anode materials in sodium-ion batteries. Journal of Energy Chemistry 42, 91-107.
93. Priyanka G, Sujatha P, Haider M A, Suddhasatwa B(2022) Understanding the Design of Cathode Materials for Na-Ion Batteries *ACS Omega* 7(7)5605.
94. Wang Y, Ding Y, Pan L, Shi Y, Yue Z, Shi Y, Yu G (2016) Understanding the Size-Dependent Sodium Storage Properties of Na2C6O6-Based Organic Electrodes for Sodium-Ion Batteries Nano Lett16, 3329 - 3334.
95. Chen X, Liu L, Yan Z, Huang Z, Zhou Q, Guo G, Wang X (2016) Feasible oxidation of 17β-estradiol using persulfate activated by Bi2WO6/Fe3O4 under visible light irradiation. RSC Adv 6, 2345.
96. Zhu L, Shen Y, Sun M, Qian J, Cao Y, Ai X, Yang H (2013) Self-doped polypyrrole with ionizable sodium sulfonate as a renewable cathode material for sodium ion batteries. Chem. Commun 49, 11370.
97. Su D, Zhang J, Dou S, Wang G (2015) Polypyrrole hollow nanospheres: stable cathode materials for sodium-ion batteries.Chem. Commun. 51, 16092 - 16095.
98. Chen H Y, Armand M, Demailly G, Dolhem F, Poizot P, Tarascon J M (2008) From Biomass to a Renewable LiXC6O6 Organic Electrode for Sustainable Li-Ion Batteries. ChemSusChem 1, 348 - 355.
99. Song Z P, Qian Y M, Liu X Z, Zhang T, Zhu Y B, Yu H J, Otanibd M, Zhou H S (2014) A quinone-based oligomeric lithium salt for superior Li–organic batteries Energy Environ. Sci. 7, 4077 - 4086
100. Koshika K, Sano N, Oyaizu K, Nishide H (2009) An ultrafast chargeable polymer electrode based on the combination of nitroxide radical and aqueous electrolyte. Commun. 836 -838.

101. Choi W, Harada D, Oyaizu K, Nishide H (2011) Aqueous Electrochemistry of Poly(vinylanthraquinone) for Anode-Active Materials in High-Density and Rechargeable Polymer/Air Batteries J. Am. Chem. Soc.133, 19839- 19843.

102. Kim D J, Jung Y H, Bharathi K K, Je S H, Kim D K , Coskun A, Choi J W (2014) An Aqueous Sodium Ion Hybrid Battery Incorporating an Organic Compound and a Prussian Blue Derivative, Adv. Energy Mater 4, 1400133.

103. Zhou M, Xiong Y, Cao Y L, Ai X P, Yang H X (2013) Electroactive organic anion-doped polypyrrole as a low cost and renewable cathode for sodium-ion batteries. J. Polym. Sci., Part B: Polym. Phys 51, 114 - 118.

104. Sun T, Li Z j, Wang H g, Bao D, Meng F l, Zhang X b (2016) A Biodegradable Polydopamine-Derived Electrode Material for High-Capacity and Long-Life Lithium-Ion and Sodium-Ion Batteries Angew. Chem., Int. Ed 55, 10662 - 10666.

105. Zhu L, Niu Y, Cao Y, Lei A, Ai X, Yang H (2012) n-Type redox behaviors of polybithiophene and its implications for anodic Li and Na storage materials. Electrochim. Acta 78, 27 - 31.

106. Liu T, Kim K C, Lee B, Chen Z, Noda S, Jang S S, Lee S W (2017) Self-polymerized dopamine as an organic cathode for Li-and Na-ion batteries , Energy Environ. Sci 10, 205- 215.

107. Wang Y, Kretschmer K, Zhang J, Mondal A K, Guo X, Wang G (2016) Organic sodium terephthalate@graphene hybrid anode materials for sodium-ion batteries RSC Adv 6, 57098 - 57102.

108. Zhao X, Qiu W, Ma C, Zhao Y, Wang K, Zhang W, Kang L, Liu J.(2018) Superposed Redox Chemistry of Fused Carbon Rings in Cyclooctatetraene-Based Organic Molecules for High-Voltage and High-Capacity Cathodes. ACS Appl. Mater. Interfaces 10, 2496 - 2503.

109. Luo C, Zhu Y, Xu Y, Liu Y, Gao T, Wang J, Wang C(2014) Graphene oxide wrapped croconic acid disodium salt for sodium ion battery electrodes. J. Power Sources 2014, 250, 372 - 378.

110. Chen J, Liu Y, Li W, Wu C, Xu L, Yang H (2015) Nanostructured polystyrene/polyaniline/graphene hybrid materials for

electrochemical supercapacitor and Na-ion battery applications. J. Mater. Sci. 2015, 50, 5466 - 5474. Guo C, Zhang K, Zhao Q, Pei L(2015) High-performance sodium batteries with the 9,10-anthraquinone/CMK-3 cathode and an ether-based electrolyte. J. Chen, Chem. Commun. 2015, 51, 10244 - 10247.

111. Deng W, Qian J, Cao Y, Ai X, Yang H.(2016) Graphene-Wrapped Na2C12H6O4 Nanoflowers as High Performance Anodes for Sodium-Ion Batteries. Small 2016, 12, 583 - 587.
112. Ruijuan S, Shilong J, Qianqian Y, Guangqin G, Kai Z, Yong Z(2022) REVIEW Challenges and advances of organic electrode materials for sustainable secondary batteries.2(4) 20220066.
113. John J S, Chao L(2020) Organic Electrode Materials for Metal Ion Batteries. *ACS Applied Materials & Interfaces 12* (5) 5361.
114. Muench S, Wild A, Friebe C, Haupler B, Janoschka T,Schubert U S(2016) Polymer-Based Organic Batteries. Chem. Rev116 (16) 9438−9484.
115. Zhang K, Monteiro M J, Jia Z(2016) Stable Organic Radical Polymers: Synthesis and Applications. Polym. Chem. 7 (36) 5589−5614.
116. Heiska J, Nisula M, Karppinen M(2019) Organic Electrode Materials with Solid-State Battery Technology. J. Mater. Chem. A 7 (32) 18735−18758.
117. Mauger,A, Julien C, Paolella A, Armand M, Zaghib K(2019) Recent Progress on Organic Electrodes Materials for Rechargeable Batteries and Supercapacitors. Materials 12 (11) 1770.
118. Liang Y, Tao Z, Chen J(2012) Organic Electrode Materials for Rechargeable Lithium Batteries. Adv. Energy Mater. 2 (7) 742−769.
119. Kim H, Kwon J E, Lee B, Hong J, Lee M, Park S Y, Kang K(2015) High Energy Organic Cathode for Sodium Rechargeable B atteries, Chem. Mater. 27, 7258 - 7264.
120. Chen H Y, Armand M, Demailly G, Dolhem F, Poizot P, Tarascon J M (2008) From Biomass to a Renewable LiXC6O6 Organic Electrode for Sustainable Li-Ion Batteries. ChemSusChem 1, 348 - 355.
121. Song Z P, Qian Y M, Liu X Z, Zhang T, Zhu Y B, Yu H J, Otanibd M, Zhou H S (2014) A

quinone-based oligomeric lithium salt for superior Li–organic batteries. Energy Environ. Sci. 7, 4077.

122. Wang C L, Xu Y, Fang Y G, Zhou M, Liang L Y, Singh S, Zhao H P, Schober A, Lei Y (2015) Extended π-Conjugated System for Fast-Charge and -Discharge Sodium-Ion Batteries. J. Am. Chem. Soc. 137, 3124 – 3130.
123. Z Song, Y Qian, X Liu, T Zhang, Y Zhu, H Yu, M Otani, H Zhou (2014) A quinone-based oligomeric lithium salt for superior Li–organic batteries. Energy Environ. Sci. 7, 4077 - 4086.
124. Shamara K, Ahmed W, Alzharani A, El-Kaderi H M(2019) Redox-Active Porous Organic Polymers as Novel Electrode Materials for Green Rechargeable Sodium-Ion Batteries, ACS Applied Materials & Interfaces. 11, 26, 1-8.
125. Arab P, Parrish E, Işlamoğlu T, El-Kaderi H M(2015) Synthesis and Evaluation of Porous Azo-Linked Polymers for Carbon Dioxide Capture and Separation. J. Mater. Chem. A 3, 20586−20594.
126. Xu J, Deshpande R D, Pan J, Cheng YT, Battaglia V S(2015) Electrode Side Reactions, Capacity Loss and Mechanical Degradation in Lithium-Ion Batteries. J. Electrochem. Soc.162, A2026−A2035.
127. Yan Y, Hao B, Wang D, Chen G, Markweg E, Albrecht A, Schaaf P (2013) Understanding the fast lithium storage performance of hydrogenated TiO2 nanoparticles. J. Mater. Chem. A 1, 14507−14513.
128. Lee S W, Yabuuchi N, Gallant B M, Chen S, Kim B-S, Hammond P T, Shao-Horn Y(2010) High-Power Lithium Batteries from Functionalized Carbon-Nanotube Electrodes. Nat. Nanotechnol. 5, 531−537.
129. Liang Y, Luo C, Wang F, Hou S, Liou S-C, Qing T, Li Q, Zheng J, Cui C, Wang C(2019) An Organic Anode for High Temperature Potassium-Ion Batteries. Adv. Energy Mater. 9, 1802986.
130. Kudo T, Hibino M (1996) Consideration on the potential composition relationships observed with amorphous intercalation systems such as LixWO3. Solid State Ionics 84, 65−72.
131. Okubo M, Hosono E, Kim J, Enomoto M, Kojima N, Kudo T, Zhou H, Honma I(2007) Nanosize Effect on High-Rate Li-Ion

Intercalation in LiCoO2Electrode. J. Am. Chem. Soc. 129, 7444−7452.

132. Okubo M, Kim J, Kudo T, Zhou H, Honma I(2009) Anisotropic Surface Effect on Electronic Structures and Electrochemical Properties of LiCoO2. J. Phys. Chem. C 113, 15337−15342.

133. Huang Q, Loveridge M J, Genieser R, Lain M J, Bhagat R(2018) Electrochemical Evaluation and Phase-related Impedance Studies on Silicon−Few Layer Graphene (FLG) Composite Electrode Systems. Sci. Rep. 8, 1386.

التطورات الحديثة في تطبيقات المواد العضوية المتقدمة لبطاريات الصوديوم الايونية

أحمد الزهراني

كلية العلوم، جامعة الباحة ، المملكة العربية السعودية

الملخص

تتعدد مميزات الصوديوم كعنصر أكثر وفرة في الطبيعة سهل الحصول عليه ورخيص الثمن. تم تطوير بطاريات الصوديوم بصورة متسارعة في السنوات الأخيرة نظرا لاستخدام المواد العضوية المتطورة في تطوير وتحسين خواص بطاريات الصوديوم. من أشهر المواد العضوية التي تم استخدامها لتطوير بطاريات الصوديوم هي مواد الازو والمركبات غير متجانسة الحلقة والمواد العضوية الكربونية و البوليمرات. تعد البوليمرات العضوية والمواد الكربونية المشتقة منها ضرورية للتنمية الخضراء والمستدامة عند استخدامها كقطب موجب (أنود) لبطاريات أيون الصوديوم لأنها وفيرة في الموارد ، ولها تأثير بيئي مقبول ، ولها تصميمات هيكلية يمكن التحكم فيها. نظرًا لمرونتها المتأصلة، تعد البوليمرات العضوية مفيدة جدًا أيضًا في بطاريات أيون الصوديوم المرنة. فيما يتعلق ببطاريات أيون الصوديوم، تمت مناقشة تطور مواد البوليمر العضوية المرنة والمواد الكربونية المرنة المشتقة من مواد البوليمر المرنة. سنستعرض طرق المعالجة المختلفة والسلائف لمركبات الكربون القائمة على البوليمر. من المتوقع أن تتطور مواد البوليمر المرنة المتجددة في المستقبل. الصوديوم معدن متاح على نطاق واسع وهو بديل ممتاز لأجهزة تخزين الطاقة الكهروكيميائية. العائق الرئيسي لتطوير بطاريات أيون الصوديوم ذات العمر الافتراضي الطويل هو نقص مواد القطب الكهربي المناسبة لتفاعلات الأكسدة والاختزال العكسية لأيون الصوديوم. توفر البوليمرات النشطة في الأكسدة والاختزال فرصًا لتطوير مواد إلكترود جديدة لبطاريات أيونات الصوديوم نظرًا لمرونتها الهيكلية ووظائف السطح القابلة للاستمرار والتكلفة المنخفضة. يلخص هذا البحث المرجعي ويلقي الضوء علي التطورات الحالية في المواد البوليمرية المركبة لبطاريات أيون الصوديوم. ستتم معالجة العديد من المشكلات المتعلقة بمواد وعمليات القطب الكهربي البوليمر من أجل تحسين الأداء الكهروكيميائي لمواد البوليمر المستخدمة كأقطاب كهربائية لبطارية أيون الصوديوم. تركز المراجعة الحالية على أحدث التطورات في مجال تعديل المواد العضوية لبطارية أيون الصوديوم.

الكلمات المفتاحية: بطاريات أيون الصوديوم، المواد المتقدمة، مواد القطب، التنمية المستدامة؛ البوليمرات العضوية ، ازو -الأطر العضوية التساهمية ، أزو- الأطر العضوية الفلزية.

A Study of the possibility of a next pandemic outbreak arising from Avian Influenza H5N1 using machine learning approaches

Dr Prakash Kuppuswamy[1], Dr Saeed Qasim Yahya Al Khalidi Al-Maliki [2], Dr Rajan John[3], Dr Shanmuga Sundaram Marappam[4], Vijaya varshini Prakash[5]

[1]Computer Networks Engineering Department, College of CS & IT, Jazan University, Jazan, KSA
[2]Department of Information science, King Khalid University, Abha, Kingdom of Saudi Arabia
[3]Department of Computer science, College of CS &IT, Jazan University, Jazan, KSA
[4]Department of Computer science, College of CS &IT, Jazan University, Jazan, KSA
[5]PG student, Palanisamy college of Arts, Erode, Tamil Nadu, India.

Abstract

Avian influenza (AI) virus commonly causes bird flu in poultry and mammalian species. In the past 20 years, avian influenza has been one of the most vulnerable disease-causing viruses in the world, particularly in the developing world, where 63 countries have reported cases. This high mutation rate not only makes the virus highly pathogenic but also makes it vulnerable to attack. The World Health Organization (WHO) defines avian influenza as one of the most widespread animal diseases of all time due to its presence in birds and rooster farmsteads. A flu pandemic that is more severe than the other flu could result from the transmission of an avian influenza virus among humans. The objective of this paper is to analyze the recent public controversy surrounding the transmission of highly pathogenic avian influenza among animals. There is a tenuous bond between the group due to the commitment to pandemic preparedness. The artificial intelligence tool is helping us analyze the possibility of an outbreak of Avian flu causing the next pandemic and that leads to identifying the risks and areas of urgency. We collected datasets from WHO's data repository for this study. Our method of choice in this research article is the J48 classifier, which is among the best Artificial Intelligent learning algorithms for categorizing and continuously monitoring data in order to predict an avian flu pandemic in the near future. The early detection of diseases is made possible by machine learning-based technology, and if a pandemic occurs, the government and health authorities can take action right away.

Keywords: H5N1, Avian influenza, Bird flu, Pandemic, Regulation, Machine learning algorithm, Artificial intelligence etc**.,**

1. Introduction

The 1918 influenza pandemic led to the death of 50 million people due to the influenza A virus. In the past century, we have learned much about influenza evolution, origins, and epidemiology thanks to phylogenetic methods and modern sequencing technology. Our study focuses on avian influenza history through genetic analysis of the 1918 H1N1 strain, epidemics in birds with highly pathogenic strains, and the modern strains. In addition to discussing the assortment and aggressive of novel influenza virus in wild and domestic bird populations, we also discuss how wild bird relocation contributes to their long-range spread. Furthermore, zoonotic influenza H5 and H7 viruses have been invading humans over the last couple of decades, and an emergence of highly pathogenic avian influenza viruses is talked about. As avian influenza spreads around the world, it poses a serious threat to human health. Control of domestic bird populations can minimize that risk, but a human pandemic is possible.

.

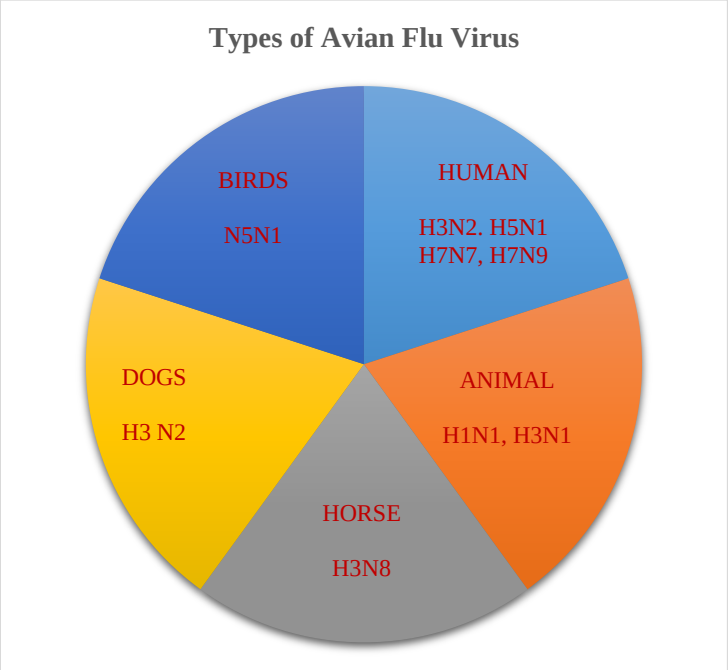

Figure 1. Avian Influenza mutations
Source: https://www.cdc.gov/flu/avianflu/influenza-a-virus-subtypes.htm

H5N1-sometimes named bird flu-is a type of avian influenza that roots serious respiratory disease in birds. The classification of various avian influenza is shown in figure 1. A first detection was made in 1959 in chickens in Britain, and a second in 1996 in geese in southern China and Hong Kong. China and Hong Kong reported the first human cases of the disease in 1997, when 18 people, six of whom died, were infected by animals [1]. A number of bird types have been diseased with this virus, including crows, swans, ducks, eagles, gulls, pelicans, vultures, owls, and geese. Due to the

enormous amount of birds exaggerated, the risks of being exposed to other animals have been high. As well as minks and seals, other mammals confirmed to have contracted the disease include badgers, bobcats, coyotes, dolphins, ferrets, fishing cats, foxes, leopards, lynxes, opossums, otter, pigs, polecats, porpoises, raccoons, raccoon dogs, and skunks [2].

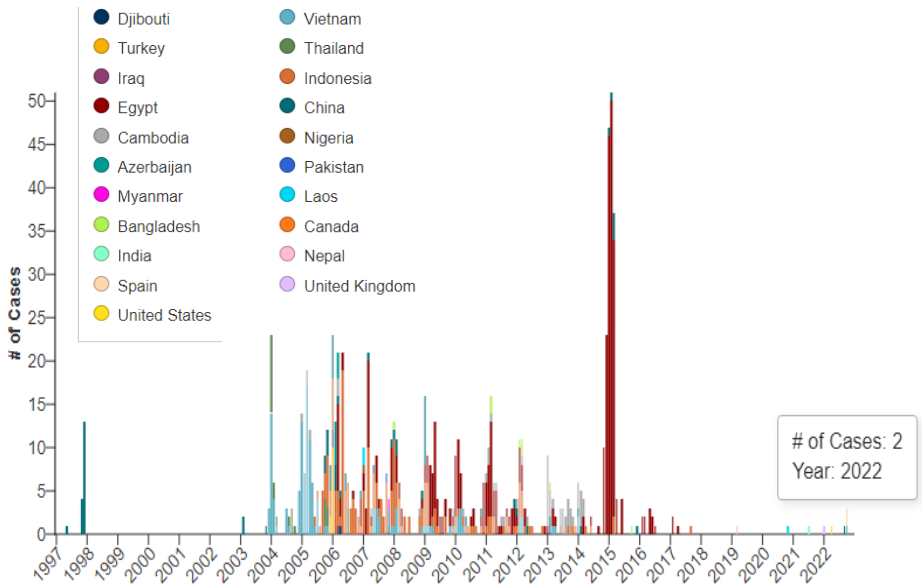

Figure 2. H5N1Countrywide data 1997-2022

The above figure 2 shows all human infections with HPAI H5N1 bird flu virus reported to the World Health Organization (WHO), since the first human cases in 1997. There are two types of H5N1 bird flu circulating in the world today. The first is genetically distinct from earlier strains of the virus and has emerged as the predominant subtype of H5AI H5 in the fall of 2021. In many countries, these viruses have caused sporadic rooster infections and outbreaks. As a result of all bird flu virus infections, humans have suffered varying degrees of illness, from mild illness to severe conditions that have resulted in death.

This research study explores the problem of mining patterns for outlying sequences in sequence data [3, 14]. Globally, there is proof that bird flu outbreaks are increasing due to spillover from domestic birds to humans. Chicken diseases, such as bird flu, not only cause economic losses to farmers but also pose a serious threat to human health [4, 16]. The first large mammal-to-mammal outbreaks of H5N1 have occurred. The epidemics, along with the virus' ongoing transmission in wild birds and poultry, and the increased infections in wild mammals, may lead to an outbreak in humans. As per the WHO's statistical data, the present classification of avian influenza is identified huge numbers in North America and Europe. Since October 2021, H5N1 has killed or culled over 58 million birds, according to different reports [5].

As a government, one of its major responsibilities is to build the capacity to locate, isolate, test, and monitor the situation in order to deal with the pandemic fatality. There is a greater impact in densely populated countries and cities. Technical and financial assistance is needed by several low- and middle-income countries to respond effectively against influenza viruses [6]. In machine learning (ML), the systems analyze large data sets to discover outlines and make predictions. The healthcare industry has a number of successful applications of machine learning, so it's no wonder that the technology is gaining a lot of traction [7] [6] [15].

Table 1. Avian Flu-Low and High Pathogenic

AVIAN INFLUENZA	
Low Pathogenic Avian Influenza (LPAI)	H6N1, H7N2, H7N3, H7N4, H7N7, H7N9, H9N2, H10N8
Highly Pathogenic Avian Influenza (HPAI)	H5N1, H5N6, H5N8, H7N3
Human to Human transmission AI	H5N1, H7N7, H7N9

Source: https://www.cdc.gov/flu/avianflu/influenza-a-virus-subtypes.htm

During avian flu outbreaks in wild birds and/or poultry, those who have come into contact with infected or potentially sick animals, including any that could have eaten contaminated birds, should be aware of their health and look out for fever or other signs of infection. From the above table 1, LPAI and HPAI: Low pathogenic avian influenza viruses cause either no symptoms or only mild ones in poultry. Many avian influenza A viruses are low pathogenic, causing few signs of illness in wild birds [20]. Within 48 hours, some low-pathogenic poultry influenza viruses can transform into highly pathogenic ones, causing serious disease and death rates (up to 90%).

One of the most significant ways in which AI is helping during the pandemic is by enabling rapid detection and diagnosis of the virus. AI-powered tools can analyze large volumes of data from various sources, including medical records, social media, and news reports, to identify potential outbreaks and track the spread of the virus. This allows healthcare professionals to respond quickly and efficiently to contain the virus, saving countless lives. AI is also playing a vital role in developing treatments and vaccines for current pandemic situation. AI-powered drug discovery platforms can analyze vast amounts of medical data to identify potential drug targets and speed up the drug discovery process. Similarly, AI can help researchers develop vaccines by predicting how different strains of the virus will mutate and evolve over time.

2. Background Study

The virus can infect humans when it enters their eyes, nose, or mouth, or if they inhale it. Inhaling the virus from the air or tender something that has the virus on it and then touching the nose, eyes, or mouth can cause this. Close contact with a person who has bird flu is very rare, and when it has happened, it has not resulted in continued spread [19].

Cuiying Lin, Yajuan Guo, Mengmeng Zh ao, Mi Sun, Fang Luo, Longhua Guo, Bin Qiu, Zhenyu Lin and Guonan Chen (2017) This study has created a colorimetric immune sensor that is both highly selective and straightforward to detect influenza virus H5N1. The considerable amount of horseradish peroxidase when the substrate was added, which then catalyzed the oxidation of TMB with hydrogen peroxide. This change in color could be seen with the naked eye or through ultraviolet-visible spectra. Detection threshold was estimated to be 0.04 ng/mL at 0.1 ng/mL and increased with a rise in H5N1 concentration from 0.1 to 4.0 ng/mL. As compared to enzyme-linked immunosorbent assays, the proposed biosensor is much more sensitive. In clinical medicine, food safety examinations, and environmental monitoring, this proposed immune detector may have a promising outlook due to its simplicity, low cost, sensitivity, and specificity [8].

Andrew Lakoff (2017) The author of this paper discusses the recent controversy surrounding avian influenza originating from laboratories that can transmit to mammals. n order to better understand the contours of the controversy around emerging diseases, actors, institutions, and devices need to be brought together. There is a tenuous bond held by 'pandemic preparedness'. It is a controversial topic to conduct research in a field characterized by urgency and uncertainty. The purpose of gain-of-function research is to improve pandemic preparedness, but can only be judged according to its declared objective. The normative rationality of preparedness makes it impossible to assess risks and benefits formally. The issue of estimating the likelihood of uncertain risks still exists in the event of a lab accident or a mutation in the wild. There still remains a challenge connecting envisioned benefits such as using molecular signatures to detect viral mutations in chickens and selecting vaccine strains to actual benefits [9].

Raj and J.G. Jayanthi (2018) One of the major agriculture businesses is Poultry Management. Identifying the disease early and preventing it from spreading is a big challenge in poultry. There is usually a lot of labor and training involved. A monitoring system that can distinguish the affected birds from the rest is proposed. As a result, the user is able to detect sick units earlier and will be able to offer a cost-effective solution to the poultry industry. This paper addresses the development of an embedded IOT system that connects with the server to monitor poultry farms. As a second objective, the current work in sound analysis for the poultry industry will be presented [10].

Samantha Lycett, Florian Duchatel, Paul Digard. Lycett SJ, Duchatel F and Digard P (2019) During the past couple of decades, humans have been infected with highly pathogenic avian influenza viruses, including avian H5 and H7 viruses. A newly discovered avian influenza virus remains a potential cause of a pandemic, despite control of domestic bird populations. As part of the theme issue 'Modeling infectious diseases outbreaks in humans, animals, and plants: approaches and relevant themes', this article is available online. As this brief history of bird flu demonstrates, avian influenza has been circulating and diversifying in wild bird populations for at least 100 years. Humans and wild birds rarely interact; however, domestic bird species do transmit disease to humans; especially in Asian markets for live birds, this is due to the low frequency of human contact with wild birds. [11].

Ali Javed, Byung Suk Lee, and Donna M. Rizzo (2020) An all-time series data repository is used to develop a time series clustering benchmark. To ensure unbiased results, the benchmark examines eight popular clustering algorithms representing three types of clustering algorithms and three types of distance measures. A phased evaluation approach was then used to summarize and discuss the assessment metrics. Also, based on the benchmark study presented, the dataset-level assessment metrics can be used to formulate evaluation frameworks to address different research questions. In order to reduce bias, this study outlined six restrictions. It is worth noting that eight popular clustering methods covered three categories of clustering algorithms and three distance measures. Six external evaluation measures are used to report dataset-level assessment metrics. This paper uses the adjusted Rand Index as its default measure [12].

Saadh and Aldalaen (2021) H5N1 flu antiviral pills are available, however they go through from antiviral drug resistance and damaging aspect effects. As a result, this work examined epigallocatechin gallate (EGCG) in aggregate with zinc ions and silver nanoparticles. Tests to determine cytotoxicity were conducted using MTS. The find out about confirmed for the first time that EGCG mixed with zinc II and AgNPs might also have a right threat of being used in the remedy and prevention of infections due to its potential to inhibit the entry of H5N1 influenza viruses into host cells. Protease, polymerase, hemagglutination, and neuraminidase may all be inhibited in order to destroy the virus particle. A new multi-activity topical therapeutic agent in opposition to the H5N1 avian flu virus may want to be developed the use of the potentiated antiviral residences of EGCG co-administered with zinc II and AgNPs. Infection resistance is limited by this mix, which prevents viral adaptation and does not affect virus mutations [13].

3. Research Significance

There are only a few cases of human infection with some types of bird flu viruses (avian influenza viruses). Infections with the bird flu virus have caused a range of illnesses in humans, from mild illness to death-causing diseases. Virus infections in human beings most frequently appear after shut or extended unprotected contact with contaminated birds or locations the place unwell birds or their saliva, mucous, and feces are present. Infections with H5-type viruses, H6-type viruses, H7-type viruses, H9-type viruses, and H10-type viruses have caused respiratory illness in humans. The majority of infections in people occur from H5N1 and H7N9 viruses. The Bird Flu Virus Infections in Humans website provides more information about bird influenza in humans.

Avian influenza refers to an illness in birds caused by the presence of avian (bird) influenza (flu) Type A viruses. Over a hundred different species of wild birds around the globe have had Avian influenza A viruses identified in them. These viruses are typically observed amongst wild aquatic birds globally and can unfold to the home rooster as properly as different hen and animal species. Infected birds can transmit avian influenza Viruses thru their saliva, nasal secretions, and feces. When uncovered to the virus, prone birds may additionally end up contaminated if they come into contact with it when shed by means of unwell birds. Domesticated bird avian influenza outbreaks are a matter of concern for several reasons. Primarily, there is the opportunity for low pathogenic A(H5) and A(H7) viruses to remodel into tons greater

risky rather pathogenic forms, which may want to have huge agricultural implications. Furthermore, at some point of outbreaks of relatively pathogenic avian influenza, there is the viable for speedy unfolding and extreme sickness and loss of life amongst poultry. This can cause a significant economic impact as well as trade limitations due to an outbreak of this nature. Moreover, it's conceivable that avian influenza viruses could be transmitted to humans in contact with infected birds.

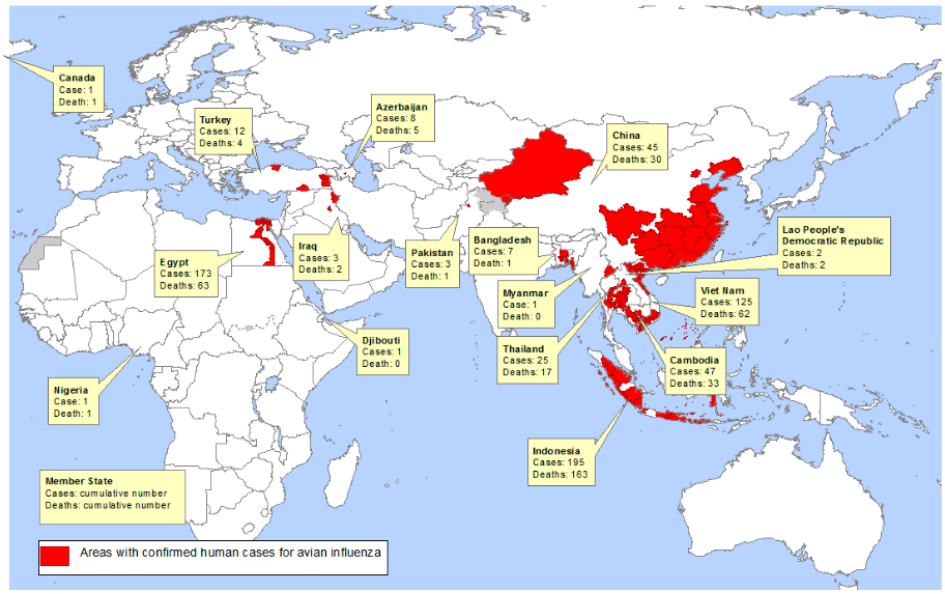

Figure 3. Cases and Deaths (2003-2013)
Source: https://www.who.int/images/default-source/maps/2003_2013_avianinfluenza

In 1997, a strain of avian influenza (H5N1) caused serious illness in humans in Hong Kong, resulting in the death of 4 out of 9 infected children and 5 out of 9 infected adults. According to the World Health Organization, between 2003 and 2023 there were 868 officially reported cases of human infection with H5N1 worldwide. Of those who contracted it, 457 people died - a mortality rate of 53 percent. Observing data from figure 3, the number of cases and death rate compared to Covid-19, this strain is much more deadly when contracted by humans; thus, further research is essential to better understand its future potential for harm.

4. Methods and Materials

The information has analyzed the usage of a variety of statistical techniques, such as classification, clustering, and anomaly detection. This paper focuses on the j48 classifier. Classification is a normal unsupervised desktop mastering technique for dividing records factors into agencies such that observations inside the identical classification have a tendency to be extra comparable than these in exceptional classifiers. Sources make openly accessible paper metadata, and in most cases, sources associated with each type of different variant of influenza.

4.1 Data source

This is a prospective cohort study of 767 instances of the outbreak since 2022 to date with 5 attributes persons who had close contact and worked with poultry farms with confirmed cases. The facts sources cited in figure.4 had been accumulated from the

Centers for Disease Control and Prevention (CDC) records repository [17]. The Weka device model 3.9.5 bundle used to focal point on this learn about was once the ailment as adverse to the virus; hence, we refrained from together with search phrases such as "avian virus/Bird flu".

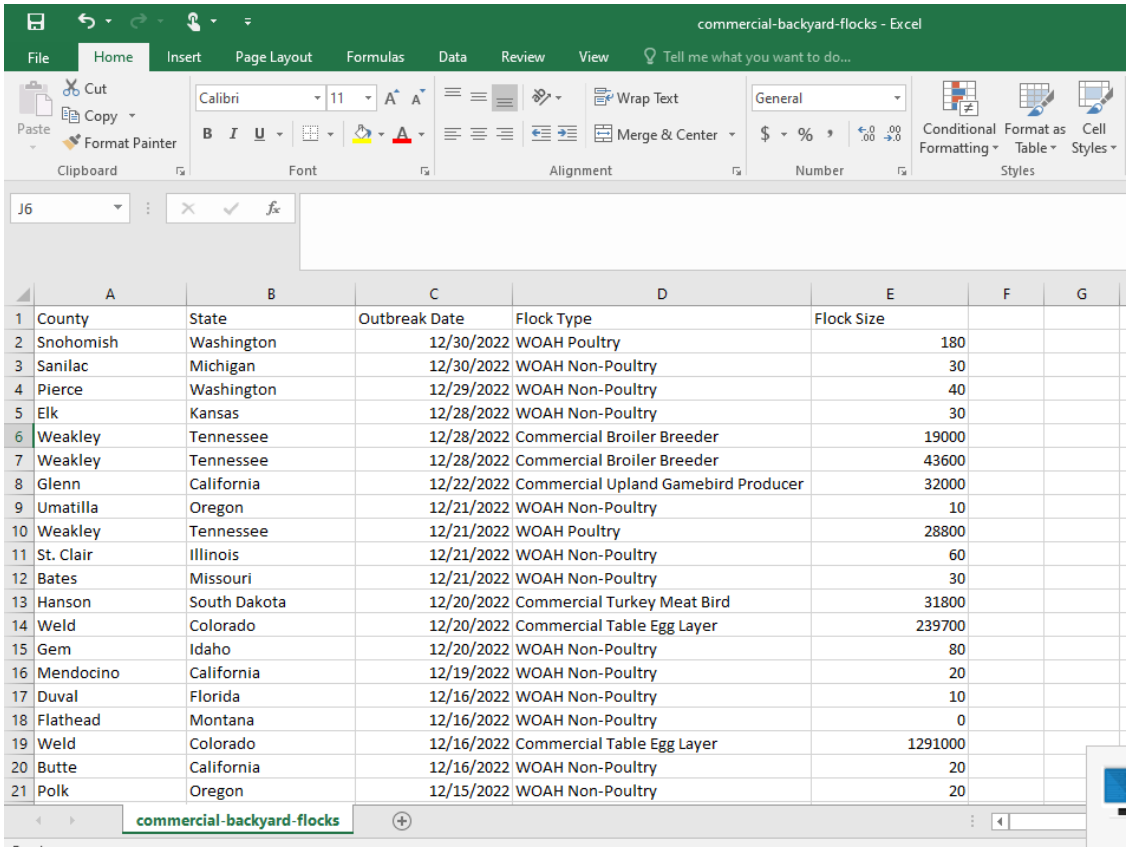

commercial-backyard-flocks - Excel

	A	B	C	D	E	F	G
1	County	State	Outbreak Date	Flock Type	Flock Size		
2	Snohomish	Washington	12/30/2022	WOAH Poultry	180		
3	Sanilac	Michigan	12/30/2022	WOAH Non-Poultry	30		
4	Pierce	Washington	12/29/2022	WOAH Non-Poultry	40		
5	Elk	Kansas	12/28/2022	WOAH Non-Poultry	30		
6	Weakley	Tennessee	12/28/2022	Commercial Broiler Breeder	19000		
7	Weakley	Tennessee	12/28/2022	Commercial Broiler Breeder	43600		
8	Glenn	California	12/22/2022	Commercial Upland Gamebird Producer	32000		
9	Umatilla	Oregon	12/21/2022	WOAH Non-Poultry	10		
10	Weakley	Tennessee	12/21/2022	WOAH Poultry	28800		
11	St. Clair	Illinois	12/21/2022	WOAH Non-Poultry	60		
12	Bates	Missouri	12/21/2022	WOAH Non-Poultry	30		
13	Hanson	South Dakota	12/20/2022	Commercial Turkey Meat Bird	31800		
14	Weld	Colorado	12/20/2022	Commercial Table Egg Layer	239700		
15	Gem	Idaho	12/20/2022	WOAH Non-Poultry	80		
16	Mendocino	California	12/19/2022	WOAH Non-Poultry	20		
17	Duval	Florida	12/16/2022	WOAH Non-Poultry	10		
18	Flathead	Montana	12/16/2022	WOAH Non-Poultry	0		
19	Weld	Colorado	12/16/2022	Commercial Table Egg Layer	1291000		
20	Butte	California	12/16/2022	WOAH Non-Poultry	20		
21	Polk	Oregon	12/15/2022	WOAH Non-Poultry	20		

Figure 4. Avian Influenza Data set
Source: https://www.cdc.gov/flu/pandemic-resources/monitoring/global-monitoring.html

4.2 Processing metadata

The resulting processing collection of source metadata is collected from the WHO Data repository. It is structured data consisting of 767 instances and 5 attributes. We perform the following operations to harmonize all metadata entries. Classifying metadata using the J48 algorithm, Selecting the canonical attribute and predicting the attributes. Here, the dataset was analysed with more than 700 metadata entries and 5 segments such as Country, State, Outbreak date, Flock type and size of the flock.

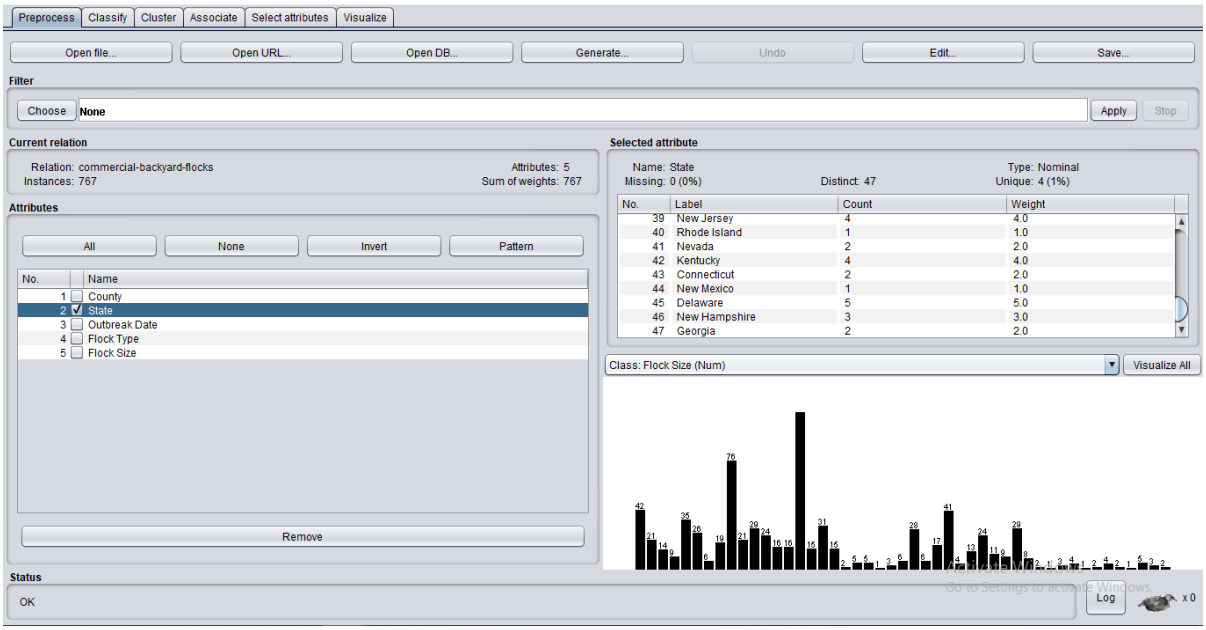

Figure 5. Statewide-data preprocessing

We applied the CSV data using the Weka tools. We considered the country of the state-wise and date-wise outbreak i.e mentioned in the following figure 5 and 6. To identify future predictions of the vulnerability of avian flu, two attributes of the database have been selected for the trial. Next, the statistics set has manually assessed all recognized values as practicable randomized output values to decide their genuine cost with the cross-validation method. The root mean square error (RMSE) and root relative square error (RRSE) on hold-out records are then chosen as the prediction value. The utilized statistics set is really useful due to the fact the equal algorithm can have exclusive efficiencies on different records attributes. To consider the dataset, we used a check pattern and imply mean and median as overall performance metrics.

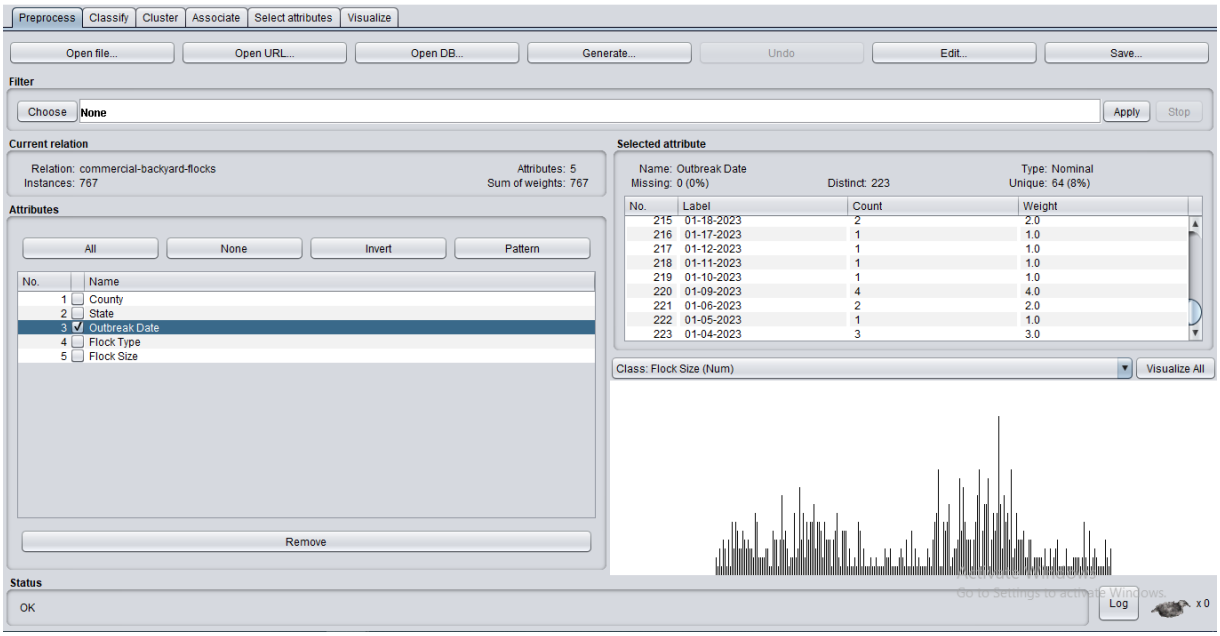

Figure 6. Date of out-break preprocessing result

4.3 Prediction

There are now H5N1 bird flu viruses used to infect wild birds and poultry around the world. These viruses differ genetically from earlier variants. As the dominant subtype of HPAI H5, these viruses emerged in the fall of 2021. Viruses caused by these viruses are causing outbreaks in a number of countries. A study conducted earlier found H5N1 to be more susceptible than covid-19. In order to identify predictions for avian flu, a linear regression prediction algorithm and machine learning techniques were applied. This article includes a detailed description of the avian flu data set from the WHO repository. Using Linear Regression and J48 models, avian flu vulnerability can be predicted. The World Health Organization's web portal provides training data that can be used for testing. This interface made it possible to run all algorithms simultaneously and compare their results.

The classifier models were able to correctly identify and predict the value based on the trained data sent along with the actual data set. Studies of the use of the model have been carried out in sociology, biostatistics, medicine, psychology, econometrics, and marketing, and are frequently in contrast with research on the use of computer learning. These classification techniques have many benefits in addition to being powerful and accurate. J48 classifiers are built independently using bootstrap aggregation using a selected sample of the training data. However, the J48 method continues to dominate the field of predicting with a high level of certainty. On the basis of the J48 classifier model validation results, a measure of overall performance was calculated.

In the early studies, only a few studies discussed the possibility that the avian flu might cause a new pandemic. Besides diagnosing and predicting diseases, the Weka tool can also be used for other purposes. Therefore, medical practitioners and researchers can expand their research activities in an efficient and cost-effective manner. In addition to solving clinical research problems, Weka machine learning tools apply to solve other problems too. Another benefit of using Weka for disease

prediction is that it can diagnose any type of disease easily with the required datasets.

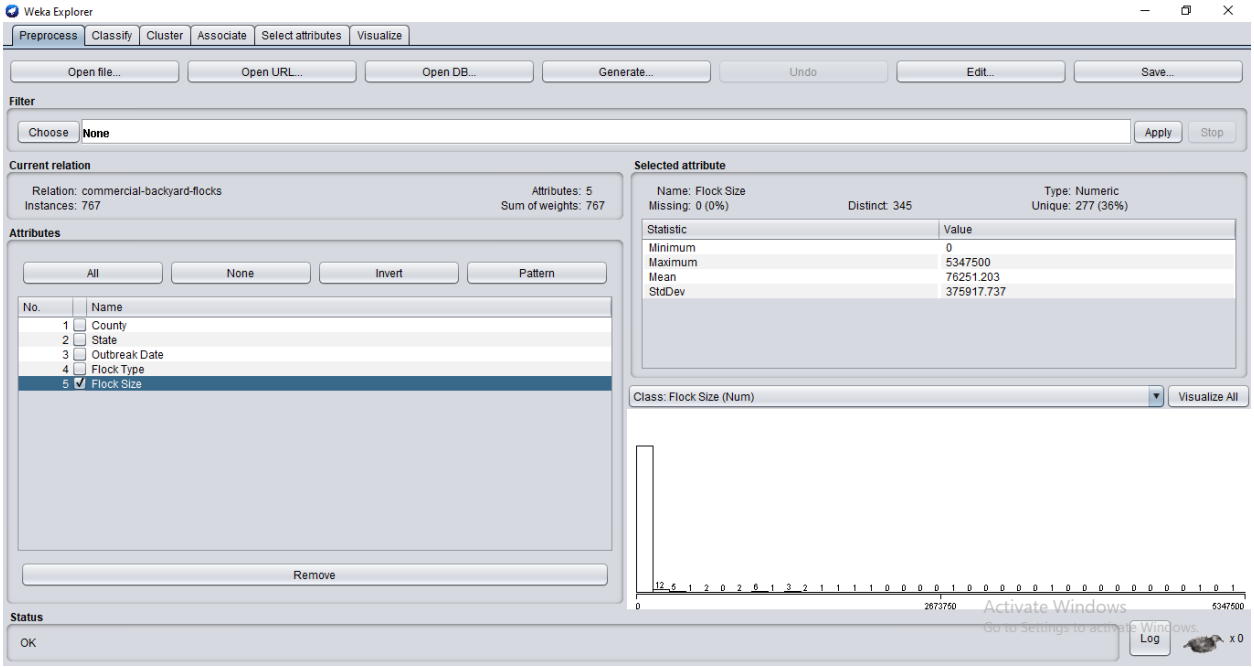

Figure 7. Mean and Median of Flock size

Normally, prediction variables are identified using the J48 classifier based on the values of mean, standard deviation, and linear regression that are shown in figure 7. ROC curves were calculated to predict avian flu. Additionally, we calculated accuracy (AC), Kappa statistics, root-mean-squared errors (RMSE), and relative absolute errors (RSE).

In order to build classifier models, Weka (Version 3.9.5) was used. Users can use Weka tools to perform their tasks in a desired manner by using graphical user interfaces and visualizations. Between December 2022 and January 2023, 767 instances and 5 attributes were collected.

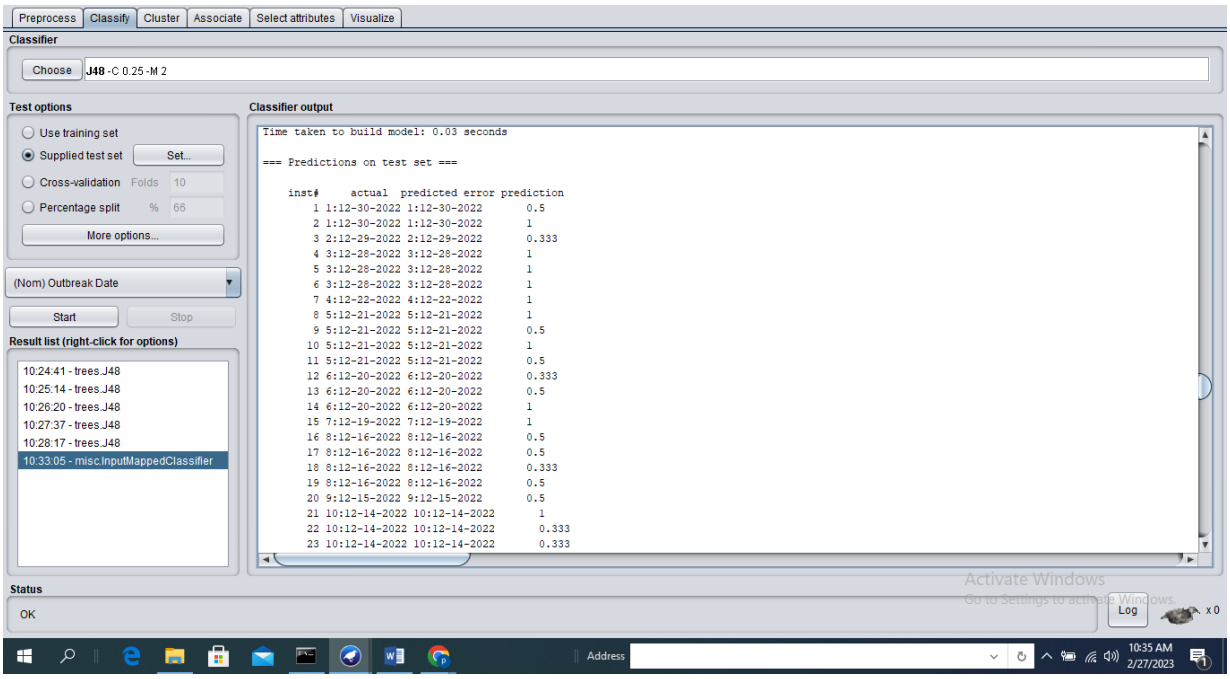

Figure 8. Prediction test using j48 classifier

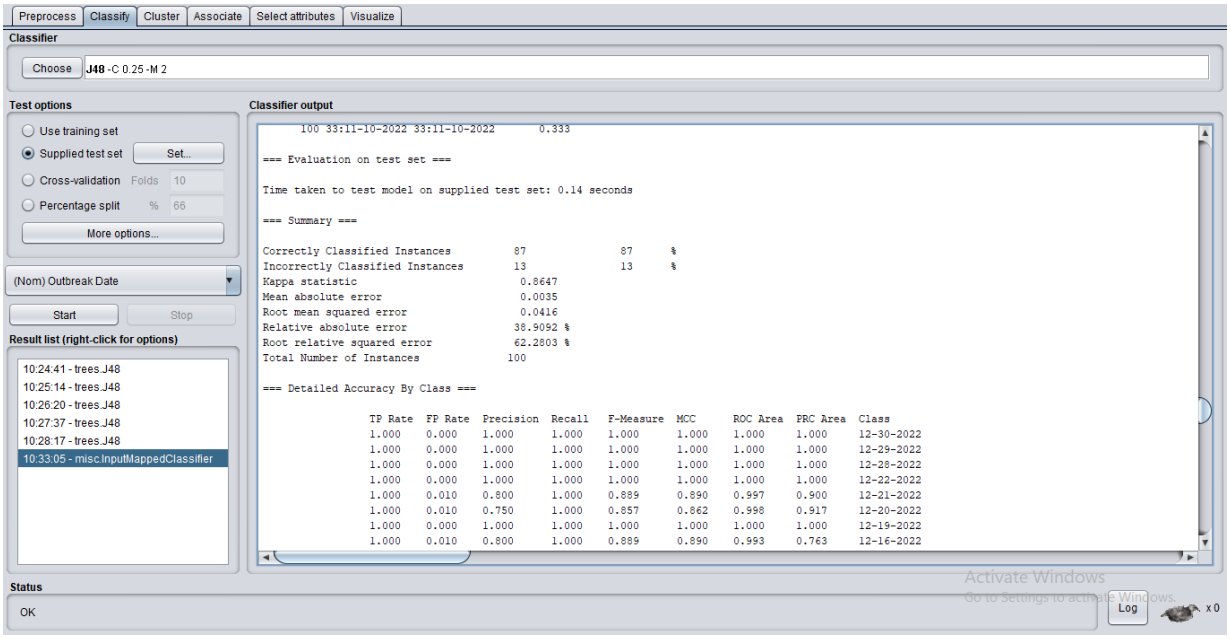

Figure 9. Classification of instances

4.4 Test Result

As per the above test model mentioned above in figure 8, processing the data using the J48 classifier algorithm and in figure 9, shows that the probability value of kappa statistics indicates a 0.8647 positive rate and mean absolute error (MAE) rate is 0.0035, root mean squared error (RMSE) is 00.0416, relative absolute error (RAE) rate is 38.9092 and root relative squared error (RRSE) is 62.2803. In general, a relative absolute error rate of more than 10% is considered acceptable. Based on the data set to be used in the machine learning algorithm, if the

value is between 1 and 10%, more attention is required for the problem.

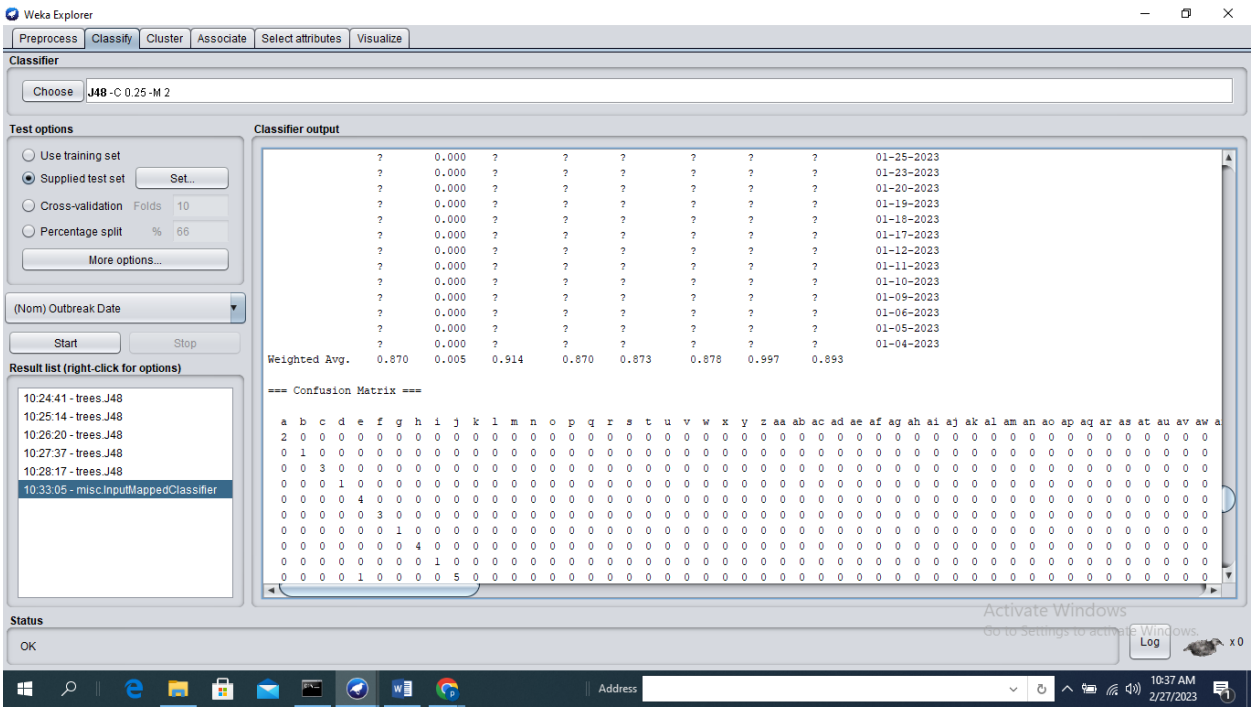

Figure 10. Weighted average of prediction result

The weighted average of the Receiver Operating Characteristic Curve (ROC) value is 0.997. It is appropriate to use the ROC when observations are evenly distributed between classes, while the precision-recall curve (PRC) is appropriate when datasets are imbalanced. As shown in figure 10, the weighted average value of PRC is 0.893. Figure 11 shows the values of the actual predicted and error prediction values that indicate the possible outcome of the next pandemic. As per artificial intelligent tools and based on the given data, the next pandemic from avian flu is dilution.

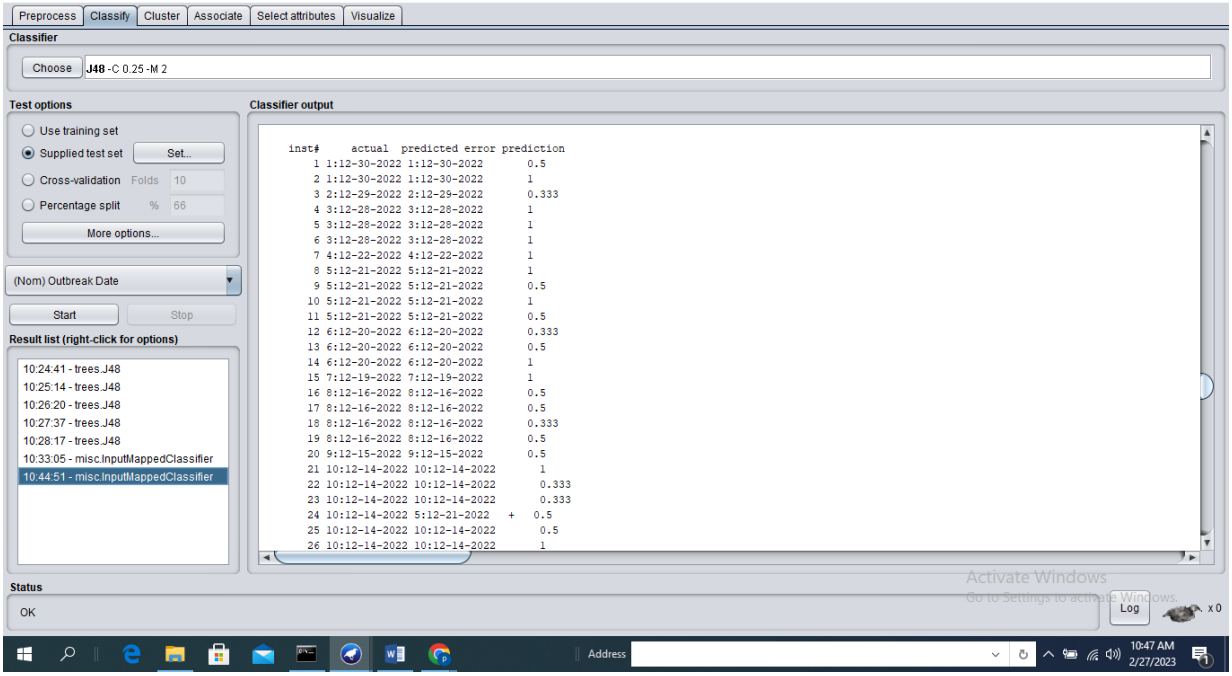

Figure 11. Actual predicted error prediction

5. Guidelines for preventing influenza

The best way to observe wild birds is from a distance and avoid direct contact whenever possible. Avian influenza (flu) A virus can be transmitted from wild birds even if they don't appear ill. Birds whose health appears to be in danger or those that have already died should never be handled unprotected [17].

- ❖ Use safety gear, such as gloves, an N95 respirator, or a surgical mask.
- ❖ After coming into contact with birds, refrain from touching your mouth, nose, or eyes.
- ❖ Steer clear of areas that could be covered in feces, mucus, or saliva from wild or domestic birds.
- ❖ After frequently handling birds, always wash your hands with soap and water.
- ❖ Before handling domestic poultry and after handling wild birds, take care and change into new clothing.
- ❖ Frequently wash your hands with soap, and alcohol-based hand sanitizer.
- ❖ If at all possible, stay away from going to poultry farms, bird markets, or other locations where live chickens are raised, kept, or sold.
- ❖ Avoid consuming any poultry items that are raw or undercooked, and wash your hands after handling uncooked poultry.
- ❖ Maintain a clean and hygienic environment [17].

6. Discussion

As per the evaluation model, it has been trying to identify the level of risk that will bring possible outbreak transmission among close contacts with poultry farms and pet animals. This study provided further evidence that people who have close contact with animals such as older aged people, middle-aged people and household contacts were infected taken into account of this research. The symptomatic cases with abnormal expectoration symptoms had a higher transmission capacity that should treat with immediate medical assistance. As a result of the report, control measures have

been evaluated and global responses have been guided based on evidence. As per the derived dataset from the resource pool and present scenario, asymptomatic persons have a lower risk of transmission to others. Therefore, it is significant to focus on symptomatic persons, in order to avoid critical conditions and higher death rates.

Therefore, it is of great public health significance to strictly monitor the closer contact of those who are working on poultry farms and close contact with the animals. After, the new pandemic, the WHO gave wonderful guidelines that bring massive movement returning to the workplace and the school. Guidance of self-protection and active isolation of close contact with infected animals/people should be continuously followed. This study is limited by the small sample size and limited data attributes on the prediction algorithm. Large-scale multicenter and clinical studies are needed to cross-verify these findings of the machine learning-based research tool.

7. Conclusion

Public health and healthcare systems, as well as providers of essential community services, will be challenged by an influenza pandemic, regardless of its severity. Global pandemic response capacity has been increased by the WHO. Identifying a novel influenza A virus' pandemic risk, evaluating the risk and potential public health impacts, understanding the possible progression of the virus, creating a vaccine-candidate virus that can be used in a pre-pandemic scenario, and evaluating the severity and transmissibility so that public health interventions can be informed. The study has a few notable limitations. Firstly, the data do not indicate the course of the disease, so we cannot fully understand the course of the disease. Furthermore, because of the low incidence of people with virus-related illnesses and high viral mortality (20 to 30% of infected people), logistic regression analysis was used instead of direct proportional risk modeling. In addition, there may be a recall bias among the source cases and secondary cases regarding symptoms at onset. Data on large numbers of moving animals is also lacking in information regarding its accuracy and use. Through the use of datasets, we were able to achieve high validation rates for our model. According to our linear regression classifier, we were able to achieve an accuracy of 86.37%. The dataset we used in our model was fixed. This research study concluded that the avian flu won't cause panic the same way as COVID-19, so governments and people shouldn't worry. From the learn about of given data, we have concluded, the subsequent pandemic from avian flu is weakening. To improve and further investigate our probability findings, we plan to add other Artificial Intelligence techniques such as deep learning techniques in the near future.

References

[1] Elisabeth Mahase, “H5N1: Do we need to worry about the latest bird flu outbreaks?”, BMJ 2023; 380 Page 401, February 8, 2023, doi: https://doi.org/10.1136/bmj.p401.

[2] Jeffery K., Taubenberger, David M, Morens, “H5Nx Panzootic Bird Flu—Influenza’s Newest Worldwide Evolutionary Tour”, Emerg Infect Dis, February; 23(2), 2017, 340–342, doi: 10.3201/eid2302.161963.

[3] Tingting Wang, Lei Duan, Guozhu Dong, Zhifeng Bao, “Efficient Mining of Outlying Sequence Patterns for Analyzing Outlierness of Sequence Data”, ACM Transactions on Knowledge Discovery from Data, Vol. 14, No. 5, 2020.

[4] Barbara C. Canavan, "Opening Pandora's Box at the roof of the world: Landscape, climate and avian influenza (H5N1)", Acta Tropica, Pages 93-101, Volume 196, August 2019.

[5] Jennifer Abbasi, "Bird Flu Has Begun to Spread in Mammals—Here's What's Important to Know", JAMA. Published online February 8, 2023, doi:10.1001/jama.2023.1317.

[6] Dr Prakash Kuppuswamy, Dr Saeed Q. Al-Khalidi Al-Maliki, Mohammad Khamruddin, Syed Ameen Saadullaha Hussaini Quadri, Ahamed Ali Shaik Meeran, "The COVID-19: Saudi Government's Comprehensive Guide to Safety Measures Analysis with Big Data", Journal of Pharmaceutical Negative Results Vol.13, Special Issue 02, 2022.

[7] Kobayashi, Jung, Linton, "Communicating the risk of death from novel coronavirus disease (COVID-19)", Journal of Clinical Medicine, Vol. 9, Page 580, 2020, https://doi.org/10.3390/jcm9020580.

[8] Cuiying Lin, Yajuan Guo, Mengmeng Zhao, Mi Sun, Fang Luo, Longhua Guo , Bin Qiu, Zhenyu Lin, Guonan Chen, "Highly sensitive colorimetric immune sensor for influenza virus H5N1 based on enzyme-encapsulated liposome", Analytica Chimica Acta, Volume 963, , Pages 112-118, 22 April 2017.

[9] Andrew Lakoff, "A fragile assemblage: Mutant bird flu and the limits of risk assessment", Social Studies of Science Vol. 47(3) 376–397, 2017. DOI: 10.1177/0306312716666420.

[10] Raj G, Jayanthi, "IoT-based real-time poultry monitoring and health status identification", 2018 11th International Symposium on Mechatronics and its Applications (ISMA), Sharjah, United Arab Emirates, 2018, pp. 1-7, doi: 10.1109/ISMA.2018.8330139.

[11] Samantha J. Lycett, Florian Duchatel, Paul Digard. Lycett SJ, Duchatel F, Digard P., "A brief history of bird flu", Phil. Trans. R. Soc. B 374: 20180257, 2019, http://dx.doi.org/10.1098/rstb.2018.0257.

[12] Ali Javed, Byung Suk Lee, Donna M. Rizzo, "A benchmark study on time series clustering", Machine Learning with Applications 1, 2020, www.elsevier.com/locate/mlwa.

[13] Saadh M.J, Aldalaen S.M., "Inhibitory effects of epigallocatechin gallate (EGCG) combined with zinc sulfate and silver nanoparticles on avian influenza A virus subtype H5N1", European Review for Medical and Pharmacological Sciences Vol. 25: 2630-2636, 2021.

[14] Mirza Imran Shahzad, Muhammad Arslan, Hina Ashraf, Muhammad Naeem Iqbal, "Computational Screening of Bird Flu Viral Strains to Find Conserved Epitopes for Vaccine Development", Montenegrin Journal of Economics, Volume 17, Number 3, September 2021.

[15] Dr. Saeed Q Al-Khalidi Al-Maliki, Dr. Prakash Kuppuswamy, Dr. Rajan John, Dr. Nithya Rekha Sivakumar, "COVID-19: An Efficient Big Data Analytics for SARS-CoV-2 Mutations Prediction: A Machine Learning Approach", Indian Journal of Science and Technology, Volume: 15, Issue: 21, Pages: 1022-1031, 2022. DOI: 10.17485/IJST/v15i21.374.

[16] Tesia Bobrowski, Cleber C Melo-Filho, Daniel Korn, Vincicius, M. Alves, Konstantin Popov, Scott Auerbach, Charles Schmitt, Nathaniel, Alexander tropsah, "Learning from history: do not flatten the curve of antiviral research", Drug Discovery Today, Vol.25, Issue 9, Pages 1604-1613, September 2020.

[17] Centre for Disease Control and Prevention (CDC), https://www.cdc.gov/flu/avianflu/inhumans.htm Accessed on 10/3/2023.

[18] World Health Organisation, https://www.who.int/emergencies/disease-outbreak-news/item/2023-DON445 Assessed on 10/3/2023.

[19] Reina Yamaji, Magdi D. Saad, Charles T. Davis, David E. Swayne, Dayan Wang, Frank Y.K. Wong, John W. McCauley, J.S. Malik Peiris, Richard J. Webby, Ron A.M. Fouchier, Yoshihiro Kawaoka, Wenqing Zhang, "Pandemic potential of highly pathogenic avian influenza clade2.3.4.4 A(H5) viruses", John Wiley & Sons Ltd.Rev Med, February, 2020. https://doi.org/10.1002/rmv.2099.

[20] Sisi Luo, Zhixun Xie, Zhiqin Xie, Liji Xie, Li Huang, Jiaoling Huang, Xianwen Deng, Tingting Zeng, Sheng Wang, Yanfang Zhang & Jiabo Liu, "Surveillance of Live Poultry Markets for Low Pathogenic Avian Infuenza Viruses in Guangxi Province, Southern China, from 2012–2015", Scientific RePorTS, Nature.com, | 7: 17577 | DOI:10.1038/s41598-017-17740-0

دراسة احتمالية تفشي جائحة قادم ناشئ عن إنفلونزا الطيور H5N1 باستخدام مناهج التعلم الآلي

براكاش كوبسوامي ١ ، دكتور سعيد قاسم يحيى الخالدي المالكي ٢ ، دكتور راجان جون ٣ ، الدكتورة شانموجا سوندارام مارابام ٤ ، فيجايا فارشيني براكاش ٥

١ قسم هندسة شبكات الحاسوب ، كلية علوم الكمبيوتر وتكنولوجيا المعلومات ، جامعة جازان ، المملكة العربية السعودية

٢ قسم علم المعلومات ، جامعة الملك خالد ، أبها ، المملكة العربية السعودية

٣-قسم علوم الحاسب ، كلية علوم الحاسب وتكنولوجيا المعلومات ، جامعة جازان ، المملكة العربية السعودية

٤ قسم علوم الحاسب ، كلية علوم الحاسب وتكنولوجيا المعلومات ، جامعة جازان ، المملكة العربية السعودية

٥ طالب PG ، كلية الفنون Palanisamy، Erode ، تاميل نادو ، الهند.

الملخص

يتسبب فيروس إنفلونزا الطيور (AI)بشكل شائع في أنفلونزا الطيور في أنواع الدواجن والثدييات. في السنوات العشرين الماضية ، كانت إنفلونزا الطيور من أكثر الفيروسات المسببة للأمراض عرضة للخطر في العالم ، لا سيما في العالم النامي ، حيث أبلغت ٦٣ دولة عن حالات إصابة. هذا المعدل المرتفع للطفرات لا يجعل الفيروس شديد الإمراض فحسب ، بل يجعله أيضًا عرضة للهجوم. تُعرِّف منظمة الصحة العالمية (WHO)أنفلونزا الطيور بأنها واحدة من أكثر الأمراض الحيوانية انتشارًا في كل العصور نظرًا لوجودها في الطيور ومزارع الديوك. يمكن أن ينتج جائحة إنفلونزا أكثر حدة من الأنفلونزا الأخرى عن انتقال فيروس أنفلونزا الطيور بين البشر. الهدف من هذه الورقة هو تحليل الجدل العام الأخير حول انتقال أنفلونزا الطيور شديدة العدوى بين الحيوانات. هناك رابط ضعيف بين المجموعة بسبب الالتزام بالتأهب للجائحة. تساعدنا أداة الذكاء الاصطناعي في تحليل احتمالية تفشي أنفلونزا الطيور التي تسبب الوباء التالي ، مما يؤدي إلى تحديد المخاطر والمجالات الملحة. جمعنا مجموعات بيانات من مستودع بيانات منظمة الصحة العالمية لهذه الدراسة. طريقتنا المختارة في هذه المقالة البحثية هي المصنف J48 ، وهو من بين أفضل خوارزميات التعلم الذكي الاصطناعي لتصنيف البيانات ومراقبتها باستمرار من أجل التنبؤ بجائحة إنفلونزا الطيور في المستقبل القريب. أصبح الاكتشاف المبكر للأمراض ممكنًا من خلال التكنولوجيا القائمة على التعلم الآلي ، وفي حالة حدوث جائحة ، يمكن للحكومة والسلطات الصحية اتخاذ الإجراءات على الفور.

الكلمات المفتاحية: H5N1 ، إنفلونزا الطيور ، إنفلونزا الطيور ، الوباء ، التنظيم ، خوارزمية التعلم الآلي ، الذكاء الاصطناعي ، إلخ .

A Flexible Linear-To-Circular GNSS Polarizer Receiver Based On Conducting Fabric For KSA

Hidayath Mirza[a], Nishat Sultana[b], Rais Ahmad Sheikh[a,c], Bilquis Banu[d]

[a]Department of Electrical Engineering, College of Engineering, Jazan University, Jazan University, Kingdom of Saudi Arabia.

[b]Department of Business Adminstration, Applied College, Jazan University, Jazan Kingdom of Saudi Arabia

[c] Advanced Communication Engineering (ACE) CoE, School of Computer and Communication Engineering, Universiti Malaysia Perlis (UniMAP), Pauh Putra, 02600, Arau, Perlis, Malaysia.

[d] Department of Management, Applied College, Jazan University, Jazan University, Kingdom of Saudi Arabia.

Abstract

This article presents a single-layered and single-sided fabric flexible linear-to-circular polarizer that may be used for GNSS/GPS applications that run at 1.57542 GHz and are related to the L1 band. The polarizer is made from a flexible linear-to-circular polarizing fabric. The polarizer was created using a flexible linear-to-circular polarizer that was produced from a fabric with a single face. In contrast to the rear side of the polarizer, which is devoid of any kind of structure whatsoever, the front side of the device features a structure in the shape of perpendicular rectangular strips. In the case of the wavelength in free space, the Unit-cell has dimensions that are, respectively, $0.29\lambda \times 0.255\lambda \times 0.01\lambda$. The operational frequency is centered at about 1.5754 GHz, and the lowest feasible value for the axial ratio that can be achieved is 0.1 dB, which is very close to zero dB. The entire construction can flex, allowing it to be worn as part of the garment. The fractional bandwidth for the 3 dB axial ratio is 1.2544-1.83 GHz, which results in a value of 37.32%. In comparison, the fractional bandwidth for the conversion efficiency spanning 90% is 50.55%, which is (1.1315-1.8971).

Keywords*: GNSS; GPS; L1 band; circular polarization; polarizer; periodic surface; CubeSats, LEO satellites.*

1. Introduction

In 1978, the Global Positioning System (GPS) was launched for military purposes such as spy satellites and communications satellites, as well as to provide satellite-based navigation(Munoz-Martin et al., 2019). GPS was used for remote sensing and measuring the Earth's atmosphere in addition to military applications (Ware et al., 1996; Yunck, Lindal, & Liu, 2003). These days, there has been a sporadic increase all over the world in location, tracking, and navigation. As a result of this, nations have started launching their individual satellites because many of these countries were looking for an alternative to GPS. Satellites like these can be found in sub-orbital, orbital, interplanetary, and, last but not least, intergalactic areas. The Global Navigation Satellite System, also known as GNSS, is comprised of a network of satellites that collaborate provide precise positioning, navigation, and timing information (PNT) on both a national and worldwide scale(Munoz-Martin et al., 2019; Wanhill, Barter, & Molent, 2019; Zavorotny, Gleason, Cardellach, & Camps, 2014). These proliferating aims is to provide accuracy and agility to the user. For instance, BeiDou Navigation Satellite System (BDS) by China uses 35 satellites, Galileo operated by Europe plans to put more than 24 satellites, GLONASS (*Globalnaya Navigazionnaya Sputnikovaya Sistema*, or Global Navigation Satellite System) also uses more than 24 satellites, India Regional Navigation Satellite System (IRNSS) or Navigation Indian Constellation (NavIC) this system uses 7 satellites and last but not least Quasi-Zenith Satellite System by Japan uses 4 satellites and plans to use 7 satellites by 2023(Bonnor, 2014; Subirana, 2020; U.S. Space Force, 2021).

No matter if the satellite is transmitting an uplink or a downlink, the signal is always transmitted in circular polarization (CP). A power divider network with alternating phases is typically required for a CP antenna's two probes, making CP antenna designs quite complicated. In addition, the GNSS signal strength is low and the CP antenna has low gain. It's a result of numerous factors, including the presence of mountainous terrain, foggy climes (like much of Europe), and abundant precipitation (in nations like Malaysia and Indonesia) near the equator. Antenna designers have a frustrating challenge when tasked with creating a high-gain antenna that also has the qualities that make it suitable for use by people who need to wear it.

Alternatively, the linearly polarized antenna can be converted to a CP antenna with the use of a linear to circular polarizer. As this is a pragmatic and realistic approach to circumvent the design challenges of the CP antenna. The subtle nature of the polarizer is that it can be incorporated into a cap or a hat (Hassan & Attiya, 2018). Using a polarizer for converting the linear wave to CP wave idea has been implemented in many but the major drawback was the polarizer is made with a rigid substrate and has multiple layers(Fonseca & Mangenot, 2016; Molero et al., 2019; Munoz-Martin et al., 2019; Ren, Shen, & Li, 2013; Xu, Wang, Qi, Cai, & Cui, 2013a). This makes the integration of the polarizer difficult. In this manuscript, we present a linear to circular polarizing surface made with electro-fabric and felt. The surface is flexible and can be worn by a person. The targeted frequency is an L1 band and the frequency is 1.57542 GHz, this frequency is also used in The Kingdom of Saudi Arabia for GPS location and tracking.

2. Linear-To-Circular Polarizers: Concept and Performance Characteristics

2.1 Requirements of Circular Polarization

Let's assume that the incident wave falling or passing through the polarizer Unit cell is divided into two parties namely the electric field in the *x* direction and the electric field in the *y* direction. In the cartesian system the intensity of the transmitted wave E^t and incidence waves are related to the linear components from the Jones Matrix. They can be rewritten as shown in equations (1) and (2)(Xu, Wang, Qi, Cai, & Cui, 2013b)

.

$$E^i = E_x^i T_x - j\, E_y^i T_y \quad (1)$$

$$E^t = E_x^i T_x - j\, E_y^i T_y \quad (2)$$

The CP wave can be rewritten after solving the Jones Matrix. The subscript presented is + for lefthanded CP and – for righthanded CP.

2.2 Polarization Conversion

The parameter in equation (3) can change any linearly polarized wave to a CP. Using the lefthanded and righthanded co-efficient conversion efficiency can be calculated as mentioned in equation (4).

$$\begin{pmatrix} C_+^t \\ C_-^t \end{pmatrix} = \begin{pmatrix} E_x^t + jE_y^t \\ E_x^t - jE_y^t \end{pmatrix} = \mathbf{T_{cl}} \begin{pmatrix} E_x^i \\ E_y^i \end{pmatrix} \quad (3)$$

$$\eta_{conv} = \frac{(|C_-|^2 - |C_+|^2)}{(|C_-|^2 + |C_+|^2)} \times 100 \quad (4)$$

However, to attain CP the wave needed to have the following conditions to be met.

$$|T_x| = |T_y| \quad (5)$$

$$\Phi_{T_x} - \Phi_{T_y} = 90^0 \quad (6)$$

The ellipticity of the wave determines whether or not it is solely circularly polarized or if it is linearly polarized. If the value of η is equal to zero, then it is purely linearly polarized, and if is equal to forty-five degrees, then it is purely circularly polarized. If η is positive then the wave is lefthanded, if the η is negative then the wave is righthanded.

$$\eta = \tan^{-1}\left(\frac{|C_+| - |C_-|}{|C_+| + |C_-|}\right) \quad (7)$$

3. Polarizer Design and Operation Principles

An electromagnetic full-wave solver is used in the design and optimization of each component of the Unit cell. In the directions, *x* and *y* of a Unit cell, the boundary condition that is applied is an infinite boundary, whereas the boundary that is specified in the *z* direction is an open border. To be more accurate, Unit cell boundary conditions for the *Xmin*, *Xmax*, *Ymin*, and *Ymax* directions while leaving the *Zmin* and *Zmax* directions unbounded(H. Mirza, Soh, et al., 2018).

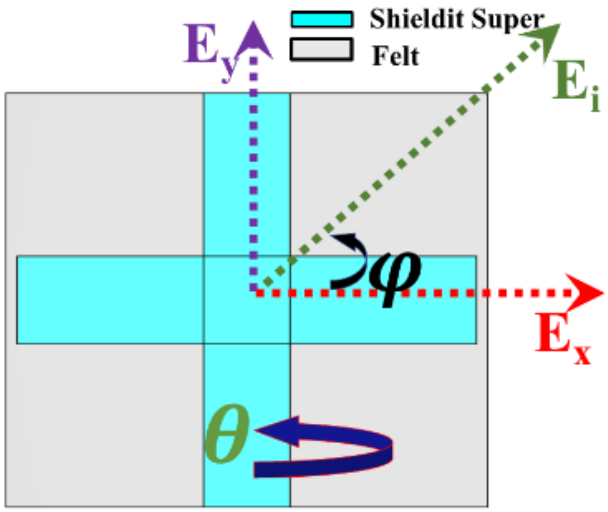

Figure. 1 Unit cell with incidence wave with electric field components in *x* and *y* directions.

Floquet ports have been added in the *z*-direction., and a numerical result of T_x and T_y has been computed using equations (1), (2), and (3) by utilizing the inbuild function of the CST Microwave Studio with the help of a templated-based processing option that is present in the program.

To get the phase difference of 90º the magnitude of the T_x and T_y, at microwave frequencies, the metallic strips act as the inductive nature to the incidence wave, and the gap between the two-unit cell in a periodic surface act as a capacitive nature for the incidence wave. This notion has been well explained in many articles(A. Munk, 2000; Hossain et al., 2019; H. Mirza, Hossain, et al., 2018; Hidayath Mirza et al., 2018). The phase difference between the elements is 90º. The inductance and capacitance values in the unit cell needed to be optimized and tuned crucially to achieve the CP wave. As observed in Figure 2(a).

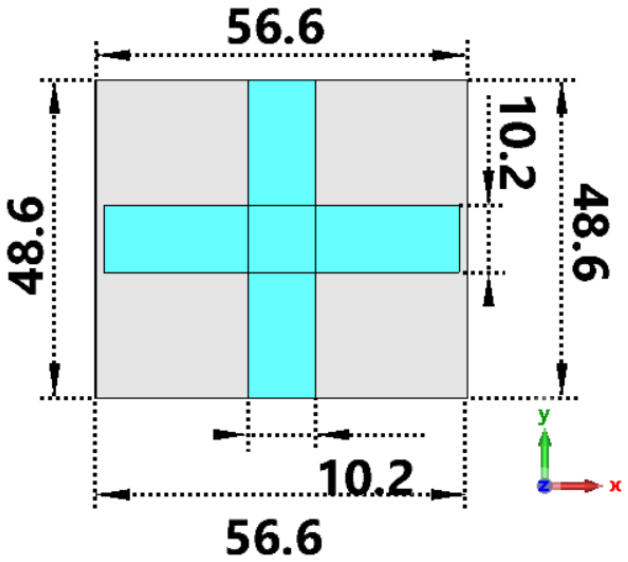

(a)

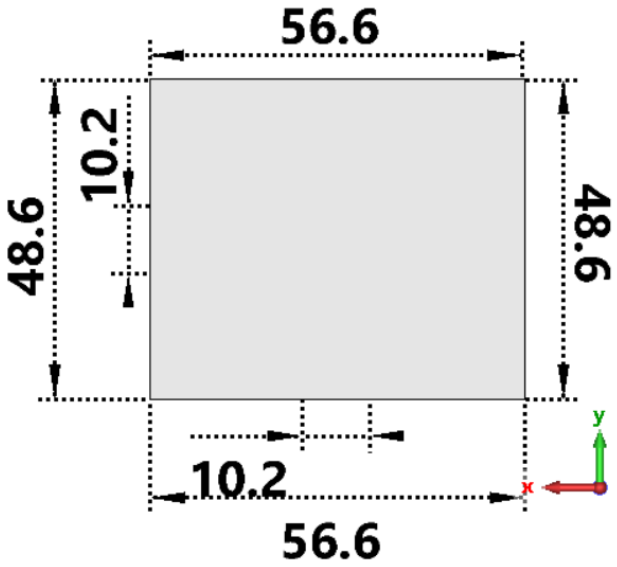

(b)

Figure. 2, (a) Shows a front view of a polarizer, (b) is a back perspective of the polarizer.

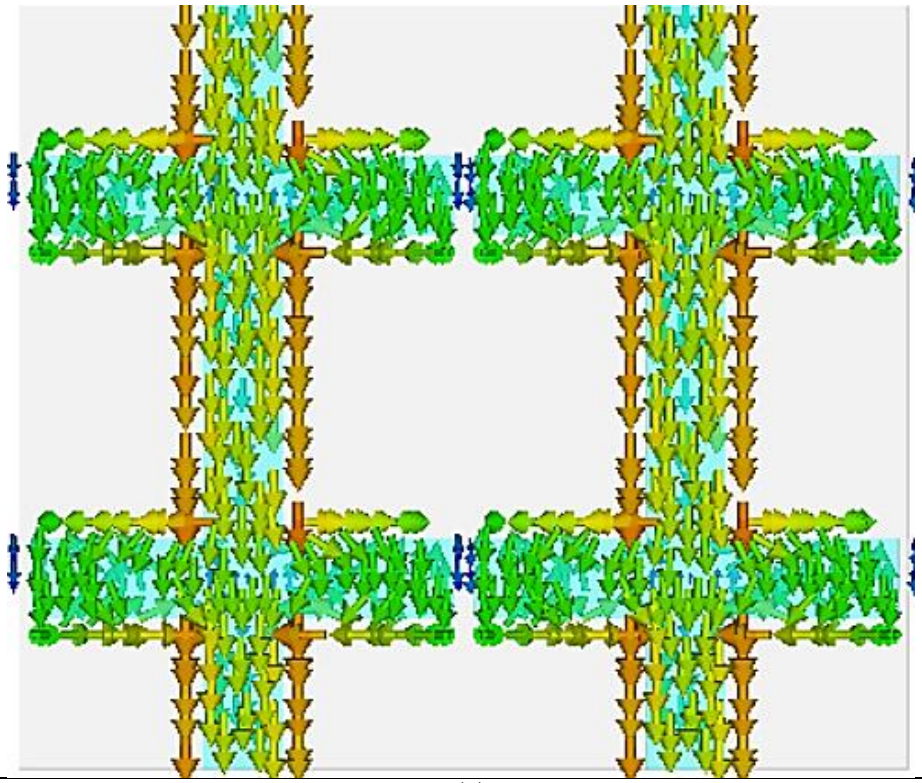

(a)

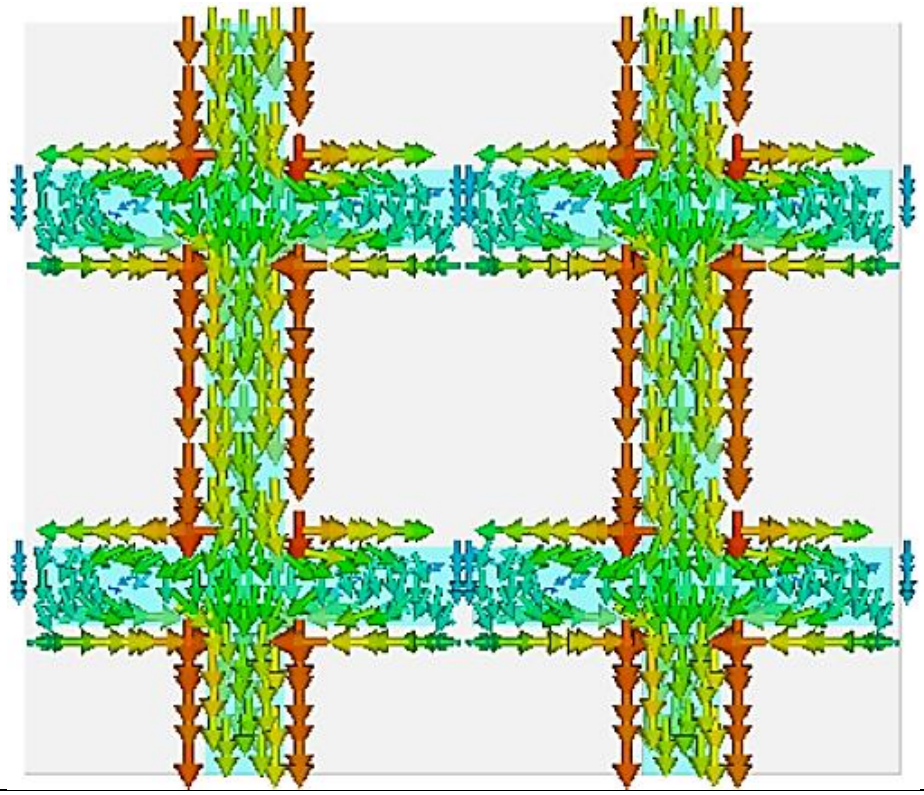

(b)

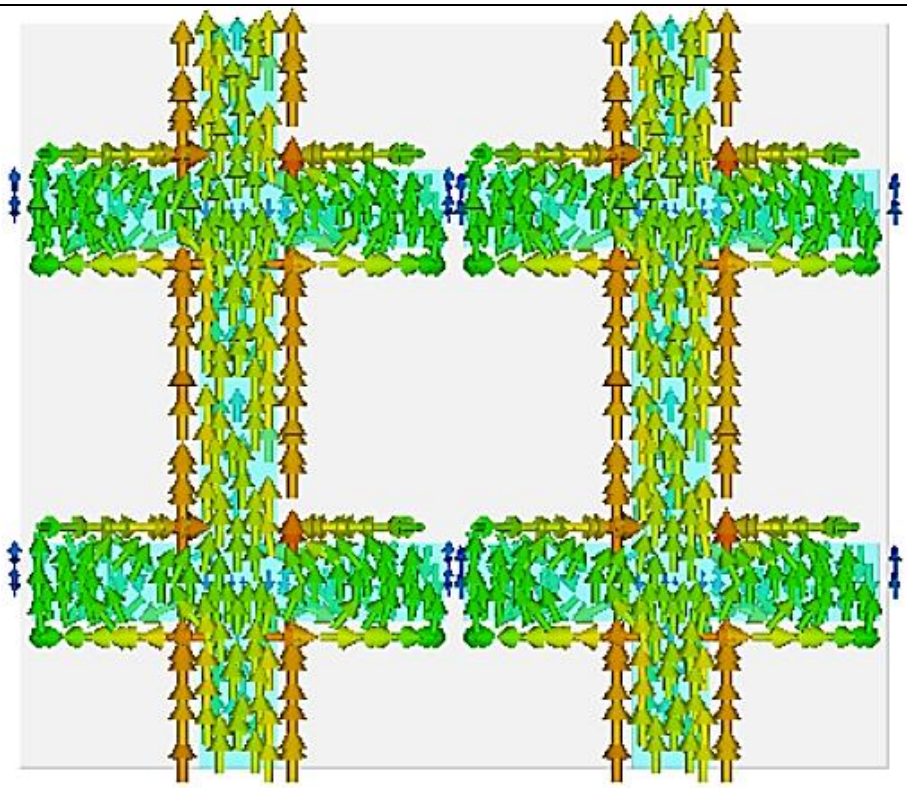

(c)

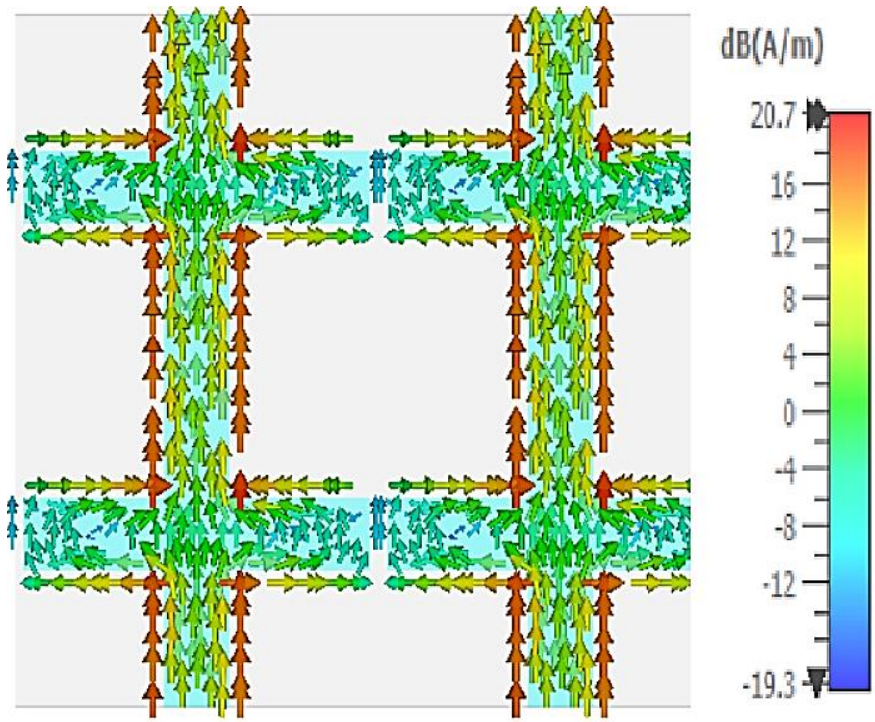

(d)

Figure. 2 Depicts the *x*-polarized wave surface current (a)0º (b)90º, (c)180º and (d)270º

For the *x*-polarized wave Figure 2 (a), (b), (c), and (d), it is possible to detect that only the vertical strip is actively having surface current density for various phases spanning from 0 degrees to 270 degrees. This may be seen by looking at the vertical strip. In contrast, the surface current along the horizontal strip is almost nonexistent. This indicates that the vertical strip has an inductive influence on the characteristics of the incidence wave it is interacting therewith.

Figures 3 (a), (b), (c), and (d) demonstrate the varied surface currents concerning the distinct phases of the *y*-polarized wave. There are phases ranging from 0 degrees to 270 degrees. It is possible to see that just the horizontal strip is active, or that the amount of the surface current density is high on this strip, and the end of the strip creates a gap when the second unit cell is together. This is something that may be observed. As a result of the wave's incidence, this gap evolves into a capacitance(Mantash & Denidni, 2019b, 2019a).

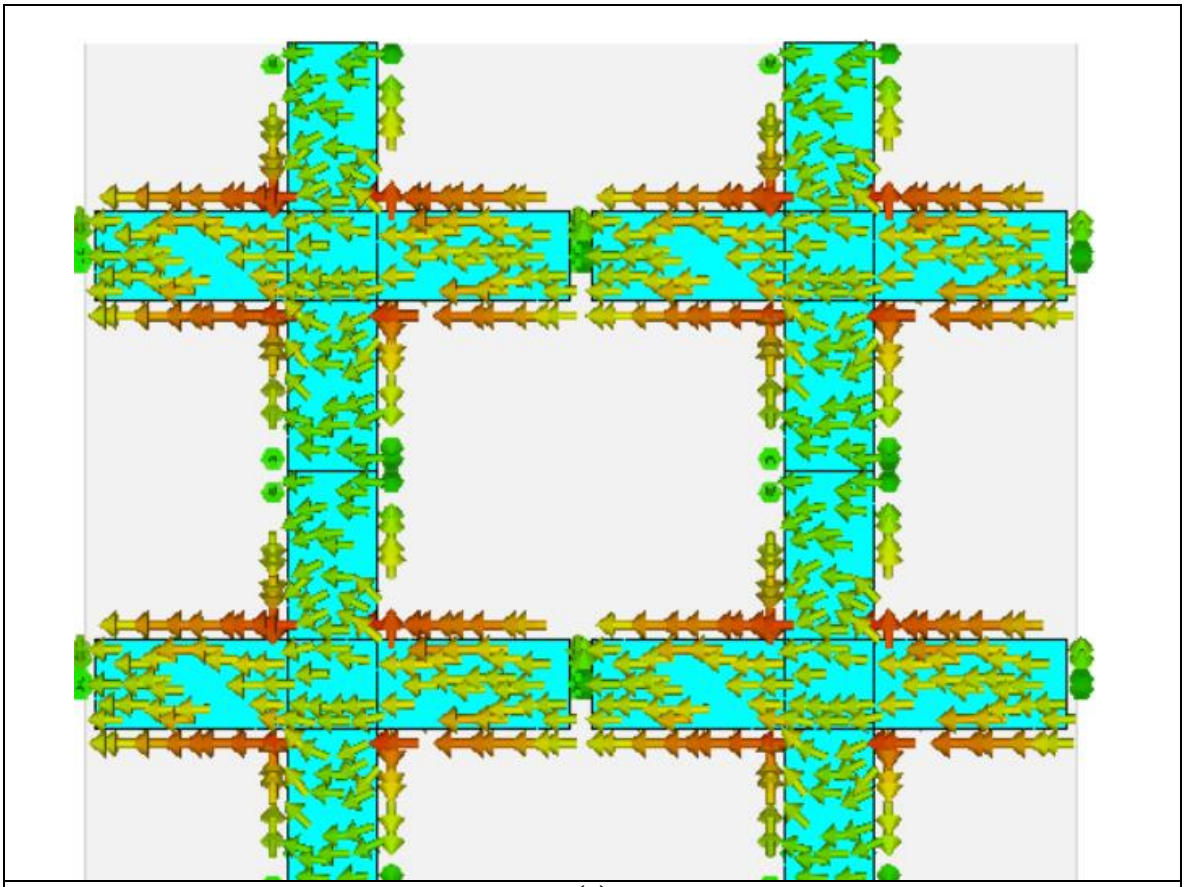

(a)

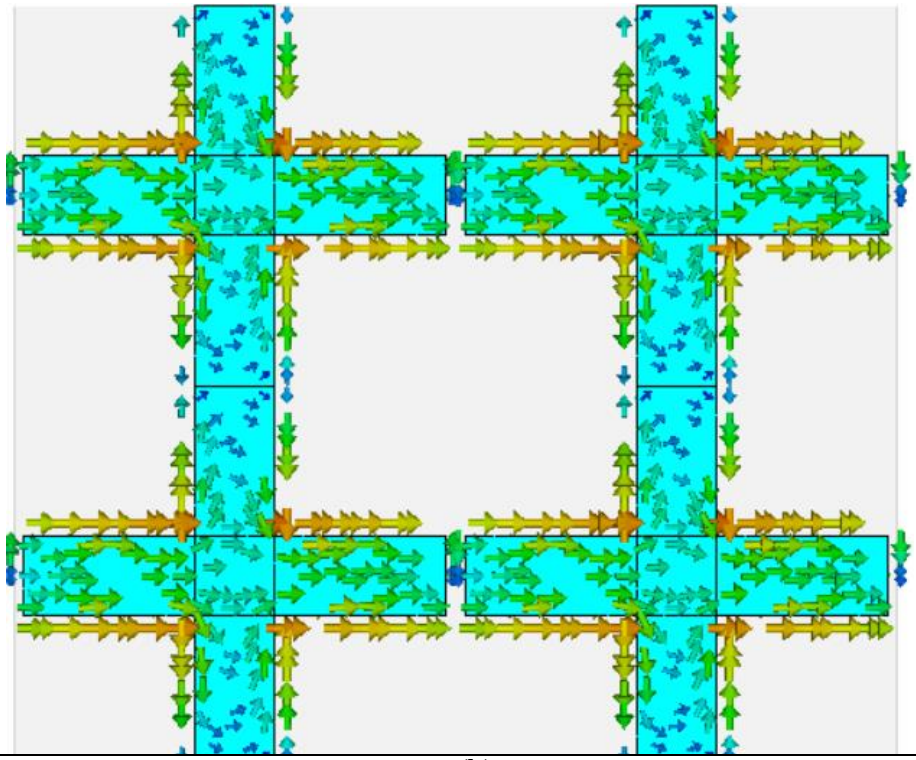

(b)

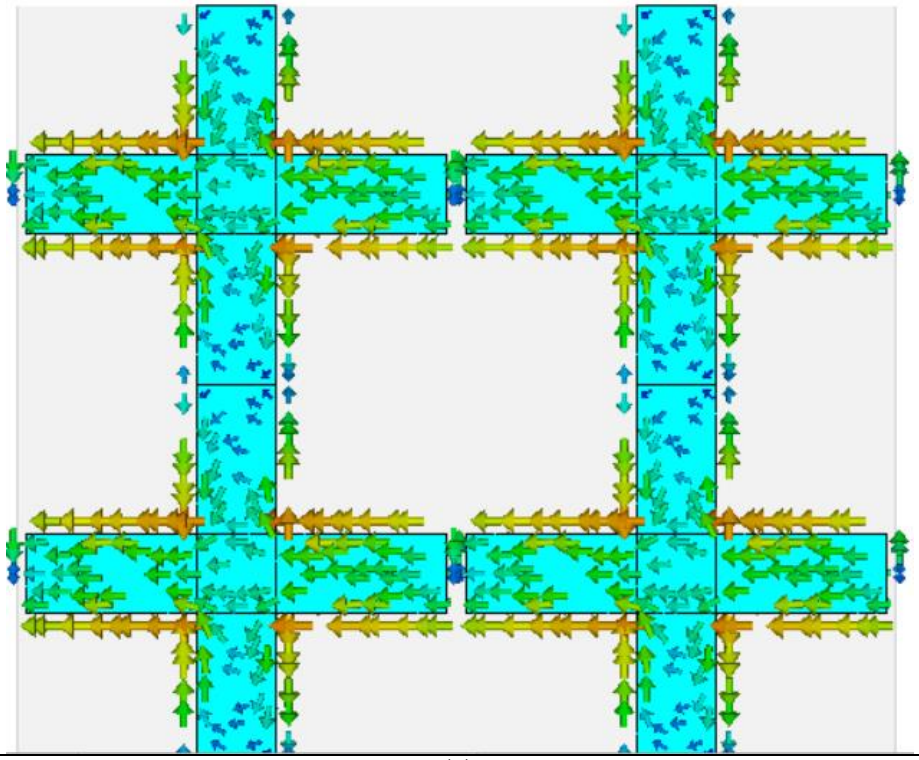

(c)

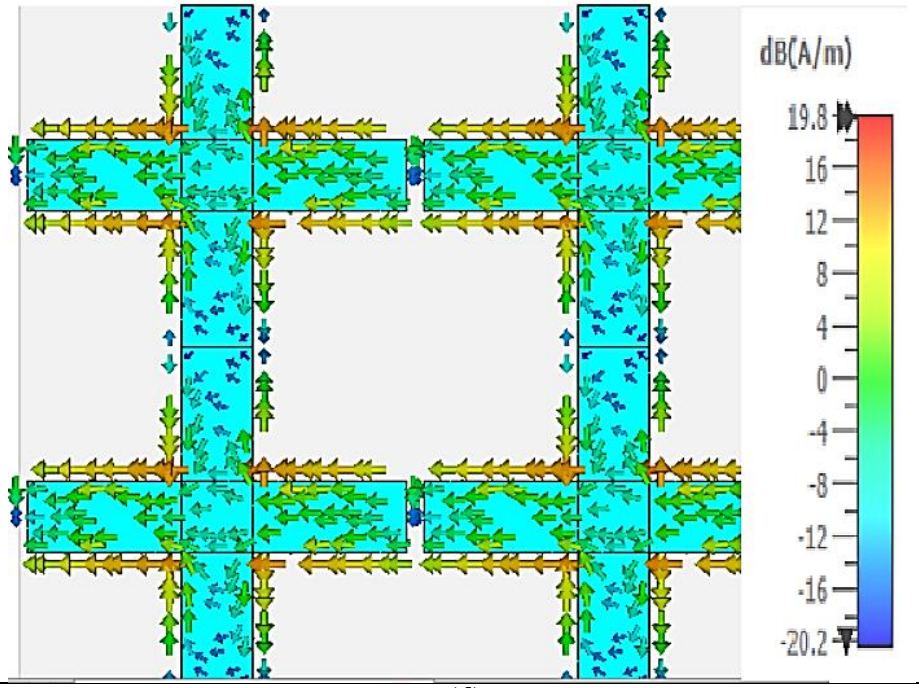

(d)

Figure.3 Shows the *y*-polarized wave surface current (a)0º, (b)90º, (c)180º and (d)270º

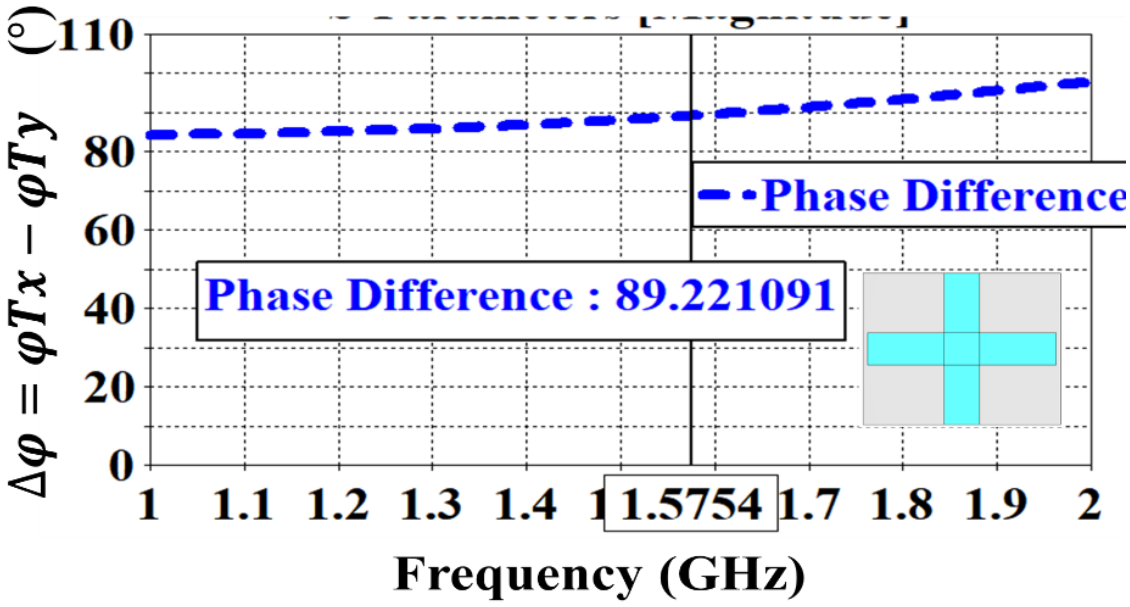

Figure. 4 Phase difference of the two electric fields

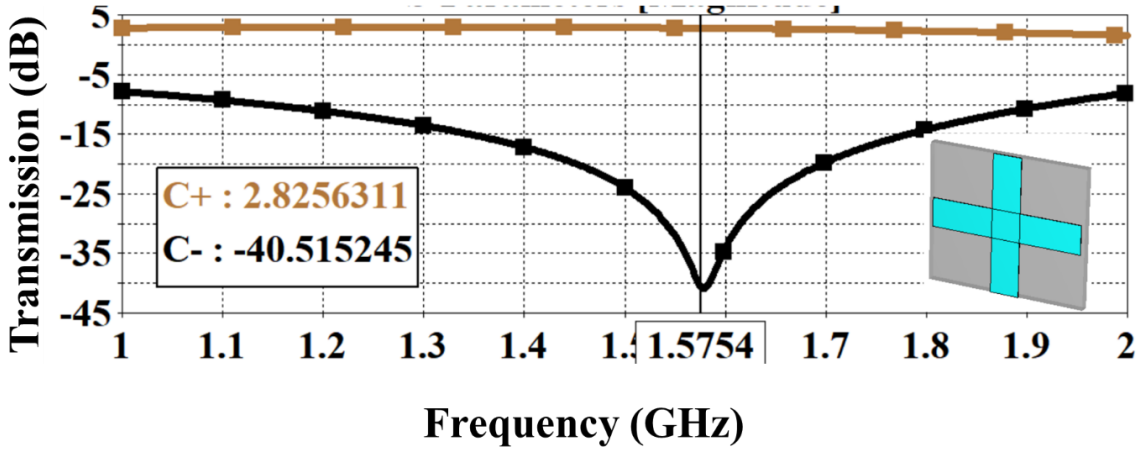

Figure. 5 Transmission of reflection coefficients of the two electric fields

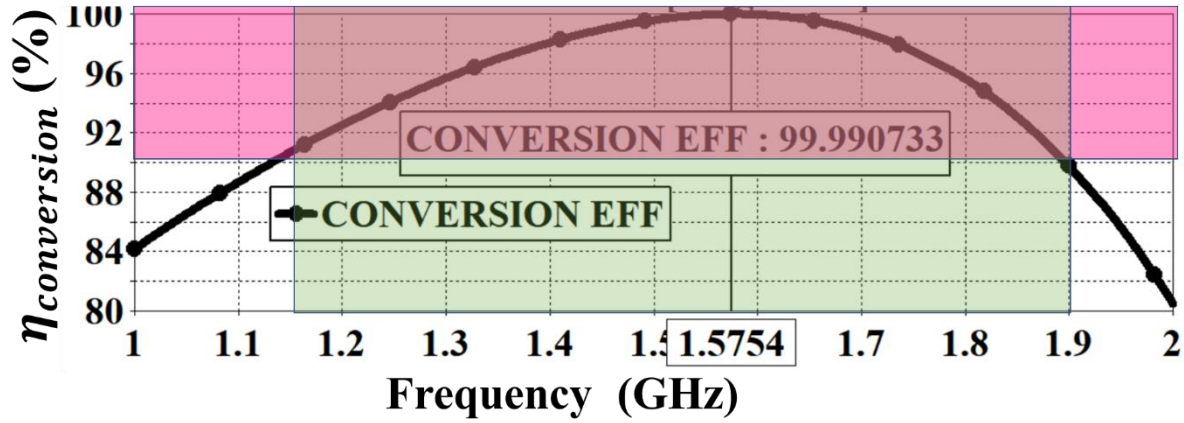

Figure. 6 Conversion efficiency of the unit cell

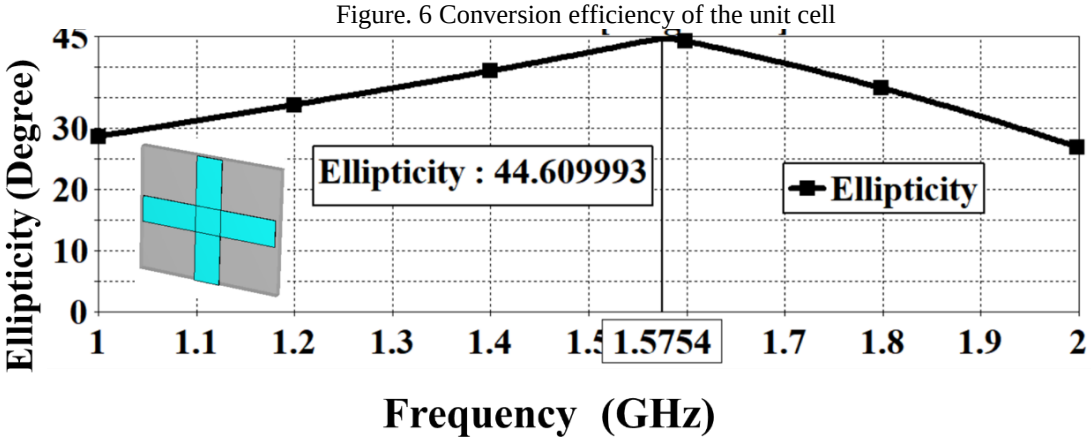

Figure. 7. Elllipticity of the wave

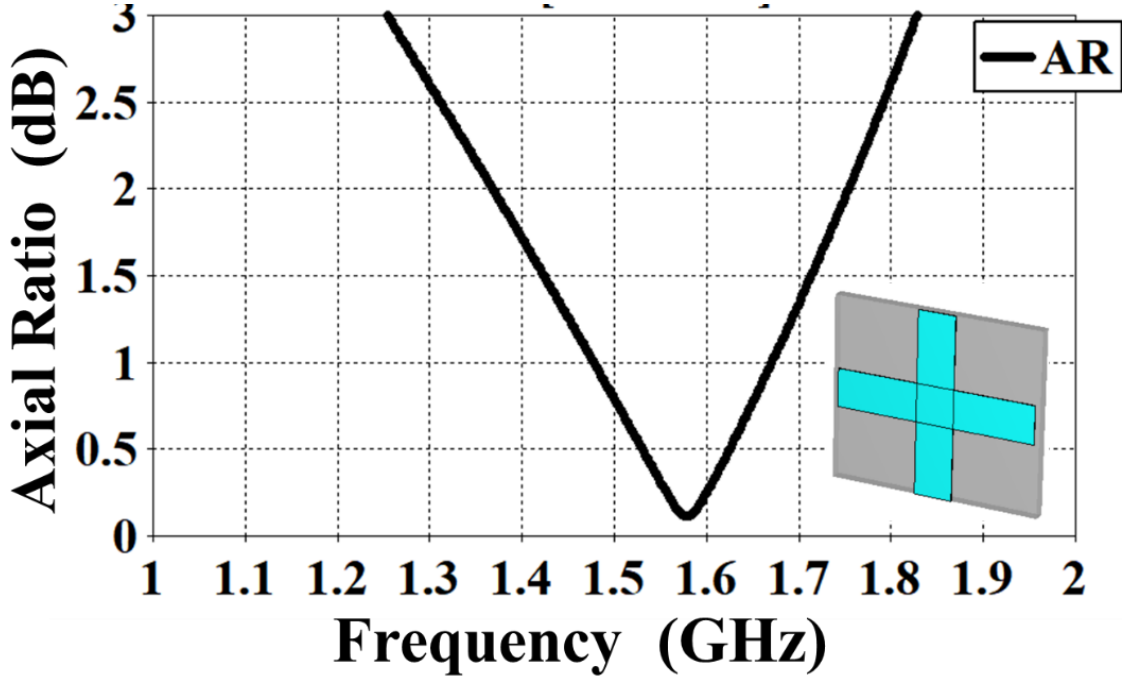

Figure. 8. The axial ratio of the ellipse

Figure 4, portrays the phase difference between the two transmission coefficients of electric fields, T_x and T_y. It can be seen that at 1.57542 GHz the value is nearly equal to 89.22º which is equal to nearly 90º. The phase difference ± 10 % of 90º, will be 81º and 99º, it can be observed that the phase difference with ± 10 % difference covers the whole frequency range of from 1-2 GHz and is cent percent at the target frequency.

Figure 5 shows the conversion coefficient of the CP wave. Usually between the two C_- and C_+ anyone's coefficient will be lower and the other will be higher. This is because one is inductive and the other will is capacitive. In our case, C_-, the righthanded CP is the lowest near about -40 dB.

Figure 6, shows the conversion efficiency of the unit cell. The conversion efficiency is derived from the conversion coefficients. The fractional bandwidth for the conversion efficiency covering the above 90% (highlighted in the magenta color) is 50.55% frequency ranging from 1.1315 GHz - 1.8971 GHz (highlighted with the green color). As per the author's knowledge, this is the highest range reported for the first time in the GPS L1 band.

Figure 7 and 8, depicts the ellipticity and axial ratio of the ellipse coming out of the polarizer. For the pure CP wave, the ellipticity value is 45º and for the linear wave, it is 0º. However, at the target frequency of the L1 band, the ellipticity value is 44.6º. The axial ratio fractional bandwidth for a 3 dB axial ratio is 1.2544-1.83 GHz, and it ranges from 1.2544-1.83 GHz. which results in a value of 37.32% 0.1 dB is the minimum available value of the axial ratio that may be attained. This is because the value of ellipticity is not exactly 45º therefore there is a difference in an axial ratio not reaching the 0 dB.

Table 1. Assessment of the polarizer's performance at the GPS/GNSS L1 band

S. No.	Frequency (GHz)	Phase Difference in degrees	$\eta_{conversion}$ (%)	Axial Ratio (dB)
1	1.57542	89.22	99.99	0.1

Conclusion

The polarizing surface that has been developed consists of just one layer. When it comes to GNSS, the polarizing surface performs most effectively around 1.57542 GHz. Fabrics are used in the development of the polarizer throughout its entirety. Felt serves as the substrate, while ShieldIt Super is employed as a substitute for metal in this application. According to the findings, It is evident that the proposed polarizing surface can convert an incoming linear wave into a circular wave at frequencies between 1.1315 GHz and 1.8971 GHz. The polarization converter that was proposed was tested, and the findings revealed that an ideal axial ratio value of 0.1 dB could be attained at 1.57542 GHz.

References

[1] A. Munk, B. (2000). Frequency selective surface: Theory and design.

[2] Bonnor, N. (2014). Principles of GNSS, Inertial, and Multisensor Integrated Navigation Systems – Second EditionPaul D. Groves Artech House, 2013, 776 pp ISBN-13: 978-1-60807-005-3. *Journal of Navigation*, *67*(1), 191–192. https://doi.org/10.1017/s0373463313000672

[3] Fonseca, N. J. G., & Mangenot, C. (2016). High-Performance Electrically Thin Dual-Band Polarizing Reflective Surface for Broadband Satellite Applications. *IEEE Transactions on Antennas and Propagation*, *64*(2), 640–649. https://doi.org/10.1109/TAP.2015.2509011

[4] Hassan, W. M., & Attiya, A. M. (2018). 2018 , 35 th NATIONAL RADIO SCIENCE CONFERENCE Textile Antenna Integrated with a Cap for L1 GPS Application 2018 , 35 th NATIONAL RADIO SCIENCE CONFERENCE, (Nrsc), 38–46.

[5] Hossain, T., Mirza, H., Soh, P. J., Member, S., Jamlos, M. F., Member, S., & Sheikh, R. A. (2019). Broadband Single-Layered , Single-Sided Flexible Linear-to-Circular Polarizer Using Square Loop Array for S-Band Pico-Satellites. *IEEE Access*, *7*, 149262–149272. https://doi.org/10.1109/ACCESS.2019.2944901

[6] Mantash, M., & Denidni, T. A. (2019a). 3D FSS polarizer for millimeter-wave antenna applications. *International Journal of RF and Microwave Computer-Aided Engineering*, *29*(8), 1–5. https://doi.org/10.1002/mmce.21767

[7] Mantash, M., & Denidni, T. A. (2019b). Design of GNSS Antenna Using Polarizer. *13th European Conference on Antennas and Propagation, EuCAP 2019*, *1*(EuCAP), 13–15.

[8] Mirza, H., Hossain, T. M., Soh, P. J., Jamlos, M. F., Ramli, M. N., Hassan, E. S., … Yan, S. (2018). Single layered swastika-shaped flexible linear-to-circular polarizer using textiles for S-band

application. *International Journal of RF and Microwave Computer-Aided Engineering*, *28*(7). https://doi.org/10.1002/mmce.21463

[9] Mirza, H., Soh, P. J., Jamlos, M. F., Hossain, T. M., Ramli, M. N., Al-Hadi, A. A., … Yan, S. (2018). A crossed dodecagonal deployable polarizer on textile and polydimethylsiloxane (PDMS) substrates. *Applied Physics A: Materials Science and Processing*, *124*(2). https://doi.org/10.1007/s00339-018-1602-9

[10] Mirza, Hidayath, Hossain, T. M., Soh, P. J., Jamlos, M. F., Ramli, M. N., Al-Hadi, A. A., … Yan, S. (2018). Deployable Linear-to-Circular Polarizer using PDMS Based on Unloaded and Loaded Circular FSS Arrays for Pico-Satellites. *IEEE Access*, 1–1. https://doi.org/10.1109/ACCESS.2018.2885381

[11] Molero, C., Garcia-Vigueras, M., Zhao, Y., Qing, A., Meng, Y., Song, Z., … Denidni, T. A. (2019). Cross-Polarization Reduction of Linear-to-Circular Polarizing Reflective Surfaces. *IEEE Transactions on Antennas and Propagation*, *66*(4), 5623–5627. https://doi.org/10.1109/ACCESS.2017.2746800

[12] Munoz-Martin, J. F., Fernandez, L., Ruiz-De-Azua, J., Camps, A., Edwards, R. M., Khattak, M. I., … Ur Rehman, M. (2019). A Low Profile, Dual-band, Dual Polarized Antenna for Indoor/Outdoor Wearable Application. *13th European Conference on Antennas and Propagation, EuCAP 2019*, *77*(1), 1221–1232. https://doi.org/10.1109/IGARSS.2019.8898402

[13] Ren, H., Shen, Z., & Li, B. (2013). Linear-to-circular polarization converter based on a two-dimensional periodic array of inhomogenously filled waveguide. *IEEE MTT-S International Microwave Symposium Digest*, 9–11. https://doi.org/10.1109/MWSYM.2013.6697557

[14] Subirana, J. S. (2020). GNSS signal, 1–5.

[15] U.S. Space Force. (2021). Other Global Navigation Satellite Systems (GNSS), 2–3. Retrieved from https://www.gps.gov/systems/gnss/

[16] Wanhill, R., Barter, S., & Molent, L. (2019). Historical Review. *SpringerBriefs in Applied Sciences and Technology*, 1–20. https://doi.org/10.1007/978-94-024-1675-6_1

[17] Ware, R., Exner, M., Feng, D., Gorbunov, M., Hardy, K., Herman, B., … Trenberth, K. (1996). GPS sounding of the atmosphere from low earth orbit: Preliminary results. *Bulletin of the American Meteorological Society*. https://doi.org/10.1175/1520-0477(1996)077<0019:GSOTAF>2.0.CO;2

[18] Xu, H.-X., Wang, G.-M., Qi, M. Q., Cai, T., & Cui, T. J. (2013a). A single-layer circular polarizer based on hybrid meander line and loop configuration. *IEEE Transactions on Antennas and Propagation*, *65*(10), 1–10. https://doi.org/10.1109/TAP.2015.2462128

[19] Xu, H.-X., Wang, G.-M., Qi, M. Q., Cai, T., & Cui, T. J. (2013b). Compact dual-band circular polarizer using twisted Hilbert-shaped chiral metamaterial. *Optics*

[21] Zavorotny, V. U., Gleason, S., Cardellach, E., & Camps, A. (2014). Tutorial on remote sensing using GNSS bistatic radar of opportunity. *IEEE Geoscience and Remote Sensing Magazine*, *2*(4), 8–45. https://doi.org/10.1109/MGRS.2014.2374220

[20] Yunck, T. P., Lindal, G. F., & Liu, C.-H. (2003). The role of GPS in precise Earth observation, 251–258. https://doi.org/10.1109/plans.1988.195491

Express, *21*(21), 24912. https://doi.org/10.1364/OE.21.024912

جهاز استقبال GNSS Polarizer خطي إلى دائري مرن يعتمد على النسيج الموصّل للمملكة العربية السعودية

هداية ميرزا [ا] ، نشأت سلطانة [ب] ، رئيس أحمد شيخ [ا،ت] ، بلقيس بانو [د]

ا قسم الهندسة الكهربائية ، كلية الهندسة ، جامعة جازان ، جامعة جازان ، المملكة العربية السعودية.

[ب] قسم إدارة الأعمال ، الكلية التطبيقية ، جامعة جازان ، المملكة العربية السعودية.

[ج] هندسة الاتصالات المتقدمة CoE (ACE) ، كلية هندسة الكمبيوتر والاتصالات ، Universiti Malaysia Perlis (UniMAP)، Pauh Putra، أراو ، بيرليس ، ماليزيا.

[د] قسم الإدارة ، الكلية التطبيقية ، جامعة جازان ، المملكة العربية السعودية.

الملخص

تقدم هذه المقالة مستقطبًا مرنًا أحادي الطبقة وخطيًا أحادي الجانب من القماش يمكن استخدامه لتطبيقات GNSS / GPS التي تعمل عند ١,٥٧٥٤٢ جيجاهرتز وترتبط بالنطاق L1. المستقطب مصنوع من قماش مرن مستقطب خطي إلى دائري. تم إنشاء المستقطب باستخدام مستقطب مرن خطي إلى دائري تم إنتاجه من قماش ذو وجه واحد. على عكس الجانب الخلفي من المستقطب ، الذي يخلو من أي نوع من الهياكل على الإطلاق ، يتميز الجانب الأمامي للجهاز بهيكل على شكل شرائط مستطيلة عمودية. في حالة الطول الموجي في الفضاء الحر ، تكون لخلية الوحدة أبعادًا ، على التوالي ، $0.29\lambda \times 0.255\lambda \times 0.01\lambda$ درجة. يتركز تردد التشغيل حول ١,٥٧٥٤ جيجا هرتز ، وأقل قيمة ممكنة للنسبة المحورية التي يمكن تحقيقها هي ٠,١ ديسيبل ، وهي قريبة جدًا من صفر ديسيبل. الهيكل بأكمله قادر على الثني ، مما يسمح بارتدائه كجزء من الثوب. عرض النطاق الترددي الكسري للنسبة المحورية ٣ ديسيبل هو ١,٢٥٤٤-١,٨٣ جيجا هرتز ، مما ينتج عنه قيمة ٣٧,٣٢٪. وبالمقارنة ، فإن عرض النطاق الترددي الكسري لكفاءة التحويل الممتد ٩٠٪ هو ٥٠,٥٥٪ ، وهو (١,١٣١٥-١,٨٩٧١).

الكلمات المفتاحية: GNSS :؛ GPS ؛ الفرقة L1 استقطاب دائري المستقطب. سطح دوري CubeSats، سواتلLEO .

Influence of Machining Parameters and Blasting Erosion Arc Machining on Material Removal Rate in Electrical Discharge Machining (EDM): A Review

Haitham Hadidi [1*]

[1]Department of Mechanical Engineering, College of Engineering, Jazan University, Jazan, Kingdom of Saudi Arabia.

Abstract

Electrical Discharge machining (EDM) is a valuable method to fabricate and shape hard to machine materials. Due to EDM process ability to machine any conductive materials and because most of those materials are widely used in various applications, it became a necessity to improve material removal rate (MRR) for better performance, cost and time reduction, and higher accuracy. Material removal rate (MRR) is a very important performance measure, which led investigators to focus on its improvement and evaluation. Despite what approaches have been followed, research in this field share the same goals which focuses on increasing the MRR, reducing the tool wear rate, and improving the surface quality. This paper outlines studies and works concerning the development of MRR with various process parameters along with deep focus on a recent ongoing developing approach called bundled electrodes in a process named blasting erosion arc- machining (BEAM) and its influence of the MRR.

Keywords: Electrical discharge machining (EDM); Blasting erosion arc-machining (BEAM); Material Removal Rate (MRR); Tool wear (TWR); Bundled electrode; Arc dimensional machining (ADM); Sustainability.

1. Introduction

Electrical discharge machining (EDM) is an effective and competitive machining process, which is capable to machine any electrically conductive material regardless their stiffness or hardness. EDM is a non-conventional machining process that involves the controlled removal of material from a workpiece using sparks generated by an electrical discharge. EDM is used to fabricate and produce molds, dies, aerospace and automotive parts, medical and surgical components. The efficiency and quality of the EDM process depend on various factors, including the machining parameters and the use of auxiliary techniques such as blasting erosion arc machining (BEAM). This process is capable to machine a variety of shapes and geometry regardless the hardness of the workpiece material. Most of the applications are requiring hard to cut materials and that's why industries tend to use EDM as it can be clear looking at the historical information and experiments that one important hard to cut material is Titanium alloys [1]. In recent years, researchers have focused on optimizing the EDM process to enhance its performance and reduce the production time and cost. In this context, a comprehensive review of the literature on the influence of machining parameters and BEAM on the material removal rate in EDM can provide valuable insights into the process and provide a guide for future research efforts.

This paper aims to review all related aspects to the improvement of process performance namely material removal rate (MRR), tool wear rate (TWR), and surface roughness. A deep insight on the use and performance of new electrode design so called Bundled electrode in EDM is also discussed in this paper. Being a critical performance measure, the development and improvement of MRR have been a major part of emphasis for researchers, which certainly need a review introducing previous and current contributions. In addition, a review of different implemented electrode design and techniques are revised for the sake of comparison with the method intended for this paper. The last part of this paper identifies the major research contributions done towards the development of EDM process performance, especially, the influence of blasting erosion arc machining (BEAM) on material removal rate, tool wear rate, and surface roughness.

1.1. EDM Working Principal

The electrical discharge machining (EDM) is a non-traditional machining process, which utilizes thermal energy to remove material from the machined part during machining. EDM converts the electrical energy into thermal energy which is considered the drive factor of the process. Both tool and workpiece are submerged into a dielectric fluid. The workpiece and tool electrode are not in direct contact and are separated by a small gap defined as spark gap. This created electrical energy between electrode and workpiece is transmitted through the gap medium where this spark gap is ranging between (10-1000 μm) [2]. The gap is filled by an insulating dielectric liquid usually de-ionized water or hydrocarbon oil. The gap works as a link connecting the spark on the electrode side to the workpiece material. Figure (1) illustrates the basic EDM process set up.

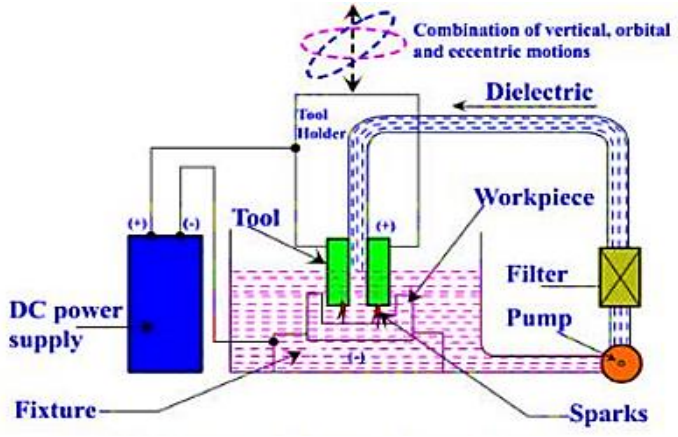

Figure 1: EDM Process Setup [3].

The material removal process depends on many factors such as tool material, electric parameters (current and voltage), polarity, dielectric type, flushing pressure, and electrode motion. EDM working principle is described in figure (2), the electrode starts to move towards the workpiece until a designated spark gap is reached so that the voltage is enough to ionize the dielectric. Usually a series of voltage pulses ranging from 20 to 120 V are applied between electrode tool and workpiece [4]. Once dielectric is ionized then it is not an insulator anymore and works as a conducting medium. Discharge pulses (sparks) are generated with relatively small duration ranging between (0.1 to 4000µs). The electrical resistance of the dielectric influences the discharge energy and the time of spark initiation [5]. Heat is generated due to the sparking action within the dielectric fluid where high temperatures of about 8000 to 12,000°C and heat fluxes up to 1017 W/m2 are achieved. Dielectric fluid works and helps to concentrate the discharge energy into a small cross sectional area channel as to increase the erosion effect. Then, the material from workpiece melts in small quantities by the conduction heat transfer effect generated by the discharge energy. During the On Time, sparks are occurring and subsequently once the pulses duration is over and material is melted, the debris is removed and flushed away by the dielectric fluid. Dielectric fluid works as an insulator before the sparking process begins, contributes in initiating channel of the discharge energy with small cross section area to increase heat effect. In addition, it cools both electrode and workpiece and enhances the process of debris removal and ejection.

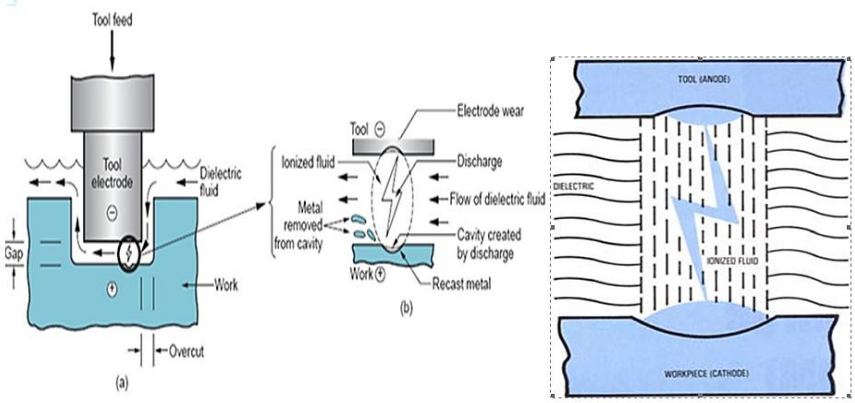

Figure 2: Electrical discharge machining (EDM) working principle [6].

2. Performance Measure and Process Parameters

Based on previous research, one can classify parameters affecting machining performance measure/ characteristics such as MRR, surface finish and TWR as depicted in figure (3):

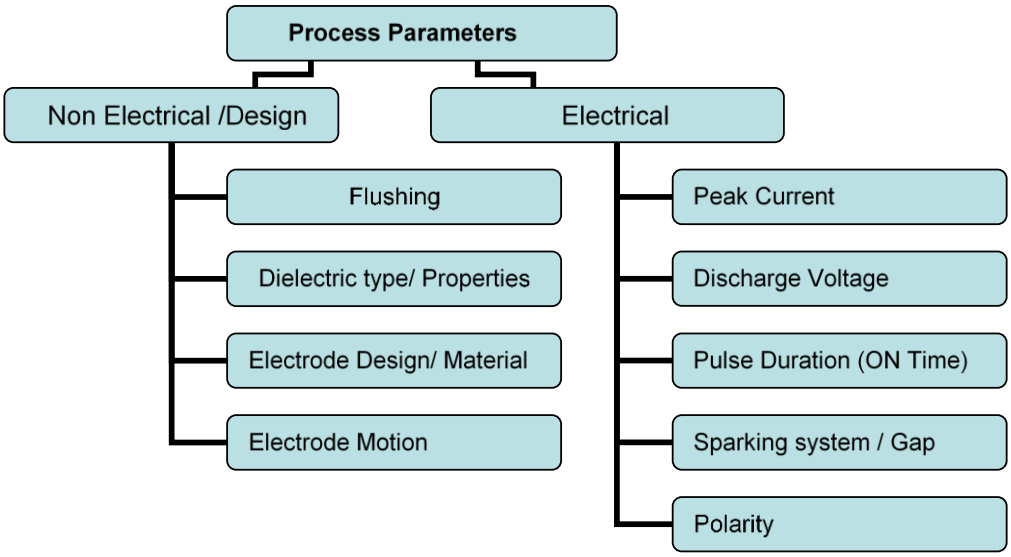

Figure 3: Classification of EDM Process Parameters.

2.1. Material Removal

Material removal rate (MRR) is an important performance measure in most machining processes specifically in the non-conventional machining. Electrical Discharge Machining (EDM), is amonge these non-conventional machining processes where MRR is of creat importance. Therefore, immense research and experimentation took place investigating the effect machining parameters have on MRR relation.

2.1.1. Methods of Improving Material Removal Rate (MMR)

EDM process performance depends on many factors including electrode design (geometry), electrode material, electrode manufacturing process as well as process electrical parameters.

2.1.1.1 Influence of electrode design/ material on process performance

Numerous research has been done to improve MRR by modifying the tool design. Some researchers tended to study the suitability of tool electrode material with a particular work piece material. Meanwhile, others have investigated the proper geometry design to attain high MRR and Low TWR. EDM process primarily used 3-D tool electrode to create a negative image on the sample, but the preparation of a complex 3-D profile is time consuming and costly, therefore, alternatives have been investigated [7]. A lot of work has gone into the EDM tooling complications concerning manufacturability, cost, and material availability [8,9]. Rajeev Kumar et al. [10] discussed different type of Electrode design and their contribution to the process performance. Rajeev reported the major differences among frame, plate, and ball ended cylindrical tool designs. Frame tool and plate tool had

been widely explored and it was revealed that plate type tools are limited in their capabilities regarding required machining profile. M. Bayramoglu and A.W. Duffill [11, 12] discussed how plate type tool is good for basic shapes (spheres, conics and simple 2D sweeps) and intermediate shapes (complex 2D sweeps, ruled surfaces and fillets) but not for complex shaped deep cavities, where it results in poor dielectric flow causing debris accumulation and hence lower MRR and low surface quality. Electrode and work piece materials interaction varies from material to another, hence a determination of surface characteristics and integrity depends on what materials are been used. Sumi et al. [13] studied the cracks and voids generation in TiC and Si layer by electrical discharge coating with S50C work piece. Investigation revealed that cracks and voids exist in TiC meanwhile voids alone appears in SiC layer. Defects existence mainly related to workpiece and electrode material interaction and nature, such that cracks are generated in TiC due to the tensile stress of it being brittle but not in Si due to its toughness as it forms amorphous layer. The grain size effect showed little influence on MRR and TWR but strong correlation with roughness when machining PCD with tungsten carbide electrode as revealed by Tai et al. [14].

2.1.1.2 Influence of electrode motion on process performance

Different studies have showed that even a small amount of electrode / work piece vibration or orbital movement could influence the process performance and surface roughness. Prihandana et al. [15] found out the shortest distance between the tool and sample can be achieved by having low frequency vibration. This vibration results in lower TWR and better surface roughness because the vibration enhances the flushing, which tends to improve both surface roughness and MRR. Rajurkar et al. [16] found that electrode orbital movement, which reduces flow disruption, affects machining accuracy and stability. Mohan et al. [17] analyzed the influence of electrode rotation on EDM performance when machining Al–SiC MMCs with 20 and 25 vol.% SiC using copper and brass electrodes. The study revealed that increasing the speed of the rotating electrode resulted in a positive effect with MRR, TWR and better SR than at stationary. The explanation for that is with rotating electrode flushing has better effect on gap debris removal resulting in higher MRR and better surface finish. Guu and Hocheng [18] provided a sample rotary motion to improve the circulation of the dielectric fluid in the spark gap and temperature distribution of the sample yielding improved MRR and SR. Increasing external hydro-static pressure decreases the MRR due to the increase in electrode boiling point, hence lower bubble formation occurs causing low debris ejection. Stable tool motion with low pressure enhances the bubble formation therefore MRR is improved as revealed by Koyano et al. [19].

2.1.1.3 Influence of process's electrical parameters on process performance

Peak current, discharge voltage, polarity, and pulse duration are characterized as EDM process electrical parameters. An increase or decrease in one of which results in either a decrease or increase on process performance measure. T. Muthuramalingam and B. Mohan [20] emphasized on the importance of enhancing the electrical process parameters since they are the key factors for improving the process effectiveness. The explanation to that is EDM process is thermo dependent material removal process where the thermal energy is produced from the applied electrical energy/discharge. Ghoreishi et al. [21] found that when applying voltage excitation of the pulse a higher MRR and lower TWR of 2% can be

achieved do the effective pulses produced as a result of the excitation. Hence, pulses in the existence of voltage excitation possess longer discharge time and less delay time which contributes in higher thermal effect on work piece and less influence on tool electrode since short delay time is applied on electrode side.

The effect of current impulses on EDM performance measures has been investigated when machining tungsten carbide using coper electrode by Tsai and Lu [22]. Based on the results, an improvement in MRR have been noticed due to the increase of energy density obtained by current impulses rise such that, an increase in current rising slope increases the MRR with similar trends even using different initial current. According to Muthuramalingam and Mohan [23] the efficiency of using pulse generator in EDM process is determined by the improvement in the MRR. Mohan et al. [17] analyzed the influence of discharge current on EDM performance when machining Al–SiC and it was found that MRR increased with an increase in discharge current and for a specific current MRR decreased with an increase in pulse duration. Hirotaka et al. [24] studied the influence of single discharge on low melting temperature alloy, it was found that an increase in the pulse duration result to an increase in the diameter of discharge crater, depth of crater and consequently resulted in an increase of MRR. Contrary, the volume removed MRR decreased over 200µs pulse duration using negative polarity electrode and kerosene oil as dielectric due to the shallow depth under such conditions. Maintaining Volt-Ampere of discharge gap is essential in generating better MRR and it mainly depends on the size of the gap such that gap voltage is kept above threshold voltage Fan et al. [25]. SiC & SiSiC were machined using brass multi-hole electrode and the process indicated that increasing ignition voltage and reducing pulse duration causes spalling and micro cracking for brittle materials and hence improve MRR [26].

2.1.1.4 Influence of polarity on process performance

According to Mohan et al. [17] polarity effect was analyzed when machining Al–SiC and it was found that MRR increased when polarity is positive compared with negative polarity. In addition, Wang et al. [27] revealed that positive polarity caused higher MRR in the presence of high discharge energy. In contrast, Zhao et al. [28] had alternated the electrode polarity to be a positive in one case and negative in the other with so called blasting erosion arc machining (BEAM) EDM process as to examine its effect on process performance. They have found that polarity plays a giant effect in the consistency of plasma channel and accordingly resulting in higher MRR. Polarity where changed on and a dramatic increase in MRR was observed when negative polarity is used compared to a better surface roughness and lower MRR when using positive polarity. The reason behind such contradiction is due to many factors as work piece/electrode material, flushing system, and plasma arc breaking system. Hirotaka et al. [24] showed that polarity effect on MRR depends on the dielectric used and also depends on pulse duration. Kerosene oil resulted in lower removed volume with negative polarity and higher MRR with positive polarity; while using de-ionized water shows increasing trends in both polarity situations. Negative polarity coupled with high speed rotating graphite pipe resulted in MRR of 21494 mm3/min when machining (Ti6Al4V) [29]. Electrode negative polarity a companied with shorter pulse duration and high voltage optimized process output (MRR, electrode wear, hole diameter) in SiSiC and SiC drilling process Kliuev et al. [26].

2.1.1.5 Influence of dielectric medium and flushing

Dielectric or working fluid in electrical discharge machining plays an important role in process characteristics, which results in higher MRR as well as better surface quality and longer tool life. Palanisamy et al. [30] found that applying high-pressure coolant results in longer tool life and better surface finish. S.L. Chen et al. [31] investigated the influence of using kerosene and distilled water on machining characteristics of Ti6Al4V. It was concluded that the MRR is higher and TWR is relatively smaller when using distilled water rather than kerosene. In contrast, distilled water tends to create more micro cracks whereas using kerosene causes a formation of carbide (TiC) layers and these layers are reasons behind having lower MRR as they require large discharge energy to melt down since they have higher melting temperature. Quantity and type of lubricants are also important as revealed by Sadeghi et al. [32]. The vegetable oil exhibits higher cooling influence than synthetic oil when machining Ti6Al4V. Lee et al. [33] have inspected the influence of dielectric flushing on process outcomes, it was concluded that high flushing helps in different aspects such as reducing the TWR by minimizing the localized temperature on tool side and better evacuate generated debris. While low flushing did not contribute in removing gaseous and solid debris. An optimal dielectric flushing had found it helps in minimizing the recast layer thickness and cracking as investigated by Wong et al. [34]. Zhao et al. [28] showed the influence of flushing pressure on both positive and negative polarity when using blasting erosion arc machining which tends to increase MRR in both cases but more remarkably with negative polarity.

Discharge frequency increases if sparking gap condition is improved by strengthened flushing. While Lin Gu et al. [10] showed that a significant feature of using bundled electrode in EDM is the result of having lower TWR beside very high MRR when machining same work piece material; and that is due to the extensive flushing effects resulted from the electrode design by having multi inner flushing holes. Jahan et al. [35] investigated dry and wet EM in Nano-scale and found that machining medium plays an important role in material removal mechanism and intensity.

Dry EM causes heat localization, which turns to evaporate tool electrode material, and retained the tool quality enabling it to utilize more feature in a single step. On the other hand, Oxygen, Argon and Deionized-water were used to investigate micro drilling EDM process characteristics such as erosion time and electrode relative wear on machining Si3N4-TiN, Uhlmann et al. [36]. The study revealed that oxygen is having shorter erosion time (3.8 s) but causes higher electrode wear 9.2 % therefore it is good as roughing process. Meanwhile Argon has the longest erosion time (72 s) and the lowest tool wear due to its properties as inert gas. Whereas water showed erosion time of (13 s) and better electrode wear than oxygen, therefore it is good for finishing process. Further development in EDMed surface finish and characteristic was reached when using Chromium powder mixed as working fluid. Toshimitsu et al. [37] investigated SKD11 alloy tool steel surface roughness and hardness when different dielectrics were used and better surface characteristics were obtained using Chromium powder with variant concentration (1-5 g/L) and discharge current (0.4- 1.6A) with the observation that higher concentration could result in poor surface roughness due to in sufficient stirring and low discharge current.

2.2. Bundled Electrode

Bundled electrode is a new innovative type of tool electrode used in the field of Electrical discharge machining. It consists of multiple tubes lumped together in one pipe to form one multi-hole electrode as shown in figure (4). The goal of using bundled electrode is to obtain a better machining effectiveness and performance in EDM process while maintaining good surface quality.

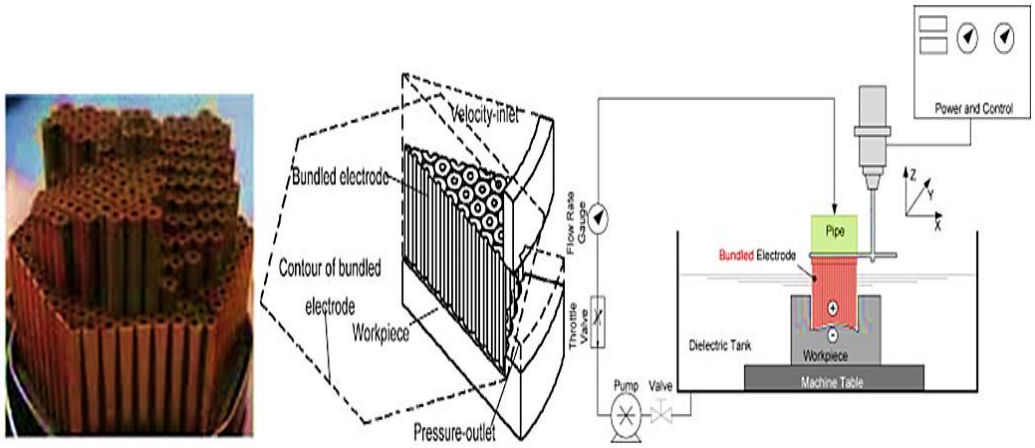

Figure 4: Bundled Electrode Schematic.

2.2.1. Mechanism of material removal of bundled electrode in EDM

Blasting Erosion Arc Machining (BEAM) is the concept of the mechanism by which material removal occurs in EDM process using bundled electrode with high flushing effect and plasma arc initiation and breaking. BEAM is low cost and high efficiency process. There are two types of plasma arc breaking mechanism as described in W. Zhao et al. [38] named mechanical motion arc breaking and hydrodynamic arc breaking. The first considers an effective mechanism to distort or break the plasma channel and causing the arcing to occurs; however, it has limitation on electrode shape (either tubular or disc are used) hence it restricts shapes proceeds and is applied on process like electro contact dimensional machining (ECDM), electro chemical arc machining (ECAM) and electro melting explosion. The latter is even better since it is capable to machine or create complex cavities (concave and convex shapes are produced) where it can be found in processes like Arc dimensional machining (ADM) and blasting erosion arc machining (BEAM).

BEAM process with 3-D end surface (bundled electrode) with multi-hole and inner flushing increase machining efficiency, MRR, and reduce cost and time lead related to electrode preparation not only this but also enhance the gap condition as a result of high velocity dielectric flow Dursun et al. [39]. Utilizing the benefits of BEAM are strongly connected to the issue of arc plasma channel distortion and/or breaking. It is important to maintain the transient arcing, which happens as consequence of high velocity flushing that, extend and elongate the plasma channel as going from the center to the peripheral where a crater is formed as a result of the distortion and extension of the arc plasma channel. Wang et al. [40] study revealed that Steady arcing causes localize hear and high energy in one spot or small area which may ruin both tool electrode and work piece therefore, high and effective flushing is recommended.

3. Comparison of MRR using Bundled Electrode and other Techniques

3.1. Bundled (bunched) electrode EDM

The idea of bunched (bundled) electrode efficiently contributed to improve process performance by having higher MRR and comparably lower tool wear ratio (TWR) than most other electrode tool design used in the process of EDM. Process performance using graphite bundled electrode with multi-hole and high flushing velocity on machining Inconel718 indicated that process characteristics were much better compared to that gotten with solid electrode as shown on [38]. The process had the following:

- Material removal rate of 11300 mm3/min;
- Peak current endurance up to 600 A;
- Tool wear ratio less than 3% due to the electrode material (graphite properties) as well as the energy distribution on anode side rather than cathode side;
- The heat-affected zone is less than 200µm because of the effective flushing effect by rejecting the heat out of the gap.

Meanwhile, In the case of machining Ti6Al4V with copper bundled electrode having 217 tubes [11], the process tend to have more limitation and low capability if it would be machined with solid electrode due to the physical and mechanical properties of Ti6Al4V. Typically, a high melting temperature and high thermal diffusivity is required for tool electrode material to prevent high erosion rate of electrode as well as not to have localized heating zone along the tip of electrode, which may result in electrode deformation and failure beside low process effectiveness (MRR) and high TWR. On the other hand, it is not the case in machining Ti6Al4V, where it has higher melting temperature and higher specific heat, leading to complicate the material removal and increase the energy required during heating process [10]. Consequently, an effective way to overcome such complication is to have an electrode able to create more than one spark or have better heat provision to melt down the work piece material. Meanwhile it is also essential to provide a cooling system to reduce the localized heat on the part. The Bundled electrode with multi inner flushing seen in figure (5) is the answer for similar situation where it can utilize high heat provision and cooling effect.

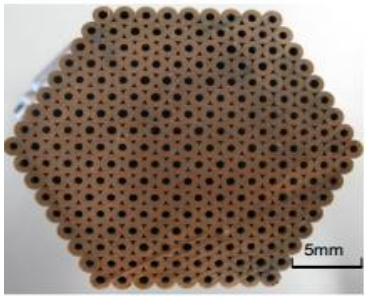

Figure 5: Bundled Electrode with Inner Flushing System [10].

Lin Gu et al. [10] showed that when using bundled electrode for processing Ti6Al4V MRR is 5 times higher (150 mm3/min) than that when using solid electrode under similar machining circumstances as shown in the result of figure (6). The analysis of this big difference simply because the generated heat in the gap is cooled down while debris are flushed out with assist of high flushing velocity coming through inner holes of bundled electrode. This critical feature enables electrode to sustain and allow high current causing more material removal opposite to the insufficient flushing in solid electrode.

Likewise, tool wear ration is less with bundled electrode because the high flushing helps reducing the debris concentration and localized heat beside the carbon formed by dielectric deionization is deposited on the electrode forming protective layer.

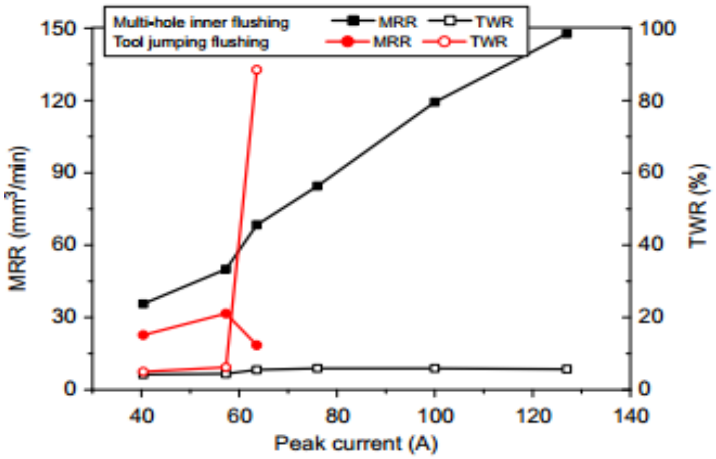

Figure 6: Peak current – MRR & TWR relation when machining Ti6Al4V with multi-hole inner flushing and tool jumping flushing [10].

3.1.1. Polarity Effect on BEAM Process Performance

Polarity where changed on BEAM process as to examine its effect on the BEAM process performance. Operating with same technique of hydrodynamic arc breaking and high flushing effect Zhao et al. [28] have alternated the electrode polarity to be a positive in one case and negative in other with varying the process parameter and have found that polarity plays a giant effect in the consistency of plasma channel and hence affect the MRR accordingly. This experiment has revealed that negative electrode polarity results in high MRR (14000 mm3/min) when machining AISI D2 and rough surface up to 300µm with trailing crater evidence. This is driven from the increase of peak current, which increases the energy density in negative electrode polarity by which more material is removed.

Positive electrode polarity results in an increase in MRR as current increases but does not compared to the negative polarity. This is because in positive polarity when peak current increase, the discharge current does not increase proportionally as it is the case in negative polarity.

TWR in positive polarity is 18% high than that is negative polarity 1% due to the fast arc plasma distortion an ability to be fully developed and more energy is distributed on tool side in positive case, the following can be summarized:

- Current increase result in MRR increase in both cases with some limitation on positive polarity for above mentioned reasons;
- Flushing pressure increase result in an increase in MRR but more in negative case;
- No major change on TWR with pressure increase.

Therefore, for rough machining with high MRR, negative polarity electrode is preferred. Meanwhile, better surface finish is obtained using positive polarity associated with low MRR. Hence, a combination of both negative and positive polarity may be of predominant performance on BEAM process to have high MRR and good surface finish.

3.2. High Current Density EDM

Wang et al. [40] suggested and experimented to machine Iconel718 with a graphite pipe electrode to measure the performance of the process. The concept of high current density process is to use a rotary standard electrode with a source of high voltage pulse generator and DC power source with high current and side flushing pump. What makes this process significant is how the ignition takes place after pulse generator is switched on which enables to maintain high discharge current producing high temperature and pressure into the plasma channel; whereas the fluid flushing tends to brake the plasma arch and has a transient plasma effect helping in more generated heat and MRR. In contrast, the traditional EDM in the discharging interval phase, the discharge is ended by switching of the pulse generator.

Figure (7) Shows the effect of high current density method on ED milling. The process revealed:

- High MRR up to 15062 mm3/m;
- Process endure 920 A when using a rotary standard electrode with a source of high voltage pulse generator and DC power source with high current;
- TWR was about 1.7%;
- Major increase in MRR is because of the high current source, rotary motion, and flushing effect.

Arc dimensional machining (ADM) is similar in concept of BEAM process where both use the same arc breaking mechanism and both capable to obtain high MRR and sustain high peak current values. Meanwhile, solid electrode, plate frame electrode, multi sparks method are limited to certain current value due to the insufficient flushing and electrode design. High current density method is using the same concept of breaking the arc as BEAM process in addition it uses the rotary motion for better breaking effect.

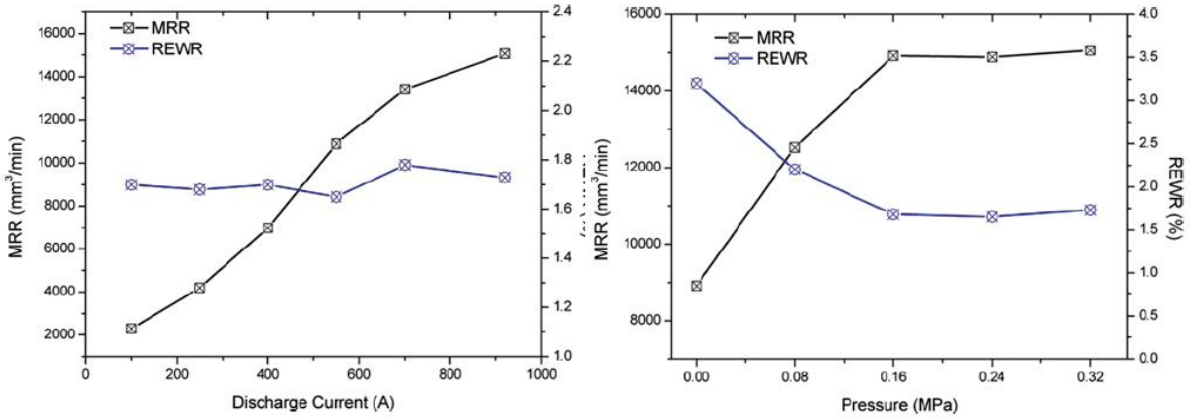

Figure 7: High Current Density Influence on ED Milling Performance [40].

3.3. Compound Machining Using Super High Speed EDM and Arc Machining

High speed and arc machining have proven their ability to create higher MRR when utilized individually. Combining both techniques has been carried out by Fei Wang et al. [28] where graphite pipe with 3000 rpm, power supply (pulse generator & power source), negative polarity, and arcing are lumped together to machine Ti6Al4V. The experiment resulted in MRR of 21494 mm^3/min associated with 700 A; whereas TWR of 1.7 % was achieved.

3.4. Blasting Erosion Arc Machining (BEAM)

In this process a blasting arc machining (BEAM) concept is applied to improve process performance MRR, TWR, and surface roughness. Ti-6Al-4V alloy was machined under different process variables (peak current, pulse dura-

tion, and pulse interval) with negative polarity since negative polarity has shown its ability to create more inconsistent arc plasma, help increasing the temperature, and hence erode more material. Jipeng Chen et al. [41] have recently developed the concept of BEAM using tubular electrode with several flushing holes to perform intensive flushing. Experiments revealed that when peak current was 500 A and pulse duration was 8 ms, MRR could achieve 16,800 mm3 /min, and could reach 20,100 mm3 /min when adopting the optimized parameters (peak current 600 A, pulse duration 8.8 ms, and pulse interval 3.0 ms). Although TWR was stable around 3 ± 1 %, meanwhile influence of feeding direction on surface roughness has been studied and results that the feeding direction had great influence on the surface roughness; surfaces machined in axis feeding mode were coarser than that machined in horizontal feeding mode.

As BEAM process taking places three major factors (pulse duration, discharge current, and flushing pressure) are influencing its performance. Roughness is decreased with high flushing pressure while it decreases with raising peak current but not much changes in roughness is observed with pulse duration change when machining stainless steel with two-hole cylinder electrode. on the other side, BEAM polarity attributes in surface characteristics as smooth surface and thin affected zone is generated with positive polarity but rough surface and large affected zone are associated with negative polarity as indicated by Zhu et al. [42]. Peak current, pulse duration, pulse interval, and multi-hole electrode material and design play critical role in the performance of BEAM process performance and product characteristics. Chen at al. [43] investigated the effect of electrical parameters on machining 50 vol.% SiC/Al matric composite using cylindrical multi-hole graphite electrode. Result indicated that SiC/Al composite was successfully machined using BEAM and high MRR was achieved. Optimum values of 500 A peak current, 8 ms pulse duration, and 2 ms pulse interval, led to a MRR of 6000 mm3/min, however, the existence of SiC particles negatively influence TWR of graphite electrode due to their temperature dependent heat characteristics when compared to pure aluminum, fig.8. The attainment of high MRR in EDM process is associated with high roughness surfaces. Overcoming high roughness EDM parts was achieved with combining BEAM process with CNC milling [44]. Two stages process starting with negative BEAM step using 600 A peak current, resulted in MRR of 10,200 and 7500 mm^3/min for 20 vol.% SiC/Al and 50 vol.% SiC/Al composites respectively, however thick heat affected zone and higher surface roughness were dominant. The CNC milling stage was able to overcome the side effects of BEAM in term of rough surface and the heat affect zone attaining a roughness lower than Ra 0.5 μm after machining.

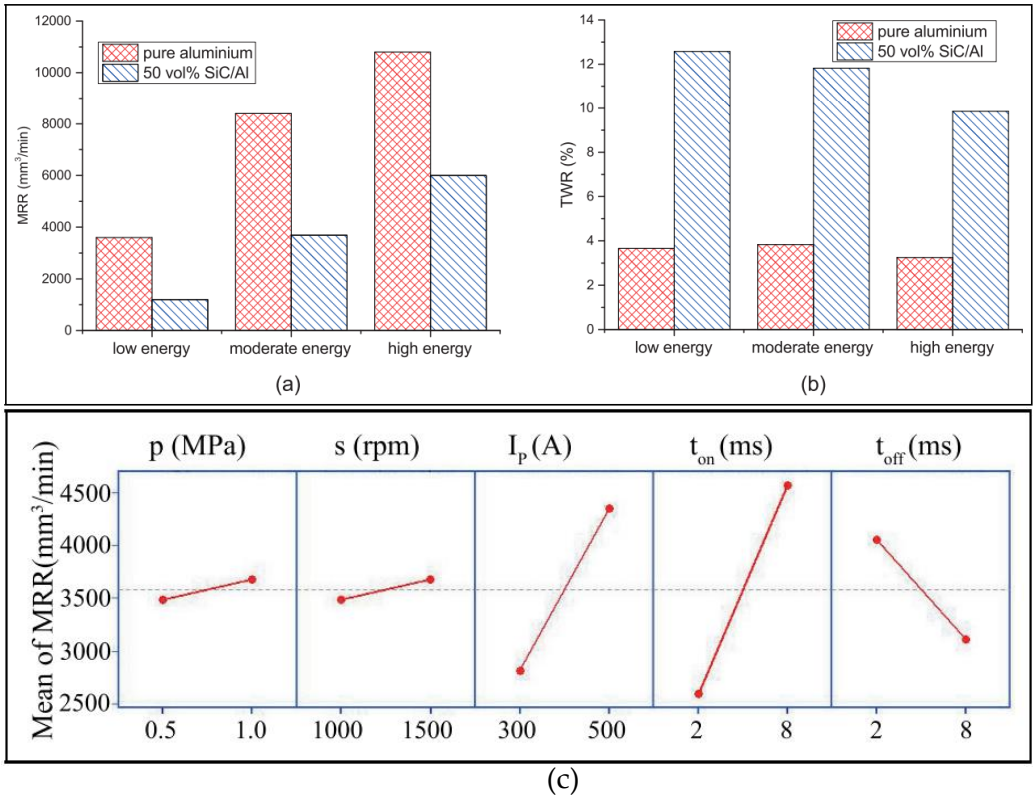

Figure 8: BEAM Performance Comparison (50% SiC/Al & pure aluminum): (a) MMR, (b) TWR, and (c) Process parameters Main effects for the MRR [43].

3.5 Chronological Comparison

A chronological order of previous research for the purpose of studying, improving, and optimizing MRR are listed in Table 1.

Table 1. Chronological Comparison on the Effect of EDM Process Parameters on the Performance and the Improvement of MRR.

Author	Year	Contribution	Workpiece material	Electrode material	Parameters & Finding
H.M Zaw, J.Y.H Fuh et al. [45]	1999	The effect of using solid/liquid state sintering fabricated electrodes (using RP technique) on MRR compared to conventional electrode materials: graphite, Cu.	Tool steel	Compound of ZrB2 and TiSi with Cu	Constant machining condition: Peak current, pulse interval, discharge time, + polarity, fixed flushing pressure.
S.L.Chen et al. [31]	1999	The effect of using different dielectric fluid	Ti6Al4V	Copper	Negative polarity, voltage of 150 V, current of 3-24A, and pulse duration of 10-200µm.

		(Kerosene and distilled water).			It was found that MRR is higher and TWR is lower when using distilled water rather than kerosene.
Kunieda and Muto [46]	2000	Compared process characteristics of multi spark EDM electrode with the single electrode spark EDM.	Steel SUJ2	Copper	Voltage, current, and polarity effects are studied. It was found that the multi spark resulted in higher MRR and TWR was arithmetically lower than the single positive and negative tool electrode.
Lin et al. [47]	2000	Combined EDM with ultrasonic machining to increase material removal rate.	Ti6Al4V	Copper	Dielectric type, abrasive size, concentration of abrasive in the dielectric fluid, discharge peak current and pulse duration. Combination EDM/USM process can increase the MRR and decrease the thickness of the recast layer and can dramatically reduce abnormal discharge.
Aspinwall et al. [48]	2001	Studied hybrid high speed process (EDM/HSM).	Steel, Inconel 718	Copper	Voltage as electrical parameter and Electrode rotation as non-electrical parameter
Guu, Y.H., Hocheng, H [18]	2001	Studied workpiece rotary motion.	AISI D2 tool steel	Copper	Rotation enhanced the dielectric flow, thus more debris removed from the gap. In addition MRR increased with the rotation speed of the workpiece.
Bayramoglu & Duffill [11]	2004	Studied plate type tool and compared the performance With 3-D form tool.	Steel	Copper	Voltage, current, on- time, off –time. 3-D form tool generally resulted in higher MRR, but plate type can achieve high MRR accompanied with high TWR also result in good dimensional accuracy and better surface finish since

					good flushing condition can be achieved.
Shibayam & Kunieda [49]	2006	Used tool electrode which has micro holes for jetting dielectric Liquid.		Copper	Higher Dielectric Flow rate. "Higher MRR"
Kadir Dursun & Can Cogun [39]	2009	Used electrodes formed by using copper wire Bunches (WBEs) to measure MRR and compare it with other tool design in EDM.		Copper	The increase in number of wires and pulse energy result in decrease of relative wear for each wire in the electrode as well as an increase in machining area and MRR.
Han et al. [50]	2009	Proposed a high speed EDM Milling method using moving electric arcs.	Mild steel	Copper	Open voltage, peak current, and electrode rotation. More than 3 times higher MRR is obtained with moving electric arc compared to the stationary electrode of EDM. TWR is about 2% in the conventional electrode while it tends to not exist in rotational electric electrode arcing process due to the longer pulse duration and higher carbon deposition on the tool electrode which protects from eroding. Also the inconsistency of arcing.
Govindan & Joshi [51]	2010	Experimented MRR in dry electrical discharge drilling using rotating electrode.	SS304	Copper	Gap voltage, discharge current, spindle rotational speed, pulse off-time, oxygen pressure. It was noticed that current is the most dominant affecting factor in increasing the MRR as well as rotational speed and voltage for certain extinct.

Lin Gu et al.[10]	2012	Using Bundled electrode with multi hole inner flushing in Die-sinking EDM and comparing that with solid electrode using same workpiece and electrode material.	Ti6Al4V	Copper	Fluid flow, Peak current, and pulse duration. Better MRR and TWR were obtained.
Singh & Verma [52]	2013	Experimented EDM drilling with three different machining parameters to study their influence on MRR.	Al-7075	Brass	Pulse On-time, Pulse OFF-time, and water pressure. It was found that pulse on-time is the most influencing factor on increasing MRR since longer current duration increases spark energy which in turn obtain higher MRR opposite to pulse off-time.
Wang et al. [40]	2013	Using high current density electrical discharge milling to improve MRR and TWR.	Inconel718	Graphite (pipe)	Peak current, gap voltage and flushing pressure. MRR was very high up to 15062 mm3/m and process endure 920 A when using a rotary standard electrode with a source of high voltage pulse generator and DC power source with high current. TWR was about 1.7 % less than that obtained by bundled electrode which was 3%.
Fei Wang et al. [29]	2014	Compound machining using super speed EDM milling and arc machining with high power supply.	Ti6Al4	Graphite (pipe)	Negative Polarity, Power supply (pulse generator, DC power source), high speed, high flushing. Negative polarity coupled with tool rotation speed of 3000 rpm and peak current of 700 (A) resulted in MRR of 21494 mm3/min.

					Polarity, pulse duration, peak current, and flushing pressure.
Wanshenq Zhao et al. [28]	2015	Blasting erosion arc machining process and Polarity effect on performance.	AISI D2	Graphite	Negative electrode polarity results in high MRR (14000 mm3/min) rough surface up to 300µm with trailing crater evidence. TWR in positive polarity is18% high than that is negative polarity 1%.
Yan Zhang et al [53]	2015	Electro-chemical discharge machining with super high interior flushing pressure.	Ti6Al4V	Tube electrode	High flushing pressure and different electrode diameter are applied. More effective debris removal and enhanced machining efficiency and surface quality reached (MRR 176.471 µm/s).
T.Y. Tai, K.T Nguyen [14]	2016	Investigated the effect of grain size of polycrystalline diamond (PCD) on MRR, TWR and surface integrity using EDM.	Polycrystalline diamond (PCD)	Tungsten Carbide	Current, pulse on-time/off-time and grain are the process parameters. Grain size shows little influence on MRR & TWR when machining PCD. While, current has the great impact on machining characteristics. Optimal machining parameters for highest MRR and low TWR are 6µm grain size with 0.5 A and 2µs on time. meanwhile, surface roughness was optimal at 1.7µm, 4A and 8µs on time.
Kliuev et al. [26]	2016	Using multi-hole electrode with internal flushing, different polarity and pulse duration to study process performance when drilling and shaping SiC & SiSiC.	SiC & SiSiC	Copper/ brass multi-hole electrode	Tool polarity, pulse duration, and ignition voltage. Result indicate new material mechanism besides melting and vaporization is presented for brittle material and called micro spalling due to shorter impulse duration & frequency. Negative polarity & high voltage gives high

					MRR with SiSiC(120V & <1µs) and SiC (250V & 8µs). Electrical conductivity increases due to temperature rise and copper solidification on workpiece.
Jipeng Chen et al. [41]	2016	BEAM using tubular electrode with several flushing holes to perform intensive flushing.	Ti6Al4V	Cylinder Graphite electrode	Peak current, pulse duration, and pulse interval. Results revealed that when peak current was 500 A and pulse duration was 8 ms, MRR could achieve 16,800 mm3 /min, And could reach 20,100 mm3 /min when adopting the optimized parameters (peak current 600 A, pulse duration 8.8 ms, and pulse interval 3.0 ms). Although TWR (around 3 ± 1%).
Shen et al. [54]	2016	Hybrid machining of EDM and Arc machining.	AISI 304 SS	Tubular Graphite	Negative tool polarity, peak current, peak voltage pulse duration, air flow rate, electrode rotational speed. Result showed that high efficient dry hybrid machining can achieve MRR of 5534 mm3 /min with high machining energy, high air speed, and high electrode rotation. Arc machining provide high energy and EDM generate high voltage for discharge gap. SR decreases with high air flow rate, peak voltage of EDM and tool rotation but decreases with high current of Arc machining. NO crack was observed.

Gotoh et al. [55]	2016	EDM of Ceramics using electrical conductive layer.	Si3N4	Copper (wire & solid)	A control of discharge duration by a pulse voltage is the key in creating a conductive surface layer enabling EDM process to be stable. Long discharge/pulse duration of 500µs up to 1000µs beside waveform control is prone to form stable conductive layer causing stable machining. Machining rate was improved as discharge duration stays longer than set value consequently surface roughness was high in the conductive layer than the ceramic.
Fu et al. [56]	2016	Studied white layer properties in both EDM & Laser cut Nitinol machined surface.	Nitinol	Brass wire /fiber laser	The white layer obtained is has different properties. EDM white layer hardness is higher than the bulk material due to alloying hardening and oxide formation while Laser white layer hardness is lower than the bulk material hardness. The distribution of while layer is uniform in laser white layer but non-uniform in EDM white layer. Whereas roughness is higher in laser white layer than that in EDM ones.
Chen et al. [43]	2017	Blasting erosion arc machining (BEAM) with multi-hole cylinder electrode.	50 vol.% SiC/Al composites & pure aluminum	Cylinder graphite multi-hole electrode	Peak current, pulse duration, and pulse interval. A peak current of 500 A, 8 ms pulse duration, and 2 ms pulse interval, resulted in the highest MRR of 6000 mm3/min. MRR of 50 vol.% SiC/Al is much lower than that of the

					pure aluminum, and the TWR of the 50 vol.% SiC/Al is much higher Because the MRR mechanism of the BEAM is directly related to the heat effect, and the heat characteristics of the SiC particles are distinct from the pure aluminum.
Chen et al. [44]	2018	Combined machining using BEAM and CNC milling.	20&50 vol.% SiC/Al composites	Cylinder graphite multi-hole electrode	Using 600 A peak current and 1 ms pulse interval resulted in MRR of 10,200 and 7500 mm^3/min and Ra less than 0.5 μm for 20 vol.% and 50 vol.% SiC/Al composites respectively.
Wu et al. [57]	2020	Sustainable and high-efficiency green electrical discharge machining milling	17-4 PH		A high-efficiency pulse power supply with high energy and environmentally friendly working fluids (deionized water and air). Resulted in higher machining efficiency, lower energy consumption (200% increase in energy utilization rate), and mild electrode wear. The MRR reached 900.66 mm3/min and the relative EWR was 1.20%.
Ablyaz et al. [58]	2022	Creating Textured Surfaces through using 3-D printed Selective Laser Melting Electrode Tools.	High-alloy steel 15Cr12H2MoWVNNB	Ti6Al4V 3D-printed electrode tool	Resulted in oil-retaining grooves on the parts of the friction pair. The grooves improved the performance properties of the product.
Yang et al. [59]	2022	The effect of BEAM and machining parameters (open circuit voltage, electrode	ɣ-TiAl	Graphite cylindrical electrode with the external diameter of	Results showed that MRR of 4,484.9 mm3/min, tool wear ratio of 2.74%, and surface roughness Sa of 74.14 μm, were reached using the the graphite electrode (BEAM

diameter, and cutting depth) on Titanium hard to cut alloy.	12-20 mm process) with peak current of 400 A. It was observed, MRR was greatly affected by cutting depth, while, tool wear ratio was mainly affected by electrode diameter and surface quality was influenced by all three parameters.

4. Conclusions and Recommendations

4.1. Conclusion

EDM performance using different technique were investigated and almost all work in above-mentioned studies agree upon essential common factors affecting the process performance including:

- Current, as it is the case in using solid stationary electrode, rotary electrode, powder/dielectric mixing method, multi sparks method, high current density method, and bundled electrode with inner flushing technique. The key point is how high the current can go and the process and work material can endure; here the contradiction and conflict comes from a method to another and from a tool electrode design to another;
- Tool Electrode design, bundled electrode with multi-hole inner flushing showed very good MRR and comparably better TWR when used in EDM because of arc breaking mechanism where a hydrodynamic force resulted from the high velocity flushing result in a distortion, extension and/or breakage of arc plasma channel creating so called trailing crater.

Based on tool electrode design, the following can be drawn:

- For 3D complex machining the plate, frame and ball ended cylindrical tool design is not in favor due to it is high electrode wear although it is capable of generating high MRR but not if the electrode is intended to be in service again since it will be eroded;
- On most of the experiments it was clear that fluid rate (dielectric pressure), peak current and pulse ON/OFF time play a role on machining characteristics and mainly on MRR and surface roughness;
- Polarity has major effect of BEAM process performance. High current density process is able to create high MRR with simple standard electrode pipe design with rotary motion;
- High current density EDM, BEAM, and Compound machining using super high speed EDM and arc machining have greatly shown their capability to obtain large MRR and contribute in lower TWR and enhance the surface quality due to high flushing pressure and humongous current and heat applied;
- As a development of EDM process, a further step has been taking for machining insulating material such as ceramics. Process stability was linked to the stability of the formed conductive layer which is formed using assisted electrode method and maintaining discharge (pulse) duration longer than set pulse duration;
- Workpiece grain size contributes in little influence on MRR, TWR, and surface roughness but scarcely compared to electric and flushing effect.

4.2. Recommendation

- More research needs to be conducted for work piece surface quality improvement. Bundled electrode need to be further investigated with various work piece and electrode material in order to come to a conclusion of classifying

electrode material is performing best with each work material;

- A combination of bundled electrode with high flushing and rotational motion of the electrode may obtain very high MRR, therefore, more investigation and experiment should be carried out for measuring process performance;
- Combination of both negative and positive polarity may be of predominant performance on BEAM process to have high MRR and good surface finish;
- EDM of insulating Ceramics was conducted and process of WEDM milling on Si3N4 was realized [53]. A control system to create conductive surface layer on insulating material in sinking EDM is an interesting topic to discover; reducing the electrode wear caused by performing this process because of the interference with the positive assisting conductive layer (electrode) is an issue should be treated either by coating or electric effect;
- Investigating the grain size effect of hard to cut materials on surface integrity by using EDM is a point on future interest;
- Examining different semi-conductive materials to determine the limit of conductivity that EDM process could attain with no assist of applying conductive layer is good to be under investigate;
- Additive manufacturing (AM) processes such as powder bed fusion and direct energy deposition are of great potential and capability to shape a complex electrode with inner flushing channel, which can acquire high MRR and yet resist the wear and maintain good surface integrity.

References

[1] Sharma, A., Sharma, M. D., & Sehgal, R. (2012). Experimental study of machining characteristics of titanium alloy (Ti–6Al–4V). Arab J Sci Eng Arabian Journal for Science and Engineering, 38(11), 3201-209.

[2] Kunieda, M., Lauwers, B., Rajurkar, K. P., & Schumacher, B. M. (2005). Advancing EDM through fundamental insight into the process. CIRP Annals - Manufacturing Technology, 54(2), 64-87.

[3] Indian Agricultural Statistics Research Institute. (n.d.). Statistical Genetics. Retrieved May 16, 2023,from http://ecoursesonline.iasri.res.in/mod/page/view.php?id=128438.

[4] Singh, J., & Kumar, V. (2012). Investigation on the material removal mechanism and the thermal aspects in the electrical discharge machining process. International Journal of Engineering and Technology, 2(9), 1503-507.

[5] Kunieda, M., Lauwers, B., Rajurkar, K. P., & Schumacher, B. M. (2005). Advancing EDM through fundamental insight into the process. CIRP Annals - Manufacturing Technology, 54(2), 64-87.

[6] Groover, M. P. (2012). Fundamentals of modern manufacturing: materials, processes and systems (4th ed.). John Wiley & Sons. ISBN 978-0470-467002.

[7] Ho, K. H., & Newman, S. T. (2003). State of the art electrical discharge machining (EDM). International Journal of Machine Tools and Manufacture, 43(13), 1287-1300.

[8] Gough, P. J. C. (1985). Electrode manufacturing: Conventional and new techniques. Proceedings of the First Electrical Machinery Symposium (EM85), 64-81.

[9] Carter, G. A., & Jergas, I. (1983). Choice of electrical discharge machining tooling. In E. C. Jameson (Ed.), Methods and Applications (pp. 57-61). Society of Manufacturing Engineers.

[10] Gu, L., Li, L., Zhao, W., & Rajurkar, K. P. (2012). Electrical discharge machining of Ti6Al4V with a bundled electrode. International Journal of Machine Tools and Manufacture, 53(1), 100-106.

[11] Bayramoglu, M., & Duffill, A. W. (2004). CNC EDM of linear and circular contours using plate tools. Journal of Materials Processing Technology, 148, 196-203.

[12] Bayramoglu, M., & Duffill, A. W. (1992). Production of three dimensional shapes using computational electrical discharge machining. In Proceedings of the International M.T.D.R. Conference (pp. 107-112).

[13] Sumi, N., Kato, C., Shimada, K., Yuzawa, T., Teramoto, H., Mizutani, A., & Kuriyagawa, T. (2016). Mechanism of defect generation in the TiC layer and Si layer by electrical discharge coating. Procedia CIRP, 42, 221-225.

[14] Tai, T. Y., & Nguyen, K. T. (2016). The grain size effect of polycrystalline diamond on surface integrity by using micro EDM. Procedia CIRP, 42, 305-310.

[15] Prihandana, G. S., Mahardika, M., Hamdi, M., Wong, Y. S., Miki, N., & Mitsui, K. (2013). A novel approach to improve machining accuracy using electrical discharge machining. International Journal of Precision Engineering and Manufacturing, 14(10), 1817-1822.

[16] Rajurkar, K. P., & Zhu, D. (1999). Improvement of electrochemical machining accuracy by using orbital electrode movement. CIRP Annals - Manufacturing Technology, 48(1), 139-142.

[17] Mohan, B., Rajadurai, A., & Satyanarayana, K. G. (2002). Effect of SiC and rotation of electrode on electric discharge machining of Al– SiC composite. Journal of Materials Processing Technology, 124, 297–304.

[18] Guu, Y. H., & Hocheng, H. (2001). Effects of workpiece rotation on machinability during electrical discharge machining. J. Mater. Manuf. Processes, 16(1), 91–101.

[19] Koyano, T., Suzuki, S., Hosokawa, A., & Furumoto, T. (2016). Study on the effect of external hydrostatic pressure on electrical discharge machining. Procedia CIRP, 42, 46-50.

[20] Muthuramalingam, T., & Mohan, B. (2015). A review on influence of electrical process parameters in EDM process. Archives of Civil and Mechanical Engineering, 15(1), 87-94.

[21] Ghoreishi, M., & Tabari, C. (2007). Investigation into the effect of voltage excitation of preignition spark pulse on the electrodischarge machining process. Materials and Manufacturing Processes, 22, 833-841.

[22] Tsai, Y. Y., & Lu, C. T. (2007). Influence of current impulse on machining characteristics in EDM. Journal of Mechanical Science and Technology, 21, 1617-1621.

[23] Muthuramalingam, T., & Mohan, B. (2013). Influence of discharge current pulse on machinability in electrical discharge machining. Materials and Manufacturing Processes, 28(4), 375-380.

[24] Kokubo, H., Takezawa, H., Horio, K., Mohri, N., & Yamazaki, T. (n.d.). A study on the material removal mechanism in EDM - single discharge experiments with low melting temperature alloy [Technical report]. Retrieved May 16, 2023, from http://www.jampt.jp/journal/vol48-2/files/48-2-5.pdf.

[25] Fan, Y., Bai, J., Li, Q., Li, C., Cao, Y., & Li, Z. (2016). Research on Maintaining Voltage of Spark Discharge in EDM. Procedia CIRP, 42, 28-33.

[26] Kliuev, M., Maradia, U., Boccadoro, M., Perez, R., Stirnimann, J., & Wegener, K. (2016). Experimental Study of EDM-Drilling and Shaping of Si-SiC and SiC. Procedia CIRP, 42, 191-196.

[27] Wang, C. C., & Yan, B. H. (2000). Blind hole drilling of Al2O3/6061 Al composites using rotary EDM. Journal of Materials Processing Technology, 102(1-3), 90-102.

[28] Zhao, W., Xu, H., Gu, L., Hong, H., & Rajurkar, K. P. (2015). Influence of

Polarity on the Performance of Blasting Erosion Arc Machining. CIRP Annals - Manufacturing Technology, 64(1), 213-216.

[29] Wang, F., Liu, Y., Zhang, Y., Tang, Z., Ji, R., & Zheng, C. (2014). Compound Machining of Titanium Alloy by Super High Speed EDM Milling and Arc Machining. Journal of Materials Processing Technology, 214(3), 531-538.

[30] Palanisamy, S., McDonald, S. D., & Dargusch, M. S. (2009). Effects of Coolant Pressure on Chip Formation While Turning Ti6Al4V Alloy. International Journal of Machine Tools and Manufacture, 49(9), 739-743.

[31] Chen, S. L., Yan, B. H., & Huang, F. Y. (1999). Influence of Kerosene and Distilled Water as Dielectrics on the Electric Discharge Machining Characteristics of Ti-6A1-4V. Journal of Materials Processing Technology, 87(1-3), 107-111.

[32] Sadeghi, M. H., Haddad, M. J., Tawakoli, T., & Emami, M. (2008). Minimal Quantity Lubrication-MQL in Grinding of Ti-6Al-4V Titanium Alloy. The International Journal of Advanced Manufacturing Technology, 44(5-6), 487-500.

[33] Lee, S. H., & Li, X. (2003). Study of the surface integrity of the machined workpiece in the EDM of tungsten carbide. Journal of Materials Processing Technology, 139, 315-321.

[34] Wong, Y. S., Lim, L. C., & Lee, L. C. (1995). Effects of flushing on electro-discharge machined surfaces. Journal of Materials Processing Technology, 48(1-4), 299-305.

[35] Jahan, M. P., Rajurkar, K. P., & Malshe, A. P. (2016). A comparative study on machining capabilities of wet and dry nano-scale electro-machining. Procedia CIRP, 42, 155-160.

[36] Uhlmann, E., Schimmelpfennig, T.-M., Perfilov, I., Streckenbach, J., & Schweitzer, L. (2016). Comparative analysis of dry-EDM and conventional EDM for the manufacturing of micro holes in Si3N4-TiN. Procedia CIRP, 42, 173-178.

[37] Toshimitsu, R., Okada, A., Kitada, R., & Okamoto, Y. (2016). Improvement in surface characteristics by EDM with chromium powder mixed fluid. Procedia CIRP, 42, 231-235.

[38] Zhao, W., Gu, L., Xu, H., Li, L., & Xiang, X. (2013). A novel high efficiency electrical erosion process – blasting erosion arc machining. Procedia CIRP, 6, 621-625.

[39] Dursun, K., & Cogun, C. (2009). Use of wire bunch electrodes in electric discharge machining. Rapid Prototyping Journal, 15(4), 291-298.

[40] Wang, F., Liu, Y., Shen, Y., Ji, R., Tang, Z., & Zhang, Y. (2013). Machining performance of Inconel 718 using high current density electrical discharge milling. Materials and Manufacturing Processes, 28(10), 1147-1152.

[41] Chen, J., Gu, L., Xu, H., & Zhao, W. (2015). Study on blasting erosion arc machining of Ti-6Al-4V alloy. The International Journal of Advanced Manufacturing Technology, 78(9-12), 1519-1526.

[42] Zhu, Y., Chen, J., Xu, H., Gu, L., & Zhao, W. (2016). Research on the surface quality of the blasting erosion arc machined stainless steel. Procedia CIRP, 42, 252-256.

[43] Chen, J., Gu, L., Zhu, Y., & Zhao, W. (2017). High efficiency blasting erosion arc machining of 50 vol.% SiC/Al matrix composites. Proc IMechE Part B: J Engineering Manufacture, 231(14), 2657-2666.

[44] Chen, J., Gu, L., Liu, X., Zhu, Y., & Zhao, W. (2018). Combined machining of SiC/Al composites based on blasting erosion arc machining and CNC milling. Int J Adv Manuf Technol, 96, 111–121.

[45] Zaw, H. M., Fuh, J. Y. H., Nee, A. Y. C., & Lu, L. (1999). Formation of a new EDM electrode material using sintering techniques. Journal of Materials Processing Technology, 89-90, 182-186.

[46] Kunieda, M., & Muto, H. (2000). Development of multi-spark EDM. CIRP Annals - Manufacturing Technology, 49(1), 119-122.

[47] Lin, Y. C., Yan, B. H., & Chang, Y. S. (2000). Machining characteristics of titanium alloy (Ti-6Al-4V) using a combination process of EDM with USM. Journal of Materials Processing Technology, 104(3), 171-177.

[48] Aspinwall, D. K., Dewes, R. C., Burrows, J. M., Paul, M. A., & Davies, B. J. (2001). Hybrid high speed machining (HSM): System design and experimental results for grinding/HSM and EDM/HSM. CIRP Annals - Manufacturing Technology, 50(1), 145-148.

[49] Shibayama, T., & Kunieda, M. (2006). Diffusion bonded EDM electrode with micro holes for jetting dielectric liquid. Annals of the CIRP, 55(1), 171-174.

[50] Han, F., Wang, Y., & Zhou, M. (2009). High-speed EDM milling with moving electric arcs. International Journal of Machine Tools and Manufacture, 49(1), 20-24.

[51] Govindan, P., & Joshi, S. S. (2010). Experimental characterization of material removal in dry electrical discharge drilling. International Journal of Machine Tools and Manufacture, 50(5), 431-443.

[52] Singh, S., & V, M. (2012). A parametric optimization of electric discharge drill machine using Taguchi approach. Journal of Engineering, Computers & Applied Science, 1(4), 39-47.

[53] Zhang, C., Wang, X., Zhang, Q., Guo, Y., & Hu, X. (2015). Investigating the use of electrochemical discharge machining with super-high pressure interior flushing for enhanced machining performance of micro holes. Journal of Manufacturing Processes, 17, 66-74.

[54] Shen, Y., Zhang, Y., Liu, Y., & Xiong, Y. (2016). A high-efficient dry hybrid machining method of EDM and arc machining. The International Journal of Advanced Manufacturing Technology, 85(5-8), 1455-1463.

[55] Gotoh, Y., Takahashi, T., Nakamura, K., & Tani, T. (2016). Electrical discharge machining of insulating ceramics by controlling electrical conductive surface layer. CIRP Annals - Manufacturing Technology, 65(1), 201-204.

[56] Fu, Y., Li, H., Yu, Y., Zhang, W., & Zhou, J. (2016). Comparing the properties of the white layer produced by laser cutting and electrical discharge machining of Nitinol shape memory alloy. The International Journal of Advanced Manufacturing Technology, 87(9-12), 3075-3084

[57] Wu, J., Wang, X., Zhang, Q., & Wei, D. (2020). A sustainable and high-efficiency green electrical discharge machining milling method. Journal of Cleaner Production, 254, 120151.

[58] Ablyaz, T. R., Khmyrov, R. S., Kudryashov, D. A., & Sokolov, I. A. (2022). Investigating the use of electrode tools obtained by selective laser melting to create textured surfaces. IOP Conference Series: Materials Science and Engineering, 1615, 012017.

[59] Yang, J., Gao, Y., Zhu, D., Gu, L., & Li, S. (2022). Experimental study on the processing of γ-TiAl using blasting erosion arc machining. International Journal of Advanced Manufacturing Technology, 118(1-4), 301-308.

دراسة شاملة لتأثير عوامل التشغيل وعملية التجريف والتشكيل بالقوس على معدل إزالة المواد (EDM)وسلامة الاسطح في عملية تصنيع وتشكيل المواد بالتفريز الكهربائي

[*1]هيثم حديدي
[1] قسم الهندسة الميكانيكية، كلية الهندسة، جامعة جازان، المملكة العربية السعودية

الملخص

الملخص: تعد عملية التفريز بالتفريغ الكهربائي (**EDM**) واحدة من الأساليب القيمة لتصنيع وتشكيل المواد الصعبة التصنيع. نظرًا لقدرة عملية التفريز بالتفريغ الكهربائي على تشكيل أي مواد موصلة للكهرباء ونظرا للاستخدام الواسع لتلك المواد في تطبيقات مختلفة ونطاق واسع، فقد أصبح من الضروري تحسين معدل إزالة المواد **(MRR)** للحصول على أداء أفضل وتقليل التكلفة/الوقت وزيادة الدقة. يعد عامل معدل إزالة المواد **(MRR)** مقياس أداء مهم للغاية وقد تم توظيف معظم الأبحاث لتقييمه وتحسينه. على الرغم من النهج والطرق التي تم اتباعها ، إلا أن الأبحاث في هذا المجال تشترك في نفس الأهداف التي تركز على زيادة معدل إزالة المواد وتقليل معدل تآكل الأدوات المستخدمة وتحسين جودة السطح للعينات.

يتمثل هدف هذه الورقة في دراسة الأبحاث والأعمال المتعلقة بتطوير معدل إزالة المواد **MRR** مع دراسة شاملة لجميع العوامل المؤثرة في عملية التفريز بالتفريغ الكهربائي (**EDM**) بالإضافة إلى التركيز في هذه الدراسة على نهج متطور لاستخدام أداة تسمى "الأقطاب المجمعة" في عملية تشكيل بالتفريغ الكهربائي بالتآكل الانفجاري **(BEAM)** وتأثيره على معدل التآكل **MRR**.

الكلمات المفتاحية: عملية التفريز بالتفريغ الكهربائي (EDM)؛ عملية تشكيل بالتفريغ الكهربائي بالتآكل الانفجاري (BEAM)؛ معدل إزالة المواد (MRR)؛ معدل تآكل أدوات التشغيل (TWR)؛ الأقطاب المجمعة.

Estimation of gamma attenuation from high energy laser-material interactions using Monte Carlo simulation

A. M. Ali* and W. A. Ghaly

Physics Department, Faculty of Science, Jazan University, Jazan, Kingdom of Saudi Arabia.

Abstract

The present work demonstrates the gamma rays resulting from the high energy laser interaction with the material, the laser intensity ranging from 10^{19} to 10^{21} W/cm^2 and produces gammas ray with different energies between 20 keV – 25 MeV. MCNP code is used to simulate the penetration of gamma rays with two groups of concrete samples, with and without steel fiber at corresponding energies to that produced by laser beam. MCNP code and Phy-X/PSD code were also used to calculate some shielding parameters such as atomic cross section (ACS), effective atomic number (Zeff), mass attenuation coefficient (MAC), linear attenuation coefficient (LAC), tenth value, half value layers (TVL, HVL), mean free path (MFP) and effective electron number (Neff) of concrete samples. The concrete samples under investigation are of densities ranging from 2.095 g/cm^3 to 2.9 g/cm^3. Both results of Phy-X/PSD and MCNP show good agreement in the studied energy range. The ilmenite-limonite concrete sample shows better shielding properties than the other concrete samples.

Keywords: High-intensity laser, Gamma ray, Concrete target, Monte Carlo simulation method and Phy-X/PSD program.

1. Introduction

Laser devices have experienced rapid development in the last two decades and it has become possible to produce a laser beam with high intensity reach to 10^{21} W/cm^2 or more and this development has been followed by production of hot electrons, accelerated ions, High Harmonic Generation, pulsed neutrons, hard x-rays and intense gamma rays. Gamma rays with energies multi-MeV with highest peak brilliance $\sim 2 \times 10^{20}$ photons $s^{-1}mm^{-2}mrad^{-2}$ (Wu D. et. al., 2018), or more can be produced from the interaction of high intensity laser beam with the material. Different laboratories measured the produced gamma ray energies from 20 to 150 KeV (Badziak J. et. al., 2002), 200 to 600 keV (Xue K. et. al., 2020), 9, 15 and 25 MeV (Kelardeh H. et. al., 2015, Brauckmann aus Arnsberg S. K., 2017 & Schille J. et. al., 2021). Also, computational methods and computer simulation are used to predicate and estimate the gamma rays from laser-material interaction (Vysko˘cil g. J. et. al., 2018 & Phuoc K. T. et. al., 2012). Moreover, Monti Carlo simulation and PhyX/PSD codes are used in many research studies to investigate gamma ray penetration through different materials (F. Afaneh et. al., 2022, F Moradi et. al., 2019, Gurinder Pal Singh et. al., 2020, Mohamed Hegazi Ghozza, 2023)

Now there is a need for the preparation of laboratories and places to serve the production of gamma rays by the laser technology in small and compact area. In present work, a study is being conducted on the interaction of gamma rays produced by laser technology with a material. Ordinary concrete, hematite–serpentine concrete, ilmenite–limonite concrete, cement fiber concrete and cement fiber magnetite concrete samples were investigated by MCNP 4C code and Phy-X/PSD program.

Penetration of gamma photons through different samples is simulated by MCNP 4C (Judith F. Briesmeister, 2000) code. MCNP software dealing with photon energy range 1eV-100MeV. Different parameters could be output directly by Phy-X/PSD codes. Mass attenuation coefficients, (MAC), mean free path (MFP), cross section could be calculated by both MCNP 4C and Phy-X/PSD codes (Singh, V.P. et. al., 2015, Sayyed M. I. et. al., 2018 & Askın A., 2020). Investigated samples are considered to be homogeneously. 20keV, 150 keV, 200 keV, 300 keV, 500 keV, 600 keV, 9 MeV, 15 MeV and 25 MeV are the most interest energies in this study (Sadawy M.M. et. al., 2013, Sadawy M.M. et. al., 2008, Ziying Z., 2012, Sadawy M.M., 2008, Sadawy M.M. et. al., 2011, Büyükyıldız M., 2017).

MCPLIB22 library provides MCNP code by the required cross section date. Relative error less than 0.01%. is achieved with results of MCNP. In MCNP simulation, the energies of the photon are chosen down to very low for photoelectric absorption region to demonstrate the applicability in low energy region. A comparison between the results of MCNP 4C code and Phy-X/PSD program (Sakar E. et al., 2020) is presented. This study is considered as a pilot study for laboratories that wish to protect their researchers and provide basic lines for the establishment of laboratories based on this technology.

and elemental composition of concrete samples (Abdo A. El-Sayed et al, 2003, Bashter I. I., 1997).

Elemental analysis (fraction by weight %)	Samples				
	S1 (ordinary concrete)	S2 (Hematite serpentine)	S3 (Ilmenite Limonite)	S4 (Cement Fiber)	S5 (Cement Fiber Magnetite)
H	0.0094	0.0129	0.0066	0.0284	0.0178
B	0	0	0	0	0.0929
C	0.0009	0	0	0.1091	0.09457
O	0.5365	0.4350	0.3645	0.4323	0.3282
Na	0.0046	0	0	0	0
Mg	0.0015	0.0664	0.0015	0.00602	0.005
Al	0.0132	0.0167	0.0080	0.0151	0.0061
Si	0.3673	0.1053	0.0306	0.0644	0.0258
S	0.0008	0.0009	0.0008	0.0043	0.0017
K	0.0031	0	0	0	0
Ca	0.0564	0.0597	0.0583	0.3162	0.1268
Ti	0	0	0.1603	0	0.0287
Cr	0	0	0	0	0.00164
Fe	0.0063	0.3031	0.3694	0.0294	0.2742
Density (g/cm^3)	2.3	2.5	2.9	2.095	2.858

2. Materials and Methods:

This study is devoted to evaluate the radiation shielding performance of five different samples of concretes using Phy-X/PSD program and Monte Carlo simulation MCNP 4C code. The chemical composition and physical properties of concrete samples has been taken from (Abdo A. El-Sayed et al, 2003, Bashter I. I., 1997), and are shown in table 1. The method of calculation of different shielding parameters are given and discussed in the following sections.

2.1 Gamma-ray shielding parameters:

The performance of shielding materials against gamma photons can be performed by evaluating different parameters such as HVL, MAC, TVL, N_{eff}, Z_{eff}, and MFP. Mass attenuation coefficient MAC in (cm^2/g) is the most important parameter which describes the photon penetration in materials, which can be computed by the following relation:

$$I = I_0 e^{-\mu x} \quad (1)$$

$$MAC = \left(\frac{\mu}{\rho}\right) = \frac{ln(I_0/I)}{\rho x} \quad (2)$$

Where I_0 is incident beam and I is transmitted beam, x is the mass thickness and ρ is density of investigated sample. μ is linear attenuation coefficient (LAC)

Both TVL and HVL estimate directly the layer thickness needed to absorb the radiation by factor of □ and ½ respectively. TVL and HVL can be calculated from (μ) as follows (Taqi A. H., et al., 2021, Reda A. M. et al, 2020, Tellili B., et al, 2017, Elmahroug Y., 2015)

$$HVL = \frac{0.693}{\mu} \quad (3)$$

$$TVL = \frac{2.303}{\mu} \quad (4)$$

Mean free path (MFP), is the average path between two successive collisions of gamma photons and can be calculated by using the following relation (Reda A. M., 2021)

$$MFP = \frac{1}{\mu} \quad (5)$$

The electronic cross-section (σ_e) and atomic cross-section (σ_a), could be obtained by equations 6,7 (Taqi A. H., et. al., 2021, Reda A. M. et. al., 2020, Tellili B., et. al., 2017, Elmahroug Y., 2015, Reda A. M., 2021) :

$$\sigma_a = \frac{\mu/\rho}{N_A \sum_i \frac{W_i}{A_i}} \quad (6)$$

$$\sigma_e = \frac{1}{N_A} \sum_i \frac{f_i A_i}{Z_i} \left(\mu/\rho\right)_i . \quad (7)$$

Where N_A is the Avogadro's number and w_i is fractional weight, A_i is atomic weight, f_i is fractional abundance, Z_i is atomic number, μ is linear attenuation coefficient (LAC), and $(\mu/\rho)_i$ is mass attenuation coefficient (MAC) of the i^{th} element in the composition of the shielding material.

Effective electron number (N_{eff}) and effective atomic number (Z_{eff}) could be evaluated by equations 8,9

$$Z_{eff} = \frac{\sigma_a}{\sigma_e} \quad (8)$$

$$N_{eff} = \frac{\mu/\rho}{\sigma_e} \quad (9)$$

2.2 MCNP simulation:

MCNP 4C code can be used to simulate the penetrated flux of gamma rays through investigated concrete samples. In MCNP 4C simulation, gamma ray source is isotropic, monochromatic point source, photon mode is used, the photon importance is one inside all cells and zero in cutoff area. Flux of transmitted gamma rays is estimated using F4 tally. Figure 1 shows the geometry of the simulation. The geometry consists of source collimator, detector collimator and investigated sample with the dimension shown in figure 1. The transmitted gamma photons are calculated behind different layer thicknesses (1-5 cm) of each sample then the mean value is calculated. The elemental analysis of investigated samples was input to MCNP 4C code.

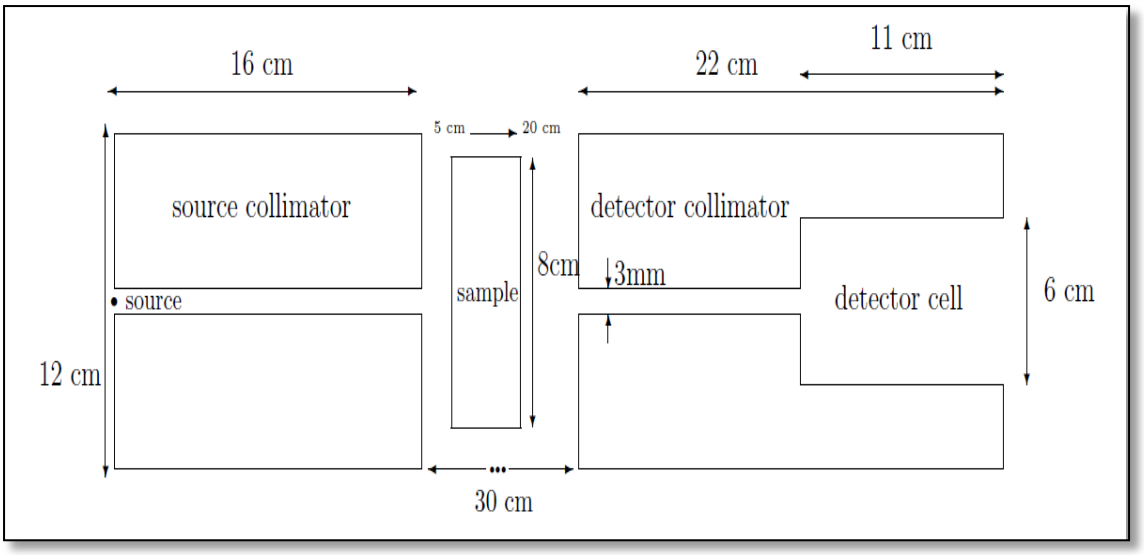

Fig. 1. Geometrical design of MCNP4c simulation of penetrated gamma rays through concrete samples.

3. Results and Discussion

3.1 Mass attenuation coefficient (MAC)

Mass attenuation coefficient (MAC) is the most important parameter which can explain material absorbing characterization. For better gamma radiation protection materials, MAC should be higher (Attix. F., 1986). The obtained results of mass attenuation coefficient (cm^2/g) for the investigated samples, ordinary and hematite serpentine concrete samples, ilmenite-limonite, cement fiber and cement fiber magnetite, have been shown in figure 2.

MAC of each sample estimated by both MCNP 4C and Phy-X/PSD codes are displayed in figure 2. Figure 2 shows a good agreement between MCNP and Phy-X/PSD results. The ilmenite–limonite sample showed higher mass attenuation coefficient than the cement fiber magnetite sample, MAC values of cement fiber magnetite sample is higher than MAC values of cement fiber, while ordinary and hematite serpentine concrete samples shows the lowest values of MAC.

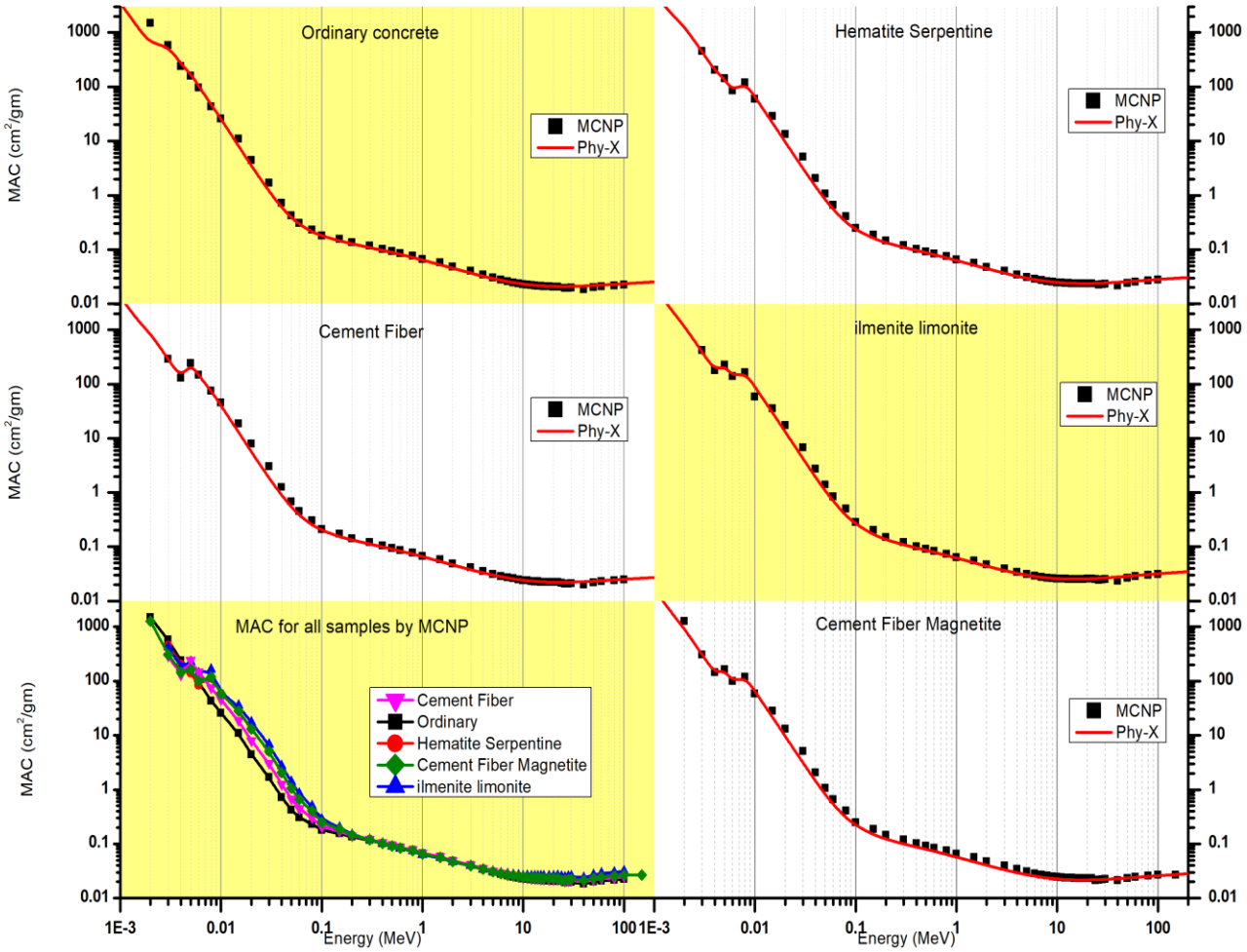

Fig. 2. Variations of MAC for the investigated concrete samples versus photon energy in MeV.

3.2 Linear attenuation coefficient (LAC)

Linear attenuation coefficient is another beneficial parameter to estimate the attenuation shielding of the investigated samples against gamma-rays. The variation of linear attenuation coefficient for the studied samples against photons energy was displayed in figure 3. Figure 3 shows LAC of each sample estimated by both MCNP 4C code and Phy-X/PSD software program. Figures 3 shows a good agreement between Phy-X/PSD and MCNP results. The variation of LAC can be explained using photoelectric absorption cross section for low-energy range, Compton scattering cross section for intermediate-energy range and pair production cross section for high-energy range. At 10 keV energy, the values of LAC are of order hundreds which decrease due to the photoelectric cross section is inversely proportional to $E^{7/2}$ (Das A. and Ferbel T.,2005). At low-energy range (E < 100 keV), LAC has very large values. The values of LAC of all the samples decrease to below 10 cm^{-1} as photon energy reaches 100 keV. As photon energy increases greater than 100 keV, the decreasing rate of LAC was very slow. It is due the fact that the interaction cross section is linearly dependent on atomic number in Compton scattering region. It was observed that the difference was very small between energy range 0.2 and 2 MeV, where Compton region.

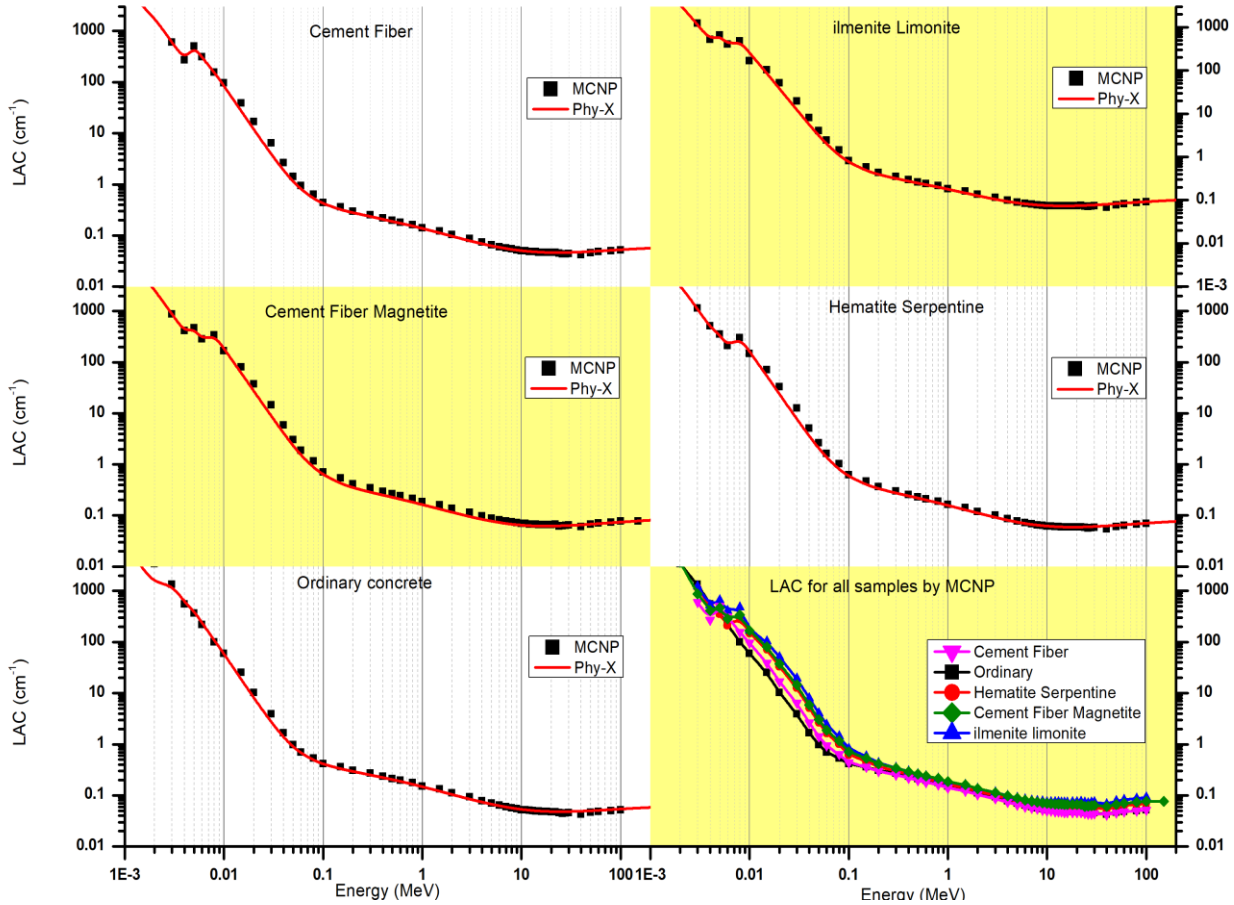

Fig. 3. Variations of LAC for investigated concrete samples versus photon energy in MeV.

3.3 Mean free path (MFP)

MFP is the most important quantity that expresses the capability of such material to attenuate or stop γ-radiation. It has been reported that material with lower value of MFP has better shielding efficiency (Al-Hadeethi Y and Sayyed MI,2020, Askın A., 2020). The obtained results of MFP variation with photon energies were displayed in figure 4.

This figure shows that, photons of high energy can penetrate concrete samples. Higher density sample like ilmenite-limonite is of lower MFP values than that of cement fiber magnetite. In addition, MFP values of cement fiber magnetite sample is higher than MFP values of hematite and ordinary concrete samples. So, ilmenite-limonite concrete sample is a good absorber of gamma-ray photons while ordinary concrete has lowest values of MFP. In the energy range below 100 keV, MFP values increase rapidly from few micrometers up to 1 cm, while MFP values slowly increase to 10 cm in the range 100 keV-10 MeV. Above 10 MeV, the MFP values are saturated. The MFP of photons of highest interest energy (25 MeV) is 14 cm for ilmenite-limonite concrete and 22 cm for ordinary concrete.

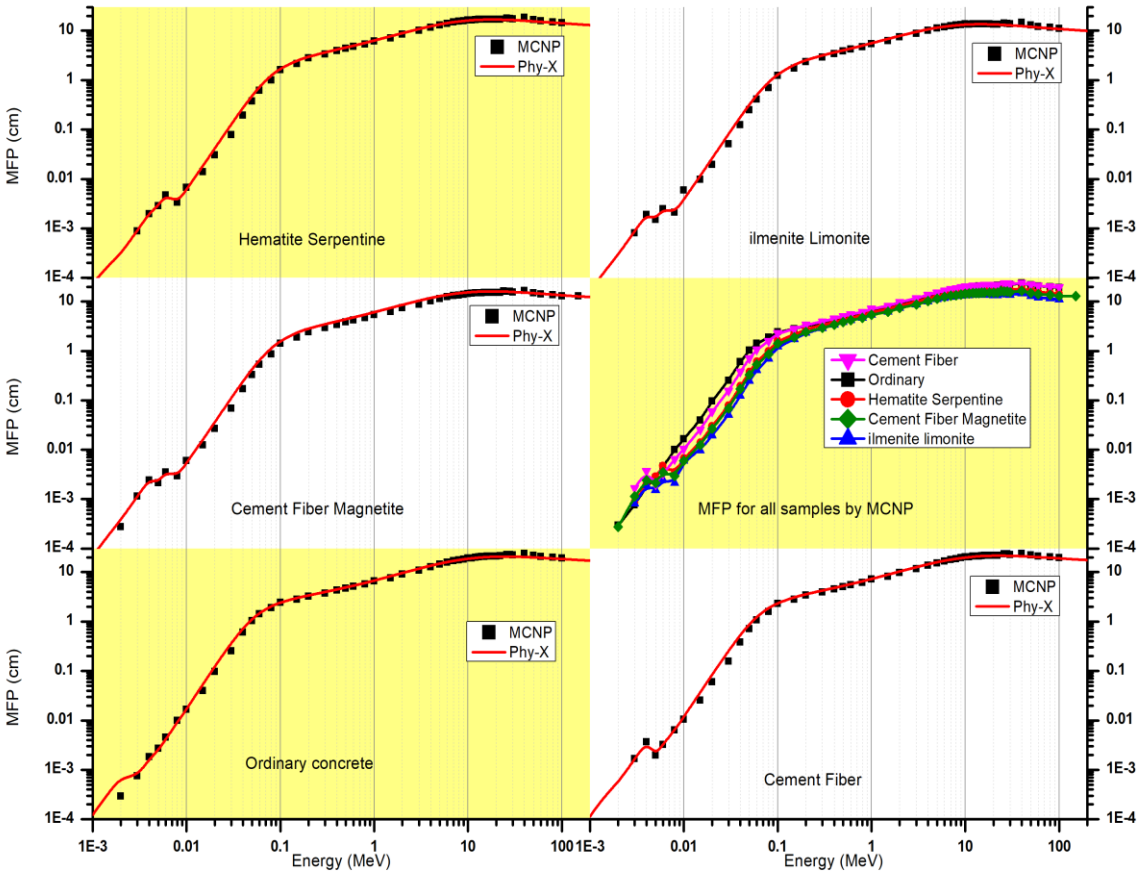

Fig. 4. Variations of MFP for the investigated concrete samples versus photon energy (in MeV).

3.4 Half value layer (HVL)

Half value layer determines the required thickness to absorb the half of incident intensity of gamma photons (Al-Hadeethi Y and Sayyed MI, 2019). Figure 5 represents the HVL for the samples under study. From figure, it is clear that by increasing sample density, HVL decreases. Ilmenite-limonite concrete sample has highest density, so HVL is least, which shows that it has a better attenuation than the other examined concrete samples. HVL values increase rapidly in the energy range below 100 keV due to photoelectric interaction which is the main interaction in that range. In the range 100 keV-10 MeV, HVL values increase slowly. Above 10 MeV, HVL values are saturated. HVL value of 25 MeV photons is 10 cm for ilmenite-limonite concrete sample and 15.6 cm for ordinary concrete sample.

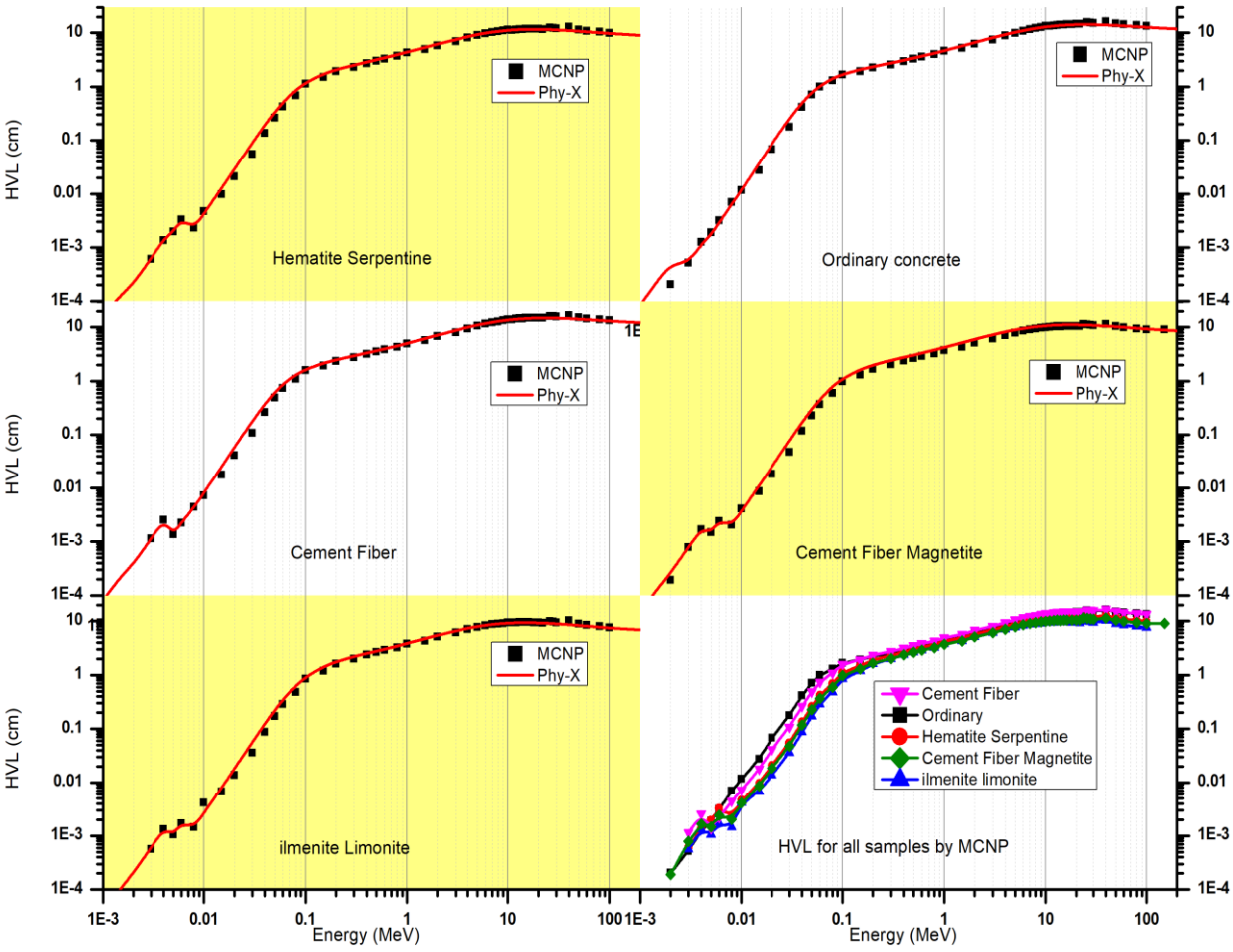

Fig. 5. Variations of HVL for the investigated concrete samples versus photon energy in MeV.

3.5 Tenth value layer (TVL)

Attenuation proficiency of material can also be estimated by its TVL value. Materials of lower TVL required lower layer to stop γ-rays (Al-Hadeethi Y and Sayyed MI, 2020). The TVL for the sample under investigation is displayed in figure 6. This figure shows that TVL gives almost the same behavior to HVL. Of course, the layer needed to transmit 10% of incident gamma rays (TVL) is greater than the layer needed to transmit 50% of the incident gamma rays (HVL). TVL value of 25 MeV photons is 35 cm for ilmenite-limonite concrete sample and 52 cm for ordinary concrete sample.

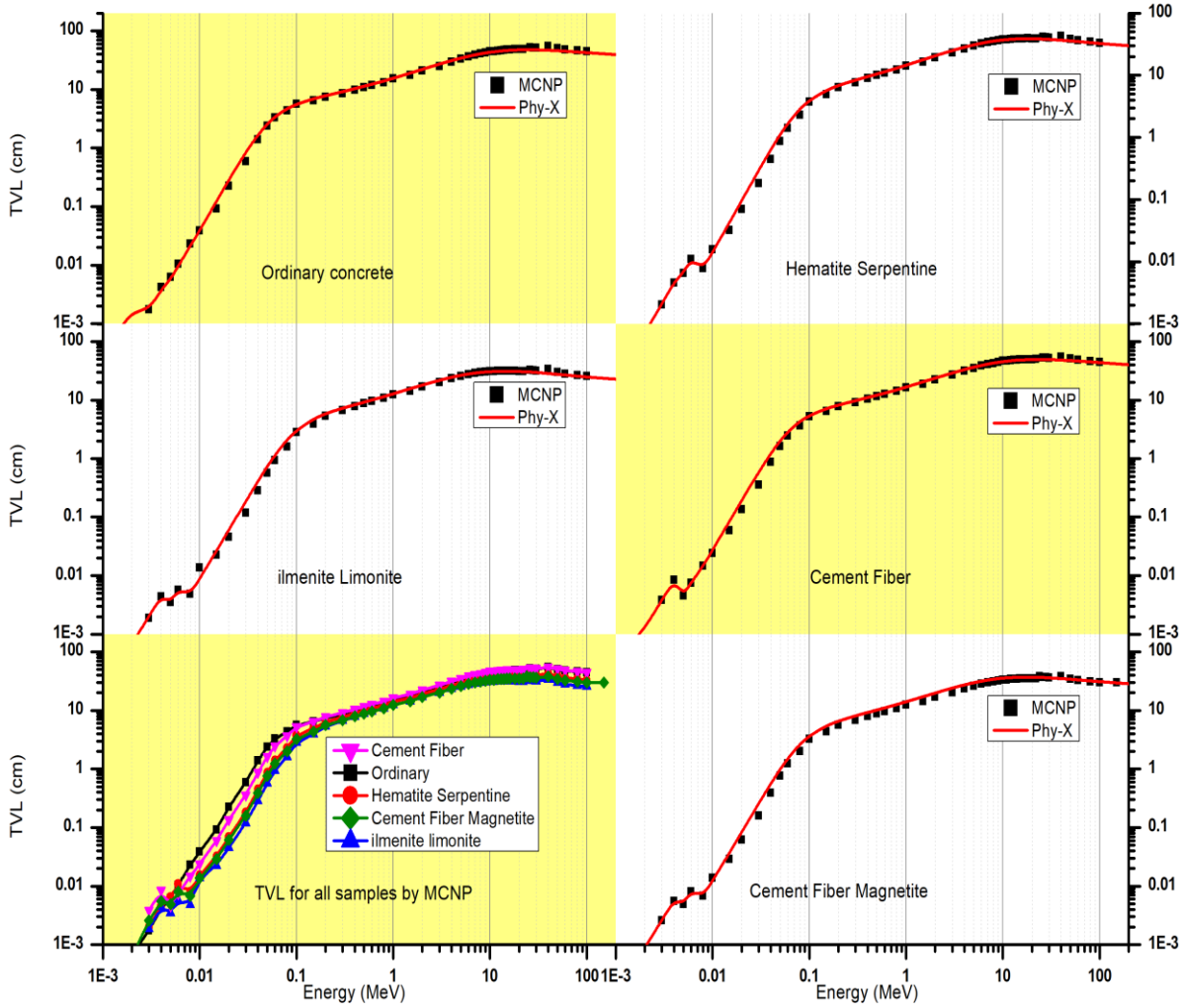

Fig. 6. Variations of TVL for the investigated concrete samples versus photon energy in MeV.

3.6 Atomic cross section (ACS)

The calculated ACS values for concrete samples are plotted in figure 7. It is clearly shown that the values of ACS depend on densities of investigated concrete samples and the energy of the incident photon. The plots of ACS with photon energy have the same profile as MAC plots. So, the change in ACS with incident photon energy for the investigated samples can be discussed in terms of mass attenuation coefficients (see equation 6).

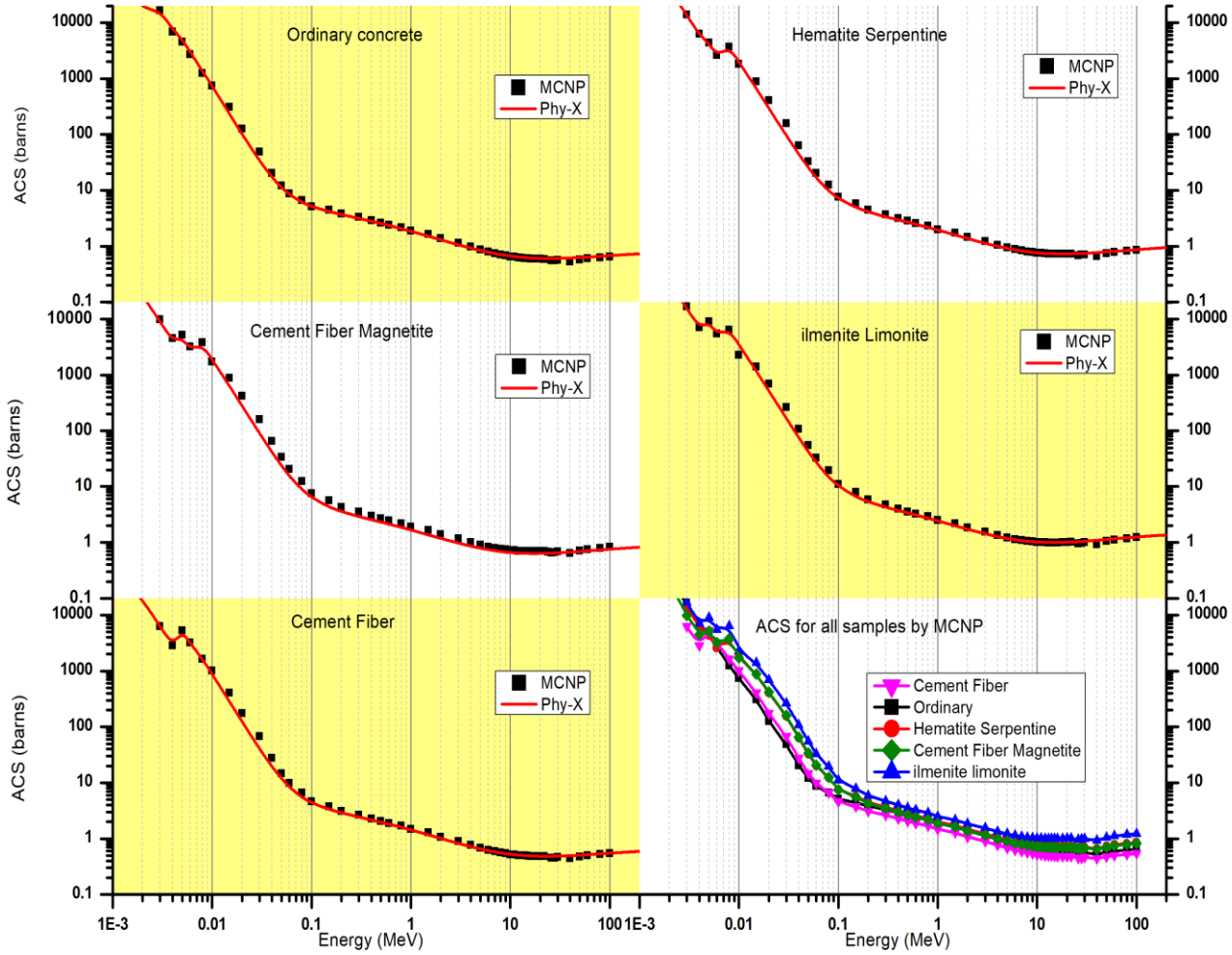

Fig. 7. Variations of ACS for the investigated concrete samples versus photon energy (in MeV).

3.7 Dependency of iron percentage

As mentioned, 20 keV, 150 keV, 200 keV, 300 keV, 500 keV, 600 keV, 9 MeV, 15 MeV, 25 MeV are the photon energies produced as a secondary radiation of high intensity laser beam. The mass attenuation coefficients of investigated concrete samples for most interest energies is tabulated in table 2. From this table, it is clear that ilmenite-limonite and hematite–serpentine concrete samples have higher values of mass attenuation coefficient which means

that these concrete samples have higher shielding performance than the other samples.

The iron percentage dependency of mass attenuation coefficient is displayed in figure 8. It is clear that, the mass attenuation coefficient increases as the iron percentage increases. This dependency is more clearance for 20 keV which leis in photoelectric effect region.

Table 2. Mass attenuation coefficients at interested energies and iron percentage of concrete samples.

Energy (MeV)	Ordinary concrete	Cement fiber	cement fiber magnetite	hematite–serpentine	ilmenite–limonite
Fe %	0.0063	0.0294	0.2742	0.3031	0.3694
0.020	4.45782	8.00598	13.12642	13.24912	17.54067
0.150	0.15522	0.17058	0.18618	0.18619	0.20093
0.200	0.13392	0.14097	0.14407	0.14415	0.14808
0.300	0.11672	0.12054	0.11942	0.11955	0.11959
0.500	0.09228	0.09425	0.09151	0.09165	0.09011
0.600	0.08465	0.08639	0.08373	0.08384	0.08227
9.00	0.02375	0.02471	0.02498	0.02529	0.02615
15.00	0.02113	0.02233	0.02309	0.02362	0.02516
25.00	0.0193	0.02065	0.02173	0.0223	0.02421

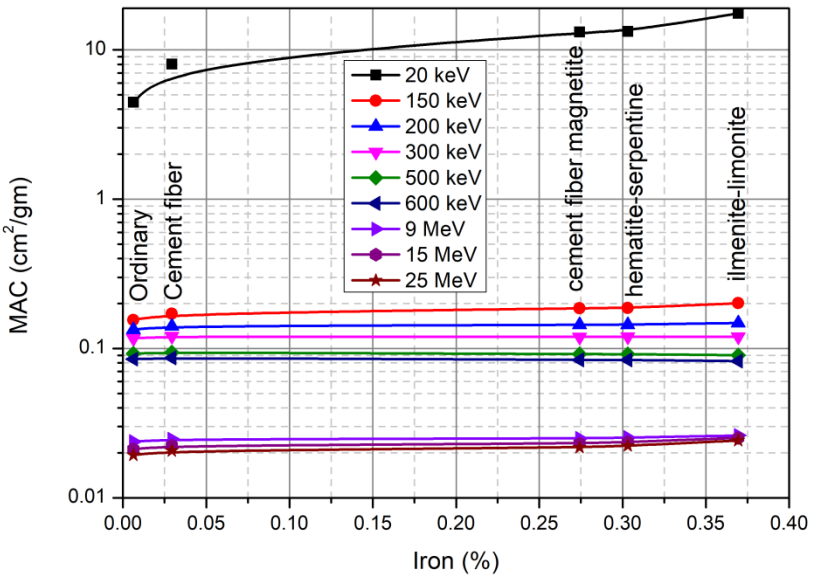

Fig. 8. Variations of mass attenuation coefficient of the investigated concrete samples versus percentage of iron content (%).

3.8 Dependency of density

The mass attenuation coefficients of investigated concrete samples for most interest energies as a function of sample density is displayed in figure 9.

In general, the attenuation properties of materials depend on materials density but in low energy the photoelectric interaction is prevalent, so the attenuation properties are more sensitive to the atomic number (σ_{photo} α Z^5) (Das A. and Ferbel T., 2005). Iron (Z=26) is the element of highest atomic number in the constituent of samples under investigation, so the sample of higher ratio of iron will show more shielding efficiency in low energy range even it has lower density such as cement fiber and ordinary concrete samples. Although, cement fiber concrete sample has lower density (density= 2.095 g/cm^3) than ordinary concrete sample (density=2.3 g/cm^3), it has more shielding efficiency than ordinary concrete sample in low energy. This is due to cement fiber has more iron percentage (0.0294) than ordinary concrete (0.0063).

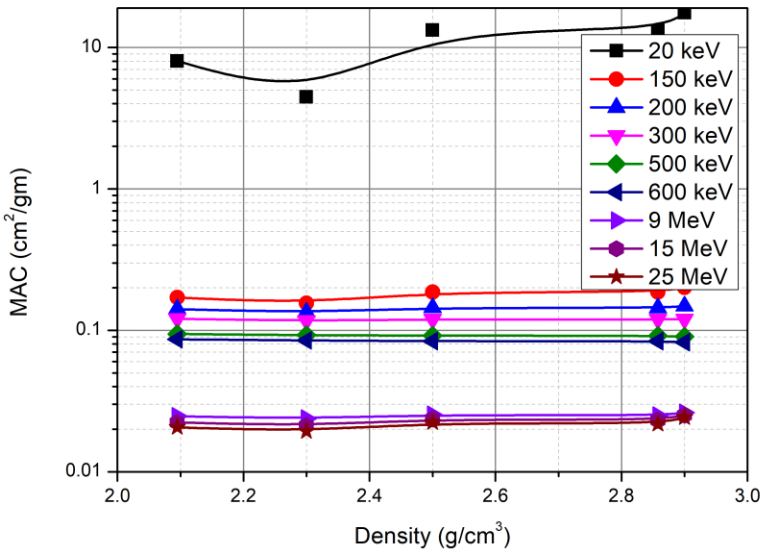

Fig.9.Variations of mass attenuation coefficient of the investigated concrete samples versus sample density.

3.9 Effective atomic number (Z_{eff})

Z_{eff} is a very useful parameter that determines the attenuation capability of studied samples. Materials of higher value of Z_{eff} have higher γ-rays shielding efficiency (Al-Hadeethi Y and Sayyed MI, 2019). The Z_{eff} calculation for the investigated samples is calculated using both MCNP 4C and Phy-X/PSD programs. Figure 10 shows the relation between Z_{eff} values of the samples under investigation and photon energy. At lowest photon energy, Z_{eff} has higher value. Z_{eff} decreases rapidly in the energy range 30-300 keV. After 300 keV, the curve shows slowly increasing in the Z_{eff} values. Moreover, Z_{eff} also depends on the density of the

sample. It is noted that ilmenite–limonite sample has largest value of Z_{eff}. These results are further in favor that examined samples can be used to have high shielding properties.

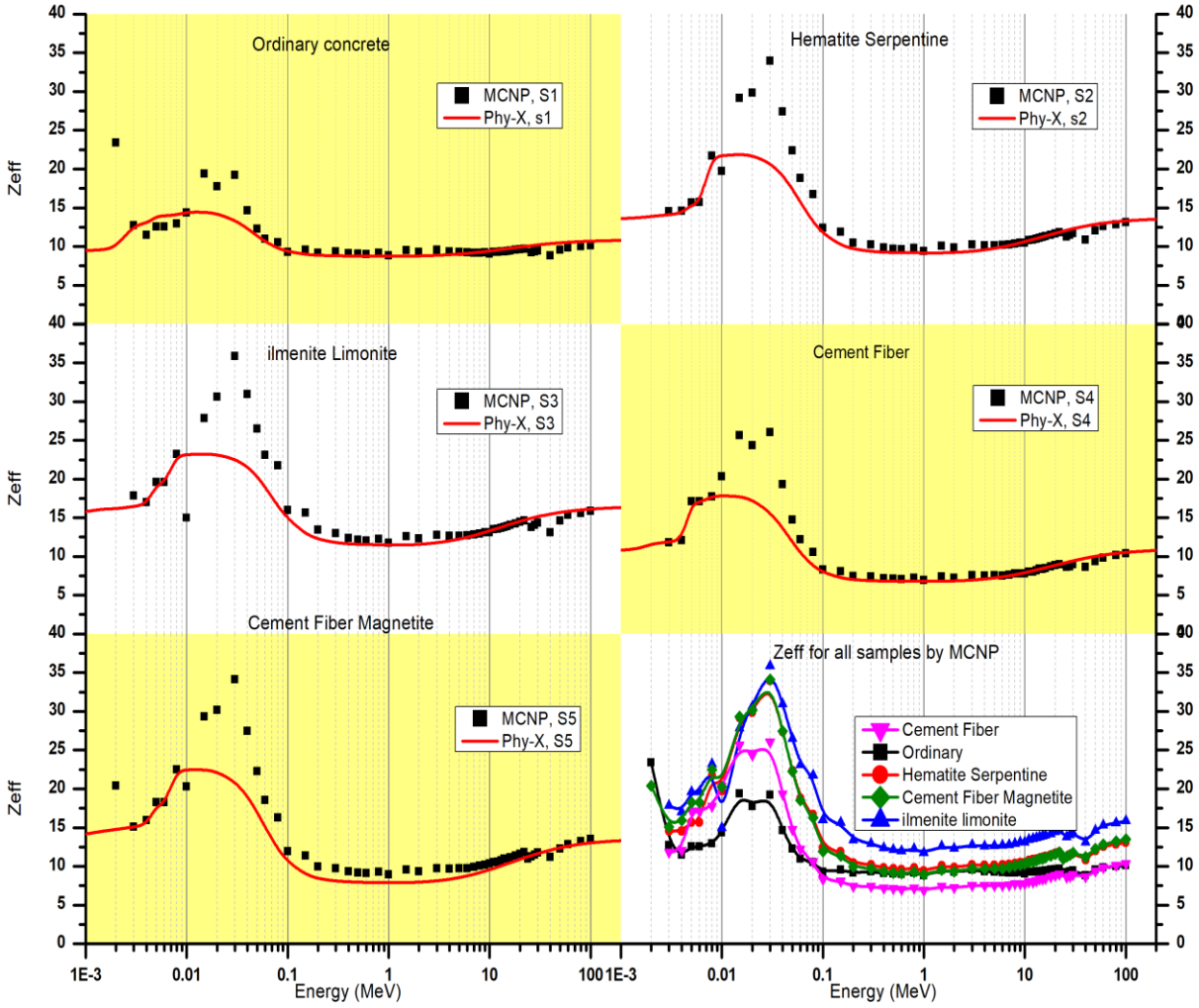

Fig. 10. Variations of Z_{eff} for the investigated concrete samples versus photon energy in MeV.

3.10 Effective electron number (N_{eff})

The other important quantity called "effective electron number or effective electron density" is defined as the electrons per unit mass of the absorber (I. Akkurt, 2011). The behavior of N_{eff} for concrete samples versus photon energy is shown in figure 11. It is observed that N_{eff} effective electron density has maximum values at 20 keV and reduced rapidly until 300 keV. All samples have the same value of effective electron density in the range (300 keV-10 MeV).

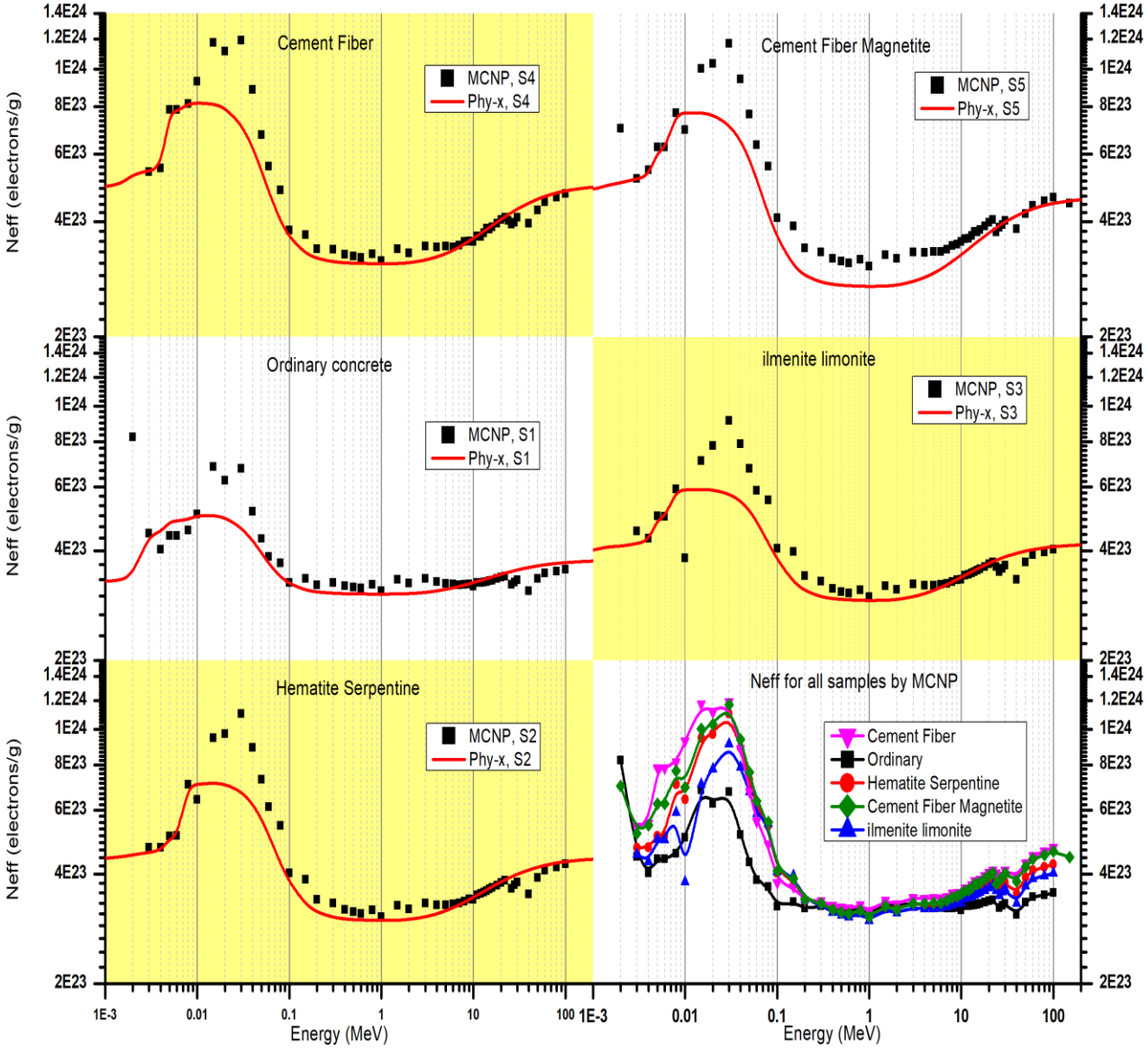

Fig. 11. Variations of N_{eff} for the investigated concrete samples versus photon energy in MeV.

Conclusion

In this study the photon attenuation parameters of concrete samples with and without steel fibers are calculated by Phy-X/PSD and simulation by MCNP for energies 20 keV, 150 keV, 200 keV, 300 keV, 500 keV, 600 keV, 9 MeV, 15 MeV and 25 MeV. By comparing the results of Phy-X/PSD and MCNP, it can be concluded that:

- The mass attenuation coefficients, atomic cross-sections, HVL, TVL, MFP of both Phy-X/PSD and MCNP methods are in good agreement.
- The ilmenite–limonite sample showed higher mass attenuation coefficient than the cement fiber magnetite sample, MAC values of cement fiber magnetite sample is higher than MAC values of cement fiber,

while ordinary and hematite serpentine concrete samples shows the lowest values of MAC.

- The MFP of photons of highest interest energy (25 MeV) is 14 cm for ilmenite-limonite concrete and 22 cm for ordinary concrete.
- HVL value of 25 MeV photons is 10 cm for ilmenite-limonite concrete sample and 15.6 cm for ordinary concrete sample.
- TVL value of 25 MeV photons is 35 cm for ilmenite-limonite concrete sample and 52 cm for ordinary concrete sample.
- The mass attenuation coefficient and thereby cross section of the concrete samples increases as the iron percentage increases.
- Ilmenite–limonite concrete sample has largest value of Z_{eff}.
- Ilmenite-limonite concrete sample has the highest shielding efficiency followed by cement fiber magnetite concrete sample. This is due to that, these samples have the highest densities and highest percentage of iron (see table 1) in comparison to the other concrete samples.
- The simulated MCNP results, which have 0.01% relative error, showed a good agreement with Phy-X/PSD values. This agreement indicates that Monte Carlo method may be used to perform more calculations on the photon attenuation characteristics of different nuclear materials.

Reference:

Abdo A. El-Sayed & Ali M. A., Ismail M.R. (2003), "Influence of magnetite and boron carbide on radiation attenuation of cement–fiber/composite", Annals of Nuclear Energy, 30, 391–403

Al-Hadeethi Y and Sayyed MI (2020), A comprehensive study on the effect of TeO2 on the radiation shielding properties of TeO_2-B_2O_3-Bi_2O_3-$LiFeSrCl_2$ glass system using Phy-X/PSD software. Ceram Int; 46, 6136 – 6140.

Al-Hadeethi Y and Sayyed MI (2019), Analysis of borosilicate glasses doped with heavy metal oxides for gamma radiation shielding application using Geant4 simulation code. Ceram Int; 45, 24858 - 64.

Askın A. (2020), "Evaluation of the radiation shielding capabilities of the $Na_2B_4O_7$-SiO_2-MoO_3-Dy_2O_3 glass quaternary using Geant4 simulation code and Phy-X/PSD database". Ceram Int., 46, 9096-102.

Attix, F., (1986), Introduction to Radiological Physics and Radiation Dosimetry. Wiley, New York. Aznar, M.C., Andersen.

Badziak J., Jablonski S., Makowski J., Parys P., Ryc L., Vankov A. B., Wolowski J. & Woryna E. (2002),"X-ray emission from high-intensity interaction of picosecond and sub nanosecond laser pulses with solid targets", Optica Applitica, XXXII, No.1-2

Bashter I. I. (1997), "Calculation of radiation attenuation coefficients for shielding concretes", Ann. Nucl. Energy, 24(17), 1389-1401.

Brauckmann aus Arnsberg S. K. (2017), "X-ray generation by high intensity laser pulses", Doctoral Thesis, Faculty of Mathematic, University of Heinrich -Heine,

Düsseldorf. Retrieved from https://d-nb.info/1152076256/34

Briesmeister Judith F. (2000) (Ed.), MCNP–A General Monte Carlo N–Particle Transport Code Version 4C, Los Alamos National Laboratory Report, LA–13709–M,.

Büyükyıldız M., Kurudirek M., Ekici M., Içelli O. & Karabu Y. (2017), "Determination of radiation shielding parameters of 304L stainless steel specimens from welding area for photons of various gamma ray sources", Prog Nucl Energy, 100, 245-54.

Das A. and Ferbel T. (2005), Introduction to Nuclear and Particle Physics, 2nd edition, World Scientific Publishing Co. Pte. Ltd.

Elmahroug Y., Tellili B. & Souga C. (2015), "Determination of total mass attenuation coefficients, effective atomic numbers and electron densities for different shielding materials", Ann. Nucl. Energy, vol. 75 268–274

F. Afaneh, Z.Y. Khattari, M.S. Al-Buriahi (2022), "Monte Carlo simulations and phy-X/PSD study of radiation shielding and elastic effects of molybdenum and tungsten in phosphate glasses", journal of materials research and technology;19:3788-3802

F Moradi, Mayeen Uddin Khandaker, T Alrefae, H Ramazanian, D A Bradley, (2019), "Monte Carlo simulations and analysis of transmitted gamma ray spectra through various tissue phantoms", Appl Radiat. Isot;146: 120-126

Gurinder Pal Singh, Joga Singh, Parvinder Kaur, Simranpreet Kaur, Deepawali Arora, Ravneet Kaur, Kulwinder Kaur, D.P. Singh (2020), "Analysis of enhancement in gamma ray shielding proficiency by adding WO3 in Al2O3-PbO-B2O3 glasses using Phy-X/PSD", journal of materials research and technology; 9(6) :14425-14442.

I. Akkurt (2011), "Determination of effective atomic number and electron density of chitin by gamma-ray attenuation", International Journal of the Physical Sciences Vol. 6(21), pp.5048-5050, available online at http://www.academicjournals.org/IJPS

Kelardeh H. K., Mahdieh M. (2015), "Numerical Study of Kα X-ray Emission from Multi- layered Cold and Compressed Targets Irradiated by Ultrashort Laser Pulses", Computational Physics project, Retrieved from https://doi.org/10.48550/arXiv.1508.00592

Mohamed Hegazi Ghozza (2023), Radiation Attenuation Properties of BaMnO3 Doping Nickel Semiconductor Perovskite Using Phys-X/PSD Software, Arab J. Nucl. Sci. Appl., Vol. 56, 3, 27-40.

Phuoc K. T. et al. (2012), "All-optical Compton gamma-ray source", Nat. Photonics 6, 308 .

Reda A. M. & El-Daly A. A. (2020), "Gamma ray shielding characteristics of Sn-20Bi and Sn-20Bi-0.4Cu lead-free alloys". Prog. Nucl. Energy, 123 103304

Reda A. M. , El-Daly A. A. , Eid E.A. (2021), "Neutron/gamma radiation shielding characteristics and physical properties of (97.3–x)Pb–xCd–2.7Ag alloys for nuclear radiation applications". Phys. Scr. , 96 125321.

Sadawy M. M. & Elsharkawy E. R. (2013), "Prediction and modeling of corrosion in steel oil storage tank

from nondestructive inspection". J Mater Sci Eng, B,3(12), 785-792.

Sadawy M.M. (2008), "Investigation of alloying elements and nonmetallic inclusions effects on the corrosion and electrochemical behavior of high alloying steel", J. Al. Azhar Univ. Eng. Sect.,3(9), 1143e9.

Sadawy M.M., Shirinov T.U. & Heseinov R.G. (2011), "Corrosion and electrochemical behavior of martensitic-austenitic stainless steel in hydrochloric acid solutions", Int J Pure Appl Chem, 6(3),855e61.

Sakar E. et al. (2020), Phy-X/PSD, "Development of user friendly online software for calculation of parameters relevant to radiation shielding and dosimetry". Rad Phys Chem, 166, 108496.

Sayyed M. I. et al. (2018), "Radiation shielding properties of pentaternary borate glasses using MCNPX code". J Phys Chem Solid, 121, 17-21.

Singh, V.P., Medhat & M., Shirmardi, S. (2015), "Comparative studies on shielding properties of some steel alloys using Geant4, MCNP, WinXCOM and experimental results". Radiat. Phys. Chem., 106, 255–260

Schille J., Kraft S., Pflug T. , Scholz Ch. , Clair M. , Horn A. and Loeschner U (2021), " Study on X-ray Emission Using Ultrashort Pulsed Lasers in Materials Processing", Materials, 14, 4537. Retrieved from https://doi.org/10.3390/ma 14164537

Taqi A. H., Ghalib A. M. & Mohammed H. N. (2021), "Shielding properties of Cu-Sn-Pb alloy by Geant4", XCOM and experimental data Mater. Today Commun., 26 101996

Tellili B., Elmahroug Y., Souga C. (2017), "Investigation on radiation shielding parameters of cerrobend alloys". Nucl. Eng. Technol. , 49 1758–71 .

Vysko˘cil g. J., Klimo O., and Weber S. (2018),"Simulations of bremsstrahlung emission in ultra-intense laser interactions with foil targets", Plasma Phys Controlled Fusion, 60, 054013.

Wu D., Yu W., Zhao Y.T., Fritzsche S. & He X.T (2018), "Characteristics of X/g-ray radiations by intense laser interactions with high-Z solids: The role of bremsstrahlung and radiation reactions", Matter and Radiat. Extremes, 3, 293-299.

Xue K., Dou Z., Wan F., Yu T., Wang W., Ren J., Zhao Q.,Zhao Y., Xu Z., & Li J. (2020), " Generation of highly-polarized high-energy brilliant γ-rays via laser-plasma interaction", Matter and Radiat. Extremes, 5, 054402, 1-8

Ziying Z. , Zhiyu W. , Yiming J., Hua T., Han D., Yanjun G & Li J. (2012), "Effect of post-weld heat treatment on microstructure evolution and pitting corrosion behavior of UNS S31803 duplex stainless-steel welds", Corros Sci,62, 42e50.

تقدير اضعاف اشعة جاما الناتجة من تفاعلات المادة مع الليزر عالي الطاقة باستخدام أسلوب المحاكاة بطريقة مونت كارلو"

على مصطفى على، وليد احمد غالى
قسم الفيزياء – كلية العلوم – جامعة جازان – جازان - المملكة العربية السعودية

ملخص

توضح الدراسة فى هذا البحث مدى اختراق أشعة جاما الناتجة من تفاعلات المادة مع الليزر عالي الطاقة. تكون شدة الليزر المتفاعلة مع المادة فى المدى من 10^{19} إلى10^{21} واط/سم^{٢}. لقد لوحظ ان تفاعل الليزر مع المادة ينتج أشعة جاما بطاقات مختلفة يقع مداها بين ٢٠ كيلو فولت الى 25 ميغا فولت. لقد تم استخدم كود مونت كارلو (MCNP) لمحاكاة اختراق أشعة جاما الناتجة من تفاعل الليزر مع المادة. تم اقتراح مجموعتين من عينات الخرسانة للدراسة، على ان تكون المجموعة الأولى من العينات الخرسانية ممزوجة بالألياف الفولاذية والمجموعة الثانية بدون الألياف الفولاذية. كما تم استخدام برنامج Phy-X/PSD بجانب كود المونت كارلو لحساب بعض معاملات التدريع لهذه العينات مثل معامل المقطع العرضي الذري(ACS)، ومعامل العدد الذري الفعال (Zeff)، ومعامل الاضعاف الكتلي (MAC)، ومعامل الاضعاف الخطي (LAC)، ومعامل قيمة الاضعاف للعشر (TVL)، ومعامل قيمة الاضعاف للنصف (HVL)، ومعامل متوسط المسار الحر (MFP) ومعامل عدد الإلكترون الفعال (Neff). العينات الخرسانية التى تم دراستها ذات كثافة تتراوح من 2.095 جم/سم^{٣} إلى 2.9 جم/سم^{٣}. أظهرت النتائج التى تم الحصول عليها من برنامج Phy-X/PSD وكود المونت كارلو توافق جيد عند الطاقات التي تم دراستها كما أظهرت عينة الخرسانة الإلمنيت-ليمونيت خصائص تدريع أفضل من عينات الخرسانة الاخرى.

الكلمات المفتاحية: الليزر عالي الكثافة – أشعة جاما – الخرسانة – طريقة محاكاة مونت كارلو – برنامج Phy-X/PSD

Antibacterial activity of *Blumea bovei* (DC.) Vatke, Linn. extracts on selected pathogenic bacteria

Mohamed Abdullah Al Abboud
Department of Biology, College of Science, Jazan University, Jazan, Saudi Arabia

Abstract

The present study evaluated the potential antibacterial activity of *Blumea bovei* (DC.) Vatke, Linn. extracts through different organic and aqueous solvents. The test bacteria were pathogenic types; *Listeria monocytogenes*, *Pseudomonas aeruginosa* and *Staphylococcus aureus*. There were different affinities for the studied organic solvents besides aqueous one. MIC values were confirmed on using *Blumea bovei* (DC.) Vatke, Linn. extracts as an alternative natural antibacterial inhibitory agent.

Keywords: *Listeria*, *Pseudomonas*, *Staphylococcus*, morphology, correlation, Jazan.

Introduction

Most of secondary metabolites of phytochemicals are derived biosynthetically from phyto-primary metabolites. They can be classified according to their medical values into several groups. The active and medical phytochemicals are alkaloids, tannins, steroids, volatile oils, glycosides, fixed oils, phenols, resins and flavonoids which are efficacy in treating many diseases. These phytochemical constituents are deposited in specific parts such as flowers, leaves, seeds, bark, roots and fruits **(Parekh and Chanda, 2007; Farooq and Hafiz, 2010)**.

Most of medicinal plants have been reported to have antimicrobial activities against many infectious and pathogenic microorganisms. Currently, scientists prefer natural substituents to synthetic additives because they have no side effects besides are safe to the environment. Therefore, many published articles are focused on using plant extracts as natural antibiotics with the recommendations from therapeutic physicians **(Nurul *et al*., 2022; Mariola *et al*., 2022)**.

Blumea bovei (DC.) Vatke, Linn. is a medicinal plant species belonging to family Asteraceae. It is a paleotropic genus with 50 species in different countries; Tropical East Africa, North Africa, Arabian Peninsula, Palestine, Pakistan, India and Sri-Lanka. Only one species is present in Saudi Arabia **(Ahmed *et al*., 2005)**. It is described as pungent, bitter, antipyretic, curing for thirst, fever and burning sensation besides it is good for bronchitis **(Salisu *et al*., 2015)**.

The aim of this study is to evaluate the antimicrobial activity of *Blumea bovei* (DC.) Vatke, Linn. through different organic and aqueous solvents against selected pathogenic bacteria.

Material and Methods

Plant collection and identification

The plant material *Blumea bovei* (DC.) Vatke, Linn. were collected from Wadi Lejib, Jazan region, KSA located at 17°35′27.5″ latitude, 42°55′39.9″ longitude in September 2022. The identification of studied plant species was issued by the herbarium of the Biology Department, College of Science, Jazan University (JAZUH). The whole plant species were dried in hot air oven at 50^{o}C for 24 hr and blended into powder, this powder of *Blumea lacera* were used for aqueous and other organic solvents; acetone, butanol, chloroform, diethyl ether, ethanol and methanol. Each whole plant extract was prepared by standard methods of **Yasser *et al*. (2019)**. For each solvent, the treated

filtrate evaporates, and the dried residue was dissolved in dimethyl sulfoxide (DMSO) and stored at -20^{o}C for further use. Three replicates were performed for each solvent extraction and standard deviations were obtained **(Maria *et al*., 2023)**.

Antibacterial Activity

The disc-diffusion assay was used to determine the antibacterial activity of plant extracts. Each plant solvent extract was dripped on sterile filter paper discs (9 mm diameter, Whatman No. 3 chromatographic paper). Each filter paper discs were loaded with 2 mg of each plant extract. After that, they were placed on Mueller-Hinton II agar medium plates inoculated with Reference bacterial American Type Culture Collection strains which were used in antimicrobial screening and incubated at 35^{o}C±2.5^{o}C for 24 hr. A paper disc with dimethyl sulfoxide (DMSO) was used as a negative control. Commercial 6-mm diameter discs containing 0.01 mg of Streptomycin were used as a positive control. The diameter of the clear zone surrounding the plant extract loaded discs was measure in millimeter by Vernier caliper as the antibacterial activity of the given extracts **(Mariola *et al*., 2022)**.

Minimum Inhibitory Concentration (MIC) evaluation was determined for each tested bacteria by a serial micro-dilution of plant extract in DMSO solution following the protocol described by **Kosti´c *et al*. (2017)** besides Minimum Bacterial Concentration (MBC) was determined according to **Joshi (2010)**.

Statistical Analysis

Correlation among MIC values and regression between bacterial strains are achieved according to **(Shaban, 2005 and Tamhane, 2009)**. P values for significance tests based on degrees of freedom were determined according to **Dutilleul (1993)** approach. MIC values were subjected to statistical analysis to work out ANOVA to compare means. Standard error was calculated following **Steel *et al*., (1997)**.

MIC values were tested for significance using Duncan's range test (Duncan, 1951). This test was to evaluate the differences among tissues. Statistical tests were conducted using SPSS software (ver. 22) for Windows **(Deya El-deen and El-Shabasy A. 2020)**. The representation of correlated data was done by the linear regression approaches which explored the extent effect for MIC values **(Maindonald, 1992; Miller and Franklin, 2002)**.

Results

Plant morphology studies

It is a perennial herb with 20-60 cm tall. The stems are more branched with glabrous surfaces. Leaves are sessile, linear-oblong, obscurely denticulate margin with auriculate at base. They are glabrous but sometimes present on the median vein below. Inflorescences are terminal corymb with 4-7 cm long and 5-7 mm wide. Florets are bluish. Achenes are oblong and brown pubescent.

Antibacterial analysis

Different organic solvents of *Blumea bovei* (DC.) Vatke, Linn revealed potential antibacterial effects on tested bacteria except acetone solvent. It was obvious on *Listeria monocytogenes* which had been inhibited in growth. Butanol extract was the most inhibitor agent with the largest inhibition zone (120.0±0.02 mm) while ethanol extract showed the lowest inhibition one (20.0±0.30 mm). On the other hand, *Pseudomonas aeruginosa* and *Staphylococcus aureus* were inhibited with the less number of organic solvents; butanol and chloroform besides butanol only respectively. Aqueous solvents hadn't any effects on bacterial growth but there was promoting in growth in *Pseudomonas aeruginosa* after aqueous solvent treatment. DMSO (negative control) inhibited only *Listeria monocytogenes*. Streptomycin (positive control) showed predominantly activity against different tested bacteria.

Considering MIC values for butanol extracts for all treated bacteria achieved because the butanol extract was the only common inhibitor agent in the present study. The values were more or less close to each other except *Staphylococcus aureus* which has the lowest MIC value. *Listeria monocytogenes* showed significantly the highest MIC value. In contrast, *Pseudomonas aeruginosa* showed the lowest MBC value while *Listeria monocytogenes* was still the highest value.

The analysis of variance for various MIC values by ANOVA test showed significant differences for all tested bacterial strains. *Listeria monocytogenes* versus *Staphylococcus aureus* showed extremely significant with *F* test equals 11.01. Correlation analysis showed that *Pseudomonas aeruginosa* and *Staphylococcus aureus* had a highly positive significant correlation However, *Pseudomonas aeruginosa* and *Listeria monocytogenes* had a low positive significant correlation. Regression describes the co-variation among MIC variables.

Simple Linear Regression curves indicate the significant relationships among them.

Discussion

Blumea genus was regarded as the most medicinal plant having ethnobotanical information in local people all over the world **(Singh *et al*., 2010)**. **Nurul *et al*. (2022)** reported that *B. balsamifera* extracts show antimicrobial activities against Gram-positive and Gram-negative bacteria. Moreover, **Mukesh and Rahul (2017)** confirmed that *Blumea lacera* possessed activity against *S. aureus, E. coli, S. pyogens, K. pneumonia* and *S. typhi*.

The search for medicinal plant extracts exhibiting antimicrobial activity is increased due to the World Health Organization (W.H.O.) reports indicating the rise of antimicrobial resistance **(Kebede *et al*., 2021)**. The choice of organic solvent is the proper use in extraction of natural resources. It was clear in this study which covered many number of different organic solvents besides aqueous one. The butanol solvent was the most convenient extract in this investigation due to high polarity with medium molecular weight comparing to other organic solvents. Chloroform ranked the best second organic solvent due to medium polarity and high molecular weight. *Staphylococcus aureus* was regarded as the most resistant bacterial strain while *Listeria monocytogenes* was the most susceptible one. Aqueous solvent had no effect but it was growth promoting that means there may be natural products in the extract which enhanced the growth not reduced. DMSO was the better negative control due to less inhibited zones created.

MIC is an accepted standard for measuring the sensitivity of any microorganisms and MBC is a tool for inoculum load which withstand the inhibitory factors **(Fahd *et al*., 2020)**. MIC values are the main goal for any alternative natural growth inhibitors. *Listeria monocytogenes* was the most resistant bacterial strain due to having the highest MIC value while *Staphylococcus aureus* was the most sensitive one as it had the lowest value. MBC revealed nearly values throughout different solvent extracts versus the tested microorganisms that facilitate to obtain more or less natural inhibitory alternative with the same dose.

However, according to alteration in life style and mode of nutrition which lead to genetic mutations in bacterial properties that enforce pathogenic bacteria to be more resistant, hence, the discovery of novel antimicrobial compounds is important for

future antibiotic security **(Exner *et al*., 2017)**.

Simple linear regression curves showed positively correlation among MIC values which confirmed on the importance of this plant extract and focus on highly significant affinity on the studied bacteria. Regression among tested ones paved the way to influence on other types of pathogenic bacteria.

Conclusion

1- The need for natural alternative becomes the world demand nowadays

2- *Blumea bovei* (DC.) Vatke, Linn has the best antimicrobial activity

3- Butanol solvent records the most favorable natural extract.

References

Ahmed H. Alfarhan, Turki Ali Al-Turki, Abdullah Yahya Basahy (2005). Flora of Jizan Region, Final Report, Vol.- 1, 418-419.

Deya El-deen M.Radwan and El-Shabasy A. (2020). Comparative Analysis of Five *Heliotropium* species in Phenotypic Correlations, Biochemical Constituents and Antioxidant Properties, *Catrina*, 21(1): 1-8.

Duncan D. B. 1951. A significance test for differences between ranked treatments in an analysis of variance. Virginia Polytechnic Institute. pp. 13.

Dutilleul, P. 1993. Modifying the t test for assessing the correlation between two spatial processes. Biometrics 49, 305–314.

Exner M, Bhattacharya S, Christiansen B, Gebel J, *et al*. (2017). Antibiotic resistance: What is so special about multidrug-resistant Gram-negative bacteria? *GMS Hyg Infect Control* ;12.

Fahd A. Nasr, Omar M. Noman, Ramzi A. Mothana, Ali S. Alqahtani and Abdullah A. Al-Mishari (2020). Cytotoxic, antimicrobial and antioxidant activities and phytochemical analysis of *Artemisia judaica* and *A. sieberi* in Saudi Arabia, Vol. 14(8), pp. 278-284.

Farooq Anwar, Hafiz Muhammad Abdul Qayyum (2010). Antioxidant activity of 100% and 80% methanol extracts from barley seeds (*Hordeum vulgare* L.): Stabilization of sunflower oil. *Grasas Y Aceites*, 61 (3):237-243.

Joshi, R.K., 2010. In vitro antimicrobial and antioxidant activities of the essential oil of *Craniotome furcata*. *J. Appl. Nat*. Sci. 2, 57–62.

Kebede T, Gadisa E, Tufa A. (2021). Antimicrobial activities evaluation and phytochemical screening of some selected medicinal plants: A possible alternative in the treatment of multidrug-resistant microbes. PLoS ONE;16.

Kosti´c M., Smiljkovi´c M. Petrovi´c J. *et al*. (2017). Chemical, nutritive composition and a wide range of bioactive properties of honey mushroom *Armillaria mellea* (Vahl: Fr.) Kummer, *Food & Function*, vol. 8, no. 9, 3239–3249.

Maindonald, J.H., (1992). Statistical design, analysis, and presentation issues. New Zealand, *J. Agric. Res*. 35 (2), 121–141.

Maria Evelina Bordean, Rodica Ana Ungur, Dan Alexandru Toc, Ileana Monica Borda, Georgiana Smaranda Mart, Carmen Rodica Pop, Miut,a Filip, Mihaela Vlassa, Bogdana Adriana Nasui , Anamaria Pop, Delia Cinteza, Florina Ligia Popa, Sabina Marian, Lidia Gizella Szanto and Sevastit,a Muste (2023). Antibacterial and Phytochemical Screening of *Artemisia* Species, *Antioxidants* 2023, 12, 596.

Mariola Kozłowska, Iwona Scibisz, Jarosław L. Przybył , Agnieszka E. Laudy , Ewa Majewska, Katarzyna Tarnowska, Jolanta Małajowicz and Małgorzata Ziarno (2022). Antioxidant and Antibacterial Activity of Extracts from Selected Plant Material, *Appl. Sci*. 2022, 12, 9871.

Miller, J. and Franklin, J., (2002). Modeling the distribution of four vegetation alliances using generalized linear models and classification trees with spatial dependence. *Ecol. Model*. 157 (2–3), 227–247.

Nurul Ain Ismail, Azlinah Matawali, Fadzilah Awang Kanak, Ping-Chin Lee, Siew-Eng How, Lucky Poh Wah Goh, Jualang Azlan Gansau (2022). Antimicrobial activities and phytochemical properties of *Blumea balsamifera* against pathogenic microorganisms, *Journal of Medicine and Life*, 15(8): 2-3.

Parekh Jigna, Sumitra V. Chanda (2007). In vitro Antimicrobial Activity and Phytochemical Analysis of Some

Indian Medicinal Plants, *Turk. J. Biol*. 31: 53-58.

Salisu Abubakar, Etim Veronica, Nweke Ogechi, Asemota Uwem, Fatokun Olakunle (2015). A comparative study of phytochemical, antibacterial and scavenging effects of methanolic leaves extract of *Blumea lacera* (Burm. F.) DC and *Blumea aurita* (Linn F.) DC, *Pharmaceutical and Biological Evaluations*; 2(6): 264-270.

Shaban, N. 2005. Analysis of the correlation and regression coefficients of the interaction between yield and some parameters of snap beans plants. Trakia J. Sci. 3 (6), 27–31.

Singh, S Singh, Surender Singh, L Ali, Ritu Mahajan (2010). Ethnobotanical Significance and Antimicrobial Activity of *Blumea lacera* (Roxb.) DC B. *International Journal of Pharmaceutical & Biological Archives*, 1(3):314 – 316.

Steel, R.G.D., J.H. Torrie and D.A. Dickie. 1997. Principles and Procedures of Statistics-A Biometric Approach. 3rd edn. McGraw-Hill Publishing Company: Toronto, pp.5.

Tamhane, A.C. 2009. Statistical analyses of designed experiments: theory and applications, pp. 41–50.

Yasser A. El-Amier, Abd El-Nasser S. Al Borki**,** Shrouk A. Elagami (2019). Potential of wild plant *Artemisia judaica* L. as sustainable source of antioxidant and antimicrobial compounds *Journal of Experimental Sciences*, 10: 04-08.

Tables

Table (1) Antibacterial activity of the plant extract against the tested bacterial strains

Bacterial strain	Diameter of Inhibition Zone (IZ) in mm								
	Organic solvents						Aqueous solvent (g)	DMSO (Negative control) (h)	Streptomycin (Positive control) (AC)
	Acetone (a)	Butanol (b)	Chloroform (c)	Diethyl ether (d)	Ethanol (e)	Methanol (f)			
Listeria monocytogenes ATCC 19111	-	120.0±0.02	40.0±0.04	100.0±0.12	20.0±0.30	80.0±0.04	-	18.0±0.21	110±0.04
Pseudomonas aeruginosa ATCC 10662	-	3.38±0.48	0.5±0.01	-	-	-	-0.5±0.58	-	8.0±0.01
Staphylococcus aureus ATCC 25923	-	3.12±0.63	-	-	-	-	-	-	3.0±0.01

Table (2) Minimum inhibitory concentration (MIC) of the plant extracts against the tested bacterial strains.

Bacterial strain	MIC (mg/ml)							
	Organic solvents						Aqueous solvent (g)	DMSO (Negative control) (h)
	Acetone (a)	Butanol (b)	Chloroform (c)	Diethyl ether (d)	Ethanol (e)	Methanol (f)		
Listeria monocytogenes ATCC 19111	-	٢٩٥,٦١±0.٥٠	١٧٨,٠±0.٢٢	٣٠٥,١٤±0.٢٣	٢٢٥,٢٣±0.٤0	٢٤٠,0±0.0٣	-	١٧٠,٠±0.٢٣
Pseudomonas aeruginosa ATCC 10662	-	٢٤٠,٩١±0.٠٢	٣٥,٦٤±0.٣٤	-	-	-	٣٥,٦٤±0.٢٥	-
Staphylococcus aureus ATCC 25923	-	101.62±0.36	-	-	-	-	-	-
F test	L m versus P a = 2.06			Lm versus S a = 11.01			P a versus S a = 5.36	
P<0.05 *, *P*<0.01**, *P*<0.001***	*			**			*	

Table (٣) Minimum Bacterial Concentration (MBC) of the tested bacterial strains against plant extracts

Bacterial strain	MIC (mg/ml)							
	Organic solvents						Aqueous solvent (g)	DMSO (Negative control) (h)
	Acetone (a)	Butanol (b)	Chloroform (c)	Diethyl ether (d)	Ethanol (e)	Methanol (f)		
Listeria monocytogenes ATCC 19111	-	9.0±0.33	7.0±0.٢1	10.0±0.42	8.0±0.32	9.0±0.02	-	7.0±0.٢2
Pseudomonas aeruginosa ATCC 10662	-	2.0±0.٠3	2.0±0.55	-	-	-	2.5±0.35	-
Staphylococcus aureus ATCC 25923	-	4.0±0.37	-	-	-	-	-	-

Table (4) Correlation among Minimum Inhibitory Concentration (MIC) of the plant extracts against the tested bacterial strains.

	Listeria monocytogenes	*Pseudomonas aeruginosa*	*Staphylococcus aureus*
Listeria monocytogenes	1	0.32	0.40
Pseudomonas aeruginosa	0.32	1	0.98
Staphylococcus aureus	0.40	0.98	1

\

Figures

Fig (1) *Blumea bovei* (DC.) Vatke, Linn morphology

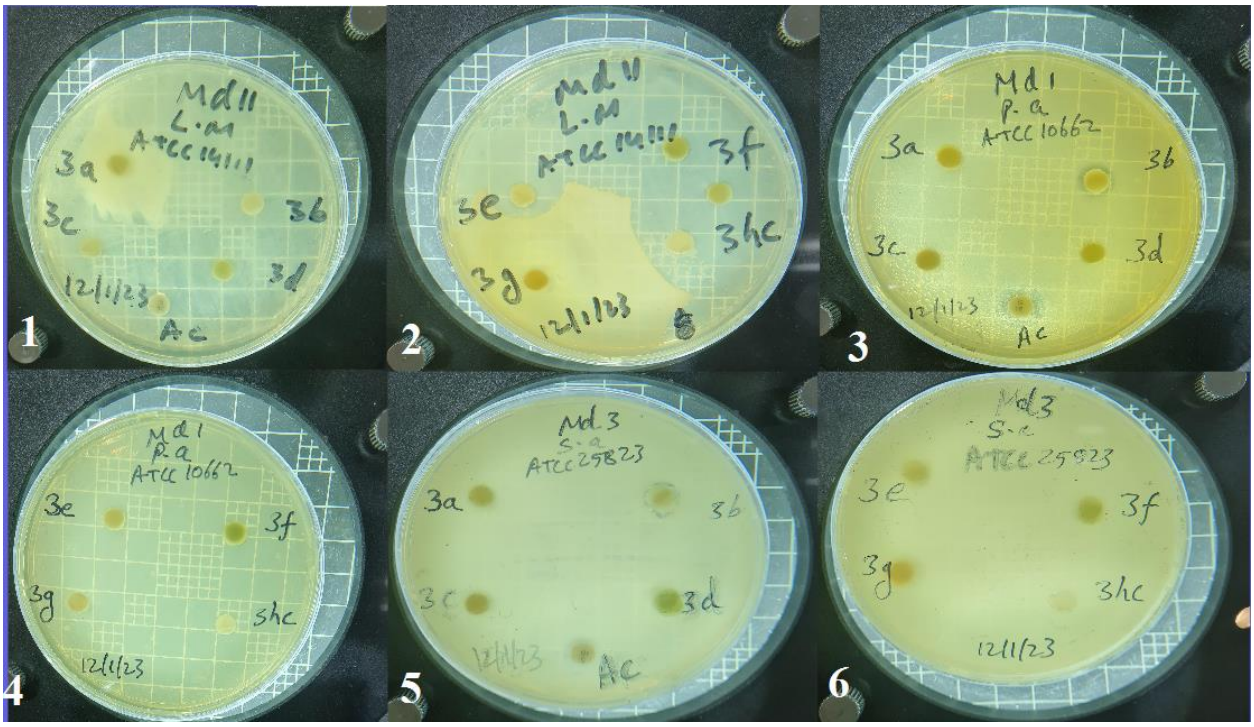

Fig (2) Antimicrobial activity of the plant extracts against the tested bacterial strains; L a (*Listeria monocytogenes*), P a (*Pseudomonas aeruginosa*), S a (*Staphylococcus aureus*), a: acetone, b: butanol, c: chloroform, d: diethyl ether, e: ethanol, f: methanol, g: aqueous, h: DMSO, Ac: Streptomycin

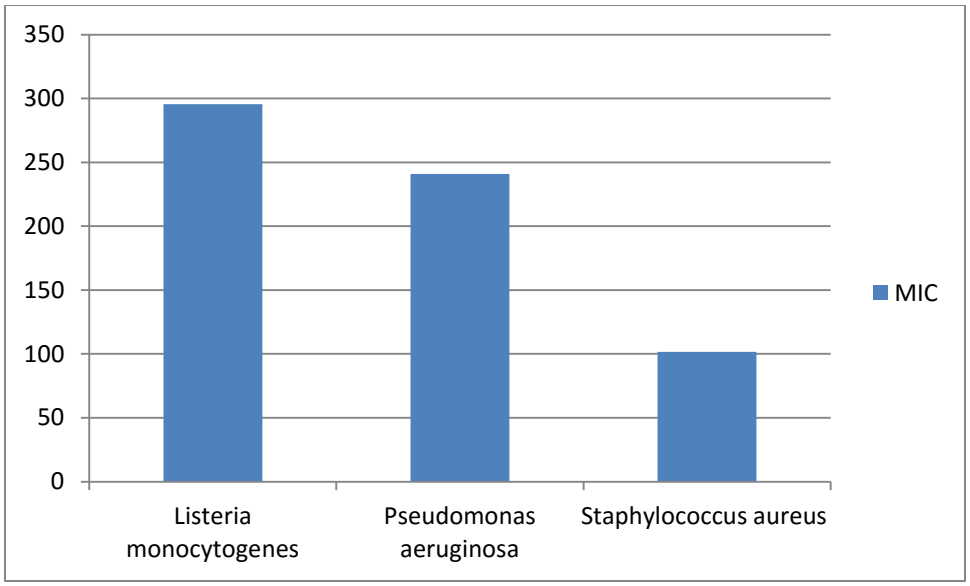

Fig (3) Minimum inhibitory concentration (MIC) of the plant extracts against selected bacterial strains.

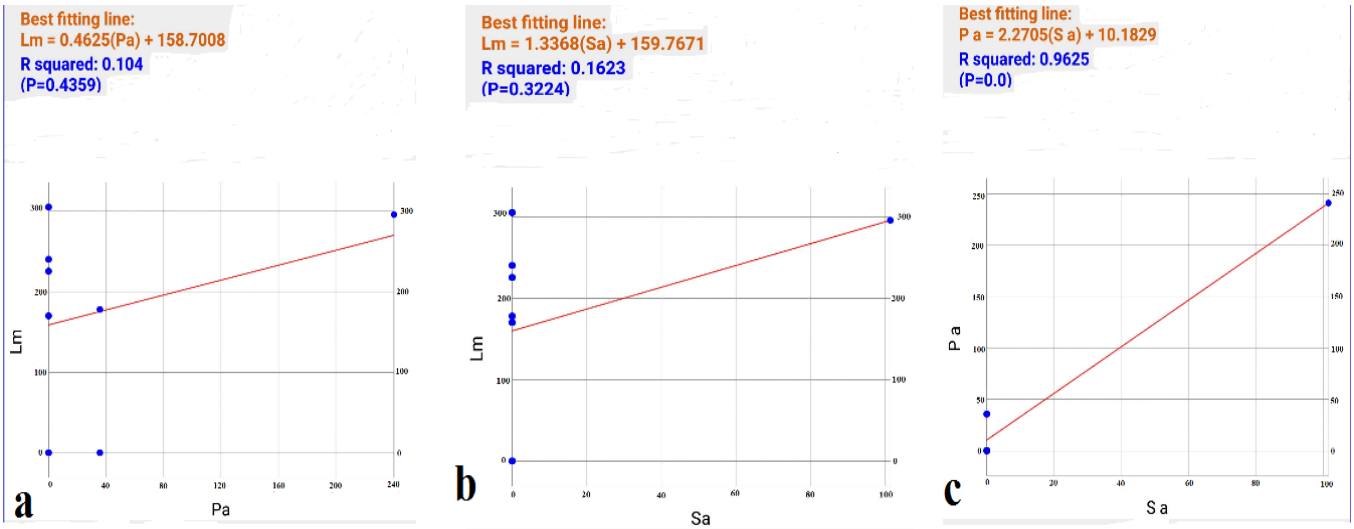

Fig (4) Simple Linear Regression of MIC values among the tested bacterial strains

النشاط الضد بكتيري لمستخلصات نبات بلوميا وادي *Blumea bovei* (DC.) Vatke, Linn. على بعض أنواع البكتيريا الممرضة

محمد عبدالله العبود

قسم الأحياء ، كلية العلوم ، جامعة جازان ، المملكة العربية السعودية

الملخص

صممت الدراسة الحالية لقياس النشاط الضد البكتيري المحتمل للمستخلصات العضوية المختلفة والمستخلص المائي لنبات بلوميا وادي. كانت البكتيريا المختارة من الأنواع المسببة للأمراض *Listeria monocytogenes* .و *Pseudomonas aeruginosa* و *Staphylococcus aureus* . كان هناك ارتباطات مختلفة للمذيبات العضوية المدروسة و المذيبات المائية. أكدت قيم MIC للمستخلصات العضوية المختلفة والمستخلص المائي لنبات بلوميا وادي إمكانية إستخدامه كعامل مثبط طبيعي بديل مضاد للجراثيم.

الكلمات المفتاحية : *Listeria, Pseudomonas, Staphylococcus,* ، مورفولوجي، إرتباط ، جازان

Association of coronavirus disease (COVID-19) vaccinations with post-COVID-19 symptoms in Saudi Arabia

Rnda I. Ashgar[1]

[1]College of Nursing, Jazan University, Jazan, Saudi Arabia

Abstract

Coronavirus disease (COVID-19) vaccinations have significantly changed the trajectory of the pandemic, by saving tens millions of lives worldwide. However, there are concerns regarding their safety, efficacy, and long-term effects. Therefore, this study seeks to determine whether receiving a complete doses of COVID-19 vaccine was linked to post-COVID-19 symptoms among adults in Saudi Arabia. This cross-sectional study included a convenience sample of 307 post-COVID-19 patients who participated in an online survey from April 2022 to August 2022. We compared demographic characteristics based on vaccination status. The chi-square analysis was utilized to compare the characteristics of participants with and without at least one post-COVID-19 symptoms. Binary logistic regression analysis was conducted to assess the degree to which vaccination status affects post-COVID-19 symptoms with reciprocal covariate adjustment. Post-COVID-19 symptoms were more common among middle-aged adults (58.5%), women (54.6%), employed individuals (72.1%), those who had no previous health problems (56.8%), and those who had incomplete vaccination status (69.4%) than their counterparts. A complete vaccination status was mostly reported among middle-aged adults (55.2%), men (51.0%), employed individuals (80.2%), and those who had no previous health problems (54.2%). Bivariate analysis showed that none of the post-COVID-19 symptoms were associated with vaccination status, except cough (adjusted odds ratio = 2.19, 95% confidence interval = 1.09–4.45, *p*-value = .028). This study found that COVID-19 vaccination was not associated with post-COVID-19 symptoms. Governments and legislators need to deal with the problem of false information flowing on social media regarding the association between vaccinations and post-COVID-19 symptoms.

Keywords: Adults, public health nurses, post-COVID-19 symptoms, COVID-19 vaccinations, Saudi Arabia.

INTRODUCTION

Since its emergence and as of 2023, coronavirus disease (COVID-19) is an ongoing global pandemic that has strained healthcare systems worldwide. The impact of the disease has been affected global economy, society, cultures, politics and other areas. Similar to other countries, Saudi Arabia has been affected by the pandemic. On March 2, 2020, the Ministry of Health confirmed the first reported case in Saudi Arabia (AlGhalyini et al., 2022). From January 3, 2020 to March 29, 2023, there were 832,709 confirmed cases of COVID-19 in Saudi Arabia, with 9,629 deaths reported to the World Health Organization (2023a). In response, Saudi Arabia has prepared public and private healthcare agencies to deal with the pandemic (Khan et al., 2021). Several strategies were undertaken by the kingdom to slow the spread of the virus, such as implementing curfew and suspending all schools, social events, sports activities, and domestic and international flights (Ashgar, 2021). On December 10, 2020, the Saudi Arabian Food and Drug Administration approved the first COVID-19 vaccine, and on January 6, 2021, the vaccination campaign was launched[5].

Saudi Arabia was one of the first countries which provide COVID-19 vaccines for free to all inhabitants. The Saudi government encouraged people to get the vaccine through daily COVID-19 press conferences and reassured them in terms of its safety and efficacy (Alshahrani et al., 2021). Vaccination against COVID-19 was executed according to a systematic plan, beginning with the most vulnerable groups, such as the elderly population and those with comorbidities. Despite mounting evidence pointing to the vaccine's benefits, there has been misinformation in the media casting doubt on its efficacy, safety, and long-term risk (Alshahrani et al., 2021). Such a dispute made people more reluctant to receive the COVID-19 vaccine and have impacted their willingness to do so (Alshahrani et al., 2021). As of April 4, 2023, 27,018,975 people received a minimum of one vaccination dosage, and 25,414,359 people were fully vaccinated (World Health Organization, 2023a). The availability of an effective vaccine has sparked optimism for controlling the transmission of the virus in Saudi Arabia; however, the public health system remains skeptical about post-COVID-19 symptoms.

Post-COVID-19 symptoms are defined as new or reoccurring health problems emerging at least 4 weeks after contracting COVID-19 (World Health Organization, 2023b; Centers for Disease Control and Prevention, 2023). The following symptoms may appear in various combinations: breathing problems, concentration problems, sleep problems, exhaustion, dizziness, post-exercise malaise, fast-beating heart, cough, chest/stomach pain, diarrhea, headache, joint and muscle pain, tingling sensation, rash, and mood changes (World Health Organization, 2023b; Centers for Disease Control and Prevention, 2023a). Even in situations of moderate sickness or no early symptoms of COVID-19, these health symptoms can manifest in anyone who has exhibited COVID-19 positive testing (Centers for Disease Control and Prevention, 2023a). Although these symptoms may improve gradually with time, post-COVID-19 symptoms can occasionally last for weeks, months, or even longer and cause disability (Centers for Disease Control and Prevention, 2023b). A full understanding of the post-COVID-19 symptoms would help decision-makers establish systematic management plans to overcome health risks and associated complications.

Previous research has indicated that post-COVID-19 symptoms are highly prevalent (74.60%) among Saudi Arabian adults (Ashgar, 2023). It was established that 1 in 10 individuals with a positive COVID-19 test result may develop post-COVID-19 symptoms for up to 12 weeks or more

(Office for National Statistics, 2020). Several contributing factors, such as advanced age، female sex, higher stress level, and having previous medical issues increases the risk for post-COVID-19 symptoms (Ashgar, 2023).

An early British trial with 66 post-COVID-19 patients indicated that in those who had received the vaccine, their symptoms had improved or disappeared compared to participants who had not received the vaccine (Arnold et al., 2021). However، a larger study included 453 post-COVID-19 patients in New York City suggested that COVID-19 immunization is not linked to a reduction in post-COVID-19 symptoms (Wisnivesky et al., 2022). In addition, no such studies have been conducted in the Saudi population. Given the differences in the context of immunization, geographical location, and culture of the Saudi population, national studies are needed to understand the effect of vaccinations on post-COVID-19 symptoms among Saudi Arabian adults. Consequently, we conducted this study to determine whether receiving a complete dose of COVID-19 vaccine was linked to post-COVID-19 symptoms among adults in Saudi Arabia. We hypothesized that post-COVID-19 symptoms would vary among adults based on their vaccination status, after controlling for age, sex, previous health conditions, and perceived stress level.

METHODS

Ethics statements

Ethical approval was obtained from Jazan University prior to data collection. Informed consent was obtained in the first page of the survey. The study was anonymous, and participation was optional.

Study design and participants

This cross-sectional survey was conducted in Saudi Arabia. Study participants were recruited online through social networking using convenience and snowball sampling. A total of 307 post-COVID-19 patients completed online survey from April 2022 to August 2022. The inclusion criteria were adults older than 18 years of age, and those with a history of positive COVID-19 result at least 1 month prior to participation. We excluded individuals with newly diagnosed COVID-19 (within <1 month), those with no history of COVID-19, and pregnant women.

Data collection

The most common reported post-COVID-19 symptoms were selected as dependent variables such as breathing problems, concentration problems, exhaustion, dizziness, post-exercise malaise, cough, chest/stomach pain, headache, fast-beating heart, joint and muscle pain, tingling sensation, mood changes. Participants were asked to select all post-COVID-19 symptoms that they were experiencing. Then, post-COVID-19 symptoms were analyzed at a dichotomous level. The independent variable was vaccination status. A single-item, three-point Likert question was used for evaluation (0 = not vaccinated, 1 = incomplete vaccination, and 2 = complete vaccination). Participants' vaccination status was deemed complete if they had received all the recommended doses of COVID-19 or incomplete if they had only received a portion of the recommended doses.

The covariates included age, sex, previous health conditions, and perceived stress level. Age was measured at a categorical level: young adult (18–39 years), middle-aged adult (40–65 years), and older adults (>65 years); however, the older adult category had no participants. Sex was classified as male or female. Previous health conditions were defined as the presence of ≥1 chronic disease prior to the onset of COVID-19. A list of the most common chronic health conditions was provided, and the participants selected all applicable conditions. Next, these

conditions were analyzed at the dichotomous level.

Herein, perceived stress refers to a person's perception of the level of stress experienced at a certain moment or period. Perceived stress was evaluated by using the Perceived Stress Scale (PSS). The 10-question PSS evaluates an individual's experience of stress by measuring a person's perception of how difficult their life is (Cohen et al., 1983). Higher scores indicate a higher perceived stress level. The PSS is valid and reliable, including in Saudi Arabian adults (Ashgar, 2023). The Arabic version has a Cronbach's alpha of 0.74 (Chaaya et al., 2010). In this study, the Cronbach's alpha was 0.86.

Statistical analysis

We compared the demographic characteristics of participants based on their vaccination status using the chi-square analysis. The chi-square analysis was used to compare the characteristics of participants with and without at least one post-COVID-19 symptoms For each outcome, binary logistic regression analysis was utilized to assess the degree to which vaccination status affects post-COVID-19 symptoms with reciprocal covariate adjustment. The Hosmer-Lemeshow test was utilized to evaluate the quality of the fit. (Fagerland & Hosmer, 2012). An alpha of <0.05 was considered statistically significant. All data were analyzed using SPSS statistics software (version 25.0, IBM Corp.).

RESULTS

A total of 307 post-COVID-19 patients were recruited. Table 1 compares the demographic characteristics of the participants according to post-COVID-19 symptoms and vaccination status. Most of those who reported having ≥1 post-COVID-19 symptom were middle-aged adults (58.5%), women (54.6%), employed individuals (72.1%), those who had no previous health problems (56.8%), those who had incomplete vaccination status (69.4%), and those who had only one COVID-19 infection history (81.2%). Complete vaccination status was mostly reported among middle-aged adults (44.8%), men (51.0%), employed individuals (80.2%), those with no previous health problems (54.2%), and those with only one COVID-19 infection history (78.1%).

Table 1. Comparison of demographic characteristics of participants by post-COVID-19 symptoms and vaccination status (n = 307).

Characteristic		Total number (n [%])	At least 1 post-COVID-19 symptoms (n [%])	No post-COVID-19 symptoms (n [%])	Complete vaccination status (n [%])	Incomplete vaccination status (n [%])
Total participants		307 (100)	229 (74.6)	78 (25.4)	96 (31.3)	211 (68.7)
Age	18-39	140 (45.5)	95 (41.5)	45 (57.7)	43 (44.8)	97 (46.0)
	40-65	167 (54.4)	134 (58.5)	33 (42.3)	53 (55.2%)	114 (54.0)
	> 65	0 (0)	0 (0)	0 (0)	0 (0)	0 (0)
Sex	Male	144 (46.9)	104 (45.4)	40 (51.3)	49 (51.0)	95 (45.0)
	Female	163 (53.1)	125 (54.6)	38 (48.7)	47 (49.0)	116 (55.0)
Work status	Employed	217 (70.7)	165 (72.1)	52 (66.7)	77 (80.2)	140 (66.4)
	Unemployed	90 (29.3)	64 (27.9)	26 (33.3)	19 (19.8)	71 (33.6)
Previous health conditions	Absent	184 (59.9)	130 (56.8)	54 (69.2)	52 (54.2%)	132 (62.6)
	1 condition	69 (22.5)	48 (21.0)	21 (26.9)	20 (20.8%)	49 (23.2)
	>1 condition	54 (17.6)	51 (22.2)	3 (3.9)	24 (25%)	30 (14.2)
Vaccination status	Not vaccinated	0 (0)	0 (0)	0 (0)	0 (0)	0 (0)
	Incomplete	211 (68.7)	159 (69.4)	52 (66.7)		211 (68.7)
	Complete	96 (31.3)	70 (30.6)	26 (33.3)	96 (31.3)	
Number of COVID-19 infections	1	254 (82.7)	186 (81.2)	68 (87.2)	75 (78.1)	179 (84.8)
	2	44 (14.3)	35 (15.3)	9 (11.5)	17 (17.7)	27 (12.8)
	3	2 (.7)	2 (.9)	0 (0)	2 (2.1)	0 (0)
	4+	7 (2.3)	6 (2.6)	1 (1.3)	2 (2.1)	5 (2.4)

COVID-19, coronavirus disease.

Unadjusted analysis showed no significant differences in all post-COVID-19 symptoms, except cough, between those who had complete vaccinations and those who had incomplete vaccinations. Table 2 shows the association between post-COVID-19 symptoms and vaccination status. Participants who reported incomplete vaccinations were more likely to experience cough for ≥1 month post-COVID-19 illness (odds ratio [OR] = 2.09, 95% confidence interval [CI] = 1.06–4.13,

p = .032). Breathing problems (*p* = .324), exhaustion (*p*= .822), dizziness (*p* = .156), post-exercise malaise (*p* = .759), concentration problems (*p* = .522), chest and stomach pain (*p* = .362), headache (*p* = .120), fast-beating heart (*p* = .706), joint and muscle pain (*p* = .524), tingling sensation (*p* = .630), and mood changes (*p* = .479) were not significantly associated with vaccination status.

Results of bivariate analysis showed that none of the post-COVID-19 symptoms were associated with vaccination status, except cough (adjusted OR = 2.19, 95% CI = 1.09–4.45, *p* = .028). Participants with incomplete vaccination status were 2.19 higher risk of experiencing cough for ≥1 month post-COVID-19 illness after adjusting for the linear effect of age, sex, previous health conditions, and perceived stress level. Breathing problems (*p* = .340), exhaustion (*p* = .798), dizziness (*p* = .179), post-exercise malaise (*p* = .732), concentration problems (*p* = .409), chest and stomach pain (*p* = .387), headache (*p* = .133), fast-beating heart (*p* = .670), joint and muscle pain (*p* = .579), tingling sensation (*p* = .451), and mood changes (*p* = .526) were not significantly associated with vaccination status after adjusting for the linear effect of age, sex, previous health conditions, and perceived stress level.

Table 2. Association of post-COVID-19 symptoms with vaccination status (n = 307).

Post-COVID-19 symptoms	Vaccination Status	Symptomatic 229 (74.60%)	OR (95% CI)	*p*-value	AOR (95% CI)	*p*-value
Breathing Problems	Complete vaccination	7 (23.33)	.64 (.26–1.55)	.324	.64 (.25–1.61)	.340
	Incomplete vaccination	23 (76.67)				
Exhaustion	Complete vaccination	27 (30.34)	.94 (.55–1.60)	.822	.93 (.50–1.68)	.798
	Incomplete vaccination	62 (69.66)				
Post-exercise malaise	Complete vaccination	19 (29.69)	.91 (.50–1.66)	.759	.89 (.46–1.69)	.723
	Incomplete vaccination	45 (70.31)				
Concentration problems	Complete vaccination	17 (27.87)	.82 (.4–1.52)	.522	.75 (.38–1.48)	.409
	Incomplete vaccination	44 (72.13)				
Cough	Complete vaccination	18 (46.15)	2.02 (1.06–4.13)	**.032**	2.19 (1.09–4.45)	**.028**
	Incomplete vaccination	21 (53.85)				
Chest/stomach pain	Complete vaccination	15 (37.50)	1.38 (.69–2.75)	.362	1.39 (.66–2.89)	.387
	Incomplete vaccination	25 (62.50)				
Headache	Complete vaccination	21 (40.38)	1.62 (.88–3.01)	.120	1.63 (.86–3.09)	.133

	Incomplete vaccination	31 (59.62)				
Fast-beating heart	Complete vaccination	8 (34.78)	1.19 (.49–2.90)	.706	1.23 (.48–3.16)	.670
	Incomplete vaccination	15 (65.22)				
Joint and muscle pain	Complete vaccination	26 (34.21)	1.20 (.69–2.08)	.524	1.17 (.67–2.07)	.579
	Incomplete vaccination	50 (65.79)				
Tingling sensation	Complete vaccination	10 (27.78)	.83 (.38–1.79)	.630	.73 (.33–1.65)	.451
	Incomplete vaccination	26 (72.22)				
Dizziness	Complete vaccination	12 (42.86)	1.74 (.79–3.84)	.165	1.79 (.77–4.16)	.179
	Incomplete vaccination	16 (57.14)				
Mood changes	Complete vaccination	23 (34.85)	1.23 (.69–2.19)	.479	1.24 (.62–2.42)	.526
	Incomplete vaccination	43 (65.15)				

Bold *p*-values indicate statistical significance.

OR, odds ratio; CI, confidence interval; AOR, adjusted odds ratio; COVID-19, coronavirus disease.

DISCUSSION

This study compared post-COVID-19 symptoms among people in Saudi Arabia based on their vaccination status. Among the 307 post-COVID-19 patients who participated in this study, we found no significant difference in the post-COVID-19 symptoms between those who received complete vaccinations and those who received incomplete vaccinations, except for cough, which does not support our hypothesis. This is the first study to examine the potential effect of COVID-19 vaccinations on post-COVID-19 symptoms in Saudi Arabian adults. These results imply that, while immunization is crucial for providing immunological protection against infection, it does not seem to be linked to modifications in post-COVID-19 symptoms. Additionally, these data support the safety of COVID-19 vaccines in the mentioned post-COVID-19 symptoms.

According to studies from China, Italy, France, and Saudi Arabia, between 15% and 84% of patients with COVID-19 may develop post-COVID-19 symptoms (Ashgar, 2023; Carfì, Bernabei, and Landi, 2020; Garrigues et al., 2020; Havervall et al., 2021; Huang et al., 2021; Lerner et al., 2021; Logue et al., 2021; Nalbandian et al., 2021; Watson et al., 2022). Several studies have been conducted to understand the mechanisms underlying the post-COVID-19 symptoms. Current literature support several theories that have been proposed to explain the continuing impact of COVID-19 symptoms such as viral reservoirs, ongoing inflammatory processes, the

production of autoantibodies, and/or organ damage after acute infection (Wisnivesky et al., 2022; Lerner et al., 2021). Moreover, after the first infection, the virus particles can stay in the stomach for up to 4–7 months. (Wisnivesky et al., 2022). As such, COVID-19 vaccines may help reduce post-COVID-19 symptoms by eliminating the viral reservoir or by resetting an immune response that was dysregulated in response to the initial infection (Wisnivesky et al., 2022).

COVID-19 vaccines have significantly changed the trajectory of the pandemic, saving millions of lives worldwide (Nalbandian et al., 2021). Nevertheless, people are still worried of the possible long-term risk of COVID-19 vaccinations (Alshahrani et al., 2021). Herein, the findings revealed no evidence linking COVID-19 vaccinations to post-COVID-19 symptoms. These findings are consistent with previous research that found no association between COVID-19 immunizations and improvement in post-COVID-19 symptoms (Wisnivesky et al., 2022).

Our study has several strengths and limitations. This descriptive cross-sectional study used an online survey to assess whether receiving a complete dose of COVID-19 vaccine was linked to post-COVID-19 symptoms among adults in Saudi Arabia. The participants' responses may have been affected by social expectations, thereby affecting the results. Furthermore, the use of social networking to recruit participants limited the participation to those with smartphones and internet access. Therefore, no older adults (≥65 years) were enrolled in this study. However, to our best knowledge, this is the first study to assess the association between COVID-19 vaccinations and post-COVID-19 symptoms among Saudi Arabian adults. This study's findings support the continued provision of the COVID-19 vaccination. Therefore, to highlight the significance of vaccination against infectious diseases in general, and in particular COVID-19, outreach initiatives are required. The latest evidence regarding the associated risk factors and long-term risks should be communicated to the public. Further research is required to fully understand the causes and risk factors of post-COVID-19 symptoms and to determine appropriate care for these individuals

CONCLUSIONS

This study revealed that receiving a complete dose of COVID-19 vaccines had no effect in post-COVID-19 symptoms. COVID-19 vaccinations are important for immunological protection against the infection, and governments are directing all initiatives to reach vaccination coverage targets. Governments and legislators need to deal with the problem of false information flowing on social media regarding the association between vaccinations and post-COVID-19 symptoms. Finally, population-based comprehensive initiatives and interventions are required to raise awareness of the benefits of COVID-19 vaccinations and to manage and control post-COVID-19 symptoms.

Acknowledgement: We would like to thank Editage (www.editage.com) for English language editing.

References

AlGhalyini, B., Shakir, I., Wahed, M., Babar, S., Mohamed, M. (2022). Does SARI Score Predict COVID-19 Positivity? A Retrospective Analysis of Emergency Department Patients in a Tertiary HospitalWHO. *Saudi Arabia Coronavirus Disease (COVID-19) Dashboard*. (2023). *Journal of Health and Allied Sciences*. https://www.thieme-connect.de/products/ejournals/pdf/10.1055/s-0042-1748806.pdf

Alshahrani, S.M., Dehom, S., Almutairi, D., Alnasser, B.S., Alsaif, B., Alabdrabalnabi, A.A., ... & Mahtab Alam, M. (2021). Acceptability of COVID-19 vaccination in Saudi Arabia: A cross-sectional study using a web-based survey. *Human vaccines & immunotherapeutics*, 17(10), 3338-47.

Arnold, D. T., Milne, A., Samms, E., Stadon, L., Maskell, N. A., Hamilton, F. W. (2021). Are vaccines safe in patients with Long COVID? A prospective observational study. *medRxiv*, https://doi.org/10.1101/2021.03.11.21253225

Ashgar, R.I. (2021). Health-promoting behaviour during the COVID-19 pandemic among Saudi Adults: A cross-sectional study. *Journal of advanced nursing*, 77(8), 3389-97.

Ashgar, R. I. (2023). Prevalence of Post Coronavirus Illness Conditions and Associated Risk Factors Among Adults in Saudi Arabia. Public Health Open Access, 7(1), 1-10. Doi: 10.23880/phoa-16000228.

Carfì, A., Bernabei, R., & Landi, F. (2020). Persistent Symptoms in Patients After Acute COVID-19. *JAMA*, 324(6), 603-5.

Centers for Disease Control and Prevention. (2023). *Post COVID conditions*. CDC. https://www.cdc.gov/coronavirus/2019-ncov/long-term-effects/index.html

Centers for Disease Control and Prevention. (2023). *Post-COVID conditions: Information for healthcare providers*. CDC. https://www.cdc.gov/coronavirus/2019-ncov/hcp/clinical-care/post-covid-conditions.html

Chaaya, M., Osman, H., Naassan, G., & Mahfoud, Z. (2010). Validation of the Arabic version of the Cohen Perceived Stress Scale (PSS-10) among pregnant and postpartum women. *BMC psychiatry*, 10, 111.

Cohen, S., Kamarck, T., & Mermelstein, R. (1983). A global measure of perceived stress. *Journal of health and social behavior*, 24(4), 385-96.

Fagerland, M. W., Hosmer, D. W. (2012). A generalized Hosmer–Lemeshow goodness-of-fit test for multinomial logistic regression models. *Stata J*, 12, 447-53.

Garrigues, E., Janvier, P., Kherabi, Y., Le Bot, A., Hamon, A., Gouze, H., ... & Nguyen, Y. (2020). Post-discharge persistent symptoms and health-related quality of life after hospitalization for COVID-19. *The Journal of infection*, 81(6), e4-e6.

Havervall, S., Rosell, A., Phillipson, M., Mangsbo, S.M., Nilsson, P., Hober, S., & Thålin, C. (2021). Symptoms and Functional Impairment Assessed 8 Months After Mild COVID-19 Among Health Care Workers. *JAMA*, 325(19), 2015-6.

Huang, C., Huang, L., Wang, Y., Li, X., Ren, L., Gu, X., ... & Cao, B. (2021). 6-month consequences of COVID-19 in patients discharged

from hospital: a cohort study. *Lancet (London, England)*, 397(10270), 220-32.

Khan, A., Alsofayan, Y., Alahmari, A., Alowais, J., Algwizani, A., Alserehi, H., ... & Jokhdar, H. (2021). COVID-19 in Saudi Arabia: the national health response. *Eastern Mediterranean health journal = La revue de sante de la Mediterranee orientale = al-Majallah al-sihhiyah li-sharq al-mutawassit*, 27(11), 1114-24.

Lerner, A.M., Robinson, D.A., Yang, L., Williams, C.F., Newman, L.M., Breen, J.J., ... & Erbelding, E.J. (2021). Toward Understanding COVID-19 Recovery: National Institutes of Health Workshop on Postacute COVID-19. *Annals of internal medicine*, 174(7), 999-1003.

Logue, J.K., Franko, N.M., McCulloch, D.J., McDonald, D., Magedson, A., Wolf, C.R., & Chu, H.Y. (2021). Sequelae in Adults at 6 Months After COVID-19 Infection. *JAMA network open*, 4(2), e210830.

Nalbandian, A., Sehgal, K., Gupta, A., Madhavan, M.V., McGroder, C., Stevens, J.S., ... & Wan, E.Y. (2021). Post-acute COVID-19 syndrome. *Nature medicine*, 27(4), 601-15.

Office for National Statistics. (2020). *The prevalence of long COVID symptoms and COVID-19 complications (2020).* Office for National Statistics. https://www.ons.gov.uk/news/statementsandletters/theprevalenceoflongcovidsymptomsandcovid19complications

Watson, O.J., Barnsley, G., Toor, J., Hogan, A.B., Winskill, P., & Ghani, A.C. (2022). Global impact of the first year of COVID-19 vaccination: a mathematical modelling study. *The Lancet. Infectious diseases*, 22(9), 1293-302.

World Health Organization. (2023). *Post COVID-19 Condition (Long COVID).* WHO. WHO. https://www.who.int/europe/news-room/fact-sheets/item/post-covid-19-condition

World Health Organization. (2023). S*audi Arabia Coronavirus Disease (COVID-19) Dashboard*. WHO. https://covid19.who.int/region/emro/country/sa

Wisnivesky, J.P., Govindarajulu, U., Bagiella, E., Goswami, R., Kale, M., Campbell, K.N., ... & Lin, J.J. (2022). Association of Vaccination with the Persistence of Post-COVID Symptoms. *Journal of general internal medicine*, 37(7), 1748-53.

العلاقة بين لقاحات مرض فايروس كورونا-٢٠١٩ (كوفيد-١٩) و أعراض ما بعد كوفيد-١٩ في المملكة العربية السعودية

رندة إبراهيم أشقر[1]

[1]كلية التمريض، جامعة جازان، المملكة العربية السعودية

ملخص

لقد غيرت لقاحات مرض فايروس كورونا-٢٠١٩ (كوفيد-١٩) بشكل كبير مسار الوباء وأنقذت عشرات الملايين من الأرواح في جميع أنحاء العالم. ومع ذلك، هناك بعض المخاوف بشأن سلامته وفعاليته وتأثيره على المدى الطويل. لذلك، الهدف من هذه الدراسة هو تقييم ما إذا كان لقاح كوفيد-١٩ مرتبطًا بأعراض ما بعد كوفيد-١٩ بين البالغين في المملكة العربية السعودية. هذه الدراسة عبارة عن دراسة مقطعية. شاركت عينة ملائمة مكونة من ٣٠٧ بالغين في استطلاع عبر الإنترنت من أبريل ٢٠٢٢ إلى أغسطس ٢٠٢٢. قمنا بمقارنة الخصائص الديموغرافية بناءً على حالة التطعيم (مكتمل التطعيم أو غير مكتمل التطعيم). تم استخدام اختبار Chi-Square أيضًا لمقارنة خصائص المشاركين الذين لديهم عرض واحد على الأقل من أعراض ما بعد كوفيد-١٩ مع أولئك اللذين ليس لديهم أي عرض من أعراض ما بعد كوفيد-١٩. تم استخدام الانحدار اللوجستي الثنائي لتقييم درجة تأثير حالة التطعيم على أعراض ما بعد كوفيد-١٩. كانت أعراض ما بعد كوفيد-١٩ أكثر شيوعًا بين البالغين في منتصف العمر (٥٨,٥٪) ، الإناث (٥٤,٦٪) ، العاملين (٧٢,١٪) ، من ليس لديهم أي مشاكل صحية سابقة (٥٦,٨٪) ، و من لديهم حالة تطعيم غير مكتملة (٦٩,٤٪). حالة التطعيم كانت مكتملة في الغالب بين البالغين في منتصف العمر (٥٥,٢%) ، الذكور (٥١,٠٪) ، العاملين (٨٠,٢٪) ، وأولئك الذين ليس لديهم مشاكل صحية سابقة (٥٤,٢٪). أظهر التحليل ثنائي المتغير أن أياً من أعراض ما بعد كوفيد-١٩ لم تكن مرتبطة بحالة التطعيم باستثناء السعال (Adjusted OR= 2.19، CI = 1.09-4.45، p-value = .028). أظهرت الدراسة الحالية أن لقاحات كوفيد-١٩ غير مرتبطة بأعراض ما بعد كوفيد-١٩. تحتاج الحكومات وصناع السياسات إلى معالجة قضايا المعلومات المضللة التي تنتشر في وسائل التواصل الاجتماعي فيما يتعلق بالارتباط بين التطعيمات وأعراض ما بعد كوفيد-١٩.

الكلمات المفتاحية: البالغين، ممرضي صحة مجتمع، أعراض ما بعد كوفيد-١٩، لقاحات كوفيد-١٩، المملكة العربية السعودية.

Sonographic measurement for spleen to left kidney ratio in healthy Saudi adult and correlation with body parameters

Meaad Elbashir [*1]

[1] Department of Diagnostic Radiography Technology, College of Applied Medical Science, Jazan University, Saudi Arabia

Abstract

This research paper investigates the relationship between age, height, weight, body mass index (BMI), the spleen and left kidney measurements and the spleen-to-left kidney ratio (SLKR). The study measured spleen length, left kidney length, and SLKR in 95 participants and analyzed the data using correlation analysis and t-tests. The study included 59 male and 36 female participants, with the mean age being 23.81±6.3 years (ranged 19-45). The BMI of the participants ranged from 14.24 to 40.25, with a mean of 23.20± 6.87. The mean for left kidney length was higher for male participants (10.34) than for female participants (9.72). The mean for spleen length was higher for male participants (9.80) than for female participants (8.74). For SLKR, the mean was slightly higher for female participants (1.12) than for male participants (1.07). However, the differences were not statistically significant ($p > 0.05$). The results suggest that BMI may impact spleen and left kidney measurements, while age does not appear to be a significant factor. The study found a significant positive correlation between spleen length and left kidney length, while SLKR negatively correlates with both spleen and left kidney length. This study provides valuable insights into the relationship between spleen and left kidney measurements and their implications for clinical practice.

Keywords: Ultrasound, Spleen, kidney, spleen to left kidney ratio

Introduction

In clinical practice, ultrasound is commonly the first-line imaging modality for assessing the visceral organ dimensions such as the spleen, liver, and kidneys[1]. The spleen is a main part of lymphatic system. It helps the immune system by storing white blood cells and helps in the creation of antibodies. Splenomegaly can be detected both clinically and sonography is commonly used for evaluating the size, shape, and texture of abdominal organs such as the liver, spleen, and kidneys [2] Size and weight of spleen is calculated by measuring length width and AP diameter . One of the important measurements derived from sonography is the spleen-to-left kidney ratio (SLKR),this ratio varies with age, and this is statistically significant in in both males and female also can be used as a measure of normality of organ dimensions [3]. This ratio has been suggested as a valuable parameter for assessing splenomegaly in various clinical conditions.

Splenomegaly is defined as enlargement of the spleen measured by size or weight. The spleen plays a significant role in hematopoiesis and immunosurveillance is a sign of a pathologic process that could have primary splenic origins or could be a symptom of disease in any other organ system. Splenomegaly may be a transient condition due to acute illness or may be due to serious underlying acute or chronic diseases [4]. the sonographic examination of the spleen. By using native B-mode and Color Doppler the underlying entity often is not elucidated. Thus, more elaborate imaging modalities topographically based imaging methods like CT and MRI scans, Ultrasound is a useful imaging modality in measuring the spleen and spares the patient radiation from CT imaging[4, 5]. Clinical evaluation of the splenic size is challenging and unreliable due to the spleen being concealed in its anatomic location under the ribs and the need for considerable enlargement to occur before the spleen is clinically palpable [6]. Therefore, imaging techniques, such as ultrasound, are used to assess the spleen's size accurately. These techniques are more reliable than clinical palpation. They can detect even a slight spleen enlargement, an essential indicator of several medical conditions such as e.g., infections, metabolism or storage disorders, and hematological abnormalities [7].

There has been increasing interest in using sonography to examine the spleen and assess its size and structure. One approach to the sonographic assessment of the spleen is to measure the ratio of its length to the length of the left kidney [8-10]. This approach helps identify various spleen-related pathologies in adults [10]. In Saudi Arabia, like many countries, there is a need for accurate and reliable sonographic measurements of the spleen in adults. However, there is currently limited research on using sonographic measurements of the SLKR in healthy Saudi adults.

Sonographic measurements for SLKR in healthy Saudi adults are an important research area that has gained increasing interest in recent years. This ratio is considered an essential tool for assessing the health of individuals, as it can provide valuable information about the size and function of the spleen and left kidney. Additionally, studies have shown that there may be a correlation between this ratio and various body parameters, such as age, height, weight, and body mass index (BMI) [9, 11]. Understanding these correlations can help clinicians better interpret sonographic measurements and diagnose more accurately.

US was used to measure maximum splenic and left kidney lengths to obtain normal values for splenic length and to determine spleen to left kidney ratio, Splenic lengths in Iraqi subjects are similar to those in American, Jordanian and Chinese subjects up to the age of 15 years. The spleen to left kidney ratio is strikingly constant with a mean value of 1. Using 2 SD ultrasound above the mean as a guide, the upper limit of normal for spleen to left kidney ratio is 1.25. with variation between male and female[12]

This study evaluates the sonographic measurements for SLKR in healthy Saudi individuals and their relationship to body parameters. The findings of this study can be added to the existing literature in the field of diagnostic imaging by providing normative data for this specific population. As there is a shortage of literature on normal reference values for this measurement in Saudi adults, this study could fill the gap and provide valuable information for clinicians to diagnose better and treat patients. Additionally, the study could aid in developing population-specific screening and diagnostic criteria for

the Saudi adult population. Therefore, this research can have significant implications for improving the quality of healthcare services provided to the people in Saudi Arabia.

Method and materials:

A prospective cross-sectional study design was used to achieve this study's objectives. A sample of healthy Saudi adults aged 18 to 60 was recruited in Jazan Region. Sonographic measurements of the spleen and left kidney were obtained, and the spleen and left kidney SLKR were calculated. Data on the participants' body parameters, such as age, gender, and BMI, were also collected. Participants with any history of disease related to the spleen or kidney, traumatic, oncologic, and hematologic conditions, sickle cell anemia, previous splenectomy, and those whose abnormal echo texture of the spleen were excluded. The sample size was calculated using an alpha of 0.05, power of 0.80, expected effect size of 0.5, and standard deviation of 0.1, based on a T-test. The minimum required sample size was 76 participants to achieve a power of 0.80 and detect a significant difference in the SLKR.

Ethical Considerations:

This study was approved by the Standing Committee for Scientific Research at Jazan University (REC-43/02/028) on 29/09/2021. Signed informed consent was obtained from all participants before recruitment. This study was performed during 2021-2022 to recruit healthy Saudi participants.

Sonographic measurements

The subjects were examined in the right lateral decubitus position, and the spleen's longitudinal and transverse views were obtained. Splenic length, width, and thickness measurements were made from the longitudinal section of the spleen, and measurements of the left kidney's length from the longitudinal section of the same position were made for SLKR calculation. All examinations were scanned with a senior sonologist and interpreted by radiologists experienced in abdomen imaging.

Statistical analysis

The statistical package for social science (SPSS), version 25, was used to analyze the data, and the results were presented in tables and figures. To determine if there were statistically significant differences in

variables, an independent sample t-test was conducted. Pearson correlation was performed to assess the correlation between variables with p-value <0.05 considered statistically significant.

Results

A total of 95 participants were included in the study, with 59 male and 36 female participants—a minimum age of 19 years and a maximum of 45 years (Table 1). The mean age was 23.81 ± years, with a standard deviation of 6.3. The participants' height ranged from 48 cm to 188 cm, with a mean of 156.84 ± 29.13 cm. The participants' weight ranged from 31 kg to 166 kg, with a mean of 69.65 ± 32.08 kg. The BMI of the participants ranged from 14.24 to 40.25, with a mean of 23.20 ± 6.87. The left kidney length ranged from 4.77 cm to 12.70 cm, with a mean of 10.10 ± 1.02 cm. The spleen length ranged from 7.17 cm to 13.80 cm, with a mean of 9.39 ± 1.38 cm. Finally, the SLKR ranged from 0.55 to 1.50, with a mean of 1.09 ± 0.14.

Table 1: Descriptive Statistics of the variables.

	Minimum	Maximum	Mean	Std. Deviation
Age (years)	19.00	45.00	23.81	6.37
Height (cm)	48.00	188.00	156.84	29.14
Weight (kg)	31.00	166.00	69.65	32.09
BMI	14.24	40.25	23.20	6.87
Left kidney length (cm)	4.77	12.70	10.11	1.02
Spleen length (cm)	7.17	13.80	9.40	1.39
Spleen to left kidney ratio	0.55	1.50	1.09	0.15

Table 2 shows the means of both genders' left kidney and spleen measurements. The mean for left kidney length was higher for male participants (10.34) than for female participants (9.72). However, the difference was not statistically significant (p = 0.493). The mean for spleen length was higher for male participants (9.80) than for female participants (8.74). However, the difference was not statistically significant (p = 0.105). For SLKR, the mean was slightly higher for female participants (1.12) than male participants (1.07). However, the difference was not statistically significant (p = 0.542).

Table 2: Independent sample t-test for compare means left kidney spleen measurements in both genders.

Measurements	Gender	Mean	Std. Deviation	P-Value
Left kidney length	Male	10.34	0.86	.493
	Female	9.72	1.15	
Spleen length	Male	9.80	1.38	.105
	Female	8.74	1.13	
Spleen to left kidney ratio	Male	1.07	0.14	.542
	Female	1.12	0.15	

Table 3 presents the results of the correlation analysis between age, height, weight, BMI, and splenic and left kidney measurements and their ratio. There were no significant correlations for spleen length with age ($r = 0.023$, $p = 0.824$) or height ($r = 0.312$, $p = 0.002$). However, weight was positively correlated with spleen length ($r = 0.259$, $p = 0.011$), indicating that heavier individuals tend to have larger spleen sizes. Additionally, BMI was positively correlated with spleen length ($r = 0.443$, $p < .001$), indicating that individuals with higher BMI tend to have larger spleen sizes.

Left kidney length had no significant correlation with age ($r = 0.077$, $p = 0.459$) or weight ($r = 0.165$, $p = 0.109$). However, height was significantly positively correlated with left kidney length ($r = 0.255$, $p = 0.013$), indicating that taller individuals tend to have longer left kidneys. Additionally, BMI was found to be strongly positively correlated with left kidney length ($r = 0.298$, $p = 0.003$), indicating that individuals with higher BMI tend to have longer left kidneys.

For SLKR, there were no significant correlations with age ($r = 0.025$, $p = 0.807$), height ($r = -0.131$, $p = 0.205$), or weight ($r = -0.169$, $p = 0.101$). However, BMI was significantly negatively correlated with SLKR ($r = -0.272$, $p = 0.008$), indicating that individuals with higher BMI tend to have smaller SLKR.

Table 3: Correlation between age, height, weight, BMI and splenic and left kidney measurements.

		Spleen length	Left kidney length	Spleen to left kidney ratio
Age	Pearson Correlation	.023	.077	.025
	P-Value	.824	.459	.807
Height	Pearson Correlation	.312	.255	-.131
	P-Value	**.002**	**.013**	.205
Weight	Pearson Correlation	.259	.165	-.169
	P-Value	**.011**	.109	.101
BMI	Pearson Correlation	.443	.298	-.272
	P-Value	**<.001**	**.003**	**.008**

The correlation analysis results between left kidney length, splenic length, and SLKR are shown in Table 4. The results indicate a significant positive correlation between spleen length and left kidney length, with a Pearson correlation coefficient of 0.426 and a p-value of <.001. Additionally, there is a significant negative correlation between SLKR and both, spleen length and left kidney length, with Pearson correlation coefficients of -0.718 and -0.306, respectively, and p-values of 0.001 and 0.003, respectively.

Table 4: Correlation of Left kidney length, splenic length and SLKR.

		Spleen length	Left kidney length	Spleen to left kidney ratio
Spleen length	Pearson Correlation	1		
	Sig. (2-tailed)			
Left kidney length	Pearson Correlation	.426	1	
	Sig. (2-tailed)	<.001		
Spleen to left kidney ratio	Pearson Correlation	-.718	.306	1
	Sig. (2-tailed)	<.001	.003	

Figure 1 shows the study's relationship between spleen and left kidney lengths. The result shows a general positive trend, suggesting a direct relationship between the two variables. The R^2 value indicates that only 18% of the variation in spleen length can be explained by left kidney length. The scatterplot also shows some variability around the line of best fit, indicating that there may be other factors affecting the spleen length that are not accounted for by the left kidney length alone.

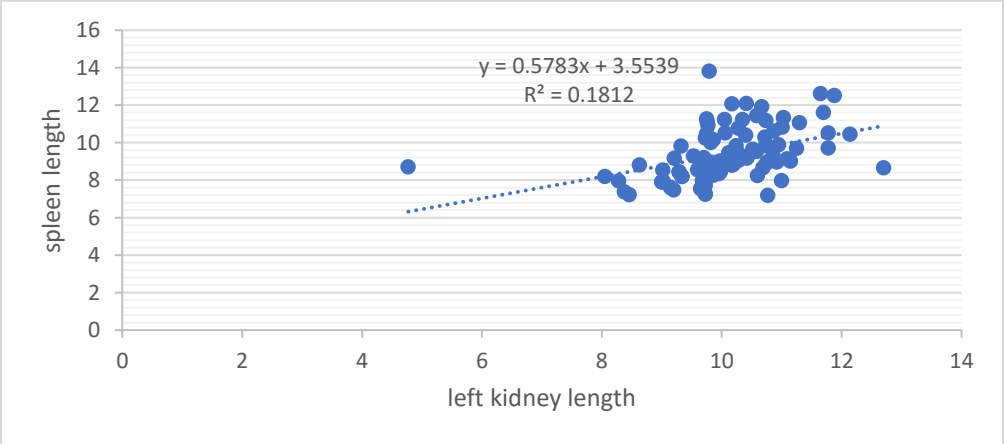

Figure (1): Relationship between spleen length to left kidney length.

Figure 2 displays the relationship between spleen length and SLKR in the study. The scatterplot shows a robust negative trend, suggesting an inverse relationship between the two variables. The R^2 indicates that 51% of the variation in SLKR can be explained by spleen length.

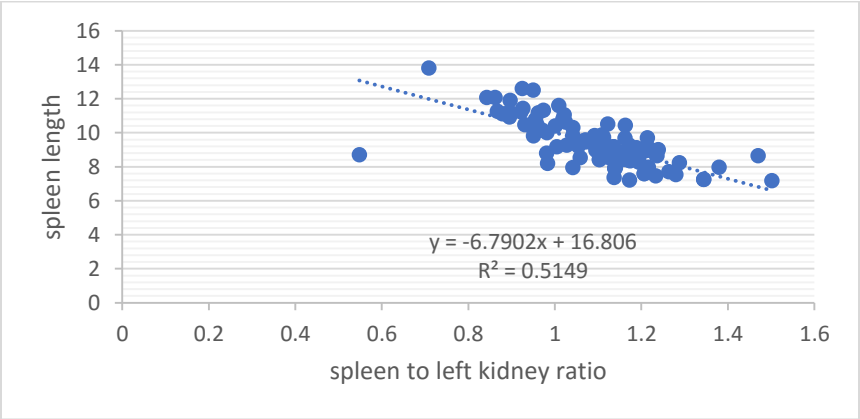

Figure (2): Relationship between spleen lengths to SLKR.

In Figure 3, The scatterplot shows a slight negative trend, suggesting an inverse relationship between left kidney length and SLKR.

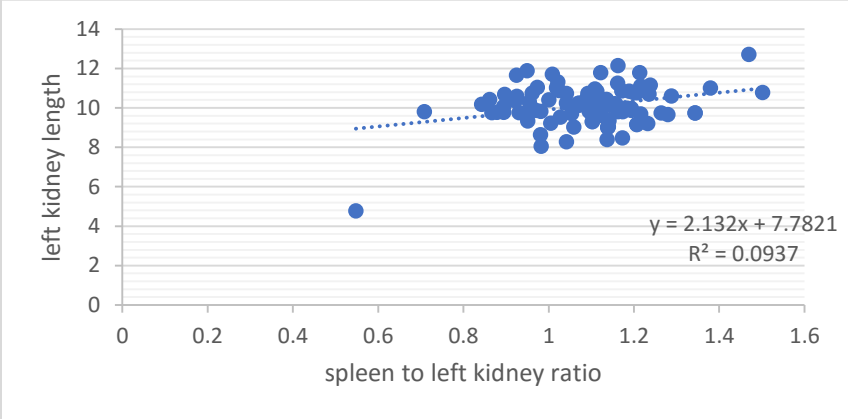

Figure (3): Relationship between left kidney lengths to SLKR.

Discussion

In this study, the mean length of the spleen and left kidney was higher for male participants than for females, with no statistically significant differences. This outcome is in line with previous studies investigating gender differences in kidney and spleen measurements. The current research, which indicates that the splenic length is longer in men than in women but that the difference is not statistically significant, is consistent with the study by Singh A. et al. [13] [14].

Additionally, a prior study revealed no connection between gender, age, and BMI and spleen length in the other hand For men with a body height of 165-199 cm and women with a body height of 155-179 cm, respectively, the authors define height- and sex-corrected normal values for spleen length and volume and offer verified algorithms to gauge the percentile of an individual's spleen size. [15, 16]. On the other hand, there are also some previous studies that reported significant gender differences in spleen and kidney measurements, such as the study of Badran et al. ($p<0.001$) [17].

However, the mean SLKR was slightly higher for female participants (1.12) compared to male participants (1.07) but not statistically significant ($p = 0.542$). The fact that there were no discernible gender differences in SLKR suggests that both males and females in the research population may have proportionate growth of the spleen and left kidney. This is in line with earlier research that found no gender differences in the lengths of the left kidney and spleen [3, 18-20]. Therefore, in the Saudi population of school-age children, gender could not be a determinant in spleen and left kidney growth [3]. However, some studies have also found that the spleen to left kidney ratio varies with age, especially in female subjects[3, 21], indicating that other factors such as hormonal changes may influence the growth of these organs over time.

The correlation analysis between BMI and splenic and left kidney measurements and their ratio suggest that BMI positively correlates with spleen and left kidney lengths. In contrast, BMI is negatively correlated with SLKR. Another study found no significant correlation between BMI with SLKR [22]. Moreover, the significant negative correlation between SLKR and both spleen length

and left kidney length suggests that as spleen length and left kidney length increase, the SLKR decreases. This finding may have implications for conditions such as kidney tumors or hydronephrosis when an increase in left kidney length may coexist with a decrease in SLKR. The diagnosis and treatment of various illnesses may benefit from this information. According to a study, left kidney length may reveal a relationship between a slightly enlarged spleen and a somewhat larger left kidney length. The lengths of the left kidney and spleen were discovered to be positively correlated.[9]. This might be normal or related to renal or splenic problems

The current research is particularly important in Saudi Arabia, where the incidence of renal and splenic diseases is increasing. The incidence of renal and splenic diseases in Saudi Arabia is higher than in many other countries. This may be due to factors such as the high prevalence of diabetes and hypertension, which are known risk factors for renal and splenic diseases[23, 24] .Therefore, understanding the relationship between body parameters and the measurements of the spleen and left kidney, as well as the SLKR, is crucial for accurately diagnosing and managing these conditions in Saudi Arabia. Moreover, this study's findings may help develop screening programs for renal and splenic diseases in Saudi Arabia. Early detection of these conditions can lead to better patient outcomes and reduce healthcare costs. Additionally, the study's findings can provide valuable information for healthcare professionals in Saudi Arabia who may encounter patients with renal or splenic conditions in their daily practice.

Limitations

One limitation of this research is the small sample size, which may affect the generalizability and applicability of the results. More research with larger and more diverse samples is needed to confirm and extend the findings on the variables of interest.

Conclusion:

The study investigated the relationship between age, height, weight, BMI, spleen and left kidney measurements, and SLKR. The findings suggest that height, weight, and BMI may impact spleen and left kidney measurements, while age does not appear significant. Moreover, the

study found a significant positive correlation between spleen length and left kidney length, while SLKR negatively correlates with both spleen and left kidney length. These findings can be helpful in the diagnosis of various conditions affecting the spleen and left kidney and provide a better understanding of the relationship between these organs.

References:

1. Mohtasib, R.S., et al., *Sonographic measurements for spleen size in healthy Saudi children and correlation with body parameters.* Annals of Saudi Medicine, 2021. **41**(1): p. 14-23.
2. Patil, S.V., et al., *Spleen and Kidney Ratio in the Assessment of Mild Splenomegaly.*
3. Akinlade, F., O. Akinlade, and A. Aremu, *Spleen–left kidney ratio and liver–right kidney ratio: novel measures of normal liver, spleen, and kidney dimensions in Southwestern Nigerian children.* Journal of Ultrasound, 2021. **24**: p. 297-302.
4. Chapman, J., et al., *Splenomegaly. 2021 Aug 11*. StatPearls. Treasure Island (FL): StatPearls Publishing, 2022.
5. Schwarze, V., et al., *Single-center study: The diagnostic performance of contrast-enhanced ultrasound (CEUS) for assessing focal splenic lesions compared to CT and MRI.* Clinical hemorheology and microcirculation, 2019. **73**(1): p. 65-71.
6. Anthony, A.O., *Sonographic Measurement of the Spleen in the healthy adult Nigerian Population in Enugu State, Nigeria.* Ibom Medical Journal, 2023. **16**(1): p. 45-50.
7. Aldulaimi, S. and A.M. Mendez, *Splenomegaly: Diagnosis and Management in Adults.* American Family Physician, 2021. **104**(3): p. 271-276.
8. Yousaf, A., et al., *Sonographic Assessment of Spleen to Left Kidney Ratio among School Going Children Ranging in Age from 8 to 15 years: Sonographic Assessment of Spleen to Left Kidney.* Pakistan BioMedical Journal, 2022: p. 51-54.
9. AlShammari, Q.T., et al., *Association of Sonographic Measurements of Kidneys and*

Spleen with Body Hight in University Age Saudi Population. Archives of Pharmacy Practice¦ Volume, 2022. **13**(2).

10. Bayramoğlu, Z., H. Ayyıldız, and B. Ersoy, *Reference Ranges of Age-Based Liver, Spleen, Pancreas, and Kidney Size in Conjunction with Waist Circumference in Children.* Turkish Archives of Pediatrics, 2022. **57**(2): p. 175.
11. Chow, K.U., et al., *Spleen Size Is Significantly Influenced by Body Height and Sex: Establishment of Normal Values for Spleen Size at US with a Cohort of 1200 Healthy Individuals.* Radiology, 2016. **279**(1): p. 306-13.
12. Al-timimy, Q.A., M.N. Al-Naddawi, and S.M. Joori, *Ultrasound assessment of normal splenic length and spleen to left kidney ratio in sample of Iraqi population.* AL-Kindy College Medical Journal, 2014. **10**(2): p. 56-61.
13. Singh, A., et al., *ULTRASONOGRAPHIC MEASUREMENT OF SPLENIC LENGTH IN RELATION WITH BODY SURFACE AREA IN ADULTS OF BIHAR.* J. Anat, 2015. **23**(1): p. 5-9.
14. Huang, Y., et al., *Ultrasound Assessment of the Relevance of Liver, Spleen, and Kidney Dimensions with Body Parameters in Adolescents.* Computational and Mathematical Methods in Medicine, 2022. **2022**.
15. Ikubor, J., S. Beryl, and O. Onajite, *Sonographic Splenic Length and Its Correlation With Biodata in Adult Nigerians in Oghara, South South Nigeria.* Journal of Research in Basic and Clinical Sciences, 2021. **2**(2): p. 53-60.
16. Chow, K.U., et al., *Spleen size is significantly influenced by body height and sex: establishment of normal values for spleen size at US with a cohort of 1200 healthy individuals.* Radiology, 2016. **279**(1): p. 306-313.
17. Badran, D.H., et al., *Ultrasonographic assessment of splenic volume and its correlation with body parameters in a Jordanian population.* Saudi medical journal, 2015. **36**(8): p. 967.
18. Elserag, T., et al., *Sonographic Measurement of Spleen to Left*

Kidney Ratio among Saudi Children. European Journal of Medical and Health Sciences, 2021. **3**(3): p. 128-130.

19. Eze, C., et al., *Sonographic determination of spleen to left kidney ratio among igbo school age children of south east, Nigeria.* African health sciences, 2014. **14**(1): p. 246-254.
20. Layton, A.T. and J.C. Sullivan, *Recent advances in sex differences in kidney function.* American Journal of Physiology-Renal Physiology, 2019. **316**(2): p. F328-F331.
21. Chemezov, S., A. Lozinskiy, and A. Urbanskiy, *Linear morphometric parameters of the spleen of children and adolescents according to the data of intravital imaging.* Pacific Medical Journal, 2021(1): p. 42-45.
22. Ehimwenma, O. and M.T. Tagbo, *Determination of normal dimension of the spleen by ultrasound in an endemic tropical environment.* Nigerian Medical Journal, 2011. **52**(3): p. 198.
23. Alsuwaida, A.O., et al., *Epidemiology of chronic kidney disease in the Kingdom of Saudi Arabia (SEEK-Saudi investigators)-a pilot study.* Saudi Journal of Kidney Diseases and Transplantation, 2010. **21**(6): p. 1066-1072.
24. Mousa, D., et al., *Prevalence and associated factors of chronic kidney disease among relatives of hemodialysis patients in Saudi Arabia.* Kidney international reports, 2021. **6**(3): p. 817.

قياس نسبة طول الطحال إلى طول الكلية اليسرى عند البالغين السعوديين الأصحاء والإرتباط بمعايير الجسم عن طريق تصوير الموجات فوق الصوتية

ميعاد البشير[١]

١قسم تقنية الأشعة التشخيصية، كلية العلوم الطبية التطبيقية، جامعة جازان، المملكة العربية السعودية

الملخص

تبحث هذه الورقة البحثية في العلاقة بين العمر والطول والوزن ومؤشر كتلة الجسم وقياسات الطحال والكلية اليسرى وكذلك نسبة الطحال إلى الكلية اليسرى قامت الدراسة بقياس طول الطحال، وطول الكلية اليسرى، ونسبة الطحال إلى الكلية اليسرى في ٩٥ مشاركًا، وحللت البيانات باستخدام تحليل واختبارات الارتباط.

اشتملت الدراسة على ٥٩ من الذكور و٣٦ من الإناث بمتوسط عمر ٢٣,٨١ ± ٦,٣ سنة (تراوحت أعمارهم بين ١٩-٤٥). تراوح مؤشر كتلة الجسم للمشاركين من ١٤,٢٤ إلى ٤٠,٢٥، بمتوسط ٢٣,٢٠ ± ٦,٨٧

بالنسبة الى طول الكلية اليسرى، كان المتوسط أعلى للمشاركين الذكور (١٠,٣٤) مقارنة بالمشاركة الإناث (٩,٧٢)

بالنسبة لطول الطحال، كان المتوسط أعلى للمشاركين الذكور (٩,٨٠) مقارنة بالمشاركة الإناث (٨,٧٤).

بالنسبة لـنسبة طول الطحال الى الكلية اليسرى، كان المتوسط أعلى قليلاً للمشاركات الإناث (١,١٢) مقارنة بالمشاركين الذكور (١,٠٧). ومع ذلك، لم تكن الفروق ذات دلالة إحصائية.

تشير النتائج إلى أن مؤشر كتلة الجسم قد يكون له تأثير على قياسات الطحال والكلى اليسرى، بينما لا يبدو أن العمر عامل مهم. وجدت الدراسة علاقة ارتباط موجبة معنوية بين طول الطحال وطول الكلية اليسرى،

بينما ترتبط نسبة طول الطحال الي الكلية اليسرى سلبًا مع كل من طول الطحال وطول الكلى اليسرى.

تقدم هذه الدراسة رؤى قيمة حول العلاقة بين قياسات الطحال والكلى اليسرى وآثارها على الممارسة السريرية.

الكلمات المفتاحية: الموجات فوق الصوتية، الطحال، الكلى، نسبة طول الطحال إلى الكلى اليسرى.

Solution of fractional type ODEs by using Method of Moments

Mehreen Shehzadi Khan

Department of Mathematics, Faculty of Sciences, Jazan University, K.S.A

Abstract

This study uses the Method of Moment (MoM), a subtype of the Method of Weighted Residual (MWR), to solve linear and nonlinear Reimann-Liouville (R-L) type fractional ODEs. The concept of using this method to fractional differential equations is completely new, and it is anticipated that the research community will be providing close attention to it. Differential equations with fractional order derivatives are subject to the Davison-Essex (D-E) definition. In order to satisfy the differential and side requirements, a trial solution for a fractional-ordered differential equation is built. The accuracy of the solution is determined by the square residual error graphs, which showed that the results were in agreement with the exact solution.

Keywords: Method of moment (MoM), Method of weighted residual (MWR), Galerkin method (GM), Least square method (LSM).

Introduction

Method of weighted residual (MWR) [7] works directly on differential equation and boundary conditions by minimize their corresponding weighted residuals, this method can be considered as a general method in which the unknown solution is expressed in the form of a trail solution [6]. Trial solution is constructed in such a way that it satisfies the essential side conditions (initial or boundary). Trial solution is expressed as a linear combination of suitable basis functions by using these basic functions, 10-20% accuracy can be achieved. We need to take help from mathematical software such as MAPLE, MATHEMATICA, or MATLAB [10]. MWR is tested on a variety of linear and nonlinear differential equations including singular equations such as Lane Emden and Emden Fowler type differential equations, partial differential equations of certain types, and fractional ordinary differential equations [7]. The Tabulated and graphical results show the effectiveness of the applied methods and trial solutions.

Method of Moment (MoM) is a subtype of the method of weighted residual (MWR) and was first developed by Yamada [1]and applied this method to solve problems related to the laminar boundary layer later on Fujita [2] used this method to estimate the nonlinear transient diffusion.

1. Method of Moment [4]

1.1 Description of the method

Method of moment is a subtype of MWR which is used for simulation of differential equations, its subtypes are Least square method (LSM) [8], Galerkin method (GM) and method of moment (MoM) all these methods varies on choice of weight functions.

In MoM weight functions are chosen in form of monomials such as $1, x, x^2 \dots x^n$, and formulated as follows:

$$W_i = V_i = {x_i}^{i-1} \ , i = 1,2 \dots . n. \tag{1}$$

Hence, we can have expressed as follows:

$$\int_{\Omega} {x_i}^{i-1} R_s d\Omega + \int_{\Gamma} {x_i}^{i-1} R_b d\Gamma = 0 \ , \quad i = 1 \dots n \, . \tag{2}$$

By integrating Eq. (2) gives system of n algebraic equations solving these equations gives values of unknowns.

1.2 Working of the method [2]

In order to illustrate the method, consider the differential equation along with I. Cs we have.

$$F(u) + b = 0 \quad \text{in} \quad \Omega. \tag{3}$$

Along with I. Cs

$$G(u) = g \quad \text{on} \ \Gamma. \tag{4}$$

In MoM the weight functions are chosen in the form of polynomials that can be expressed as $W_i = V_i = {x_i}^{i-1}$, $i = 1,2 \dots n$.

Using trial solution of the form

$$u^h(x) = \sum_i^n c[i]B[i](x). \tag{5}$$

where $c[i]$ are the unknowns and $B[i]$ are the polynomial type basis functions, Basis functions are chosen so that to satisfies the initial condition (4). Using Eq. (5) in Eq. (3) we get the residuals R_s and R_g such as:

$$R_s = F(u^h) + b \neq 0, \tag{6}$$

$$R_b = G(u^h) - g \neq 0, \tag{7}$$

therefore, by integrating over domainΩ and boundary Γ we have,

$$\int_\Omega {x_i}^{i-1} R_s d\Omega + \int_\Gamma {x_i}^{i-1} R_b d\Gamma = 0 \ , \quad i = 1 \dots n. \tag{8}$$

By integrating and differentiating resulting equation w.r.t constants we got system of algebraic equations. Solving these equations gives the unknown constants which we use in trial solution Eq. (5) to obtain approximate solution to differential Eq. (3)

2. Numerical Applications

Kansa Collocation Method (KCM) [5],[9] is used to solve ODEs of 3rd and 4th order by using RBFs but for higher ordered ODEs numerical results are diverged from their exact solutions in order to overcome this problem, Method of weighted residual (MWR) is tested on same type of differential equations as well as variety of Linear and nonlinear Lane Emden type differential equations, the methods work on such type of equations and produced numerical results that are much closer to the exact solution

2.1 Non-homogenous Fractional ODEs [3]

MWR used for the numerical solution of fractional type *Ricatti* differential equations using trial solutions in form of polynomial that satisfies the boundary conditions. To demonstrate the strength of the proposed method numerical comparison, graphical comparison and error analysis have been performed for the test problems.

2.2 Reimann-Liouville (R-L) fractional derivative operator

The Reimann-Liouville fractional derivative operator can be defined as

$$D^{\alpha}g(x) = \frac{1}{\Gamma(\eta-\alpha)}\frac{d^n}{dx^n}\int_0^x \frac{g(\beta)}{(x-\beta)^{\alpha+1-\eta}}d\beta \ , \quad \eta-1<\alpha<\eta,$$

where $\alpha > 0, x > a$ where $\alpha, a, x \in R$.

2.2.1 Example1[4]

Consider the non-homogenous fractional ODE as given below.

$$D^{0.5}U(t)+U(t) = t^2 + \frac{\Gamma(3)}{\Gamma(2.5)}t^{1.5} \ \ ; t > 0 \ . \tag{9}$$

Subject to I.C:

$$U(0) = 0. \tag{10}$$

Trial solution of the form

$$u^h(x) = 1 + x\sum_i^n c[i]B[i] \ . \tag{11}$$

Exact solution of Eq.(9) is $U(t) = t^2$. Trial solution Eq.(10) satisfies the initial condition Eq.(10) so we have residue only corresponding to Eq.(9). Numerical solution obtained by MoM is given as

$$\tilde{u}(x) = -0.15802002528047178e - 4 * x^{1}0 + 0.6103703820822552e \quad (12)$$
$$-4 * x^{9} - 0.8291700959912715e - 4 * x^{8} + 0.28826487915610344e$$
$$+0.4189445471806336e - 4 * x^{6} - 0.54442874749967494e$$
$$-4 * x^{5} + 0.2765120607469395e - 4 * x^{4}$$
$$-0.70830504453610585e$$
$$-5 * x^{3} + 1.0000008755880325 * x^{2}$$
$$-3.99514492474572 * (-8) * x.$$

Comparison with exact solution and error graph are shown in Figure 1 and Figure 2 respectively. Table 1 shows the comparison with exact values using finite values of domain.

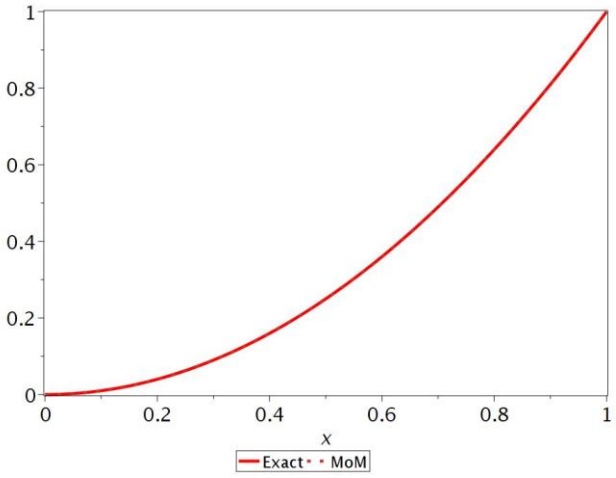

Figure 1 (Comparison along exact solution for $\alpha = 0.5$)

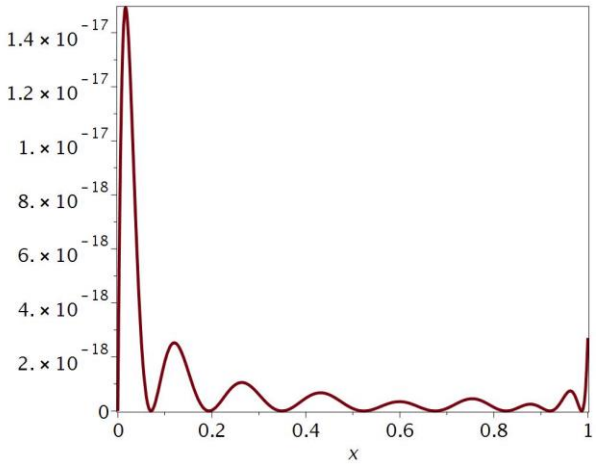

Figure 2 (Residual Error)

Table 1: Numerical results using $n = 10$.

Domain(x)	**Exact**	**MoM**	**Error**
0	0	0	0
0.1	0.010000002	0.00999994238	$5.96*10^{-8}$
0.2	0.040000004	0.040000000056	$3.44*10^{-10}$
0.3	0.090000006	0.08999999976701	$2.32982133585580*10^{-10}$
0.4	0.160000008	0.1600000000061	$6.16126594188415*10^{-12}$
0.5	0.25000001	0.250000000095067	$9.50667877752664*10^{-11}$
0.6	0.360000012	0.359999999881833	$1.18166643137130*10^{-11}$
0.7	0.490000014	0.489999999948969	$5.10311792822904*10^{-11}$
0.8	0.640000016	0.640000000078469	$7.84688980459691*10^{-11}$
0.9	0.810000018	0.809999999887954	$1.12046261158127*10^{-10}$
1	1.00000002	0.999999999886177	$1.13822729019830*10^{-10}$

2.2.2 Example 2

Consider again non-homogenous fractional order ODE given below.

$$D^{\alpha}U(t) = -U(t) + \frac{2}{\Gamma(3-\alpha)}t^{2-\alpha} - \frac{1}{\Gamma(2-\alpha)}t^{1-\alpha} + t^2 - t \quad ; t > 0; 0 \leq \alpha \leq 1.. \tag{13}$$

Subject to ICs

$$U(0) = 0. \tag{14}$$

Exact solution of Eq. (13) is$U(t) = t^2 - t$.Trial solution Eq.(11) satisfies the initial condition Eq(14) so we have residue corresponding to Eq(13).Numerical solution obtained by MoM is given as

$$\widetilde{U}(x, y) = 1.0000000017325608 * x^2 - 1.0000000013736674 * x. \tag{15}$$

Comparison with exact solution and error graph are shown in Figure 3 and Figure 4 respectively Table 2 shows the comparison with exact values using finite values of domain.

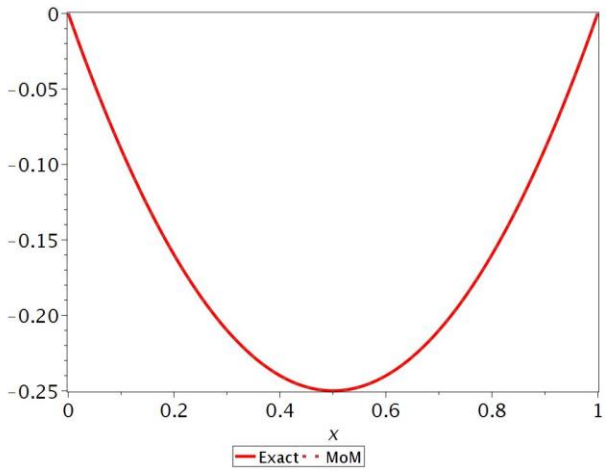

Figure 3 (Comparison along exact solution for $\alpha = 0.5$ using Maple 2020):

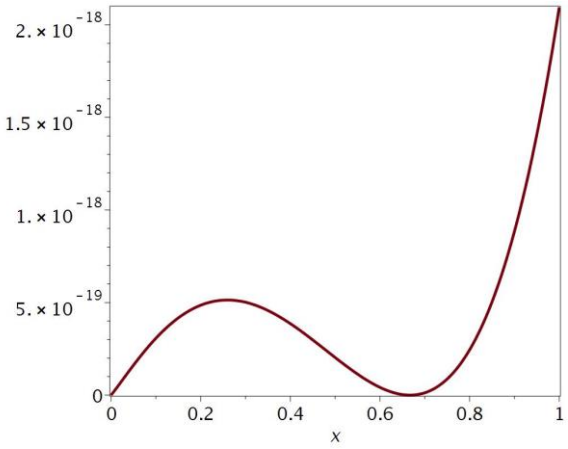

Figure 4 (Residual Error):

Table 2 Numerical results using $n = 10$.

Domain(x)	**Exact**	**MoM**	**Error**
0	-9.999999909	0	0
0.1	-0.090000008	-0.09000000012004111	$1.20041143691907*10^{-10}$
0.2	-0.160000006	-0.160000000205431	$2.05431061051087*10^{-10}$
0.3	-0.210000004	-0.210000000256170	$2.56169779833115*10^{-10}$
0.4	-0.240000002	-0.240000000272257	$2.72257272282417*10^{-10}$
0.5	-0.25	-0.250000000253694	$2.53693510643416*10^{-10}$
0.6	-0.239999998	-0.240000000200479	$2.00478633693990*10^{-10}$
0.7	-0.209999996	-0.210000000112612	$1.12612336122808*10^{-10}$
0.8	-0.159999994	-0.159999999990095	$9.90493798092018*10^{-12}$
0.9	-0.089999992	-0.8999999983292641	$1.67073604950829*10^{-10}$

2.3 Non-Linear fractional Riccati differential equation [3]

2.3.1 Example 1

Nonlinear Riccati factional differential equation is given by.

$$\frac{d^{\alpha}y(t)}{dt^{\alpha}} + y^2(t) - 1 = 0 \qquad ;0 < \alpha \leq 1. \tag{16}$$

Subject to IC:

$$y(0) = 0. \tag{17}$$

Exact solution for $\alpha = 1$ is $y(t) = \frac{e^{2t}-1}{e^{2t}+1}$. Numerical solution obtained by MoM is given as

$$\begin{aligned}\tilde{y}(t) = {} & 7885554558207064 * x^{1}0 - 11.634767182575608 * x^{9} \\ & +26.99268970701631 * x^{8} - 3.164386469903953 * x^{7} \\ & -59.71658871316277 * x^{6} + 88.58602617188026 * x^{5} \\ & -59.272618235117484 * x^{4} + 21.064031060975562 * x^{3} \\ & -4.483013574395406 * x^{2} + 1.5946413045776626 * x.\end{aligned} \tag{18}$$

Comparison with exact solution and error graph are shown in Figure 5 and Figure 6 respectively Table 3 shows the comparison with exact values using finite values of domain.

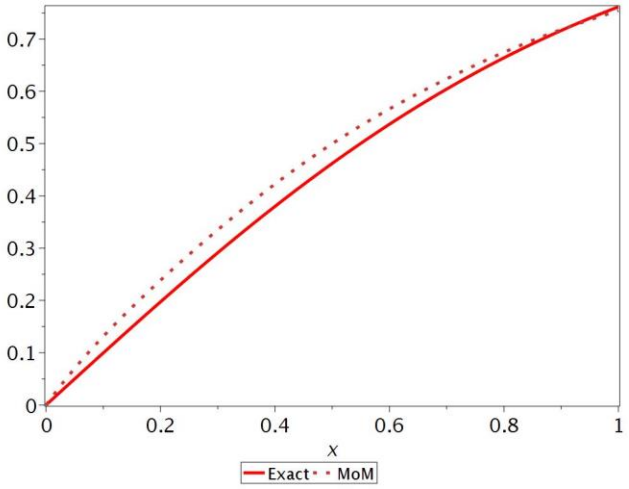

Figure 5 (Comparison along exact solution for $\alpha = 0.5$ using Maple 2020):

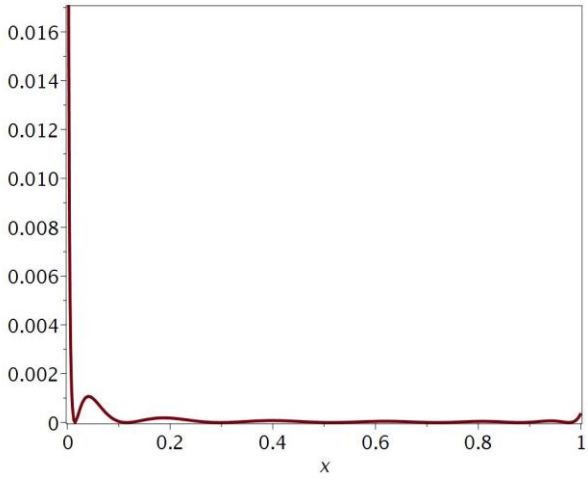

Figure 6 (Residual Error):

Table 3 Numerical results using $n = 3$

Domain (x)	**Exact**	**MoM**	**Error**
0	0	0	0
0.6	0.5370495741	0.566260522200144	$0.02921095520436 * 10^{-1}$
0.7	0.6043677835	0.623842215569434	$0.0194744384694341 * 10^{-1}$
0.8	0.6640367758	0.674637755023367	$0.0106009848233674 * 10^{-1}$
0.9	0.7162978751	0.718067090085140	$0.00176921988513978 * 10^{-1}$
1	0.7615941602	0.754641181460621	$0.00695297453937915 * 10^{-1}$

2.2.2 Example 2

Consider another nonlinear fractional Riccati differential equation.

$$\frac{d^{\alpha}y(t)}{dt^{\alpha}} + y^2(t) - 2y(t) - 1 = 0 \quad ; 0 < \alpha \leq 1. \tag{19}$$

Subject to IC:

$$y(0) = 0. \tag{20}$$

Exact solution for $\alpha = 1$ is $y(t) = 1 + \sqrt{2}\tanh(\sqrt{2}t + \frac{1}{2}\log(\frac{\sqrt{2}-1}{\sqrt{2}+1}))$ .Numerical solution obtained by MoM is given as

$$\tilde{y}(t) = 1.740105975396494 * x^5 - 4.477469274947721 * x^4 \tag{21}$$
$$+2.94041189012669 * x^3 + 0.8245510783112579e - 1 * x^2$$
$$+1.47993891782777 * x.$$

Comparison with exact solution and error graph are shown in Figure 7 and Figure 8 respectively Table 4 shows the comparison with exact values using finite values of domain.

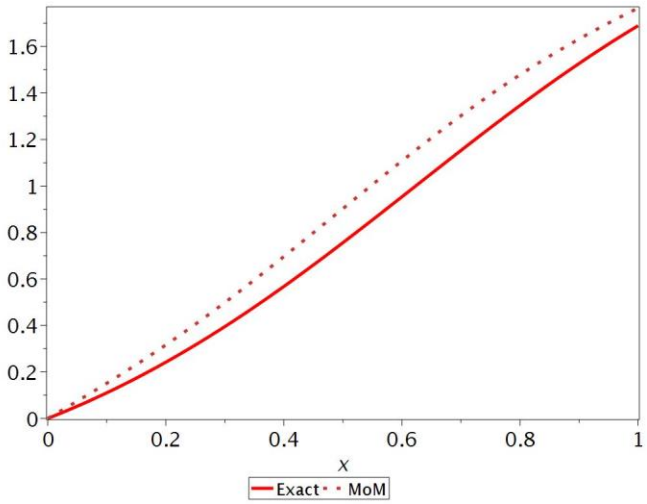

Figure 7 (Comparison along exact solution for $\alpha = 0.5$):

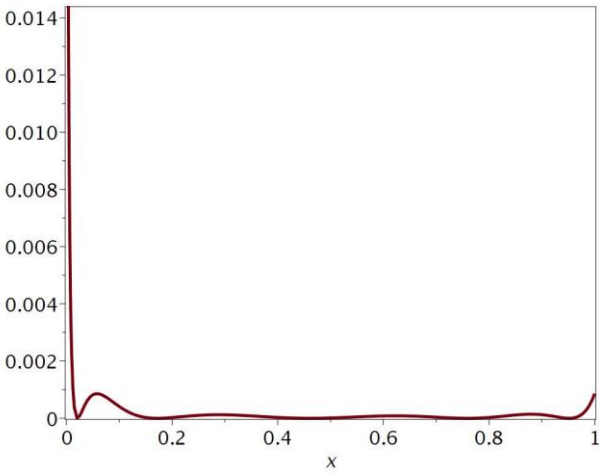

Figure 8 (Residual Error):

Table 4 Numerical results using $n = 2$

Domain(x)	**Exact**	**MoM**	**Error**
0	9.909	0	0
0.1	0.1102952088	0.151328508883474	0.04103331218347411
0.2	0.2419768135	0.316202166072023	0.07422536687202311
0.3	0.3951048644	0.498754712479690	0.103649864379690
0.4	0.5678121837	0.696550217101595	0.128738051501595
0.5	0.7560144119	0.902671204184410	0.146656811684410
0.6	0.9535662354	1.10780678039684	0.154240564896839
0.7	1.152948986	1.30234076200009	0.149391796000086
0.8	1.346363673	1.47843980201834	0.132076147018339
0.9	1.526911329	1.63214151740924	0.105230205409238
1	1.689498406	1.76544261623436	0.759442262343588

3 Finding and discussions:

The method of weighted residual (MWR) again works on construction of a trail solution involving adjustable parameters. Those parameters can be found in a way by minimizing the weighted residual error of the problem.

We have also extended the idea of MWR to fraction (R-L) type differential equations (16), (19), and numerical results are compared with the exact solution by varying the value of fractional constant. It has been observed that MWR gives numerical approximations to the differential equation much closer to the exact solution.

4. Conclusion:

In this paper fractional ordered ODEs are solved out numerically by applying method of moment MoM which is a subtype of MWR. Trial solution is constructed in form of linear combination of unknowns $c_i's$ and polynomial type basis functions. Numerical results are compared with the exact solution by varying the value of fractional constant α. It has been observed that MoM works efficiently on fractional ordered differential equation, obtained numerical results are much closer to exact solution of the differential equation.

References

[1] B. A. Finlayson and L. E. Scriven, “The Method of Weighted Residuals—A Review,” Applied Mechanics Review, vol. 19, no. 9, pp. 735–748, 1966

[2] S. N. Atluri and S. Shen, “The Basis of Meshless Domain Discretization: The Meshless Local Petrov Galerkin (MLPG) Method,” 2003.

[3]. N. A. Khan, A. Ara, and M. Jamil, “An efficient approach for solving the Riccati equation with fractional orders,” *Comput. Math. with Appl.*, vol. 61, no. 9, pp. 2683–2689, 2011.

[4] M. Krawchuk, “Applications of the Method of Moments to the Solution of Linear Differential and Integral Equations

[5] G. R. Liu and W. . GU, An Introduction to Meshfree Method and Their Programming. 2005

[6] N. Ahmed, S. T. Mohyud-Din, and S. M. Hassan, “Flow and heat transfer of nanofluid in an asymmetric channel with expanding and contracting walls suspended by carbon nanotubes: A numerical investigation,” *Aerosp. Sci. Technol.*, vol. 48, pp. 53–60, Jan. 2016.

[7] B. A. Finlayson, *The Method of Weighted Residuals and Variational Principles*. 2013.

[8] H. W. Sorenson, “Least-squares estimation: from Gauss to Kalman,” *IEEE Spectr.*, vol. 7, no. 7, pp. 63–68, 1970.

[9] E. J. Kansa, “Multiquadrics---a scattered data approximation scheme with applications to computational fluid dynamics. 1,” *Comput. Math. with Appl.*, vol. 19, no. 8, pp. 127–145, 1990.

[10] G. Fasshauer, “MATH 590: Meshfree Methods - Chapter 2: Radial Basis Function Interpolation in Matlab,” 2010.

حل المعادلات التفاضلية الجزئية من النوع الكسري باستخدام طريقة اللحظات

مهرين شهزادي خان
قسم الرياضيات، كلية العلوم، جامعة جازان، المملكة العربية السعودية

الملخص

تستخدم هذه الدراسة طريقة العزم (MoM) ، وهي نوع فرعي من طريقة الوزن المتبقي (MWR) ، لحل المعادلات التفاضلية الجزئية من النوع الخطي وغير الخطي (R-L). إن مفهوم استخدام هذه الطريقة في المعادلات التفاضلية الكسرية جديد تمامًا ، ومن المتوقع أن يهتم به الباحثون في هذا المجال .بحيث تخضع رتبة المعادلات التفاضلية الكسرية و مشتقاتها لتعريف Davison-Essex (D-E). ولقد تم التحقق من نجاح هذي الطريقة بعد الحصول على حل دقيق لهذا النوع من المعادلات الكسرية و تم تحديد دقة الحل من خلال الرسوم البيانية للخطأ التربيعي المتبقي ، و أظهرت أن النتائج كانت متوافقة مع الحل الدقيق.

الكلمات المفتاحية: طريقة العزم (MoM) ، طريقة الوزن المتبقي (MWR).

Awareness of Sickle cell anemia complications and prevention among Jazan population-Saudi Arabia

Tagwa Yousif Elsayed Yousif [1]

[1] Department of Medical Laboratory Technology, Faculty of Applied Medical Sciences, Jazan University, Gizan, 45142, Saudi Arabia

Correspondence: Tagwa Yousif Elsayed Yousif, Department of Medical Laboratory

ABSTRACT

Introduction: Sickle cell anemia is an autosomal recessive illness that is caused by the formation of abnormal hemoglobin S. Sickle cell disease has several complications such as vaso-occlusive crisis, stroke, acute chest syndrome, and gallstones. This study aimed at assessing the awareness of the Jazan community about the general knowledge and the complications of Sickle Cell Disease and to detect community awareness about triggers and prevention of Sickle Cell Disease.

Materials and Method: A cross-sectional study was conducted in 2022 among adult Saudi individuals who live in the Jazan region to assess the awareness of the community about the general knowledge and the complications of Sickle cell disease and to detect community awareness about triggers and prevention. The study was conducted using an online multiple-choice questionnaire in Arabic after obtaining consent from the participants and data was collected through questionnaires. The level of awareness was then correlated to demographic information.

Results: The study data included responses from a sample of 450 participants who have all heard of sickle cell anemia. The female who responded to the questionnaire were slightly more (n=230, 51.1%) than their male counterparts (n=220, 48.9%). Most of the respondents (n=291, 64.7%) think that having a parent affected with sickle cell anemia is a risk factor for developing the disease while n=159(35.5%) of them think that consanguine marriage is a risk factor for developing sickle cell disease. The results reveal that most of the respondents n=179(39.8%) heard about sickle cell anemia through the media channels. This is followed by those who heard about the disease through premarital check-ups or counseling (n=88,19.6%) and undergraduate studies (n=70,15.6%. n=17,3.8% of the respondents knew

or heard about sickle cell anemia after being diagnosed with the disease whereas only n=2,0.4% of them heard about sickle cell disease through health education.

Conclusion: The results of the studies indicate the need for raising knowledge regarding the disease and detecting community awareness about triggers and prevention of Sickle cell anemia. Health education campaigns would be an effective tool for increasing awareness about sickle cell disease.

Keywords: Awareness, complications, Jazan, Saudi Arabia, sickle cell disease.

Introduction

One of the hereditary conditions that affect hemoglobin and are passed down in a recessive manner is sickle cell disease[1,2]. This variant of hemoglobin is created when glutamic acid, rather than valine, is substituted in position number six of the -chain. There are multiple distinct forms of sickle cell disorders, each of which is characterized by a distinct combination of the following symptoms and characteristics. This is the most prevalent and severe type of sickle cell disease, and it's referred to as sickle cell anemia (HbSS). People who suffer from sickle cell anemia inherit two copies of the sickle cell anemia-causing hemoglobin S gene, one from each of their parents. Because the majority of their red blood cells are sickle-shaped, they suffer from chronic anemia, an increased risk of infection, and periods of excruciating agony known as vaso-occlusive crises. This kind of sickle cell illness is called sickle beta-thalassemia, and it is caused by a person inheriting one defective gene for hemoglobin S as well as one bad gene for beta-thalassemia[3,4]. A condition known as beta-thalassemia is characterized by an impairment in the formation of beta-globin chains, which are an essential component of hemoglobin. The presence of sickle hemoglobin in conjunction with a decreased synthesis of beta-globin leads to a variety of clinical manifestations, including symptoms that are associated with sickle cell disease as well as beta-thalassemia. Individuals affected with sickle hemoglobin C disease inherit one gene for sickle hemoglobin and one gene for hemoglobin C. Sickle hemoglobin C disease is a kind of sickle cell anemia. Hemoglobin C is a subtype of hemoglobin that, when combined with sickle hemoglobin, may cause a condition that is less severe than sickle cell anemia. This condition is referred to as sickle cell trait. Some patients have symptoms such as minor anemia, occasional pain crises, and organ damage that is not as severe. This is a rare form of sickle cell disease

that is produced by the combination of sickle hemoglobin with mutations that damage both the delta- and beta-globin chains[5,6]. Sickle Delta-Beta Thalassemia is the medical term for this condition. The degree of severity of the symptoms might change based on the particular mutations that are at play. This substitution causes deoxygenating-induced polymerization, which in turn causes red blood cells to take on an aberrant crescent shape[4,7]. The aberrant RBCs cause vaso-occlusive crises, ischemia, and tissue damage by blocking off the small blood capillaries in the body. The presence of Sickled hemoglobin renders red blood cells more susceptible to breaking, which can lead to both extravascular and intravascular hemolytic, which in turn leads to a decrease in hemoglobin level. To effectively treat the consequences of sickle cell disease, these complications must first be averted. This can be done by strictly sticking to the hydroxyurea and blood transfusion regimens [4]. Patients with SCD have a lower quality of life and a shorter life expectancy as a result of the disease, which also has a detrimental impact on the patient's overall quality of life[8,10,11]. It results in repeated trips to the hospital, which drives up the associated costs. Because of the high rate of consanguineous marriages in Saudi Arabia, especially in the Jazan region, which affects between 60 and 90 percent of the population, sickle cell disease is quite common there[5,9]

Sickle cell illness is prevalent in 1.4% of the Jazan region of Saudi Arabia, with the sickle cell trait ranging from 2% to 27% of the population[8]. According to the findings of a study that was carried out in Jazan, Saudi Arabia, the vast majority of recipients had consanguineous marriages [5]. This high proportion of consanguinity helps to explain the large number of patients who are affected by sickle cell disease. Because sickle cell disease is so prevalent in the Jazan region, the general populace must have a comprehensive understanding of the condition and its associated problems. The majority of persons who attended premarital counseling sessions about sick cell disease were not very aware of the problems that are associated with the disease [12,13].

There is a relatively limited amount of information available concerning the level of sickle cell disease awareness in the Jazan region. The purpose of this study is to determine the amount of community awareness regarding the consequences of sickle cell disease, as well as the level of community awareness regarding the causes and ways to prevent the disease.

Methods:

Study design

This particular cross-sectional study was carried out in Jazan, Saudi Arabia in 2022. The Scientific Research Ethics Committee of Jazan University approved this research. The study data included responses from a sample of 450 participants who have all ever heard of sickle cell anemia. Written informed consent was obtained from the participants (Appendix -Questionnaire). A section on the first page of the Google form contains a question that inquires as to whether or not the subject is interested in taking part in the research. The form will end by itself automatically if the responder decides to offer a negative answer. People who were originally from Saudi Arabia and were now living in Jazan Saudi Arabia met the requirements to participate in the research.

STUDY POPULATION

To carry out the research with a confidence level of 95%, an acceptable error margin of 5%, and a design effect factor of 2, need a sample minimum of 385 persons to participate in the study. To achieve more accuracy in the results, conducted the study with 45% more people than we had originally planned. used the tool that can be found at http://www.raosoft.com/samplesize.html to determine the appropriate sample size. The sample size was determined with a 50% ± 5% level of awareness about the general complications of sickle cell disease and detection of community awareness about triggers and prevention. The adult Saudi population that resided in the Jazan of Saudi Arabia made up the sample frame for this study.

STUDY PROCEDURE

For this study, a validated online questionnaire was used to collect data. This step was carried out after gathering the people's written informed consent on the research and its purpose. This survey was conducted online rather than using paper questionnaires since the vast majority of individuals in Saudi Arabia have access to the Internet. This has resulted in a more accurate reflection of the population's opinions. The questionnaire was constructed with a Google form and disseminated using Twitter, e-mail, and WhatsApp. The study's author addressed the participants in public settings such as shopping malls and universities. They were informed about the purpose and significance of this research, assured confidentiality regarding their identity, and then the questionnaires were sent to them; however, participation in the study was voluntary on their part, so the

questionnaires were only sent to those who volunteered for it.

Data Analysis

The (SPSS) version 27 was used to analyze the data. The results of an independent t-test were analyzed to see whether or not there was a difference that could be considered statistically significant between the two groups. The mean and standard deviation of continuous variables were calculated as a result of this investigation. The descriptive data were presented as frequencies and percentages. To calculate the median score of knowledge, one was given for each correct answer and zero for wrong answers, then the total score was calculated for every participant. Any score that was above the median value was considered good knowledge while a score below was considered poor knowledge. The collected data was expressed in the form of frequency tables, pie charts, chi-square, and ANOVA which were used to determine the significance between two variables or more (P. value <0.05).

Results

1. Demographic Profile of Respondents

Table 1. Demographical data.

		N = 450	*N %*
Age	18-29	135	30.0
	30-39	166	36.9
	40-49	110	24.4
	50-59	29	6.4
	>60	10	2.2
Gender	Male	220	48.9
	Female	230	51.1
Marital Status	Married	330	73.3
	Unmarried	118	26.2
	Divorced	2	0.5
Level of Education	Diploma	54	12.0
	Undergraduate	103	22.9
	Bachelor	215	47.8
	Master	67	14.9
	Doctorate	11	2.4
Occupation	Accounting	9	2.0
	Computer programmer	9	2.0
	Governmental	110	24.4
	Housewife	1	0.2
	Mechanical engineering	1	0.2
	Medical	68	15.1
	Military	10	2.2
	Private sector	76	16.9
	Retired	2	0.4
	Student	100	22.2
	Teacher	3	0.7
	Without work	61	13.6
Place of Residence	City	271	60.2
	Village	179	39.8

Table.1 shows that most of the respondents [166 (36.9%)] were aged between 30-39 years. 135 (30%) were aged between 20-29 years, 110 (24.4%) between 40-49

years, 29 (6.4%) between 50-59 years, and 10 (2.2%) were aged above 60 years.

The female who responded to the questionnaire were slightly more [230 (51.1%)] than their male counterparts [220 (48.9%)]. Regarding marital status, 330 (73.3%) of the respondents were married. Of those who were single, 26.2% (118) of them, while 2 (0.5%) of them had divorced. In terms of the level of education, most of the respondents had attained a Bachelor's degree [215 (47.9%)], followed by those who were in their undergraduate studies [103 (22.9%)]. 67 (14.9%) had attained a Master's level. 54 (12%) had earned a diploma, while 11 (2.4%) had gone on to achieve a doctorate. The occupation profile of respondents shows that 110 (24.4%) of the respondents worked in state (governmental) jobs, followed by those who were students [100 (22.2%)]. 76 (16.9%) worked in the private sector, 68 (15.1%) in the field of medicine, and 61 (13.6%) were without work. We had more city residents [271 (60.2%)] than villagers [179 (39.8%)] who responded to the questionnaire.

According to the data presented in the table above, most respondents [337, or 74.9 percent] believe that sickle cell anemia is a genetic blood disorder. On the other hand, 113 respondents (35.1% of the total) believe that sickle cell anemia is a disease that causes hemolysis, also known as the destruction of red blood cells (Table.1).

1. Awareness about SCD

Table 2. Awareness about Sickle Cell Anaemia.

		Count	Count %
True about sickle Cell Anemia	A disease that leads to hemolysis or breakdown of red blood cells	113	25.1
	Hereditary blood disease	337	74.9
Risk Factors for Developing Sickle Cell Anemia	Affected mother or father with sickle cell anemia	291	64.7
	Consanguine marriage	159	35.3
How have you heard about Sickle Cell Anemia	Affected family member	43	9.6
	Diagnosed with sickle cell anemia	17	3.8
	Health education in the city or neighborhood	2	0.4
	Media (TV, mobile and media, videos, and community service)	179	39.8
	Premarital check-ups or counseling	88	19.6
	School	51	11.3
	Undergraduate studies	70	15.6

Table.2 shows how the participants responded to what they knew to be true about the disease, the risk factors of developing SCD, and how they got information about sickle cell anemia.

Most respondents believe that having a parent who is affected with sickle cell anemia is a risk factor for developing the disease. On the other hand, most respondents believe that consanguine marriage is a risk factor for developing sickle cell disease (SCD). The results of how the respondents heard about the condition reveal that most of the respondents [179 (39.8%)] heard about sickle cell anemia through the media channels. This is followed by those who heard about the disease through premarital check-ups or counselling [88 (19.6%)] and undergraduate studies [70 (15.6%)]. 17 (3.8%) of the respondents knew or heard about sickle cell anemia after being diagnosed with the disease, whereas only 2 (0.4%) heard about SCD through health education (Table.2).

Table 3. Gender and Truth about Sickle Cell Anaemia.

		Gender			
		Male		Female	
		Count	Count %	Count	Count %
True about sickle cell anemia	The disease leads to hemolysis or the breakdown of red blood cells	56	12.4	57	12.7
	Hereditary blood disease	164	36.4	173	38.4

The views on the truth about sickle cell anemia across gender. The column proportions do not differ significantly for each of the pictures (Table.3).

Table 4. Association Between Gender and Truth about SCD.

Chi-Square Tests					
	Value	**df**	**Asymp. Sig. (2-sided)**	**Exact Sig. (2-sided)**	**Exact Sig. (1-sided)**
Pearson Chi-Square	.027[a]	1	.869		
Continuity Correction[s]	.003	1	.956		
Likelihood Ratio	.027	1	.869		
Fisher's Exact Test				.914	.478
Linear-by-Linear Association	.027	1	.870		
N of Valid Cases	450				

a. 0 cells (0.0%) have an expected count of less than 5. The minimum expected count is 55.24.

b. Computed only for a 2x2 table

The findings show that the p-value (0.869) is more significant than 0.05. fail to reject the null hypothesis that the association between gender and truth about SCD is substantial. It is, therefore, not evident that gender affects the truth about sickle cell anemia (Table.4).

Table 5. Age and Truth about SCD.

		Age									
		18-29		30-39		40-49		50-59		>60	
		Count	N %	Count	N %	Count	N %	Count	N %	Count	N %
True about sickle cell anemia	The disease leads to hemolysis or the breakdown of red blood cells	31	6.9	45	10.0	26	5.8	8	1.8	3	0.7
	Hereditary blood disease	104	23.1	121	26.9	84	18.7	21	4.7	7	1.6

The table shows the responses on the truth about SCD from the different age groups of the participants. The findings revealed that most (10%) of the respondents who think sickle cell anemia is a disease that leads to hemolysis or breakdown of red blood cells are between 30 and 39 years old. Similarly, most (26.9%) of those who know that SCD is a hereditary blood disease are from the same age group (Table.5).

Table 6. Education Level and Truth about SCD.

		Level of Education									
		Diploma		Undergraduate		Bachelor		Master		Doctorate	
		Count	*N %*	*Count*	*N %*	*Count*	*N %*	*Count*	*N %*	*Count*	*N %*
This is true about sickle cell anemia	A disease that leads to hemolysis or breakdown of red blood cells	14	3.1	18	4.0	59	13.1	19	4.2	3	0.7%
	Hereditary blood disease	40	8.9	85	18.9	156	34.7	48	10.7	7	1.6%

The findings show that most of the individuals who know that sickle cell anemia is a disease that leads to hemolysis or breakdown of the red blood cells are at a bachelor's degree in level of education. This is a similar case for those who know that SCD is a hereditary blood disease (Table.6).

Table 7. Association Between Education Level and Truth about SCD.

Chi-Square Tests			
	Value	**df**	**Asymp. Sig. (2-sided)**
Pearson Chi-Square	4.329[a]	4	.363
Likelihood Ratio	4.570	4	.334
Linear-by-Linear Association	1.409	1	.235
N of Valid Cases	449		

a. one cell (10.0%) has an expected count of less than 5. The minimum expected count is 2.52.

The results above show that the p-value for this test of association (0.363) is insignificant. Therefore, it needs to be evident that an individual's education level affects their knowledge about sickle cell anemia(Table.7).

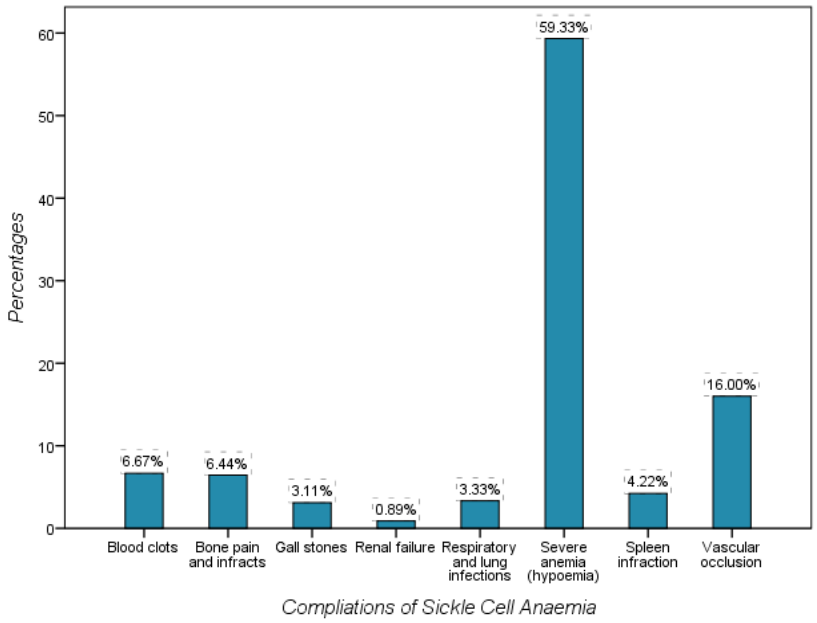

Figure 1. Awareness about SCD Complications.

Figure.1 clearly shows that most (59.3%) respondents know that severe anemia (hyperemia) is the most critical SCD complication and (Table .8) below gives further explanation of the

results.

Table 8. Awareness about SCD Complications.

		Count	Count %
Describing the seriousness of sickle cell anemia	A severe disease that may lead to death if it does not receive attention and care	362	80.4%
	I don't know	9	2.0%
	The ordinary disease that can easily cure\	79	17.6%
Most important complications	Blood clots	30	6.7%
	Bone pain and infracts	29	6.4%
	Gall stones	14	3.1%
	Renal failure	4	0.9%
	Respiratory and lung infections	15	3.3%
	Severe anemia (hyperemia)	267	59.3%
	Spleen infarction	19	4.2%
	Vascular occlusion	72	16.0%
Effects of complications	Affect the impact and performance in the school and university	216	48.0%
	The bad economic and financial impact on the family	68	15.1%
	Increased likelihood of premature death	36	8.0%
	Lack of daily activity	130	28.9%
Most important therapeutic methods	Attention to health and avoiding infection	56	12.4%
	Periodic review of the doctor	121	26.9%
	Proper nutrition	29	6.4%
	Regular blood transfusion in case of severe anemia	112	24.9%
	Take prescription drugs and vitamins regularly	132	29.3%

Regarding the severity of sickle cell anemia, the data shown in Table.8 indicate that 362 of the respondents, or 80.4% of the total, believe that SCD is a hazardous condition that might result in death if it is not treated well and promptly. The severity of sickle cell anemia is unknown to 9 people, whereas 79 (17.6%) believe that sickle cell anemia is a common condition that can be readily treated.

On the severity of complications, most of the respondents [267 (59.3%)] think that hypoxemia or severe anemia is the severest complication of the disease. This is followed by those who think that vascular occlusion is the most severe complication

[72 (16%)]. At the least, 14 (3.1%) and 4 (0.9%) think that the severe complications of the disease are gallstones and renal failure. On the effects of complications of the disease, 216 (48%) of the respondents think that it affects the impact and performance of patients in school and university. This is followed by 130 (28.9%) who think that the disease leads to a lack of daily activities. 68 (15.1%) think that SCD harms the financial and economic status of a family while 36 (8%) think that it leads to an increase in the probability of premature death.

The figure below visualizes the most important therapeutic method according to the respondents as shown in Table.8 above.

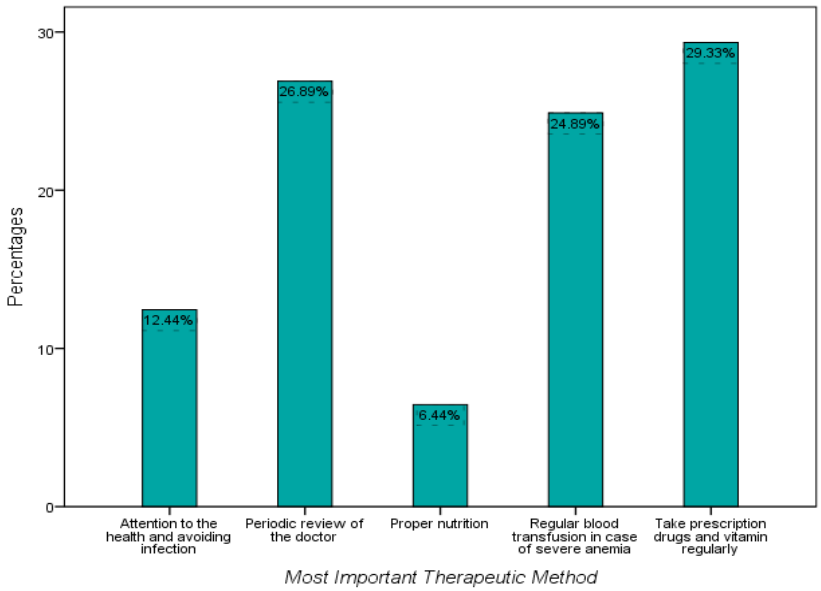

Figure 2. Most Important Therapeutic Method

Figure. 2 and Table.8 show that most [132 (29.3%)] of the respondents think that regularly taking prescription drugs and vitamin is the most important therapy for this disease. This is closely followed [at 131 (26.9%)] by those who think that patients should be periodically reviewed by the doctor. 112 (24.9%) think that patients with severe anemia should have regular blood transfusions. 56 (12.4%) and 29 (6.4%) of the respondents think that attention to health and proper nutrition, respectively, are the most important therapeutic methods.

Table.9 Ways of Preventing SCD.

		Count	Count %
Mostwaytoprevent SCD	Premarital analysis	366	81.3
	Reduce consanguineous marriage	84	18.7
The most important way to raise community awareness	Increase educational publications and videos	203	45.1
	Increasing health education campaigns in the community	195	43.3
	School health education campaigns	52	11.6

The findings show that 366 (81.3%) respondents think that the most important way to prevent sickle cell anemia is through premarital analysis. 84 (18.7%) of them think that SCD can be prevented by reducing consanguineous marriages.

On raising community awareness about the disease, most of the respondents [203 (45.1%)] think that this can be achieved through increasing educational publications and videos. 195 (43.3%) think that this should be achieved through increasing health education campaigns in the community while 52 (11.6%) of them think that this can be achieved through school health education campaigns (Table.9).

Table .10 Methods of future awareness and Age.

		Age									
		18-29		30-39		40-49		50-59		>60	
		Count	Count %	Count	Count %	Count	Count %	Count	Count %	Count	Count %
Raising community awareness	Increase educational publications and videos	64	14.2	72	16.0	55	12.2	9	2.0	3	0.7
	Increasing health education campaigns in the community	54	12.0	78	17.3	43	9.6	14	3.1	6	1.3
	School health education campaigns	17	3.8	16	3.6	12	2.7	6	1.3	1	0.2

The results show that the participants aged between 18-29 [64 (14.2%)] prefer educational publications and videos. Those aged between 30-39 [78 (17.3%)] prefer health education campaigns in the community. Those aged between 40-49 [55 (12.2%)] prefer educational publications and videos. Those aged 50-59 [14 (3.1%)] prefer health education campaigns in the community as well as those aged above 60 [6 (1.3%)] (Table.10).

Discussion

The autosomal recessive illness known as sickle cell disease has a significant impact on hemoglobin and is considered to be one of the most dangerous blood disorders [2,6,12]. Those who suffer from sickle cell disease often have a hemoglobin S variant, which causes the red blood cells to take on a crescent and sickle shape[14].

When there are fewer red blood cells than normal or not enough hemoglobin in the blood, the body cannot transport as much oxygen across the body. This condition is known as anemia. Anemia often manifests itself in several ways:

a) Persistent weariness, weakness, and loss of energy are common symptoms of anemia. They may tire easily from even little exercise and have trouble going about their regular lives.
b) Anemia is one of the causes of skin, lip, and nail bed pallor. This happens because there are fewer red blood cells, the cells whose hemoglobin gives blood its characteristic red hue.
c) Lack of oxygen in the blood may cause shortness of breath, which is particularly troublesome during exercise or other forms of physical activity. People with anemia may experience shortness of breath or fast breathing with seemingly little exertion.
d) Feelings of dizziness, lightheadedness, or fainting may occur when the brain does not get enough oxygen.
e) Increased Heart Rate: The body's response to a lack of oxygen in the blood is often to raise the heart rate by pumping blood more quickly.
f) Reduced blood flow to the extremities, such as chilly hands and feet, may be a symptom of anemia.
g) Anemia may cause headaches because the brain doesn't get enough oxygen[15,16].

Symptom relief, complication avoidance, and enhanced quality of life are the goals of therapeutic approaches to the management of sickle cell disease. Methods that are often used include:

a. Sickle cell disease is characterized by severe pain crises that need

careful management. Analgesic drugs, intravenous fluids, and other supporting measures are used in treatment to provide appropriate pain relief.

b. Therapy with hydroxyurea: This drug is used to reduce sickling of red blood cells by increasing synthesis of fetal hemoglobin. Some people with sickle cell disease have found that it lessens the frequency and intensity of pain crises and consequences.
c. In severe instances of sickle cell disease, the number of viable red blood cells may be increased and oxygen supply can be improved with regular blood transfusions. Iron overload issues may be avoided with cautious administration of this method.
d. Preventive interventions, such as prophylactic antibiotics and immunizations, are generally suggested to lessen the likelihood of infections, a major worry for people with sickle cell disease.
e. Patients and their families might benefit from counseling and psychosocial assistance as well as dietary and nutritional guidance while dealing with sickle cell disease[17,18].

Close family relationships, or inbreeding, increase the risk of passing on autosomal recessive diseases like sickle cell anemia to future generations. Because sickle cell disease is produced by a change in a single gene and is inherited in an autosomal recessive pattern, it requires mutations in both copies of the gene to be present[19]. It is more likely that both parents of a kid will possess the same recessive gene mutation if the parents are very close to one another. Therefore, there is a higher risk that their children may inherit two copies of the sickle cell gene. Therefore, in groups that practice inbreeding or consanguineous marriages, the prevalence of sickle cell illness is generally greater, as is the case in populations with a higher frequency of sickle cell disease, such as in specific parts of Africa and the Middle East. Individuals in these communities may greatly benefit from genetic counselling and information when it comes to making choices about family planning and lowering their risk of hereditary illnesses like Down syndrome[20,21,22].

Recent studies have shown that there has been an upsurge in the prevalence of sickle cell disease in the southern part of Jazan[3,19]. Patients who are affected by this kind of condition are more likely to suffer from a variety of consequences, the severity of which is directly related to their ages. The purpose of this research is to

evaluate the level of awareness that residents of Jazan have about the general knowledge and complications of SCD, as well as the level of awareness that residents have regarding the triggers and preventative measures for SCD . Thirty percent of all the people who took part in the research were between the ages of 18 and 29, which is the typical age range for getting married. Single participants made up 25.8% of the total population. I conducted the research for the study and think that individuals who are married as well as those who live a single life are the greatest demographic to focus on when trying to educate people about the problems of sickle cell disease and how to avoid them. The fact that the majority of the participants did not come from a medical background lends credibility to both the research and its purpose. Many of the participants were aware of the nature of sickle cell disease, and the majority of them were in agreement about the idea that consequence marriage and a positive family history of sickle cell disease are risk factors for the condition. According to the findings of research conducted in Jazan, the majority of SCD patients had parents who are related to each other via consanguinity[5]. Because of these discoveries, now in a position to make greater efforts to raise awareness about the consequences of SCD[23,24,26]. The findings make it abundantly evident that understanding is deficient about the consequences of SCD as well as the methods for detecting community awareness regarding the triggers and prevention of SCD [10,11]. To educate the people and patients who are afflicted by this illness, it is strongly recommended that sickle cell disease education units be established. These units should concentrate on the consequences of SCD as well as its prevention of it. According to the findings, as shown in Table 10, the participants aged between 18 and 29 [64 (14.2%)] prefer educational publications and videos to help spread awareness about the complications of SCD and its prevention shortly. This preference was found to be consistent across all three age groups. Those who are between the ages of 30 and 39 [78 (17.3%)] are most interested in community-based health education efforts. Publications and films geared at education are the go-to options for those aged 40 to 49 (12.2% of this age group). Those aged 50 to 59 [14 (3.1%)] and those aged 60 and beyond [6 (1.3%)] express a preference for health education efforts that take place in the community. The participants recommend that the Jazan community adopt the usage of video as the most effective method for obtaining visual information since it is both quicker and more widely accepted. Several techniques

and processes were used to ensure the reliability and validity of the research, as well as the findings, the data collecting, and the analysis.

Vascular occlusion is one of the consequences that sickle cell disease may bring about in the cardiovascular system. According to the findings of Hawasawi and colleagues, the complication was recognized by a few of the sixteen percent of the study's participants[15]. According to the findings of the Dammam research, 59.3 percent of the participants were aware that SDC might result in hypoxemia as a consequence. More than half of the individuals, like the people in the Dammam trial, identified hyperemia as one of the problems. These results are comparable to those of the Dammam study[16]. In a survey that was carried out in Jeddah, it was discovered that 9.9% of the participants understood that hyperemia is a condition that might be fatal. According to the research that was carried out in Jeddah, it was discovered that females were more conscious than men of the issues that were created by SCD[19]. According to the findings of the research, a person's age was inversely linked to their level of awareness, and the majority of the participants were between the ages of 18 and 29.

Conclusion

The purpose of this research was to determine how well people in the Jazan area understand the risks associated with sickle cell disease complications and how they might be avoided. People in the Jazan area showed some familiarity with the effects of sickle cell illness, but they still need to be educated more via creative channels of communication. This is due to the higher prevalence of sickle cell disease in the Jazan area. This is crucial in spreading as much information as possible regarding sickle cell disease and preventative measures to the general public. The participants agree that films, community events, and school visits are the best methods to spread information about the problem. Correlations between age groups, education levels, and degrees of awareness shown by the participants who worked in the medical profession were one of the most important findings of the study. It showed that students and working professionals did not lack the knowledge of graduates, and in fact, were much more informed than a large proportion of graduates.

References:

1. Jastaniah W. Epidemiology of sickle cell disease in Saudi Arabia. Annals of Saudi Medicine. 2011;31(3):289

2. Creary M, Williamson D, Kulkarni R. Sickle cell disease: Current activities, public health implications, and future directions. J Womens Health (Larchmt) 2007; 16:575–82. [PubMed] [Google Scholar]
3. Rees DC, Williams TN, Gladwin MT.Sickle-cell disease. Lancet.2010; 376: 2018-2031.
4. Jastaniah W. Epidemiology of sickle cell disease in Saudi Arabia. Ann Saudi Med. 2011;31:289–93. [PMC free article] [PubMed] [Google Scholar]
5. El-Hazmi MA, Al-Hazmi AM, Warsy AS. Sickle cell disease in Middle East Arab countries. Indian J Med Res .2011;134: 597-610.
6. Alotaibi MM. Sickle cell disease in Saudi Arabia: A challenge or not. J Epidemiol Glob Health. 2017;7:99–101. [PMC free article] [PubMed] [Google Scholar].
7. de Melo MB. An eye on sickle cell retinopathy. Rev Bras Hematol Hemoter. 2014;36:319–21. [PMC free article] [PubMed] [Google Scholar]
8. Lemaire C, Lamarre Y, Lemonne N, Waltz X, Chahed S, Cabot F, et al. Severe proliferative retinopathy is associated with blood hyperviscosity in sickle cell hemoglobin-C disease but not in sickle cell anemia. Clin Hemorheol Microcirc. 2013;55:205–12. [PMC free article] [PubMed] [Google Scholar]
9. al-Hazzaa S, Bird AC, Kulozik A, Serjeant BE, Serjeant GR, Thomas P, et al. Ocular findings in Saudi Arabian patients with sickle cell disease. Br J Ophthalmol. 1995;79:457–61. [PMC free article] [PubMed] [Google Scholar]
10. Al-Azri MH, Al-Belushi R, Al-Mamari M, Davidson R, Mathew AC. Knowledge and health beliefs regarding sickle cell disease among Omanis in a primary healthcare setting: Cross-sectional study. Sultan Qaboos Univ Med J. 2016;16:e437–44. [PMC free article] [PubMed] [Google Scholar]
11. Bhatt K, Reid ME, Lewis NA, Asnani MR. Knowledge and health beliefs of Jamaican adolescents with sickle cell disease. Pediatr Blood Cancer. 2011;57:1044–8. [PubMed] [Google Scholar]
12. Al-Riyami A, Ebrahim GJ. Genetic blood disorders survey in the sultanate of Oman. J Trop Pediatr. 2003;49(Suppl 1):i1–20. [PubMed] [Google Scholar]
13. King L, Knight-Madden J, Reid M. Newborn screening for sickle cell disease in Jamaica: A review – Past, present and future. West Indian Med J.

2014;63:147–50. [PMC free article] [PubMed] [Google Scholar]

14. DeBaun MR. The challenge of creating an evidence-based guideline for sickle cell disease. JAMA.2014; 312: 1004.
15. Hawasawi Z, Nabi G, Al Magamci M, Awad K. Sickle cell disease in childhood in Madina. Ann Saudi Med. 1998;18(4):293–5. https://doi.org/10.5144/0256-4947.1998.293.
16. Al-Suwaid, H.A., Darwish, M.A., & Sabra, A.A. Knowledge and misconceptions about sickle cell anemia and glucose-6-phosphate dehydrogenase deficiency among adult sickle cell anemia patients in al Qatif Area (eastern *KSA.* International Journal of Medicine and Public Health *5* (2015): 86.
17. Arrayed, Shaikha Al and Amani Al Hajeri. Public awareness of sickle cell disease in Bahrain. *Annals of Saudi Medicine.*2010;30:284-288.
18. Ann Saudi Med. 2010;30(4):284–8. https://doi.org/10.4103/0256-4947.65256.
19. Alshehri AM, Feroze KB, Amir MK. Awareness of Ocular Manifestations, Complications, and Treatment of Sickle Cell Disease in the Eastern Province of Saudi Arabia: A Cross-Sectional Study. Middle East Afr J Ophthalmol. 2019. 26;26(2):89-94. doi: 10.4103/meajo.MEAJO_200_18. PMID: 31543666; PMCID: PMC6737790.
20. Ali, Ghalib & Alshareet, Mohammed & Alsultan, Mohammed & Wabari, Mohammed & Ali, Abdulhadi & Alshareet, Ali & Alhejji, Ahmad. Awareness about Sickle Cell Disease among General Population in Al-Ahsa, Saudi Arabia. International Journal of Scientific & Engineering Research.2018; 9(10). 86-92.
21. Sun LR, Lynch JK. Advances in the Diagnosis and Treatment of Pediatric Arterial Ischemic Stroke. Neurotherapeutics. 2023 Apr 18:1–22. doi: 10.1007/s13311-023-01373-5. Epub ahead of print. PMID: 37072548; PMCID: PMC10112833.
22. Chabrier S, Ozanne A, Naggara O, Boulouis G, Husson B, Kossorotoff M. Hyperacute Recanalization Strategies and Childhood Stroke in the Evidence Age. Stroke. 2021 Jan;52(1):381-384. doi: 10.1161/STROKEAHA.120.031133. Epub 2020 Dec 22. PMID: 33349018.
23. Bender MA, Carlberg K. Sickle Cell Disease. 2003 Sep 15 [updated 2022 Nov 17]. In: Adam MP, Mirzaa GM, Pagon RA, Wallace SE, Bean LJH, Gripp KW, Amemiya A, editors. GeneReviews® [Internet]. Seattle

(WA): University of Washington, Seattle; 1993–2023. PMID: 20301551.

24. Abraham AA, Tisdale JF. Gene therapy for sickle cell disease: moving from the bench to the bedside. Blood. 2021; 138:932–41. - PMC – PubMed
25. Herity LB, Vaughan DM, Rodriguez LR, Lowe DK. Voxelotor: A Novel Treatment for Sickle Cell Disease. Ann Pharmacother. 2021 Feb;55(2):240-245. doi: 10.1177/1060028020943059. Epub 2020 Jul 16. PMID: 32674605.
26. Mangla A, Ehsan M, Agarwal N, Maruvada S. Sickle Cell Anemia. 2022 Nov 30. In: StatPearls [Internet]. Treasure Island (FL): StatPearls Publishing; 2023 Jan–. PMID: 29489205.

APPENDIX: Questionnaire

Title: Awareness of Sickle anemia general complications and Prevention among Saudi Population in the Jazan Region

Measuring the degree of community awareness of sickle cell anemia and its complications

and prevention methods. A study and statistical survey to determine the degree of awareness of the citizens of the Jazan region regarding sickle cell anemia, its complications, and ways to avoid the disease.

This study stems from the Hematology and Hematology Unit - College of Applied Sciences - Jazan University.

*Required

Do you agree to participate in the questionnaire?

- Yes.
- NO.

Section-1 Personal data:

- **Age:**
- 18-29
- 30-39
- 40-49
- 50-59
- >60
- **Gender:**

- Male
- Female

o Marital status:

- Married
- Single
- Divorced

o Educational level:

- Undergraduate.
- Diploma
- Bachelor
- MScs
- PhD

o Occupation:

- Government.
- Military
- Medical
- Without work

o Living

- City
- Village

Section 2: Awareness of sickle cell disease

o Have you ever heard about sickle cell disease?

- Yes
- No

o How did you hear about sickle cell disease?

- Affected family member
- Diagnosed with sickle cell
- Through the media (TV, mobile media, videos, community activities)
- Through my university studies
- School
- Premarital counseling
- I've never heard of it before.

- Through health education in the city or the neighborhood

o Which of the following is a true choice about Sickle cell anemia

- Hereditary blood disease
- Non-hereditary disease
- A disease that leads to hemolysis or breakdown of red blood cells

o What are the risk factors for developing sickle cell anemia?

- Consanguine marriage
- Family history of sickle cell disease
- Contact with a sick person
- I don’t know

Section 3: Awareness of sickle cell disease Complications

o How to describe the seriousness of sickle cell anemia?

- A very dangerous disease that may lead to death if it is not given attention and care
- An ordinary disease that can be easily cured
- I don't know

o What are the most important complications of sickle cell anemia?

- Severe anemia
- Vascular occlusion
- Spleen infarction
- Acute chest syndrome
- Blood and brain clots
- Heart failure
- kidney failure
- Gallstones
- Bone pain and infarcts
- Genital problems

o What are the effects of complications of sickle cell anemia?

- Increased likelihood of premature death
- Lack of daily activity
- Affect the Impact of School, university, or practical performance
- The bad economic and financial impact on the family

- What are the most important therapeutic methods for care and reducing the risk of the disease?
  - Proper nutrition
  - Attention to health and avoiding infection
  - Periodic review of the doctor
  - Regular blood transfusions in case of severe anemia
  - Take prescription drugs and vitamins regularly
  - Avoid cold, lack of oxygen, and high areas

Section-4 Prevention of sickle cell anemia

- What are the most important ways to prevent sickle cell anemia?
- Premarital analysis
- Reduce consanguineous marriages
- What is the most important way to raise community awareness of the seriousness of the disease?
  - Increasing health education campaigns in the community
  - School Health Education Campaigns
  - Increase educational and educational publications and videos

التوعية بالمضاعفات العامة لفقر الدم المنجلي والوقاية منه بين السكان السعوديين في منطقة جازان

تقوى يوسف السيد يوسف[١]

[١] شعبة تقنية المختبرات الطبية -كليه العلوم الطبيه التطبيقية- جامعة جازان- المملكة العربية السعوديه

الملخص

مقدمة: فقر الدم المنجلي هو مرض صبغي جسدي متنحي ناتج عن تكوين الهيموغلوبين غير الطبيعي . مرض فقر الدم المنجلي له العديد من المضاعفات مثل أزمة انسداد الأوعية والسكتة الدماغية ومتلازمة الصدر الحادة وحصوات المرارة. هدفت هذه الدراسة إلى تقييم وعي مجتمع جازان بالمعرفة العامة ومضاعفات الانيميا المنجلية والكشف عن الوعي المجتمعي حول محفزات الانيميا المنجلية والوقاية منها.

المواد والطريقة: أجريت دراسة مقطعية في عام ٢٠٢٢ بين الأفراد السعوديين البالغين الذين يعيشون في منطقة جازان لتقييم وعي المجتمع بالمعرفة العامة ومضاعفات داء الكريات المنجلية والكشف عن وعي المجتمع حول المحفزات والوقاية. أجريت الدراسة باستخدام استبيان متعدد الخيارات عبر الإنترنت باللغة العربية بعد الحصول على موافقة المشاركين وتم جمع البيانات من خلال الاستبيانات. ثم ارتبط مستوى الوعي بالمعلومات الديموغرافية.

النتائج: تضمنت بيانات الدراسة استجابات من عينة من ٤٥٠ مشاركا سمعوا جميعا عن فقر الدم المنجلي. كانت الإناث اللواتي أجبن على الاستبيان أكثر بقليل (ن = ٢٣٠ ، ٥١,١٪) من نظرائهن الذكور (ن = ٢٢٠ ، ٤٨,٩٪). يعتقد معظم المستجيبين (ن = ٢٩١ ، ٦٤,٧٪) أن إصابة أحد الوالدين بفقر الدم المنجلي هو عامل خطر للإصابة بالمرض بينما يعتقد ن = ١٥٩ (٣٥,٥٪) منهم أن زواج الأقارب هو عامل خطر للإصابة بداء الكريات المنجلية. كشفت النتائج أن معظم المستجيبين ن = ١٧٩ (٣٩,٨٪) سمعوا عن فقر الدم المنجلي من خلال القنوات الإعلامية. يتبع ذلك أولئك الذين سمعوا عن المرض من خلال فحوصات ما قبل الزواج أو الاستشارة (ن = ٨٨،١٩,٦٪) ومن خلال الدراسات الجامعية (ن = ٧٠،١٥,٦٪). ن = ١٧،٣,٨٪ من المستجيبين عرفوا أو سمعوا عن فقر الدم المنجلي بعد تشخيص إصابتهم بالمرض بينما سمع ن = ٢,٠,٤٪ فقط عن مرض فقر الدم المنجلي من خلال التثقيف الصحي.

الخلاصة: تشير نتائج الدراسات إلى الحاجة إلى زيادة المعرفة فيما يتعلق بالمرض والكشف عن وعي المجتمع حول محفزات فقر الدم المنجلي والوقاية منه. ستكون حملات التثقيف الصحي الأداة الفعالة في زيادة الوعي حول مرض فقر الدم المنجلي.

الكلمات المفتاحية: التوعية، المضاعفات، جازان، السعودية، مرض فقر الدم المنجلي .

مجلة جامعة جازان

للعلوم التطبيقية

دورية علمية محكمة

المراسلات

توجه جميع المراسلات إلى:

رئيس هيئة التحرير مجلة جامعة جازان للعلوم التطبيقية جازان –المدينة الجامعية –البرج الإداري – ص ب ١١٤. –الرمز البريدي ٤٥١٤

المملكة العربية السعودية أو على البريد الإلكتروني jas@jazanu.edu.sa

المملكة العربية السعودية
وزارة التعليم
جامعة جازان

مجلة جامعة جازان

للعلوم التطبيقية

دورية علمية محكمة

المجلد ١١ العدد ٢ (ربيع الثاني ١٤٤٥هـ - اكتوبر ٢٠٢٣م)

ردمد : ١٦٥٨-٦٩١٣

قواعد النشر في المجلة

مجلة جامعة جازان للعلوم التطبيقية دورية علمية محكمة تنشرها الجامعة، وهي تهدف إلى إتاحة الفرصة للباحثين لنشر إنتاجهم العلمي وتقوم المجلة بنشر المواد الآتية :

١ـ البحث : ويندرج تحت تخصص الباحث ويجب أن يحتوي على إضافة للمعرفة في مجاله .

٢ـ المقالة الاستعراضية التي تتضمن عرضًا نقدياً لبحوث سبق إجراؤها في مجال معين أو أجريت في خلال فترة زمنية محددة.

٣ـ البحث المختصر.

٤ـ نقد الكتب .

٥ـ الخطابات الموجهة إلى المحرر ، والملاحظات والردود ، والنتائج الأولية .

تقوم هيئة التحرير، بالنظر في نشر المواد المعرفية ذات الصلة بذلك الفرع، وتقدم البحوث الأصلية، التي لم يسبق نشرها، وفي حال قبول البحث للنشر تؤول كل حقوق النشر للمجلة و لا يجوز نشره في أي منفذ نشر آخر ورقيا أو إلكترونياً، دون إذن كتابي من رئيس هيئة التحرير .

تعليمات النشر في المجلة

١ـ تقديم المواد : يقدم أصل البحث مخرجا في صورته النهائية متضمنا الإشارة إلى أماكن الجداول والأشكال داخل المتن و مطبوع على هيئة صفحات مرقمة ترقيما متسلسلا، مع ضرورة إرفاق قرص ممغنط مطبوع عليه البحث على برنامج Ms Word باستخدام النظام المتوافق مع IBM ، وسيعتذر عن قبول أي بحث لا يلتزم مؤلفه بهذه التعليمات.

٢ـ الملخصات: يرفق ملخصان بالعربية والإنجليزية للبحوث و المقالات الاستعراضية والبحوث المختصرة على ألا يزيد عدد كلمات كل منهما على ٢٠٠ كلمة، وعلى عمود واحد بعرض كتابة ١٣ سم.

٣ـ لا بد من احتواء كل بحث على كلمات مفتاحية (Key Words) توضع أسفل الملخصين العربي والانجليزي على ألا تزيد عن عشر كلمات.

٤ـ الجداول والمواد التوضيحية: يجب أن تكون الجداول والرسومات واللوحات مناسبة لمساحة الصف في صفحة المجلة ١٦ ٢٤ سم بالحواشي، ويتم إعداد الأشكال الخطية على برامج الحاسب الآلي، ولا تقبل إلا أصول الأشكال. كما يجب أن تكون الخطوط واضحة ومحددة ومنتظمة من حيث كثافة الحبر وتناسب سمكها مع حجم الرسم، ويراعى أن تكون الصور الفوتوغرافية (الضوئية) الملونة وغير الملونة مطبوعة على ورق لماع، أو محملة على برنامج (Adobe Photoshop) مع كتابة عنوان لكل جدول، وتعليق لكل شكل وصورة، والإشارة إلى مصدر المادة إن كانت مقتبسة.

٥ـ الاختصارات: يجب استخدام الاختصارات المقننة دولية مثل : سم، مم، م، كم، سم، مل، مجم، كجم...إلخ.

٦ـ المراجع :يشار إلى المراجع داخل المتن بنظام الاسم والتاريخ، وتوضع المراجع جميعها في قائمة المراجع بنهاية المادة مرقمة ومتبعة نظام ترتيب البيانات الببليوجرافية التالي :

أـ يشار إلى الدوريات في المتن بنظام الاسم والتاريخ بين قوسين على مستوى السطر، أما في قائمة المراجع فيبدأ المرجع بذكر الاسم الأخير للمؤلف، ثم الاسم الأول، ثم الأسماء الأخرى أو اختصاراتها بالخط الأسود، ثم سنة النشر بين قوسين، فعنوان البحث كاملا بين علامتي تنصيص" " ، فاسم الدورية، فرقم المجلد، ثم رقم العدد : ثم أرقام الصفحات تفصل بشرطة .

مثال : هادي، أحمد بن جابر. (٢٠١١م)،" استخدام تقنية النانو لتعريف الشفرات الوراثية "مجلة جامعة جازان، ١، ١ : ٢٠٠ـ٢٢٠.

بـ يشار إلى الكتب في المتن داخل قوسين بالاسم والتاريخ . أما في قائمة المراجع، فيكتب الاسم الأخير للمؤلف، ثم الاسم الأول، ثم الأسماء الأخرى أو اختصارا تها، ثم سنة النشر بين قوسين، فعنوان الكتاب بين علامتي تنصيص، ثم بيان الطبعة، فالناشر، فمدينة النشر :ثم صفحات الكتاب إن وجدت.

مثال :

عبدالهادي، محمد علي، (١٤٣٣هـ)،" مقدمة في التقنية الحيوية"، جامعة جازان، جازان.

ويجب عدم استخدام الاختصارات المرجعية مثل :المرجع نفسه . المرجع السابق...إلخ.

٧ـ أـ الحواشي: تستخدم لتزويد القارئ بمعلومات توضيحية، ويشار إليها في المتن بأرقام مرتفعة عن السطر .وترقيم التعليقات متسلسلة داخل المتن. وفي حال الضرورة؛ يمكن الإشارة إلى مرجع داخل الحاشية عن طريق استخدام كتابة الاسم والتاريخ بين قوسين وبنفس طريقة استخدامها في المتن، وتوضع الحواشي أسفل الصفحة التي تخصها والتي ذكرت بها و تفصل بخط عن المتن وبخط أصغر.

بـ يستخدم في تخريج الأحاديث والآثار الطريقة المنهجية المعتمدة في هذا الفن وهي كالآتي : اسم المؤلف ـ اسم الكتاب ـ رقم الجزء والصفحة والحديث.

٨ـ المواد المنشورة في المجلة تعبر عن وجهة نظر صاحبها، ولا تعبر بالضرورة، عن رأي مجلة جامعة جازان.

٩ـ يتأكد الباحث من صحة اللفظ وسلامة لغة البحث، وخلوه من الأخطاء اللغوية والنحوية.

١٠ـللمجلة الحق في تحديد أولويات نشر البحوث.

١١ـالمجلة غير ملزمة بإعادة البحوث التي تصل إليها سواء أجيزت للنشر أم لم تجز.

١٢ـيتم إخضاع جميع البحوث المستلمة لفحص مبدئي، من قبل هيئة التحرير، لتقرير أهليتها للتحكيم، ويحق لها أن تعتذر عن قبول البحث دون إبداء الأسباب.

١٣ـتصدر المجلة مرتين في العام.

المملكة العربية السعودية
وزارة التعليم
جامعة جازان

مجلة جامعة جازان

للعلوم التطبيقية

دورية علمية محكمة

المجلد ١١ العدد ٢ (ربيع الثاني ١٤٤٥هـ - اكتوبر ٢٠٢٣م)

ردمد: ١٦٥٨-٦٩١٣